

Fall Final Report
RAPTR
Rapid Aerial Photographic Target Recognition

University of Colorado
Department of Aerospace Engineering Sciences
ASEN 4018

Monday 17th December, 2018



Name: Tim Moon Email: Timothy.B.Moon@lmco.com Phone: 845-521-2050	Name: Bryan Senchuk Email: Bryan.C.Senchuk@lmco.com Phone:
Name: Paul Mittan Email: Paul.Mittan@lmco.com Phone: 607-751-4471	Name: Ben Mihevc Email: Benjamin.T.Mihevc@lmco.com Phone: 315-717-5642
Name: Eileen B Liu Email: Eileen.B.Liu@lmco.com Phone:	Name: Theresa Brown Email: Theresa.M.Brown@lmco.com Phone:

Name: Austin Abraham Email: Austin.Abraham@colorado.edu Phone: (517) 442-4391	Name: Nicholas Carvo Email: Nicholas.Carvo@colorado.edu Phone: (720) 323-8272
Name: Gregory Clements Email: Gregory.Clements@colorado.edu Phone: (610) 809-7653	Name: Zachary Donovan Email: Zachary.Donovan@colorado.edu Phone: (719) 368-1788
Name: Tyler Faye Email: tyler.faye@colorado.edu Phone: (303) 884-5910	Name: Thad Gleason Email: thad.gleason@colorado.edu Phone: (727) 735-7544
Name: Everett Hale Email: ernest.haleiv@colorado.edu Phone: (904) 521-5855	Name: Jeremiah Lane Email: jela5867@colorado.edu Phone: (303) 434-5688
Name: Aubrey (AJ) McKelvy Email: Aubrey.Mckelvy@colorado.edu Phone: (864) 387-9404	Name: Logan Thompson Email: Logan.R.Thompson@colorado.edu Phone: (303) 990-4123
Name: Anna Tiberi Email: Anna.Tiberi@colorado.edu Phone: (303)-332-3321	

Customer:
Ben Mihevc, Lockheed Martin

Supervised by
Professor Dennis Akos

Table of Contents

Acronyms and Nomenclature	12
1 Project Purpose	14
2 Project Objectives and Functional Requirements	15
2.1 Concept of Operations	16
2.2 Functional Block Diagram	17
3 Concept Design	19
3.1 Key Design Alternatives	19
3.1.1 Vehicle Design	19
3.1.1.1 Rocket Powered Glider	19
3.1.1.2 Electric Aircraft	20
3.1.1.3 Traditional Rocket	21
3.1.1.4 Quad-Copter	21
3.1.2 Payload Mounting	22
3.1.2.1 Internal Nose with Aperture	22
3.1.2.2 External Gimbaled Dome	23
3.1.2.3 Deployable Payload	24
3.1.3 Landing Method	25
3.1.3.1 Deployable Parachute	25
3.1.3.2 Soft Belly Landing	26
3.1.3.3 Landing Gear	27
3.1.3.4 Crash Landing	28
3.1.4 Deployment Method	28
3.1.4.1 Hand Thrown	28
3.1.4.2 Single Fixed Rod	29
3.1.4.3 Single Variable Rod	31
3.1.4.4 Variable Rails with Hydraulic Launch Initiation	33
3.1.5 Sensor Suite	34
3.1.5.1 Attitude Determination Subsystem	34
3.1.5.2 Position Determination	37
3.1.5.3 Autopilot Subsystem	38
3.1.5.4 Imaging Subsystem	39
3.2 Trade Studies	43
3.2.1 Vehicle	43
3.2.1.1 Trade Metrics and Trade Study	43
3.2.1.2 Vehicle Trade Discussion	44
3.2.2 Payload Mounting	46
3.2.2.1 Trade Metrics and Trade Study	46
3.2.2.2 Payload Mounting Trade Discussion	46
3.2.3 Landing Methods	48
3.2.3.1 Trade Metrics and Trade Study	48
3.2.3.2 Landing Method Trade Discussion	48
3.2.4 Deployment Method	50
3.2.4.1 Deployment Method Trade Discussion	51
3.2.5 Sensor Suite	52
3.2.5.1 Attitude Determination	52
3.2.5.2 Altitude Determination	54
3.2.5.3 Autopilot Subsystem	55
3.2.5.4 Imaging Subsystem	58
3.3 Baseline Design	60

4 Requirements Development	62
4.1 Requirements Flow Down	62
5 Detailed Design	66
5.1 Structures	66
5.1.1 Detachable Engine Mechanism Design	66
5.1.2 Engine Mount Structural Analysis	68
5.1.3 Analytic Wing Bending Model	70
5.1.4 Modifying Fuselage for Flight Hardware	72
5.1.5 Vehicle and Payload Integration	75
5.2 Propulsion	76
5.2.1 Engine Choice and Design Parameters	77
5.2.2 Propulsion Models	82
5.2.2.1 RockSim	82
5.2.2.2 OpenRocket	83
5.2.2.3 MATLAB	85
5.2.2.4 Expected Sources of Error During Launch	86
5.2.3 Maximum Velocity and Weight Considerations	88
5.2.3.1 Thrust Curve Error	89
5.2.4 Parachute and Nose Cone	90
5.2.5 Launch Stand and Interface	92
5.2.6 Exhaust: Thermal Effect and Plume Characteristics	93
5.2.7 Launch Regulations and FAA Compliance	95
5.3 Aerodynamics	97
5.3.1 Aerial Vehicle Design	97
5.4 Electronics and Controls	106
5.4.1 Vehicle Electronics	106
5.4.1.1 Full Parts List	106
5.4.1.2 RAPTR Electronics Diagrams	114
5.4.2 Pixhawk IMU Uncertainty	115
5.4.3 Transmission and Reception	116
5.4.3.1 TX/RX Hardware	117
5.4.4 RAPTR Control via Pixhawk	118
5.4.5 ArduPlane Control Code	118
5.4.6 Pixhawk Control Architecture	120
5.4.7 PID Gain Approximation	121
5.4.7.1 Problem Statement	121
5.4.7.2 Problem Approach	122
5.5 Software	127
5.5.1 Target Recognition Software	127
5.5.2 GeoLocation Software	131
6 Verification and Validation	136
6.1 Test Schedule	136
6.2 Test Imaging (Software)	136
6.2.1 Test Plan	136
6.2.1.1 Introduction	136
6.2.1.2 Test Materials	136
6.2.1.3 Features to be Verified/Validated	136
6.2.1.4 Features not to be Verified/Validated	137
6.2.1.5 Approach	137
6.2.1.6 Success/Fail Criteria	137
6.2.2 Preliminary Test Results	137
6.3 Structural Test	137
6.3.1 Motor Mount Testing	137
6.3.1.1 Test Overview	137

6.3.1.2	Test Logistics	137
6.3.1.3	Materials	138
6.3.1.4	Procedure	138
6.3.1.5	Error/Uncertainty	138
6.3.1.6	Success Criteria	138
6.3.1.7	Results	139
6.3.2	Wing Bending Test	139
6.3.2.1	Test Overview	139
6.3.2.2	Design of Whiffle Tree Layout.	140
6.3.2.3	Test Logistics	142
6.3.2.4	Materials	142
6.3.2.5	Procedure	143
6.4	Thermal Test	143
6.4.1	Test Overview	143
6.4.2	Test Logistics	144
6.4.2.1	Testing Site	144
6.4.2.2	Local Emergency Services	145
6.4.2.3	Personnel Breakdown	145
6.4.3	Materials	145
6.4.3.1	Materials List	145
6.4.3.2	Safety Hazards	146
6.4.4	Go/No-Go Criteria	147
6.4.5	Procedure	147
6.4.5.1	Pre-Firing Procedure	147
6.4.5.2	Post-Firing procedure	148
6.4.6	Success Criteria	148
6.5	Wind Tunnel Testing	148
6.5.1	Test Overview	148
6.5.2	Test Logistics	148
6.5.3	Materials	149
6.5.4	Procedure	149
6.5.5	Success Criteria	149
6.6	Communications Integration Test	149
6.6.1	Test Overview	149
6.6.2	Test Logistics	150
6.6.3	Materials	150
6.6.4	Procedure	150
6.6.5	Success Criteria	151
6.7	Controls Testing/Tuning	151
6.7.1	Test Overview	151
6.7.2	Test Logistics	151
6.7.3	Materials	152
6.7.4	Procedure	152
6.7.5	Success Criteria	153
6.8	Vehicle Systems Testing	153
6.8.1	Test Overview	153
6.8.2	Test Logistics	154
6.8.2.1	Testing Site	154
6.8.2.2	Local Emergency Services	154
6.8.2.3	Personnel Breakdown	154
6.8.3	Materials	155
6.8.3.1	Safety Hazards	156
6.8.4	Go/No-Go Criteria	156
6.8.5	Procedure	156
6.8.5.1	Pre-Firing Procedure	156
6.8.5.2	Flight procedure	157

6.8.5.3	Post Flight Procedure	157
6.8.6	Success Criteria	158
6.9	Full Systems Testing	158
6.9.1	Test Overview	158
6.9.2	Test Logistics	158
6.9.2.1	Testing Site	158
6.9.2.2	Local Emergency Services	158
6.9.2.3	Personnel Breakdown	159
6.9.3	Materials	159
6.9.3.1	Safety Hazards	160
6.9.4	Go/No-Go Criteria	160
6.9.5	Procedure	161
6.9.5.1	Pre-Firing Procedure	161
6.9.5.2	Flight procedure	161
6.9.5.3	Post Flight Procedure	162
6.9.6	Success Criteria	162
7	Risk Assessment and Mitigation	163
8	Project Planning	165
8.1	Work Breakdown Structure	165
8.2	Work Plan	165
8.3	Cost Plan	166
8.3.1	Electronics Subteam Cost Breakdown	167
8.3.2	Propulsion Subteam Cost Breakdown	168
8.3.3	Structures and Manufacturing Subteam Cost Breakdown	168
8.3.4	Already Completed Purchases	168
9	Individual Report Contributions	169
9.1	Austin Abraham	169
9.2	Nick Carvo	169
9.3	Greg Clements	169
9.4	Zach Donovan	170
9.5	Tyler Faye	170
9.6	Thad Gleason	170
9.7	Everett Hale	170
9.8	Jeremy Lane	171
9.9	AJ Mckelvy	171
9.10	Logan Thompson	171
9.11	Anna Tiberi	171
10	Appendix	174
10.1	Project Budget	174
10.1.1	Completed Purchases	176

List of Figures

1	RAPTR Concept of Operations	17
2	RAPTR Functional Block Diagram	18
3	USAF Rocket Powered Target Glider	19
4	Kit Rocket Glider, Isometric View	20
5	Kit Rocket Glider, Rear View	20
6	Example of an Electric Aircraft	20
7	Example of a Traditional Rocket	21
8	Example of COTS Quad-copter. (DJI Phantom 4)	22
9	Diagram of body fixed nose aperture	23
10	Diagram of External Gimbaled Dome	24
11	Diagram of Deployable Payload	24
12	Diagram of deploy-able parachute	26
13	Diagram of Pixhawk 4	27
14	Diagram of landing gear parts	27
15	Hand Thrown Deployment Method	29
16	Single Fixed Rod Deployment Method?	30
17	Drawing of Fixed Rod	30
18	Single Variable Rod Deployment Method?	31
19	Single Variable Rod Angled Deployment Method?	32
20	Drawing of Variable Launch Rod	32
21	Variable Rail with Piston Deployment Method?	33
22	Diagram of 3-axis gyroscope, 3-axis accelerometer, and magnetometer sensor suite.	34
23	Diagram of 3-axis gyroscope, 3-axis accelerometer, and GPS sensor suite.	35
24	Diagram of 3-axis gyroscope, 3-axis accelerometer, and infrared sensor suite.	36
25	Diagram of 3-GPS sensor suite.	36
26	Diagram of a single camera imaging system	40
27	Diagram of a two camera imaging system	41
28	Diagram of camera and thermal sensor combo	41
29	Diagram of a LIDAR imaging system	42
30	Baseline Design of RAPTR	61
31	Motor mount	66
32	Motor assembly	66
33	Motor assembly drawing	67
34	Motor separation, pre-ignition	67
35	Motor separation, ignition	68
36	Motor separation, post-burnout	68
37	Motor mount Ansys analysis, view 1	69
38	Motor mount Ansys analysis, view 2	70
39	AndREaS glider ²	71
40	Model of distributed load during thrust.	71
41	Model of shear force during thrust	72
42	Model of bending moment during thrust	72
43	RAPTR vehicle three view	73
44	Some of the bulkheads that will be modified	74
45	Some of the bulkheads that will be modified	74
46	RAPTR Vehicle, View 1	75
47	RAPTR Vehicle, View 2	75
48	RAPTR Fuselage Layout	76
49	Propulsive System Design	77
50	Fully Integrated Engine	78
51	Experimental Thrust Curve from ThrustCurve.org	78
52	Engine Components - Engine and Propellant Grain	79
53	Engine Components - Engine and Case	80
54	Nominal Flight Path - Propulsive Phase	81
55	RockSim 3D CAD Model Input	82

56	OpenRocket 3D CAD Model Input	83
57	OpenRocket Simulation Calculation Steps ¹²	84
58	OpenRocket Monte-Carlo Simulation: Wind and Altitude	86
59	OpenRocket Monte-Carlo Simulation: Wind and Velocity	87
60	OpenRocket Monte-Carlo Simulation: Launch Angle Error and Altitude	87
61	OpenRocket Monte-Carlo Simulation: Launch Angle Error and Velocity	88
62	OpenRocket Weight Design Point Plot	89
63	Increased Weight MATLAB Simulation: Thrust Curve Error Plots	90
64	Increased Weight MATLAB Simulation: Thrust Curve Error Performance Plot	90
65	Nose Cone General Shape ¹⁵	91
66	Parachute Size Calculation ¹⁶	91
67	Parachute Example	92
68	Launch Lug Example	92
69	Launch Stand ²⁰	93
70	Close-Up Of Launch Rail ²⁰	93
71	Bell Nozzle Plume Expansion and Altitude Compensation ³¹	94
72	Realistic Nozzle Geometry versus Uniform Flow Simplification ³¹	94
73	Operating Requirements for High Powered Rockets	95
74	Notification Requirements	96
75	Requested Launch Schedule with Northern Colorado Rocketry Club	96
76	Fluid volume used for CFD analysis	97
77	Mesh on the exterior boundary of the interior fluid volume	98
78	Wireframe view of the mesh generated	98
79	Coefficient of pitch moment vs angle of attack	99
80	Coefficient of yaw moment vs sideslip angle	100
81	Coefficient of lift vs angle of attack	102
82	Coefficient of drag vs angle of attack	102
83	Lift to Drag ratio vs angle of attack	103
84	Course Correction Flight Path	104
85	RAPTR Performance Plot	105
86	RAPTR Performance Plot overlaid with Andreas Design Point	105
87	Turnigy Graphene Panther 2S LiPo Battery ²²	107
88	Pixhawk Common Power Module ²³	107
89	Pixhawk USB Power Consumption ²⁴	108
90	Pixhawk 4 Flight Controller ²⁵	109
91	Holybro GPS Module ²⁶	109
92	Airspeed and Integrated Temperature Sensor ²⁷	110
93	3DR Radio Telemetry Set ²⁸	111
94	FrSky X8R RC Transceiver ²⁹	112
95	Futaba S3152 Servo Motor ³⁰	112
96	Airspeed vs Control Surface Torque	113
97	RAPTR Circuit Diagram	114
98	RAPTR Wiring Diagram Overlay	115
99	Experimental Pixhawk roll test data	116
100	Experimental Pixhawk pitch test data	116
101	Example of a Wi-Fi Spectrum Analyzer Output	117
102	UMX Radian BNF remote control glider ³	119
103	Visual of ArduPlane's Mission Planner GUI	119
104	Visual of ArduPlane's Mission Planner GUI	120
105	Functional block diagram of the Pixhawk control architecture	120
106	Functional block diagram of the Pixhawk Extended Kalman Filter	121
107	PID gain input in ArduPlane	122
108	Control block diagram of the PID approximation of the Pixhawk	122
109	Longitudinal open-loop dynamics due to a pitch disturbance	123
110	Lateral open-loop dynamics due to a yaw disturbance	124
111	Longitudinal and lateral target zones	125

112	Longitudinal and lateral P control locus plot.	125
113	Longitudinal and lateral PD control locus plot.	125
114	Longitudinal and lateral design point locus plot.	126
115	Longitudinal closed-loop effects on pitch angle.	126
116	Lateral closed-loop effects on pitch angle.	127
117	Software CONOPS and Flowchart	127
118	Sliding Window Over a Target With a Blank Background	128
119	Example Image of a Target with High Contrast with Background	129
120	Saliency Map of Example Image	130
121	”Target” Hits Overlaid on the Example Image	130
122	Bounding Box Over the Target	131
123	The Known Pixel Coordinate Frame and the Unknown World Coordinate Frame	132
124	Imaging Plane and Camera Coordinate System	132
125	Plot of Geolocation Errors with Uncertainties in Attitude Angles	134
126	Target Estimate and Target Truth During Drone Test	135
127	Test Set-up	139
128	Close-up of motor mount	139
129	General Whiffle-tree Setup	140
130	Load Distribution Comparison	141
131	Whiffle-tree FBD	141
132	Actual Whiffle-tree Setup	142
133	Basic test setup	144
134	Location of testing site	144
135	Test Site	150
136	Slope Soaring Location	152
137	Example tuning plot	153
138	Launch sites	154
139	Normal Risk Matrix	164
140	Mitigated Risk Matrix	164
141	Work Breakdown	165
142	RAPTR Spring Gannt Chart	166
143	Pie Chart Visualizing the Project Budget	167

List of Tables

1	Functional Requirements	16
2	Pros and Cons of the Rocket Glider	20
3	Pros and Cons of the Electric Aircraft	21
4	Pros and Cons of the Traditional Rocket	21
5	Pros and Cons of a quad-copter drone.	22
6	Pros and Cons of the Internal Nose with Aperture	23
7	Pros and Cons of the External Gimbaled Dome	23
8	Pros and Cons of the Deployable Payload	25
9	Pros and cons of deployable parachute	26
10	Pros and cons of belly landing	27
11	Pros and cons of landing gear	28
12	Pros and cons of crash landing	28
13	Pros and Cons of Hand Thrown Deployability.	29
14	Pros and Cons of Single Fixed Rod Deployability.	31
15	Pros and Cons of Single Variable Rod Deployability.	32
16	Pros and Cons of Hydraulic and Multiple Rail Deployability.	33
17	Four possible sensor suites able to determine attitude.	34
18	Pros and Cons of a 3-axis gyroscope, 3-axis accelerometer, and magnetometer attitude sensor suite.	35
19	Pros and Cons of the 3-axis gyroscope, 3-axis accelerometer, and GPS attitude sensor suite.	35
20	Pros and Cons of the 3-axis gyroscope, 3-axis accelerometer, and infrared horizon attitude sensor suite.	36
21	Pros and Cons of the 3-GPS attitude sensor suite.	37
22	37
23	Pros and Cons of the barometer sensor suite.	37
24	Pros and Cons of the sonar proximity sensor suite.	38
25	Pros and Cons of the laser proximity sensor suite.	38
26	Four Potential Options for Autopilot Firmware	38
27	Pros and Cons of the Paparazzi Autopilot Platform	38
28	Pros and Cons of the ArduPilot Autopilot Platform	39
29	Pros and Cons of the PX4 Autopilot Platform	39
30	Four Potential Options for Target Imaging	39
31	Pros and Cons of using a single optical camera for target imaging	40
32	Pros and Cons of using multiple optical cameras for target imaging	40
33	Pros and Cons of using an optical camera and thermal sensor combination	41
34	Pros and Cons of using a LIDAR scanner for imaging the target	42
35	Vehicle Metric Description	43
36	Vehicle Metric Point Assignment	44
37	Vehicle Trade Table	44
38	Payload Mounting Metric Description	46
39	Payload Mounting Metric Point Assignment	46
40	Payload Mounting Trade Table	46
41	Landing Method Metric Description	48
42	Landing Method Metric Point Assignment	48
43	Trade Table for Landing Methods	48
44	Deployment Method Metric Description	50
45	Deployment Method Metric Point Assignment	51
46	Trade Table for Deployment Alternatives	51
47	Attitude Determination Metric Description	52
48	Attitude Determination Metric Point Assignment	53
49	Attitude Trade Table	53
50	Positional Determination Metric Description	54
51	Attitude Determination Metric Point Assignment	54
52	Attitude Trade Table	54
53	Autopilot Metric Description	55
54	Autopilot Platform Metric Point Assignment	56
55	Autopilot Trade Table	56

56	Imaging Suite Metric Description	58
57	Imaging Suite Metric Point Assignment	58
58	Imaging Trade Table	59
59	Subsystem Weight Breakdown	61
60	Functional Requirements	62
61	Derived Requirements From Functional Requirement 1	63
62	Derived Requirements From Functional Requirement 2	63
63	Derived Requirements From Functional Requirement 3	64
64	Derived Requirements From Functional Requirement 4	64
65	Derived Requirements From Functional Requirement 5	65
66	Derived Requirements From Functional Requirement 6	65
67	Potential motor mount material tensile strengths ^{14 13 11}	70
68	Strengths of potential wing spar materials ^{34 35 36}	72
69	Derived Requirements Relating to the Propulsion Subsystem	77
70	I55-9 Engine Characteristics	78
71	OpenRocket Simplifying Assumption and Analysis for its use for RAPTR ¹²	84
72	MATLAB Simulation Parameters used in the Simulation	85
73	MATLAB Simulation Assumptions and Accuracy	85
74	Thrust Curve Error Simulation Results with Increased Weight	89
75	Longitudinal stability derivatives found in CFD analysis	100
76	Lateral stability derivatives found in CFD analysis	100
77	Longitudinal stability derivatives found in Datcom analysis	101
78	Lateral stability derivatives found in Datcom analysis	101
79	Pitch stiffness during thrust and glide phases	101
80	Yaw stiffness during thrust and glide phases	101
81	Electrical components used in RAPTR.	106
82	Electrical components used in RAPTR.	117
83	Derived Requirements From Functional Requirement 1	118
84	ArduPlane's autonomous GPS waypoint interface.	120
85	Longitudinal and lateral decoupling and linearization assumptions.	122
86	Longitudinal and lateral target zone specifications.	124
87	Longitudinal and lateral PD gains.	126
88	Window Geometry	128
89	Test Plan/Schedule	136
90	Location of eye bolts for each bar	142
91	Detailed Cost Breakdown for the Electronics Subteam	167
92	Detailed Cost Breakdown for the Propulsion Subteam	168
93	Detailed Cost Breakdown for the Manufacturing and Structures Subteam	168

Acronyms

CDD	Conceptual Design Document
CDR	Critical Design Review
COTS	Commercial Off-the-Shelf
GUI	Graphical User Interface
PWM	Pulse Width Modulation
CFD	Computational Fluid Dynamics

Nomenclature

γ	Glide Slope Angle
ϕ	Bank angle, deg (5)
ψ	Yaw angle, deg (5)
ρ	Density of air, slug/ft^3 (5)
σ_{max}	Maximum stress, psi or ksi (5)
θ	Pitch angle, deg (5)
\vec{u}	Control input (5)
\vec{x}	State array (5)
E	Inertial y-position vector, ft (5)
A	Open-loop dynamics matrix (5)
B	Closed-loop dynamics matrix (5)
C	Open-loop dynamics index array (5)
C_D	Coefficient of Drag
C_L	Coefficient of Lift
$C_{L,\alpha=0}$	Coefficient of lift at zero degree angle of attack (5)
C_{m_α}	Pitch Stiffness
C_{n_β}	Yaw Stiffness
D	Closed-loop dynamics index array (5)
I_{tot}	Total Impulse, $\text{lbf} \cdot \text{sec}$ (5)
Isp	Specific Impulse, sec (5)
$K(s)$	Frequency representation of the control PID gains (5)
K_D	Derivative gain (5)
K_I	Integral gain (5)
K_P	Proportional gain (5)
ka	Lift Profile Coefficient (5)
p	Angular rate in the x-direction, deg/s (5)
P_{target}	Pixel length of the target (5)
q	Angular rate in the y-direction, deg/s (5)
r	Angular rate in the z-direction, deg/s (5)
u	Velocity in the x-direction, ft/s (5)
v	Velocity in the y-direction, ft/s (5)
v_{max}	Maximum velocity, ft/s (5)
w	Velocity in the z-direction, ft/s (5)
$X(s)$	Frequency representation of the plant (5)
a	Altitude (5)
D	Kolmogorov-Smirnov-test statistic (5)
d	diameter of spar rod, ft (5)
F	T-test statistic (5)
f	Camera focal length (5)
FOV	Camera Field of View (5)
I	Second Moment of Area for circle, ft^4 (5)
K	Camera matrix (5)
M	Bending Moment at point along wing, lbf-ft (5)
N,E,D	North, east, down target coordinates (5)
R	Rotation matrix (5)
T	T-test statistic (5)

u,v Horizontal, vertical pixel coordinates (5)

1. Project Purpose

Author: Aubrey Mckelvy

RAPTR is an acronym for Rapid Aerial Photographic Target Recognition. It is an autonomously controlled surveillance drone. The field of application for this system is any scenario where aerial images of an area within 4,000 feet of the user are needed quickly. The two primary examples of this are first: soldiers in a combat situation requiring situational awareness of an area where there may be enemies; if the possibility exists, it is important to be able to gain assurances that the area is clear before deciding how to proceed. Second: fire-fighters attempting to assist people trapped within a forest fire. They need to gain situational awareness of the obstacles that may stand in their way and be able to confirm the presence of the person whom they are assisting.

The problem this system will address is in the first letter of the acronym: Rapid. The existing systems for in-situ surveillance^{17 18} all have a common pitfall, their speed. Any drone that is small enough to be carried into and deployed in the field is powered by an electric prop. Depending on the configuration (plane or copter), the max speeds of these vehicles can range from 11 mph to about 50 mph. At these speeds, the vehicles make easy targets for enemies, or (to address the second use case) spend too long above a fire and thus fail due to over-heating. A faster vehicle means harder to destroy and less time over the flames. There is the added benefit of conducting the surveillance very quickly, but the aforementioned systems would only take a few minutes longer.

The end goal of the system is to strengthen and quicken the military's ability to gain situational awareness and to enable fire-fighters to do the same in more extreme conditions. A tertiary goal of the system is to provide one-time surveillance for a fraction of the cost of current systems. The vehicle is meant to be disposable and therefore does not require the same complexity of hardware. RAPTR uses a solid rocket motor to gain speed and altitude before dropping the motor and commencing a glide to surveil the target area. It is this propulsion system that sets RAPTR apart, making the vehicle faster, less mechanically complex, and cheaper.

2. Project Objectives and Functional Requirements

Author: Aubrey McKelvy and Logan Thompson

Success for this project is defined according to a set of objectives which are organized into three levels of success with increasing ambition. This table is split into three sections to better describe individual success for the aero and EE teams. These three sections are aligned with the three major components of the system: the vehicle, the payload, and the ground station. The aerospace team is responsible for the vehicle and the image recognition and geo-location software.

	Level I	Level II	Level III
Launch Vehicle (Aerospace Team)			
<i>Navigation</i>	The launch vehicle shall report location and altitude within 150 feet of accuracy to a user interface.	Level I	The launch vehicle will send location coordinate data corresponding to payload image data in real time.
<i>Controls</i>	The launch vehicle shall have a mathematical control model developed and validated in a simulation for expected flight conditions.	The launch vehicle shall demonstrate flight stability during wind tunnel test using simulated payload mass.	The launch vehicle shall be able to use control actuators to execute programmed maneuvers in flight.
<i>Vehicle Deployability</i>	The vehicle shall be designed and built with the intent of accepting a payload.	The launch vehicle shall be deployable from the ground with a mass simulator and remain stable for up to 1 minute.	The vehicle shall be deployable from the ground within 15 minutes of the user's decision to deploy and reach a desired location 800 feet in altitude from the ground station with integrated payload.
Payload (Electrical Team)			
<i>Communication</i>	The payload shall wirelessly transmit image data to a receiver during a ground test.	The payload shall transmit image data to the ground station at a rate of 1 image per second at a distance of 2000 feet during a ground test.	The payload shall transmit image data to the ground station at a rate of 1 image per second at a distance of 4000 feet during flight while integrated into the vehicle.
<i>Imaging System</i>	The imaging system shall capture and compress an image on the command of a CPU.	Level I	The imaging system shall have the resolution and field of view to image a 5'x5'x5' object as 25 pixels at 700 feet.
Ground Station (Both Teams)			
<i>Processing Performance</i>	The processing algorithm is able to identify a high visibility 5'x5'x5' object from a drone test using similar imaging specifications as the payload.	The processing algorithm shall be shown to identify and classify a 5'x5'x5' object from 10 different object types from 2000 feet away during a ground test and simulation.	The processing algorithm is able to identify, classify, and provide the location of a 5'x5'x5' object on the ground from 700 feet in the air in real time during a flight test.
<i>Communication</i>	The ground station shall receive and decompress image data and send to the processing software during a ground test.	Level I	The ground station shall receive and decompress all image data and send to the processing software at a range of 2000 feet during a flight test.
<i>User Interface</i>	The user interface shall display if a target has been identified by the processing algorithm during a simulation.	The user interface shall indicate which object has been identified by the software and display an image of the object to the user.	The user interface shall display the number of objects, the type of object, and the location of the object on a map to the user.

The functional requirements of the system were developed with guidance from the customer presentation as a means to satisfy these levels of success. RAPTR's functional requirements are listed in table 1.

Requirement	Description
1	The system shall survey a 2,000 foot long and at least 400 foot wide corridor beginning 2,000 feet from the user and aligned with a user defined heading.
2	The system shall be man portable.
3	The system shall transmit images and telemetry data to a ground station.
4	The system shall identify and geo-locate targets present in the captured images
5	The system shall complete its mission (launch to images processed) within 3 minutes.
6	The system shall comply with all federal and state laws regarding testing and functionality.

Table 1. Functional Requirements

2.1. Concept of Operations

The mission concept of operations is shown in Fig. 1. Once the target's presence is known, the user will set up and deploy the aerial vehicle. The user will ignite the rocket motor that is mounted to the vehicle, and the vehicle will ascend to approximately 1000 feet in altitude, and proceed to fly over the stationary 5'x5'x5' target. After the rocket motor burns out, the motor assembly will detach from the vehicle and parachute to the ground. The vehicle's imaging payload will then take overlapping images of the area, and then compress said images. At this point, the vehicle will be at an altitude of 600 feet to allow for proper imaging by the payload. The compressed images, along with vehicle telemetry and payload pointing data, will be transmitted via 2.4 GHz ISM-band frequency to the ground station. Following payload transmission, the vehicle's mission will end, and it will proceed to a belly landing, independent of the remaining elements of the mission. The ground station will decompress the data. The ground station will then utilize an image processing algorithm to identify the target through regions of interest in the images and associate the image and target location to the physical location of the target based off of the telemetry data. Using a user interface integrated into the ground station, the ground station will output target identification and location information to the user.

RAPTR CONOPs

Objective: Image and locate target within area of interest

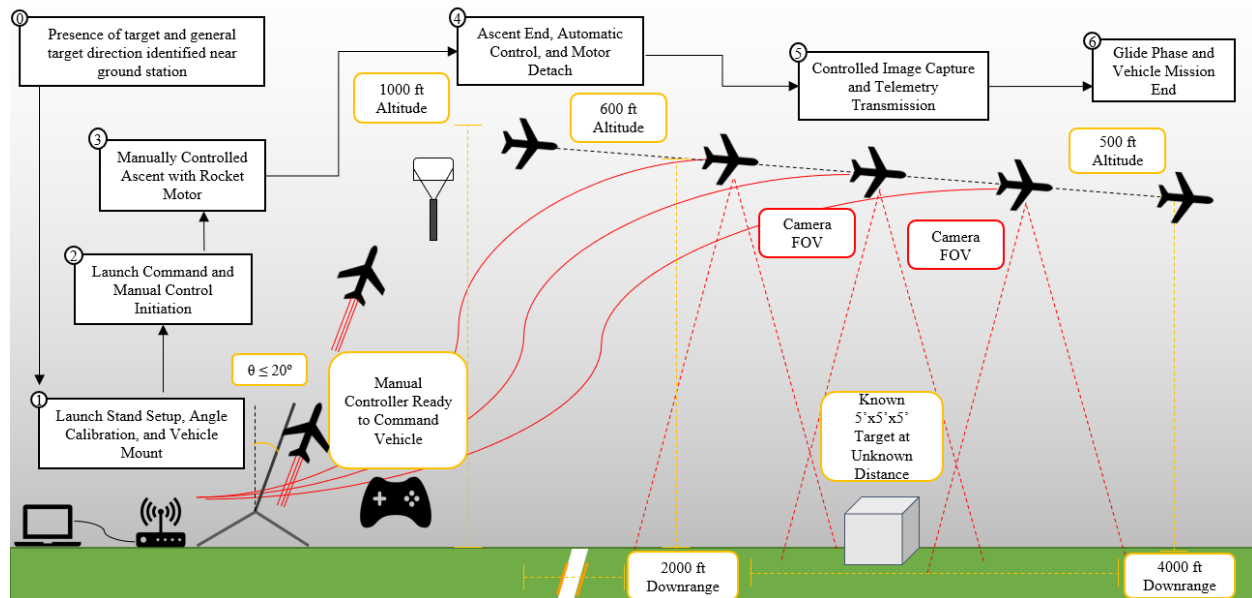


Figure 1. RAPTR Concept of Operations

2.2. Functional Block Diagram

RAPTR's Functional Block Diagram may be viewed in Fig. 2. RAPTR is composed of three primary components: the payload, the vehicle, and the ground station. The payload contains the imaging system, compression functionality, and the antenna for transmitting data back to the ground station. This component will be designed and tested by the electrical engineering team, with joint full system testing. The vehicle component, primarily designed by the aerospace engineering team, will include power, propulsion, ADCS/GNC sensors and controls. It will exchange telemetry data and power with the payload. Dependent on the vehicle solution, the vehicle will also feature RC functionality, in the event that any autopilot software does not perform nominally. The ground station component, developed jointly by both teams, contains a receiver antenna, power source, processing unit, and user interface for outputting target analysis to the user.

RAPTR Functional Block Diagram

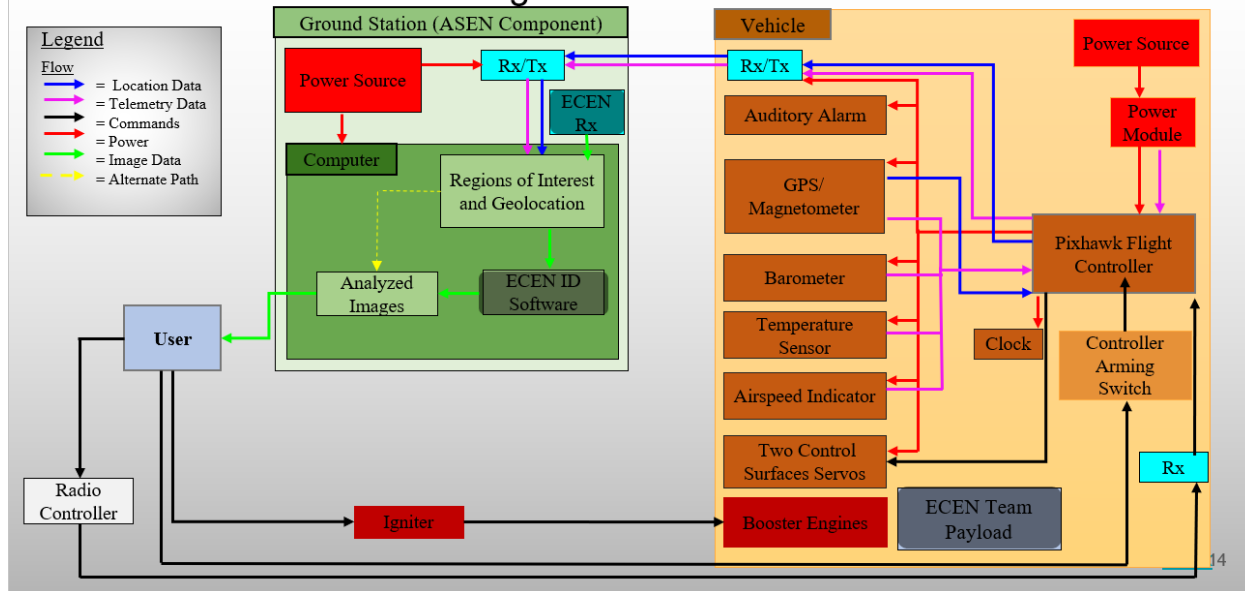


Figure 2. RAPTR Functional Block Diagram

3. Concept Design

Author: Aubrey McKelvy, Logan Thompson, Zach Donovan, Anna Tiberi, Greg Clements, Austin Abraham, Everett Hale, Thad Gleason, Nicholas Carvo, Jeremiah Lane, and Tyler Faye

The following two sections detail the design solution trade studies conducted earlier this semester. The last section details the design of RAPTR as it stands.

3.1. Key Design Alternatives

3.1.1. Vehicle Design

The vehicle must be capable of carrying the payload 2000 feet laterally, 400 feet vertically, and position itself such that the payload will be able to image the intended target area. This requirement is outlined in more detail in **DR 1.1**, **DR 1.1.1**, and **DR 5.2**. To do this, the vehicle must provide enough lift to transport its own structure and the mass of the payload. The vehicle must also be compact and travel at a high velocity to fulfill **DR 2.1** and **FR 5**. The vehicle must comply with all Federal Aviation Administration rules and regulations as outlined in **FR 6**. After considering all of the requirements, the vehicle design has been narrowed down to four options. Those options are as follows:

- Rocket Powered Glider
- Electric Aircraft
- Traditional Rocket
- Quad-Copter

3.1.1.1. Rocket Powered Glider

The first vehicle design to consider is a rocket-assisted glider. This design integrates a nacelle with a solid rocket propulsive element with control surfaces such as wings, elevators, and a tail. The control surfaces would be an integral part of this design to efficiently deliver a payload with enough stability to take quality images. A prototype design for a system such as this can be seen in Fig. 3, although for the purposes of RAPTR the concept would be considerably scaled down like the vehicle shown in Fig. 4 and Fig. 5. This vehicle option would be provided thrust and lift with elements of rocket propulsion. This simplistic propulsive mechanism means the vehicle can be tested multiple times by simply adding more fuel to the propulsion system. The control surfaces would be designed, built, and tested to last multiple flights and would therefore be very durable. As the solid rocket fuel burns away the vehicle becomes lighter, allowing for increased glide distance.



Figure 3. USAF Rocket Powered Target Glider



Figure 4. Kit Rocket Glider, Isometric View



Figure 5. Kit Rocket Glider, Rear View

Description	Pro	Con
Solid Rocket Motors are relatively cheap, simple and durable	X	
Can be controlled by off the shelf hardware and software	X	
Can reach target area quickly while maintaining control	X	
No electrical power used to provide thrust	X	
Thrust mechanism can be easily jettisoned	X	
Increased regulations and flight rules when using rocket and UAV		X
Misuse of rocket motors can cause serious injury		X
Limited examples and previous work		X

Table 2. Pros and Cons of the Rocket Glider

3.1.1.2 Electric Aircraft

An electric aircraft is another possible vehicle design. An example of an electric aircraft is shown below in Fig. 6. As seen in this example, an electric motor is used to spin a prop which provides power for the aircraft. The prop and electric motor potentially create issues. Electric motors, and the batteries needed to power them, are relatively heavy. They would consequently reduce the payload capacity of the vehicle. However, electric aircraft are widely used. This means that there are many examples and references available, there are off the shelf hardware and software systems that can control the aircraft, and there are also off the shelf products that can be used to support the design of the aircraft. These design trade-offs are summarized in Table 3 below.



Figure 6. Example of an Electric Aircraft

Description	Pro	Con
Many examples and references	X	
Many off the shelf products available to support custom design	X	
Can be controlled by off the shelf hardware and software	X	
Electric motors and batteries required to power them are heavy		X
Props can be easily broken		X

Table 3. Pros and Cons of the Electric Aircraft

3.1.1.3 Traditional Rocket

A traditional rocket, like the ones shown in Fig. 7, provides a fast way to get a payload to altitude. The simplicity of a solid rocket motor also makes the rocket easy to transport and deploy. The traditional rocket design features small fins and control surfaces. This can cause issues with stabilization and control after launch. A traditional rocket is also designed to take a payload to a high altitude and not cover a great lateral distance. This may pose a problem in reaching the required lateral distance, particularly as the lateral distance is several times larger than the height ceiling. The characteristics of the traditional rocket vehicle are summarized below in Table 4.

**Figure 7.** Example of a Traditional Rocket

Description	Pro	Con
Easy to transport	X	
Easy to deploy	X	
Little control after launch		X
Hard to recover		X
Difficult to stabilize		X
Designed for vertical distance not horizontal distance		X

Table 4. Pros and Cons of the Traditional Rocket

3.1.1.4 Quad-Copter

The last design option to consider for the vehicle is a quad copter drone with a camera. (Figure 8) This option is one that is widely available to the average consumer today and is a popular off-the-shelf option for hobbyists. These cheap drones can be flown to low altitude and provide high quality video back to the user in almost real-time. A major

drawback is that they can only generate a fraction of the lateral speed that a rocket or RC plane can. Also, they are extremely susceptible to high winds, and their stability relies entirely on the flight computer. This means that if the drone encounters too big of a disturbance it will lose stability and crash. Lastly, these drones are extremely fragile. If any of the four rotors take slightly too much damage, or are not fully operational, then the whole vehicle is essentially useless.



Figure 8. Example of COTS Quad-copter. (DJI Phantom 4)

Description	Pro	Con
Provides very stable platform for imaging	X	
Easy to deploy and recover	X	
High control after launch	X	
Very low maximum lateral velocity		X
Fragile elements make it difficult to transport		X
Susceptible to wind and other disturbances		X

Table 5. Pros and Cons of a quad-copter drone.

3.1.2. Payload Mounting

The integration of the payload into the vehicle must enable the payload to capture images of the target. This functionality is covered by **FR 1** and must specifically satisfy **DR 1.1**. Some form of pointing control must be present to assure that the payload can image the target; this will take the form of either vehicle attitude control, or a dynamic payload fixture. The three alternatives are as follows:

- Internal Nose with Aperture
- External Gimbaled Dome
- Deployable Payload

3.1.2.1 Internal Nose with Aperture

This option is the simplest of the three. Figure 9 shows a diagram of the integration. The camera is fixed to the body of the vehicle and located in the nose cone. An aperture is present on the underside of the cone to allow the camera to image directly below the vehicle. In this alternative, the attitude control of the vehicle must be used to enable pointing. This pointing would be largely limited to rotations about the body x-axis with vehicle roll as pitch or yaw would alter the flight path too dramatically. The advantages and disadvantages to this alternative are detailed in Table 6.

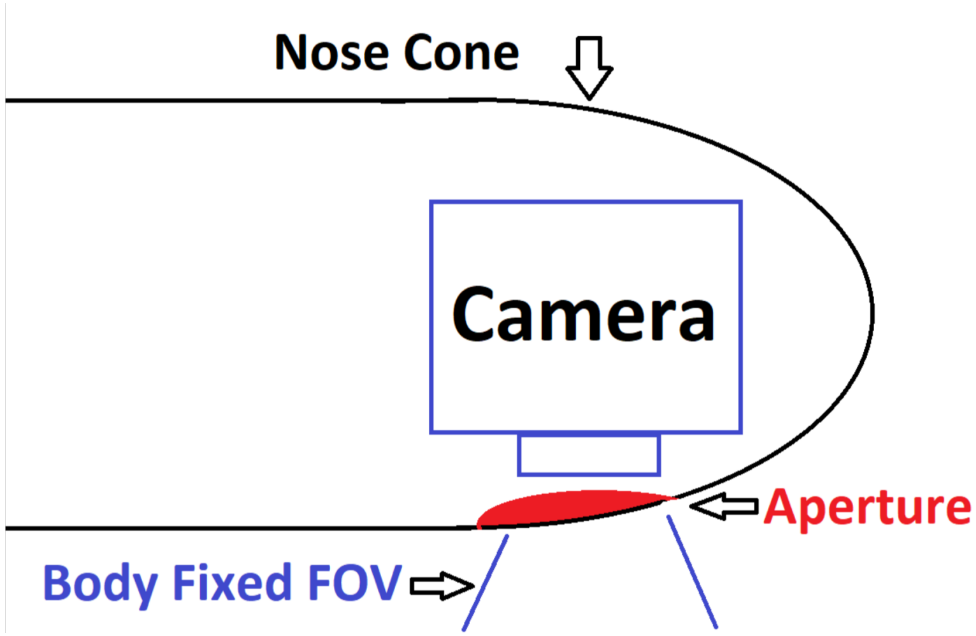


Figure 9. Diagram of body fixed nose aperture

Description	Pro	Con
No moving parts/ Simple to manufacture	X	
Pointing Location Easy to Quantify	X	
Limited (Body X) Pointing Rotations		X
Pointing requires Vehicle Attitude Changes		X

Table 6. Pros and Cons of the Internal Nose with Aperture

3.1.2.2 External Gimbaled Dome

The next alternative is to mount the camera externally in a rotating dome. A diagram of this setup is shown in Fig. 10. The camera is mounted within the dome on an actuated mount such that it can rotate up or down to change its looking azimuth. A rectangular window is placed along the dome to allow the camera to see all along its look range. This window is shaded in red in Fig. 10. The dome holding the camera is also free to rotate about the body z-axis of the vehicle. This rotation axis is shown as a dashed purple line in the diagram. With this combination of pointing control the camera could be pointed at any point on the ground visible from the vehicle's location. The vehicle would not need to adjust its attitude and also not need to fly directly over the target location. Achieving the greater pointing performance requires significant added complexity. The actuators for the two pointing directions must be controlled and quantifying the ground location of the image will require the two rotation angles to be reliably reported. The pros and cons of this alternative are detailed in Table 7.

Description	Pro	Con
Essentially Unlimited Pointing Rotations	X	
Required Vehicle Trajectory less Precise	X	
Added Control Complexity and Weight		X
Requires Rotation Angles to be Reported		X

Table 7. Pros and Cons of the External Gimbaled Dome

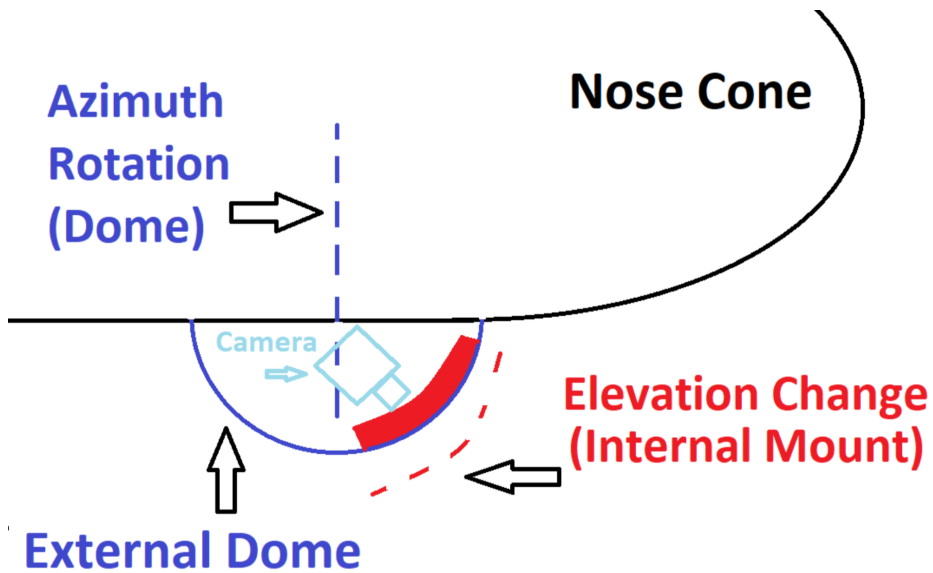


Figure 10. Diagram of External Gimbaled Dome

3.1.2.3 Deployable Payload

The final alternative is a deployable payload equipped with a parachute. For this setup, the payload is ejected from the vehicle once over the target zone. The camera is equipped with a wide field of view lens to allow room for error if the payload is not directly over the target. Images are captured and transmitted during the parachute descent. This is detailed in Fig. 11. This method requires stricter accuracy from the vehicle to assure that the payload is descending near the target. The system will also have to decide when to eject the payload with additional software and sensor considerations.

Allowing the camera to descend over the target area will allow for the target to be imaged in higher resolution, which will aid target recognition. Another key effect of this alternative is the decoupling of the vehicle requirements and the payload requirements. Under this method, the vehicle could be entirely validated without a functioning payload. The pros and cons of this alternative are summarized in Table 8.

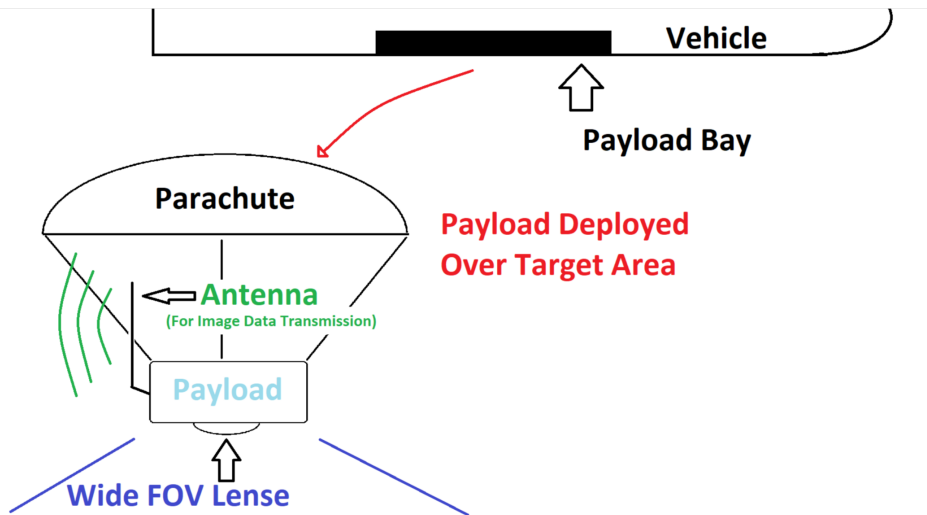


Figure 11. Diagram of Deployable Payload

Description	Pro	Con
Vehicle and Payload Functionality/System Decoupling	X	
Closer Images of Target	X	
Highly Dependant on Vehicle Trajectory		X
Vehicle/Payload must decide when to eject		X
Requires Redundant Power/Sensors/Comms for Payload and Vehicle		X

Table 8. Pros and Cons of the Deployable Payload

3.1.3. *Landing Method*

Once the vehicle and imaging systems have reached the correct altitude, captured images, and transmitted them back to the ground station, the vehicle will then need to land. This landing procedure must be controlled as required by **FR 6** and, more specifically, **DR 6.4**. Other factors that will be important when designing a landing method will be the cost, weight, and complexity. The cost is of importance due to the strict budget of this project. Providing a cheaper means of gaining imagery intelligence is also a large part of the problem statement which motivated this project to begin with. Having a landing method which adds little weight to the vehicle will allow the vehicle to reach higher altitudes faster with less thrust required from the engine. It could also allow for a heavier imaging system. The complexity of the landing method will be an important factor as well. Designing for a more complex method will require more time to implement successfully as well as increasing the risk for failure. Due to the strict time limitations on this project as well as the expensive hardware being included on the vehicle, it will be important that this method can be implemented rather quickly and with a low chance of failure. Four possible landing methods were considered for the design of this project;

- Deployable Parachute
- Soft Belly Landing
- Landing Gear
- Crash Landing

3.1.3.1 *Deployable Parachute*

A deployable parachute is one of the simplest methods for landing a UAV. Plenty of off the shelf options are available, including the Harrier Parachute Bundle shown below and sold by Fruity Chutes. Bundles like this are extremely easy to implement, they only need to be properly mounted on the vehicle, and the servo ejection channel needs to be connected to the flight controller. While this type of landing method does ensure that minimal to no damage occurs to the vehicle, it offers little to no control. Additionally, these deployable parachutes can be quite expensive and add weight to the vehicle.

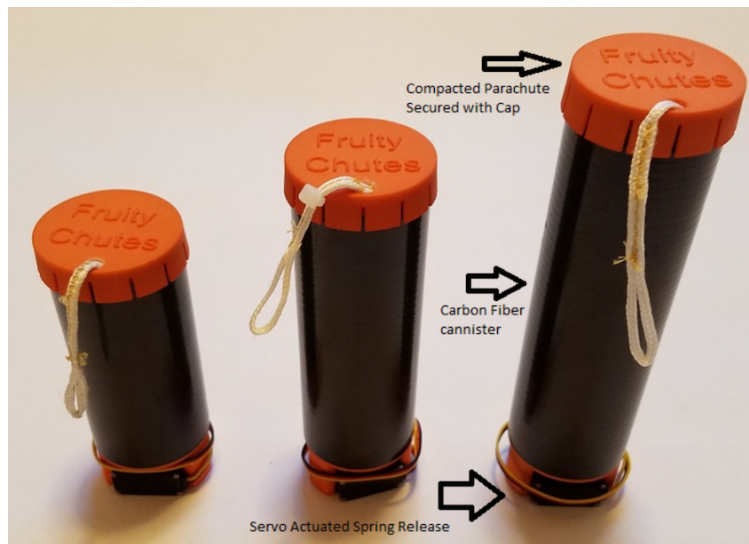


Figure 12. Diagram of deployable parachute

Description	Pro	Con
Protects vehicle/payload from damage	X	
Simple implementation	X	
Little to no control of landing		X
Can be expensive		X
Additional weight added to launch vehicle		X

Table 9. Pros and cons of deployable parachute

3.1.3.2 Soft Belly Landing

Many on board flight controllers include landing sequences. One option for landing the vehicle would be to utilize this function of the flight controller to softly touch down on its belly. Below is a diagram of the Pixhawk 4 flight controller which has available landing sequences for fixed wing aircraft. Although this would add some complexity to the project, it would add no additional weight and would provide significant control during landing. In addition, a flight controller will already be necessary for the success of this mission so taking advantage of it for landing would add little to no additional costs to the project. One concern with this method would be the risk of damaging the on board electronics. If the terrain is particularly rocky, for example, the vehicle may tumble once contacting the ground and damage the hardware. It would therefore be important to add additional protection to the electronics, such as a small skid, if this method was chosen.

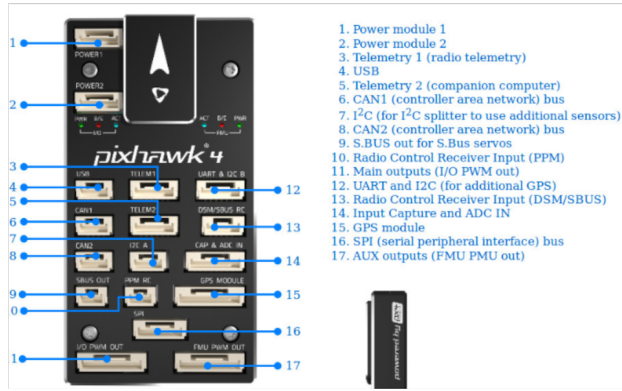


Figure 13. Diagram of Pixhawk 4

Description	Pro	Con
No additional weight added to launch vehicle	X	
Highly controlled landing	X	
No additional cost	X	
Risk of damage to electronics		X

Table 10. Pros and cons of belly landing

3.1.3.3 Landing Gear

Instead of a soft belly landing, the vehicle could also utilize a set of landing gears. Adding a landing gear to the vehicle would significantly help in protecting the electronics and adding control to the vehicle as it touches down. It would be capable of landing in a wider variety of terrain with less risk of failure. Unfortunately, the landing gear would add more weight and complexity to the vehicle. In addition, it would cost more money to implement this solution. Unless the gears were retractable, it would also affect the aerodynamic capabilities of the vehicle adding a significant amount of drag. Making the gears retractable, however, would complicate the landing method tremendously and add even more weight.

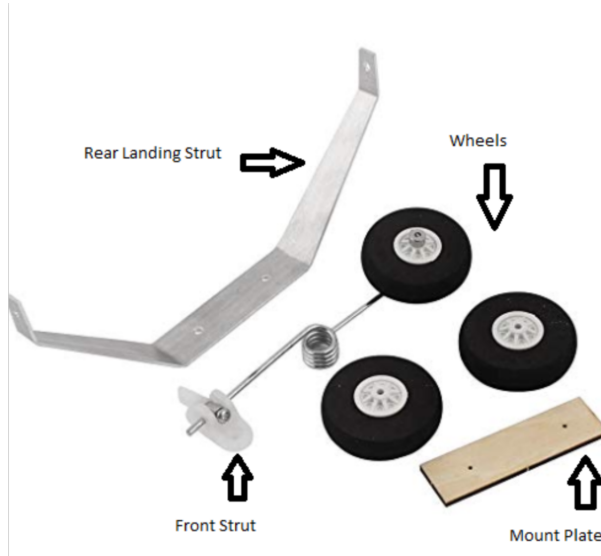


Figure 14. Diagram of landing gear parts

Description	Pro	Con
Ability to land in rugged terrain	X	
Highly controlled landing	X	
Added complexity		X
Additional cost		X
Additional weight added to launch vehicle		X

Table 11. Pros and cons of landing gear

3.1.3.4 Crash Landing

The simplest possible method of landing the vehicle would be an uncontrolled crash landing. This method has the benefit of being incredibly easy to implement; there would be no design needed for this option. Therefore the complexity and additional cost of this option is very favorable. In addition, this method would require no additional weight being added to the vehicle. A major concern, however, is in violating **DR 6.4**. It would be extremely dangerous to test a vehicle which loses all control upon landing. Additionally, the FAA requires that UAVs maintain control throughout the entire duration of their flight. Landing in this manner would also certainly destroy all on-board electronics no matter what type of terrain it is being landed in.

Description	Pro	Con
No additional weight added to vehicle	X	
No added complexity	X	
No additional cost	X	
Certain destruction of electronics		X
No control of landing		X

Table 12. Pros and cons of crash landing

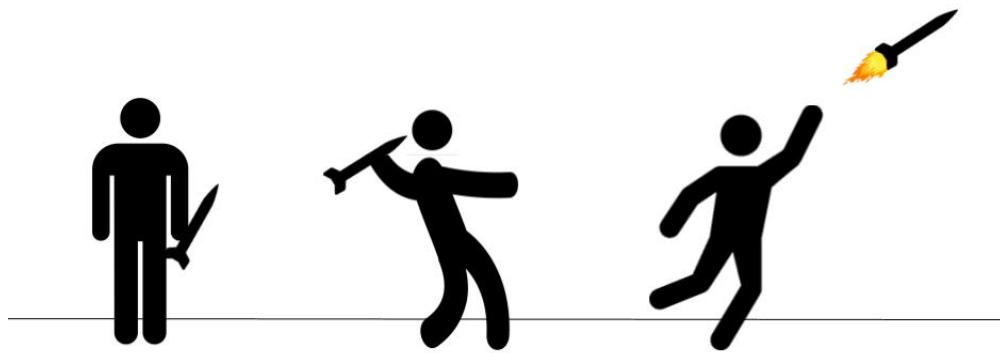
3.1.4. Deployment Method

The deployment method must be portable by one person of average strength and size and deployable in rugged and uneven terrain, up to a ten percent grade. This requirement is outlined in more detail in **FR 2**, **DR 2.1**, **DR 2.2**, and **DR 2.3**. The deployment system, in addition to being lightweight, must be small enough in size to be carried while carrying other gear - such as a backpack. After considering all of these requirements, the deployment method has been narrowed the following possibilities.

- Hand Thrown
- Single Fixed Rod
- Single Variable Rod
- Variable Rails with Hydraulic Launch Initiation

3.1.4.1 Hand Thrown

This design concept utilizes the user of the RAPTR system to launch the vehicle. This method would be designed for someone of average height and build in the United States to use. There are no design elements of this design concept as the entire method relies on the person throwing the vehicle. The user would initialize all internal elements of the vehicle, pick up the vehicle, and throw the vehicle in the general direction the user would like to investigate. At that point, the vehicle has achieved some momentum from the user throwing it and an internal accelerometer would initiate a process to commence the powered propulsive phase of the mission.

**Figure 15. Hand Thrown Deployment Method**

Description	Pro	Con
No equipment required besides a person's arm and throwing capability - weight and additional cost are zero	X	
Ability to deploy the vehicle on any terrain without concern for grade or ground composition	X	
Initial direction is dictated by the thrower, which is less exact than GPS coordinates		X
Inability to calculate and recreate a throw		X
Reliability of the person throwing the vehicle exponentially increases possibility of human error		X
The possibility of a faulty main engine start could result in more work for the thrower to retrieve the vehicle if the main engine starts late and could cause serious injury to the thrower if the main engine starts prematurely		X

Table 13. Pros and Cons of Hand Thrown Deployability.

3.1.4.2 Single Fixed Rod

This design concept would utilize a fixed rod and platform attached to stable legs as the base for the deployment method. No additional impulse would be provided to the vehicle outside of its own propulsive element. This deployment system would utilize both a launch pad and the internal propulsive system of the vehicle. The vehicle would be attached to the fixed rod upright, as seen in Figure 16. All internal elements of the vehicle and payload would then be initialized by the user. At this point the user would ignite the propulsive element, either through a connection to the brain of the vehicle, or manually at the base of the vehicle. An example of what this deployment concept might look like is shown in Figure 16.



Figure 16. Single Fixed Rod Deployment Method²

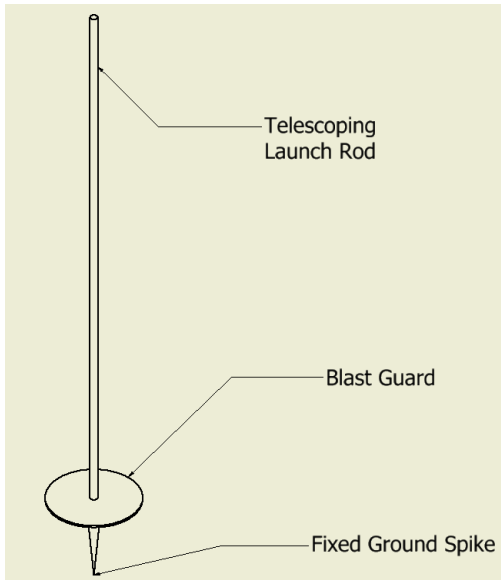


Figure 17. Drawing of Fixed Rod

Description	Pro	Con
Launch pad is stable and unlikely to be disrupted during launch	X	
Pad is structurally sound and reusable and therefore launches could be recreated to a high degree of accuracy if necessary	X	
Relatively inexpensive	X	
Launch pad is metal and therefore heavy		X
Incapable of adjusting to variable terrain		X

Table 14. Pros and Cons of Single Fixed Rod Deployability.

3.1.4.3 Single Variable Rod

This design concept would utilize a stable yet variable rod and platform attached to stable legs as the base for the deployment method. No additional impulse would be provided to the vehicle outside of it's own propulsive element. This deployment system would utilize both a launch pad and the internal propulsive system of the vehicle. The vehicle would be attached to the rod at whatever angle is desired by the user. An example photograph of one such angled installment can be seen in Fig. 19. All internal elements of the vehicle and payload would then be initialized by the user. At this point the user would ignite the propulsive element, either through a connection to the brain of the vehicle, or manually at the base of the vehicle. An example of what this deployment concept might look like is shown in Fig. 18.

**Figure 18. Single Variable Rod Deployment Method?**



Figure 19. Single Variable Rod Angled Deployment Method?

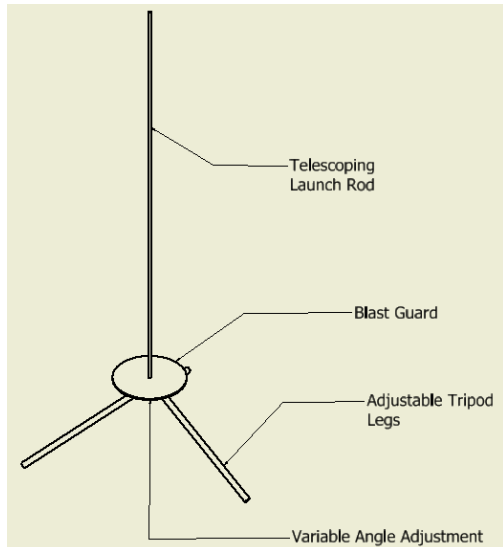


Figure 20. Drawing of Variable Launch Rod

Description	Pro	Con
Launch pad is stable and unlikely to be disrupted during launch	X	
Pad is structurally sound and reusable and therefore launches could be recreated to a high degree of accuracy if necessary	X	
Relatively inexpensive	X	
All mechanical elements are durable and do not depend on any electrical or hydraulic inputs, therefore reliability is high	X	
Mechanical elements are simple and probability of user error is low	X	
Capable of adjusting to variable terrain and incredibly sturdy for any rugged environments	X	
Variable launch angle allows for greater variability in possible range and altitude reached	X	
Launch pad is metal and therefore heavy		X

Table 15. Pros and Cons of Single Variable Rod Deployability.

3.1.4.4 Variable Rails with Hydraulic Launch Initiation

This design concept would utilize a variable rail design and platform attached to stable legs as the base for the deployment method. This design concept has the capability to introduce a secondary propulsive device, most likely hydraulic pistons, to provide extra impulse to the vehicle. This deployment system would utilize both a launch pad and the internal propulsive system of the vehicle. The vehicle would be attached to the rod at whatever angle is desired by the user. All internal elements of the vehicle and payload would then be initialized by the user. At this point, the user would initiate the hydraulic mechanism and then, after the vehicle has left the launch pad, ignite the propulsive element, using a built-in function dependent on an accelerometer readings within the nose of the vehicle. An example of what this deployment concept might look on a smaller scale like is shown in Figure 21.



Figure 21. Variable Rail with Piston Deployment Method?

Description	Pro	Con
Stable launch pad base	X	
Multiple launch rails for vehicle to sit on increases stability during launch and the first phases of flight	X	
Increased cost with addition of hydraulic element		X
Inability to launch on extreme terrain		X
Complex launch system increases weight, cost, and likelihood of user error or device malfunction and decreases reliability		X
Rail system is not collapsible and will not fit into size constraint		X

Table 16. Pros and Cons of Hydraulic and Multiple Rail Deployability.

3.1.5. Sensor Suite

3.1.5.1 Attitude Determination Subsystem

If the vehicle is to maintain stable flight, then it is essential the vehicle has an attitude determination system capable knowing the vehicle's precise attitude for use by the autopilot. The attitude determination system must be able to detect any rotation about the vehicles X, Y, and Z axis (roll, pitch, and yaw)⁷. Without this, the autopilot would be unable to accurately roll, pitch, or yaw at a given rate. The attitude determination must be able to decipher its orientation relative to the Earth. If the autopilot did not have this attribute it would still be able to roll, pitch, and yaw, but these rotations must be relative to some fixed coordinate or the vehicle will inevitably crash into the ground. Given the vehicle's attitude determination can now rotate and avoid a crash landing, the final variable necessary for stable flight is a heading. This allows the vehicle to determine the immediate direction in which it is flying. Table 17 lists the four sensor suites capable of accomplishing all three attitude determination criteria.

Number	Attitude Subsystem
1	3-Axis Gyroscope, 3-Axis Accelerometer, and Magnetometer
2	3-Axis Gyroscope, 3-Axis Accelerometer, and GPS
3	3-Axis Gyroscope, 3-Axis Accelerometer, and Infrared
4	3-GPS

Table 17. Four possible sensor suites able to determine attitude.

3-Axis Gyroscope, 3-Axis Accelerometer, and Magnetometer

The first possible attitude determination sensor suite incorporates one 3-axis gyroscope, one 3-axis accelerometer, and one magnetometer. The gyroscope provides data on the vehicles rotational speed about its own axes. This information may be interpreted by a PID controller and used to stabilize the vehicle during steady slight and maneuvers. The accelerometers are used to determine which direction is up, which direction is down, and what the current attitude is. The accelerometer does this by using the acceleration of gravity as a reference, but, because of this, the accelerometer may have trouble differentiating between the vehicle's acceleration and the Earth's acceleration. Finally, a magnetometer that controls the heading of the vehicle through magnetic interference may skew the magnetometer's readings. Figure 22 gives a graphical representation of the 3-axis gyroscope, 3-axis accelerometer, and magnetometer sensor subsystem and Table 18 lists various pros and cons of the subsystem.

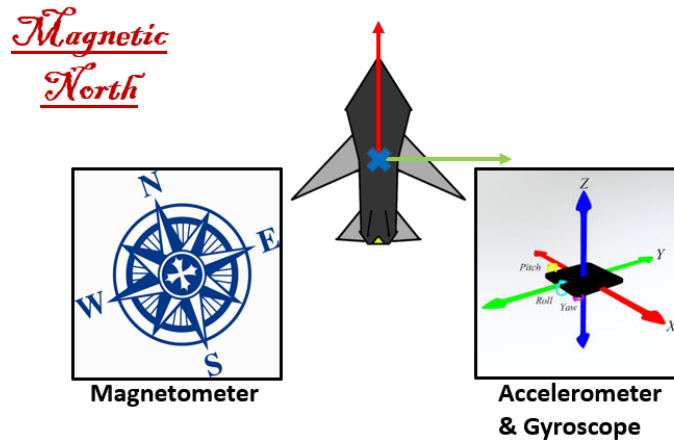


Figure 22. Diagram of 3-axis gyroscope, 3-axis accelerometer, and magnetometer sensor suite.

Description	Pro	Con
Provides rotational speed about roll, pitch, and yaw axis	X	
Can determine where is up, where is down, and current attitude	X	
Subject to magnetic field interference		X

Table 18. Pros and Cons of a 3-axis gyroscope, 3-axis accelerometer, and magnetometer attitude sensor suite.

3-Axis Gyroscope, 3-Axis Accelerometer, and GPS

The second possible attitude determination sensor suite utilizes a 3-axis gyroscope, 3-axis accelerometer, and GPS. The 3-axis gyroscope and 3-axis accelerometer function in the same method as the case above. Instead of using a magnetometer as a heading indicator, this method uses GPS. Though GPS only tracks position, GPS uses each past incremental position estimate to approximate the vehicle's heading. Due to GPS's slow update rate, this method works best for stable, slow flight. Figure 23 depicts the 3-axis gyroscope, 3-axis accelerometer, and GPS sensor subsystem and Table 19 lists pros and cons of this sensor suite.

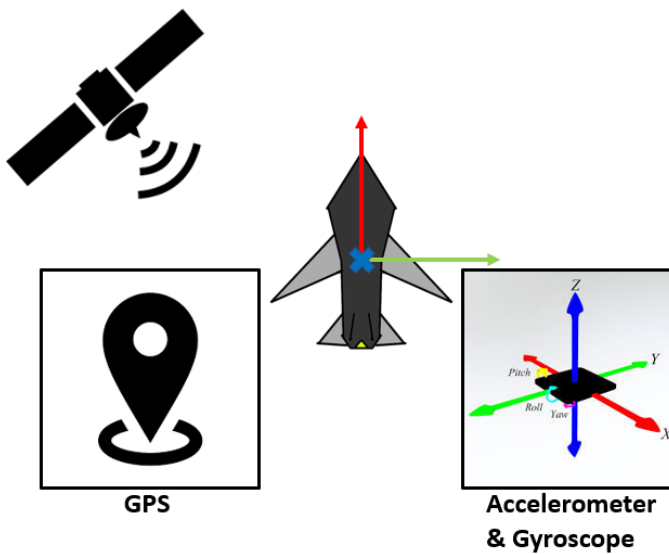


Figure 23. Diagram of 3-axis gyroscope, 3-axis accelerometer, and GPS sensor suite.

Description	Pro	Con
Provides rotational speed about roll, pitch, and yaw axis	X	
Can determine where is up, where is down, and current attitude	X	
GPS necessary for positional determination	X	
GPS has slow update rate		X
GPS subjected to short term heading errors		X

Table 19. Pros and Cons of the 3-axis gyroscope, 3-axis accelerometer, and GPS attitude sensor suite.

3-Axis Gyroscope, 3-Axis Accelerometer, and Infrared

The third possible attitude determination sensor suite implements a 3-axis gyroscope, 3-axis accelerometer, and an infrared horizon sensor. Again the 3-axis gyroscope and 3-axis accelerometer function in the same method as the previous two cases above. The infrared sensor functions by sensing a temperature difference between the Earth's surface and the sky⁷. Recently this method has become quite accurate and relatively inexpensive; however, any mountains, buildings, fires, haze, etc. will cause the infrared to produce faulty results. Figure 24 graphically presents the 3-axis gyroscope, 3-axis accelerometer, and infrared sensor subsystem and Table 20 lists pros and cons of the sensor suite.

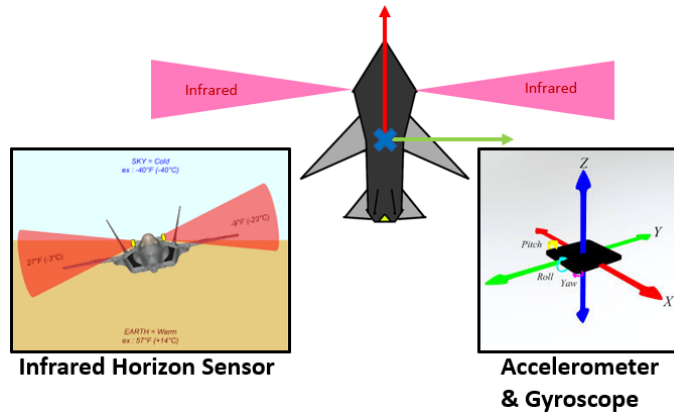


Figure 24. Diagram of 3-axis gyroscope, 3-axis accelerometer, and infrared sensor suite.

Description	Pro	Con
Provides rotational speed about roll, pitch, and yaw axis	X	
Can determine where is up, where is down, and current attitude	X	
Needs clear view of horizon		X
Environmental interference from haze, mountains, buildings, etc.		X

Table 20. Pros and Cons of the 3-axis gyroscope, 3-axis accelerometer, and infrared horizon attitude sensor suite.

3-GPS

The fourth possible attitude determination sensor suite consists of three GPS units located at strategic locations on the vehicle. Thinking of the vehicle as a plane represented by three points, the orientation of a plane may be found if the position of all three points are known. GPS coordinates located at three different locations on the vehicle would, hypothetically, allow for the vehicle's orientation to be determined. This works with larger vehicles but due to the size of the vehicle used in this project the positional error in GPS signal exceeds the actual size of the vehicle. Figure 25 displays the 3-GPS sensor subsystem and Table 21 lists the pros and cons of the sensor suites.

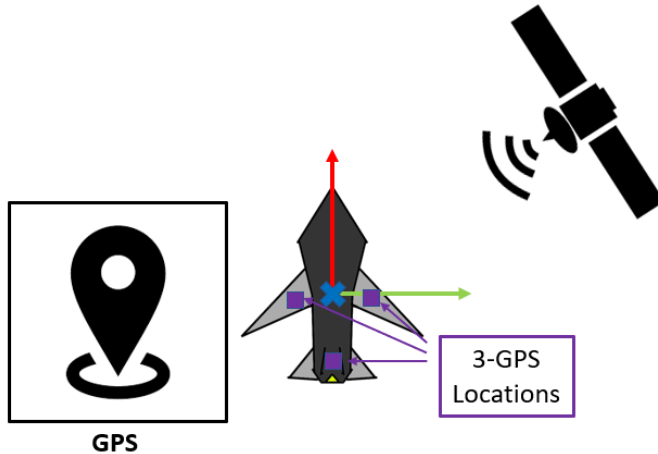


Figure 25. Diagram of 3-GPS sensor suite.

Description	Pro	Con
GPS necessary for positional determination	X	
Lack of accuracy for minute attitude adjustments		X
GPS has slow update rate		X
GPS subjected to short term heading errors		X

Table 21. Pros and Cons of the 3-GPS attitude sensor suite.

3.1.5.2 Position Determination

The attitude system alone is not enough to track the full trajectory of the vehicle. The vehicle's acceleration and rotation may be integrated; however, errors will creep into the mathematics over time. Since the purpose of this project is to precisely calculate the location of a target, this method is unacceptable. Instead GPS will be utilized to determine the position of the vehicle. This will significantly bound the positional error of the vehicle. GPS yields a particularly accurate lateral position; however, GPS's accuracy in the vertical direction is much more poor. Again the true position of the vehicle is very important to the end product so a trade study on vertical altitude sensors is necessary. Table 22 lists the three components this trade study is performed on.

Number	Method
1	Barometer
2	Sonar Proximity Sensor
3	Laser Proximity Sensor

Table 22.

Altimeter

The first method of determining the vertical altitude is an altimeter. An altimeter is the most common method used in drones. This is due to an altimeter's high level of accuracy relative to its cost (far cheaper than most alternatives). The accuracy of an altimeter is subject to the environment around it. An altimeter compares the sea level pressure to the pressure during flight to provide an altitude of the vehicle. Pressure fluctuations from inclement weather may cause these readings to be skewed. Table 23 lists the pros and cons of a barometer.

Description	Pro	Con
Only needs exposure to ambient pressure	X	
Cheap and easy to implement from COTS components	X	
Local sea level pressure must be known to determine AGL altitude		X
Prone to drift due to errors from reference pressure		X
Pressure varies with environmental changes such as wind		X

Table 23. Pros and Cons of the barometer sensor suite.

Sonar Proximity Sensor

The second method of calculating the altitude involves a sonar range finder located beneath the vehicle and pointing at the ground. The range finder emits a high frequency sound toward the ground which then bounces back and is received by the vehicle. The sonar proximity sensor measures the time taken to receive the signal and, since the speed of sound can be determined from temperature, is able to calculate the distance to the ground. Table 24 lists the pros and cons of the sonar proximity sensor suite.

Description	Pro	Con
Extremely accurate altitude reading	X	
Not affected by drift	X	
Range limited to several meters		X
Must be pointed toward the ground at all times		X
More complex than other COTS alternatives		X

Table 24. Pros and Cons of the sonar proximity sensor suite.

Laser Proximity Sensor

The third method of computing the altitude is by using a laser proximity sensor located beneath the vehicle and pointing at the ground. The laser proximity sensor projects a varying powered laser beam toward the ground which then bounces back and is received by the vehicle. The laser proximity sensor indirectly measures the time taken to receive the signal by observing the power frequency of the received beam and, since the speed of sound can be determined from temperature, is able to calculate the distance to the ground. Table 24 lists the pros and cons of the sonar proximity sensor suite.

Description	Pro	Con
Extremely accurate altitude reading	X	
Delivers speed of light altitude reading	X	
Must be pointed toward the surface at all times		X
More complex than other COTS alternatives		X

Table 25. Pros and Cons of the laser proximity sensor suite.

3.1.5.3 Autopilot Subsystem

One of the driving forces for the decision of what flight control board to choose for the RAPTR is what autopilot platforms it supports. For this project, only open source platforms are being considered mostly because closed source autopilots are thousands of dollars and an open source platform allows for more customization of the control system. The platforms being considered in this project (Table 26) are some of the more popular open source autopilot platforms because these will be the platforms that are compatible with the largest number of flight control boards.

Number	Autopilot Platform Options
1	Paparazzi
2	Ardupilot
3	PX4

Table 26. Four Potential Options for Autopilot Firmware

Paparazzi

The first autopilot platform being considered is Paparazzi UAV, the first real open source project for drone autopilot. This is the most technical of the platforms being considered, meaning that it will be more difficult to work with initially than the other platforms being considered but it will have the most features without having to change any source code.

Description	Pro	Con
Longest running open source autopilot being considered (2003)	X	
Can be written in C and Python	X	
Only runs on Linux and Mac OSX		X
Relatively difficult to obtain hardware		X

Table 27. Pros and Cons of the Paparazzi Autopilot Platform

Ardupilot

Ardupilot is one of the most popular open source autopilot platforms. This leads to it also having one of the best developer communities and forums to provide information and assistance. The ArduPilot platform being so popular also allows for it to be supported by most of the popular flight control boards so acquiring the hardware will be easy if the ArduPilot platform is used. This comes with the trade-off of the platform being created with hobbyists in mind so a much more advanced mission profile such as the RAPTR mission will require more editing of the source code.

Description	Pro	Con
Compatible with most easily available hardware	X	
Large developer community	X	
Any changes made to source code must be made public		X
Lacking in certain important mission control functions		X

Table 28. Pros and Cons of the ArduPilot Autopilot Platform

PX4

The PX4 autopilot platform is very similar to ArduPilot in many aspects such as out of the box features and supported hardware. One of the main distinguishing factors between the ArduPilot and PX4 platforms is the software licenses that they use. PX4 uses a BSD license while ArduPilot uses a GPL license. The license that PX4 uses allows for a user to make changes to the source code and keep those changes private if they so choose whereas any change that is made to the ArduPilot source code must be made public. This becomes important when the autopilot is being used for a private project that is being sold and the developer does not want to release the specifics of what they did.

Description	Pro	Con
Changes made to source code may be kept private	X	
Active community forum and slack channel	X	
Only runs on Linux and Mac OSX		X
Only major board supported is the PixHawk		X

Table 29. Pros and Cons of the PX4 Autopilot Platform

3.1.5.4 Imaging Subsystem

To satisfy the first functional requirement of being able to detect and identify targets of interest, RAPTR must be equipped with an imaging system that can provide data to the ground processing station. The detection, recognition, and identification (DRI) algorithms that will be employed by the image processing station require a certain image resolution to be able to perform these tasks, which limit the amount of options possible for the RAPTR imaging suite. Additionally, since the target of interest's location falls within an annulus of 2000-4000 feet, the imaging suite must be capable of finding the target within this region. The functional and derived requirements for imaging processing, as well as the overall problem statement and concept of operations, narrow down the potential design options to those listed in table 30.

Number	Imaging Sensor Options
1	Single Optical Camera
2	Multiple Optical Cameras
3	Optical Camera and Thermal Camera Combination
4	LIDAR Scanner

Table 30. Four Potential Options for Target Imaging

Single Optical Camera The first option considered is a single standard digital camera integrated within the vehicle. Table 31 lists the pros and cons of taking this approach, while Fig. 26 shows how the imaging suite will work with only a single camera. The most prominent benefit of the single camera is that it will be the simplest to integrate into

the vehicle, and that there will be less data needing to be transmitted to the ground in real time. This approach lacks, however, in its ability to image a wide area on the ground for a given gimbal angle, which may require a predetermined sweeping motion of either the camera mount or the vehicle itself. Furthermore, the camera requires good visibility to be able to image the target, which may not always be available when in use.

Description	Pro	Con
Simple integration, data transmission, and image processing	X	
Cheapest option	X	
Limited Field of View		X
Requires good visibility conditions		X

Table 31. Pros and Cons of using a single optical camera for target imaging

As seen in Fig. 26, the single camera will be able to image an area of approximately 540x400 ft with a resolution of approximately 4208x3120 pixels. These values were determined based on the average resolution and field of view of commonly used drone cameras, as well as by the recommendation of the electrical engineering team for how much data can be transferred in real time to the ground station. The camera will image the ground over its field of view, and then send the image data back to the ground station for further processing.

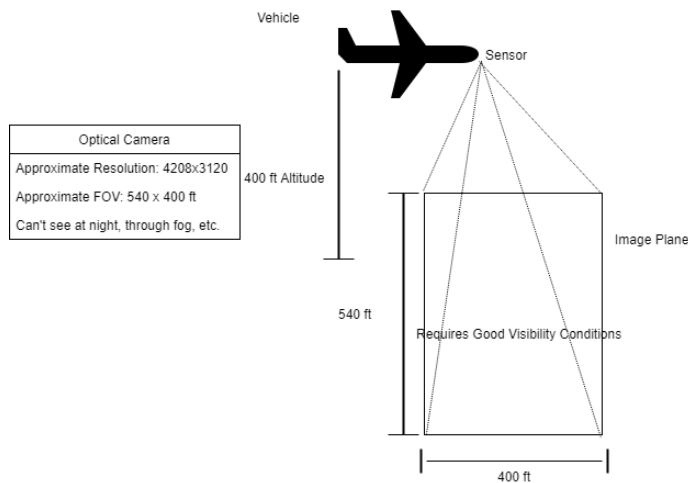


Figure 26. Diagram of a single camera imaging system

Multiple Optical Cameras Instead of limiting the imaging suite to a single digital camera, this approach considers utilizing multiple cameras at once. Table 32 lists the pros and cons to this approach, and Fig. 27 provides a diagram for how two cameras would be used in operation. this approach most notably will have a wider field of view, which will increase the ease of detecting the target of interest given its annulus of uncertainty. The primary detriment to this approach lies in the added complexity of its integration into the vehicle, as well as in the increase in data sent to the ground station.

Description	Pro	Con
Wider Field of View & higher resolution	X	
Removes need for controlled camera pointing	X	
More difficult integration, data transmission, & image processing		X
Still Requires good visibility conditions		X

Table 32. Pros and Cons of using multiple optical cameras for target imaging

The operation of a multiple camera imaging suite is very similar to that of the single camera, and only differs in the increased FOV width due to different camera gimbaling. If the cameras have no FOV overlap, then the FOV will

be effectively doubled from that of the single camera.

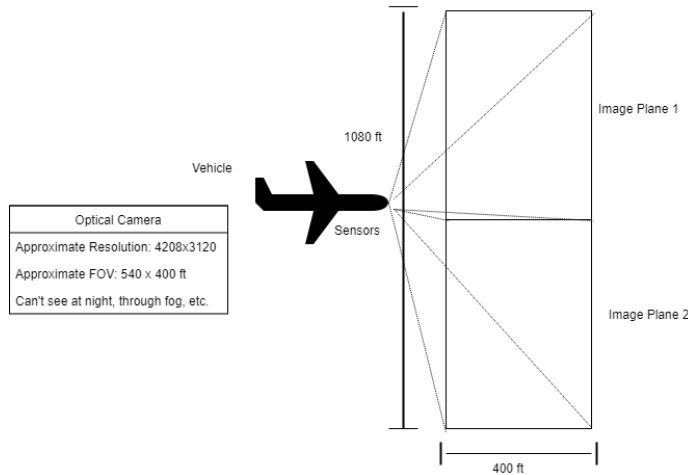


Figure 27. Diagram of a two camera imaging system

Optical and Thermal Camera Combination The next approach considers adding a thermal sensor to go along with the aforementioned digital cameras. Table 33 lists the pros and cons to this approach, and figure 28 shows a diagram of how this setup would function. A thermal sensor will be integrated along with the digital camera, where the two fields of view will overlap. The pros to this approach almost singularly lie in the thermal sensor's ability to image through low visibility, while the cons lie in the added complexity of integration as well as the cost for a thermal sensor.

Description	Pro	Con
Can image targets through poor visibility conditions	X	
Can design sensor positioning to optimize probability of target detection	X	
Very complex integration, data transmission, and image processing		X
Thermal sensors are expensive and have comparably poor resolution		X

Table 33. Pros and Cons of using an optical camera and thermal sensor combination

In Fig. 28, the camera and digital sensor have overlapping fields of view, since the ground processing can be done in a way that cross references the data from both the camera and the thermal sensor. The camera and thermal sensor will have to be integrated in such a way which accomplishes this overlap.

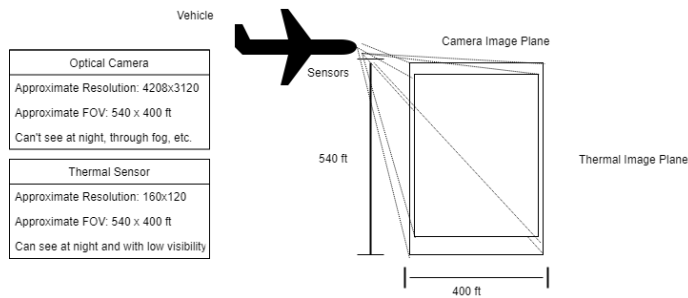


Figure 28. Diagram of camera and thermal sensor combo

LIDAR The final design option for an imaging suite is using a LIDAR 3D scanner which scans the ground as the vehicle passes overhead. The pros and cons of this approach are listed in Table 34, while the diagram for operation is given as Fig. 29. The LIDAR sensor is unique in that it measures distances instead of taking light or thermal data, which has benefits in the ability to build a 3D model of any objects that it is capable of scanning. This is the most

prominent benefit to the approach, however there are a few very notable cons. Mostly, a LIDAR scanner would be very expensive for the range that it would be operating in, and it would be very heavy in comparison to the vehicle.

Description	Pro	Con
Can generate 3D point cloud for Optimal target recognition	X	
Simple & accurate target location, can image through trees and low visibility	X	
Extremely expensive		X
Difficult integration due to size & scanning requirements		X
More difficult target identification without camera		X

Table 34. Pros and Cons of using a LIDAR scanner for imaging the target

As the LIDAR system operates, it continuously scans an area while sending back point cloud data to the ground station for processing. This width depends on the capabilities of the scanner device, however it would ideally be similar to the horizontal field of view of the two camera system shown in figure 27. This scanning will continue for the duration of the flight of the vehicle, and the LIDAR will be capable of imaging through poor visibility as well as through trees and other potential objects.

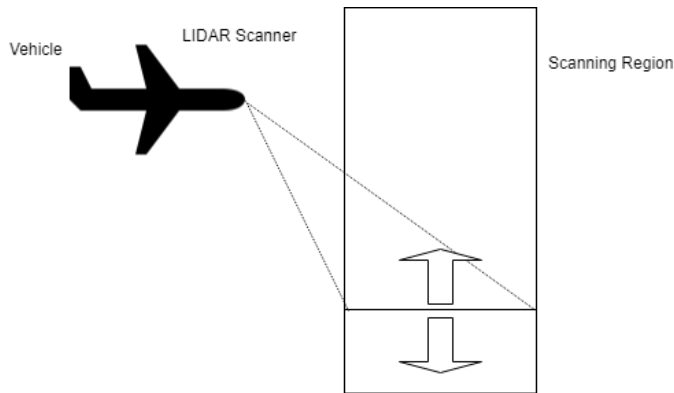


Figure 29. Diagram of a LIDAR imaging system

3.2. Trade Studies

3.2.1. Vehicle

3.2.1.1 Trade Metrics and Trade Study

Metric	Weight	Description
Ability to Meet Requirements	25%	The vehicle must be able to meet all preset functional and derived requirements in order to achieve mission success.
Manufacturability	20%	The vehicle must be able to be manufactured in approximately three months using the resources available through the University of Colorado.
Performance	20%	The vehicle will have to achieve a high airspeed to get to the target area quickly. Additionally, it must be controllable, stable, and able to deliver the payload in multiple different conditions.
Reliability	15%	The vehicle must not get broken during storage, transportation, or deployment. The propulsion system must also function properly when needed.
Level of Expertise Required	10%	The vehicle and its operating procedure must be able to be quickly understood by people with ranging levels of life experience and formal education.
Cost	10%	The cost of the vehicle must be kept to a minimum since the total budget for the aerospace portion of the project is \$ 5,000.

Table 35. Vehicle Metric Description

Metric	1	2	3	4	5
Ability to Meet Requirements	Able to meet only 1 - 2 functional requirements and very few of their derived requirements	Able to meet three of the functional requirements and some of their derived requirements	Able to meet four functional requirements and most of their derived requirements	Able to meet five functional requirements and almost all derived requirements	Able to meet all functional and all derived requirements
Manufacturability	80 percent or more of the parts needed would be custom ordered	60 - 79 percent of the parts needed would be custom ordered	40 - 59 percent of the parts needed would be custom ordered	20 - 39 percent of the parts needed would be custom ordered	0 - 19 percent of the parts needed would be custom ordered
Performance	Not able to meet minimum horizontal speed requirement or rate of climb requirement	Able to meet rate of climb requirement, but not horizontal speed requirement	Able to meet horizontal speed requirement while coming within 10 ft/s of rate of climb requirement	Able to meet both horizontal speed and rate of climb requirements on a clear, low-wind day	Able to meet both horizontal speed and rate of climb requirements in any condition.
Reliability	Rarely ever (< 25 percent of the time) works correctly, almost no durability	Works correctly 26 - 50 percent of the time in a controlled environment, not very durable	Works correctly 51 - 75 percent of the time in a controlled environment, semi-durable	Works correctly 76 - 100 percent of the time in controlled environment, durable	Works correctly 76 - 100 percent of the time in almost any open-air environment, very durable
Level of Expertise Required	Can only be operated by developers or college graduate level researchers	Could only be operated by trained specialist	Could only be operated by high school educated adults	Could be easily operated by most teenagers	Could possibly be operated by a small child
Cost	\$2500+	\$2499 - \$2000	\$1999 - \$1500	\$1499 - \$1000	Less than \$999

Table 36. Vehicle Metric Point Assignment

	Rocket Powered Glider	Electric Aircraft	Traditional Rocket	Quad-Copter
Meets Requirements (25%)	5	5	3	3
Manufacturability (20%)	4	4	5	4
Performance (20%)	5	4	2	2
Reliability (15%)	5	3	4	4
Level of Expertise (10%)	3	4	4	4
Cost (10%)	5	4	5	3
Final Score	4.6	4.1	3.65	3.25

Table 37. Vehicle Trade Table

3.2.1.2 Vehicle Trade Discussion

The metrics and the rubric used for the vehicle design trade study are shown above in Tables 35 and 36 respectively. The final results of the trade study are summarized in Table 37.

The rocket glider scored very well in all of its metrics except the level of expertise needed. This system likely needs someone with at least high school education to successfully be operated. Not only because of the danger associated with rockets, but also because the user will be needed to correctly set up the launch and possibly enter initial flight parameters (heading, wind, etc.) into the ground station. Other than that the combination of rocket and glider seems to combine the best traits of the rocket and RC plane into one. The rocket gets rid of the need for fragile propellers and extra batteries, and the glider control surfaces get rid of the lack of control one would have with a traditional rocket. Also, the cost of solid rocket motors is relatively low so multiple test flights may be a possibility later on. All in all, the rocket powered glider takes the best traits from the other vehicle options and combines them to suit the mission objectives almost perfectly.

Like the rocket powered glider, an electric aircraft will be able to fulfill all functional and derived requirements of the project. The electric aircraft also scores high in the manufacturability category. This is because of the large number of off the shelf products that are available specifically designed for electric aircraft. Moving on to Performance, the electric aircraft scores well here. There are examples of electric aircraft that achieve the required speed for this project, but the motors and batteries required to support them are heavy. This extra weight takes away from the payload capacity causing this vehicle to not get full points here. The electric aircraft struggles when it comes to reliability. This is for two reasons. The first is that this vehicle depends on fragile propellers which could be easily broken during storage or handling of the vehicle. The second is the number of electrical connections needed and the need for a fully charged battery. Both of these elements add potential failure points to the vehicle system. Electric aircraft are also easy to operate and can be built for a relatively low cost. For these reasons, this vehicle scores well in the level of expertise and cost categories. Overall, this vehicle design could perform the mission, but it does have draw backs, specifically with reliability and performance.

The traditional rocket design falls short. Since the rocket is designed to go straight up and then straight down at a high rate of speed, it is not able to meet some of the project requirements. The rocket gets full marks for manufacturability, however. This is because there are many rockets designed to carry a payload that can be bought off the shelf. The rocket scores poorly in the performance category. This is because it is designed to go straight up, but for this project a large lateral distance is required as well. Also, most rockets are designed to be spin stabilized. This would make it next to impossible for the payload to image the target area. Another benefit of the rocket is its reliability. Since solid rocket motors have no moving parts they are extremely reliable. Rockets are also relatively easy to operate, but some care must be taken with the engines since they can be dangerous. Finally, these rockets are inexpensive since there are not many parts that make them up. The traditional rocket design has many benefits; however, its shortcomings in the performance and meets requirements section make it a poor choice for the intended mission of this project.

The quadcopter is one of the better performing vehicles that can be purchased off the shelf, specifically with regards to aerial imagery. However, these quadcopters are limited by the limiting factor of all rotor driven aerial vehicles in that they usually have a slow horizontal speed. The high end quadcopters researched, such as the DJI Phantom 4, have a top lateral speed of about 65.61 ft/s which is well under the 100 ft/s requirement.⁷ Top racing drone setups can achieve speeds upwards of 240 ft/s, but with speed the cost and amount of custom parts needed goes way up.⁷ Also, not only do the rotors and intricate parts on quadcopters make them more difficult to manufacture, they mean more complex controls and less durability. In conclusion, the types of quadcopters that came close to the horizontal speed requirements already cost an upwards of \$1500, and to modify them to fit a payload could cost thousands of dollars more. The quadcopter is still a great UAV for imaging small areas and getting around obstacles, but sadly it can only travel so far so fast. That, along with other factors like poor durability, is why it ended up doing the worst out of any vehicle option on the trade study.

3.2.2. Payload Mounting

3.2.2.1 Trade Metrics and Trade Study

Metric	Weight	Description
Mechanical Complexity	25%	The payload mounting system's ultimate choice may introduce varying degrees of mechanical difficulty. As the mechanical system may be required to complete the payload's mission of successfully capturing images of the target, the mechanical system carries substantial weight.
Software Complexity	25%	Similar to the mechanical system, the needs of the payload mounting system will also increase the complexity of on-board processing actions, such as search and pointing functionality independent of the vehicle body.
Cost	10%	The price of components for each mounting alternative will be a critical piece of the mission design, as the entire aerospace project segment must be kept below the \$5,000 budget
Weight	20%	The weight of the payload mounting assembly, in conjunction with the weight of the payload, will have major impacts on the dynamics and pointing ability of the vehicle itself
Power	20%	All other payload systems will be useless without any power to drive their operations. Therefore, the power system will have to be adjusted uniquely for each mounting alternative.

Table 38. Payload Mounting Metric Description

Metric	1	2	3	4	5
Mechanical Complexity	5+ months	4 months	3 months	2 months	1 month
Software Complexity	5+ months	4 months	3 months	2 months	1 month/NA
Cost	\$1000+	\$750	\$500	\$250	\$100
Weight	4+ lbs	3 lbs	2 lbs	1 lb	Negligible mass
Power	20% draw	15% draw	10% draw	5% total draw	Negligible/No draw

Table 39. Payload Mounting Metric Point Assignment

	Internal Aperture	External Dome	Deployable Payload
Mechanical (25%)	5	2	3
Software (25%)	3	1	4
Cost (10%)	5	3	4
Weight (20%)	5	2	4
Power (20%)	5	2	3
Final Score	4.5	1.85	3.55

Table 40. Payload Mounting Trade Table

3.2.2.2 Payload Mounting Trade Discussion

The trade study of the alternatives for payload mounting may be viewed in Table 40, with descriptions of the metrics and their associated scores found in Tables 38 and 39, respectively.

The first payload mounting alternative to be considered was an internal aperture set within the nosecone of the vehicle, with a transparent material allowing the payload sight of the ground for imaging. The internal aperture is

mechanically simple, involving a fixed field-of-view (FoV) relative to the vehicle and no moving parts within the vehicle. However, the internal aperture necessitates coordination with the vehicle to correct the payload's field-of-view, should error be introduced as the system. As such, the software would be more complex with this alternative, requiring communication between the vehicle and payload to allow control surface adjustments as needed. The vehicle may also need to drastically adjust its flight path to make the FoV of the payload include the target, further increasing the software complexity. The cost of an internal aperture is trivial, requiring only a small, transparent section of material on the underside of the nosecone for the payload to "see" through and any small materials needed to secure the payload within the vehicle. A material as simple as acrylic plastic is available in thin variants of 8 square feet for only \$15 from vendors⁷. Similarly, the internal aperture does not require much excess weight. The materials involved in creating the window and internal mounts are minimal. This includes transparent materials that are relatively light weight and any screws, bolts, or otherwise composed of various metal alloys. Power is an important consideration in any system, particularly for a vehicle with a power intensive payload and transmitter. As such, the internal aperture mounting will require no power to function. Any additional power resulting from this alternative would be in the form of control surface actuation and communication between the vehicle and the payload. As a whole, this mounting option is economical in all aspects, albeit with the potential for heavy software and vehicle adjustments to ensure payload success.

The second payload mounting alternative was an external dome featuring azimuth and elevation axis rotations. This solution was created to maximize the pointing capability of the payload, independent of the vehicle. Unfortunately, this introduces extreme degrees of difficulty and risk in both the mechanical and software aspects of the mounting system. Mechanically, a two-axis rotating dome carries an immense amount of risk. If one axis of rotation should fail, or the vehicle fly too far before the gears can adjust to the targets location relative to the vehicle, then the vehicle will have failed to deliver the payload to its objective. Ensuring that the mechanical system works reliably would involve much assembly and testing. Likewise, the software aspect of the mounting system would have to include a searching functionality to locate the target in the case of a non-nominal deployment and vehicle trajectory. This would be greatly complex, and possibly beyond the scope of the year's work in ASEN 4018. Compounded with the interplay of the software and mechanical system, both may be declared to be nonviable within the scope of the project. This alternative would also cost much more than the other two options, as the materials and components required to create two-axis rotation as well as an external, mounted dome would likely require enough materials for several iterations. The increased machinery and materials would also drive up the weight of the vehicle at the location of the payload mount, affecting the dynamics of the vehicle to a greater degree than the other alternatives. The required power to actuate the payload along two axes, particularly if a "target search" function is necessary, has the potential to be immensely draining to the power system. This is undesirable, as the payload will also need a great deal of power to successfully transmit the data and communicate with the vehicle. Overall, this alternative is sub-optimal, adding complexity and unsustainable risk to the project, while accounting for potentially large issues such as vehicle flight path deviations.

The third payload mounting alternative was a mid-body, deployable payload by way of bay doors built into the vehicle. The bay doors and deployment mechanism create mechanical failure points. While not as risky as the dome option, the testing of the door operation in conjunction with the deployment mechanism of the payload would require many iterations and a long time period to ensure proper and consistent performance. The actuators to open the door would also require custom or ordered mechanical components that must be well understood to ensure proper performance. The software involved with the bay door/deployment coordination would also require intensive work. Additionally, this alternative requires the vehicle to correct its flight path following deployment to be near where the target is thought to be. This ensures the highest possible chance of payload success, at the cost of software complexity. The cost of this mounting alternative lies between the other two. While one or two actuators would be necessary for the bay door and deployment mechanism, each would also have to be less complicated than the dome case. Additionally, the material for the bay door would already exist as a part of the vehicle, reducing the demand for purchasing raw materials. This joint use of material would also help reduce the weight of the mounting system relative to the vehicle, and would shift the center of mass more towards the middle of the vehicle body. However, the mechanisms would still weigh more than the aperture alternative. Finally, the power draw of this mounting mechanism would be slightly improved over the dome, while still being more demanding than the aperture. The bay doors would have to be powered enough to open at least once, and likely close in order to not adversely affect vehicle aerodynamics for long. As such, this power cost must be included as a significant draw in power system design. This alternative features preferable options over the dome, but also potentially creates problems for the payload's imaging capability after it separates from the vehicle.

3.2.3. Landing Methods

3.2.3.1 Trade Metrics and Trade Study

Metric	Weight	Description
Cost	30%	The cost of any landing system implemented in the project is critical, as it consumes resources that could be more effectively spent elsewhere in the design and testing process. As the landing is of lesser importance than other areas of the mission, it is important that the systems implemented are a minimal resource drain.
Weight	20%	Similar to the reasoning behind the cost metric, the weight of the landing system must be kept as low as possible to minimize the additional development that is required to launch heavier vehicles.
Control/Re-usability	30%	The purpose of the landing system is to, ideally, allow for the safe recovery and ultimate reuse of the vehicle. A vehicle that lands with severe damage holds little advantage over a vehicle that simply disappears once the images have been transmitted since the recovery of a crippled vehicle provides nothing of value.
Complexity	20%	Because the landing of the vehicle is not the primary purpose of the mission, having a simple and easy to implement landing system is important because it frees up resources to be used in other mission critical areas. Less complex systems with lower failure rates are desired.

Table 41. Landing Method Metric Description

Metric	1	2	3	4	5
Cost	\$700+	\$500-699	\$300-499	\$100-299	\$100 or less
Weight	4+ lbs	3-4 lbs	2-3 lbs	1-2 lbs	1 lb or less
Control/Re-usability	Vehicle destroyed, no control over final location	Probable damage, minimal control over location	Possible damage, moderate location control	Unlikely damage, good location control	No damage, precise location control
Complexity	More than 2 months	1-2 months	2-4 weeks	1-2 weeks	Less than 1 week

Table 42. Landing Method Metric Point Assignment

	Deployable Parachute	Belly Landing	Landing Gear	Crash Landing
Cost (30%)	3	4	2	5
Weight (20%)	4	5	2	5
Control/Re-usability (30%)	3	4	5	1
Complexity (20%)	5	3	2	5
Final Score	3.7	4.0	2.9	3.8

Table 43. Trade Table for Landing Methods

3.2.3.2 Landing Method Trade Discussion

The trade study of the options for Landing Methods may be viewed in Table 43, with descriptions of the metrics themselves found in Table 41.

The simplest option for the landing method, and the baseline to which all other options were compared, was the crash landing. The reason this makes a good baseline is because it has the lowest complexity of any possible option,

since a crash landing doesn't require any additional control or components to implement. Because of this, the crash landing also scores high marks in both Cost and Weight. Since there are no added components, the cost and weight effects of a crash landing are precisely zero. Where the crash landing falls short, however, is in the Control and Re-usability category. A crash landing is, by definition, an uncontrolled landing. The operator would have no ability to determine where it would land, how it would land, or whether or not it would be re-usable after the fact.

Beyond the baseline of a crash landing, the first method to ensure the safe recovery of the vehicle that was considered is the use of a deployable parachute. Due to their widespread use in model rocketry, the cost of a deployable parachute isn't excessively expensive but it still represents a somewhat significant cost. A 36 inch chute with a 10 pound capacity costs in the neighborhood of \$100, while a 60 inch chute with a 20 pound carrying capacity would cost \$200. If the vehicle and payload are heavy enough, however, an 84 inch parachute with the capacity for 40 pounds would cost \$300. The weight of the parachute is one of its strengths, however, as even the large 84 inch parachute comes to only approximately 18 ounces in added weight. For control and re-usability, the parachute represents a large improvement over the crash landing due to the fact that it doesn't destroy the plane. What it lacks, however, is control over where the vehicle lands (due to winds) in addition to the fact that the vehicle or the parachute itself could become stuck or still be damaged during its descent. The complexity of the parachute is anything but complex, however, since off the shelf parachute kits are readily available. This means a minimum of development time would need to be devoted to this landing method if chosen.

Another option under consideration was to emulate modern aircraft, including gliders, by attaching a landing gear to the vehicle. This has the advantage of providing the most control and re-usability to the vehicle due to the nature of the landing gear. A gliding descent with wheels for landing would provide the most precise control over landing location and provide the least risk for damage due to the fact that no portion of the vehicle itself, besides the wheels, would come into contact with the ground. Unfortunately, the rest of the attributes were not as optimal on the landing gear option. The cost of a landing gear is the most prohibitive of all the options, in large part due to the complexity required. Since few landing gear kits capable of sustaining the vehicle's weight are available on the open market, a fair amount of the parts would need to be custom fabricated - driving up the cost and the time to complete it. In addition, the complexity of controls required to actually successfully land the vehicle would be no small task, with much of difficulty coming from attempting to keep the craft stable and upright upon touchdown. The final area where the landing gear loses points is its weight, as it is by far the heaviest of all the available options.

The final option presented is that of making a belly landing with the plane. This was proposed as an attempt to shore up the weaknesses offered by both the parachute and landing gear options by combining the best of each. The cost of belly landings are low, since it would simply require a tough skidplate to be added to the belly and abrasion resistant materials placed on any other surface that could come into contact with the ground. Because lightweight materials such as Nylon and other plastics may be used for this purpose the overall weight of the system is another positive, surpassing even the parachute's weight rating. In terms of control and re-usability, belly landing loses some points for having the potential of vehicle damage, simply due to uneven terrain or rocks. However, the control of this method is nearly as high as that of the landing gear landing. The biggest downfall of the belly landing, however, is the complexity. This primarily comes from the requirement that the vehicle would need to glide towards the ground in a controlled fashion at a shallow angle, increasing the difficulty in tuning the controls. It doesn't require the same complexity as the landing gear option though, since once it touches down and begins to slide there is no need to maintain control all the way up to the stop.

3.2.4. Deployment Method

Metric	Weight	Description
Stability and Accuracy	35%	Project success is dependent on the vehicle reaching a lateral distance from the user of 2000 feet and an altitude of 400 feet above the user. For these success criteria to be met the deployment method needs to provide the launch vehicle the capability to reach this distance. This capability can be achieved through the stability of the launch pad and the accuracy of the angle at which the launch vehicle is launched. The stability of the deployment method is also dependent on the terrain the user is launching the vehicle from and stability is being defined to meet the requirement for the vehicle to be deployable from terrain with a 10% grade.
Weight and Mobility	25%	An element of project success is the mobility of the entire RAPTR system, including the deployment method of the vehicle. The deployment method could easily become the largest and heaviest element of RAPTR and therefore must be chosen carefully to minimize weight and volume to allow a user of average size and strength to carry it.
Durability	20%	The deployment method must be able to support multiple uses of RAPTR and therefore needs to be durable. This is an important element of the deployment method choice because it will determine how feasible each design option is for a long project life.
User Compatibility	10%	For the project to succeed the user needs to interface with both the ground station and the vehicle. The deployment method needs to be chosen with a user of average intelligence in mind to ensure that it will be functional in any situation.
Cost	10%	Cost is a determining factor in any engineering project. As the success of the vehicle is dependent on being properly launched the cost metric has a lower weight than stability and accuracy, but the financial importance still needs to be taken into account.

Table 44. Deployment Method Metric Description

Metric	1	2	3	4	5
Stability and Accuracy	Unable to launch the vehicle accurately on command and unable to launch from any sort of variable terrain.	Able to launch the vehicle on command to a low degree of accuracy and unable to launch from terrain with a grade over 1%.	Able to launch the vehicle on command to a low degree of accuracy and unable to launch from terrain with a grade over 5%.	Able to launch the vehicle on command to a high degree of accuracy and unable to launch from terrain with a grade over 5%.	Able to launch the vehicle on command to a very high degree of accuracy and able to launch from terrain with a grade of 10%.
Weight and Mobility	Weighs more than 25 pounds and has a high likelihood of breaking during transport	Weighs more than 20 pounds and has a high likelihood of breaking during transport	Weighs 15-20 pounds and has a low likelihood of breaking during transport	Weighs 10-14.9 pounds and has a low likelihood of breaking during transport	Weighs less than 10 pounds and has a very low likelihood of breaking during transport
Durability	Unable to provide a successful launch more than once between transportation.	Unable to survive ground transportation over five miles and launch reliably.	Able to survive ground transportation over five miles and launch reliably with some adjustments.	Able to survive ground transportation over 10 miles and launch reliably with minimal adjustments.	Able to survive ground transportation over 20 miles and launch reliably with minimal adjustments.
User Compatibility	User is unable to use the deployment method without specific training lasting longer than 2 hours.	User feels uncomfortable using the deployment method without specific training lasting longer than 2 hours.	User feels uncomfortable using the deployment method without specific training lasting longer than 1 hour.	User is comfortable with the deployment method with some specific training.	User is comfortable with the deployment method with no specific training.
Cost	\$1000+	\$800 - \$999	\$600 - \$799	\$400 - \$599	Less than \$400

Table 45. Deployment Method Metric Point Assignment

	Hand Thrown	Single Fixed Rod	Single Variable Rod	Variable Rails with Hydraulic Launch Initiation
Stability and Accuracy (35%)	1	3	5	4
Weight and Mobility (25%)	5	4	3	1
Durability (20%)	5	4	4	2
User Compatibility (10%)	5	4	4	1
Cost (10%)	5	5	4	3
Final Score	3.60	3.75	4.10	2.45

Table 46. Trade Table for Deployment Alternatives

3.2.4.1 Deployment Method Trade Discussion

The criterion used for this trade study are outlined in Table 44, with the designation for each level of success explained in Table 45. The final trade study of the deployment method options is given in Table 46. The deployment method chosen was a single variable rod.

The options listed are given from the most simplistic to the most complicated. The simplest, most light weight and

cost efficient method to was throw the vehicle and have the propulsive element of the vehicle ignite after it has left the user's hand. While this method fulfills criterion for weight and cost, as no additional weight or cost is required for this deployment method, the accuracy of the throw left much to be desired. The user would throw the vehicle towards the general direction they believe the target to be and there would be no way to control the exact angle, force, and therefore initial trajectory of the vehicle. Because the metric for stability and accuracy is rated so highly for the project to meet its requirements, at 35%, this method was discarded.

The second method analyzed was the single fixed rod, which closely resembles the single variable rod method. The single fixed rod would provide more accuracy than the hand thrown method but provides less range of motion and therefore less accuracy than a single variable rod. While a variable rod has more components that need to be robust to survive transportation and is therefore heavier than a fixed rod, the increased accuracy of this method makes it superior to a single fixed rod.

The most complex method analyzed was a deployment method consisting of variable rails with hydraulic launch initiation. While this deployment method would supply increased thrust to vehicle, the increased weight, cost, and user training required for successful deployment made this option impractical.

The single variable rod scored a 5 in stability and accuracy because it allows a range of angles and initial projectile trajectories that neither the hand thrown or single fixed option offer. It would, theoretically, be able to successfully launch the vehicle on command to a very high degree of accuracy every time. The single variable rod would also have adjustable legs that make it suitable to launch from almost any terrain, including rugged terrain and terrain with a 10% grade. This method scored a 3 for weight and mobility, the lowest it scored in any metric, because it would most likely weigh between 15 and 20 pounds, based on existing models of this method, but because it is heavy and robust would most likely not break during any transport. The single variable rod deployment method scored a 4 in the durability matrix because there are several components that could break during transportation but due to the strength of the components (again in examples of this method) the likelihood of them breaking is very low and adjustments upon launch site arrival would be minimal. This method scored a 4 for both user compatibility and cost as well. The user would require minimal training to operate this deployment method and the method would, based upon research of existing models, cost somewhere between \$400 and \$500.

3.2.5. Sensor Suite

3.2.5.1 Attitude Determination

Metric	Weight	Description
Implementation Robustness	25%	The sensors shall be able to function in unison with the rest of the vehicle. This includes any sensor interference with the vehicle structure and electronics
Accuracy	35%	The attitude determination sensor suite shall be capable of accurately measuring the orientation of the vehicle. This includes the precision of any attitude information necessary for controlling the vehicle.
User Complexity	25%	The attitude determination sensor suite shall be mechanically and electrically simple enough to allow for user adjustments.
Cost	15%	The cost of the attitude determination suite shall be minimized but bounded to the quality of the sensors.

Table 47. Attitude Determination Metric Description

Metric	1	2	3	4	5
Implementation Robustness	All interference types	Structural Interference	Electrical interference	Environmental interference	Negligible interference
Error Subjectivity	< 10 degrees	< 7 degrees	< 5 degrees	< 3 degrees	< 1 degrees
User Complexity	Federal restrictions	Federal limitation	Closed source	Professional use only	College level
Cost	> \$100	< \$100	< \$50	< \$30	< \$10

Table 48. Attitude Determination Metric Point Assignment

	Accelerometer, Gyroscope, and Magnetometer	Accelerometer, Gyroscope, and GPS	Accelerometer, Gyroscope, and Infrared	3-GPS
Implementation Robustness	3	4	4	3
Error Subjectivity	5	3	5	1
User Complexity	5	2	3	2
Cost	4	2	3	1
Final Score	4.35	2.85	3.95	1.75

Table 49. Attitude Trade Table

Attitude Determination Trade Discussion

Table 47 lays out the metrics against which each attitude determination system is weighted. Each component of the attitude determination sensor suite must be able to sustain the turbulence of vehicle launch. In particular, the attitude determination subsystem must be able to function internally in the vehicle. Being inside the vehicle presents challenges as far as interference with the vehicle structure, other electronics, and the overall atmosphere at 400ft but is necessary to protect the electronics during flight. Accuracy is a substantial factor in attitude determination. If the attitude of the vehicle is not known then it will be nearly impossible to determine in which direction on board cameras are pointing. This will make the reverse engineering of a target's location extremely difficult. Due the time constraints of the project, sensor integration is also an essential trait and the attitude determination package should be made of reasonable complexity for a senior project. A significant amount of development and manufacturing costs will be necessary for other components of vehicle so cost also contributes to the sensor packages rating.

The first three attitude determination design options all incorporate a 3-axis accelerometer and a 3-axis gyroscope. This allows precise control over the vehicles movement in the X-axis and Y-axis but not the Z-axis (the heading of the vehicle). A magnetometer provides accurate heading readings but caution must be taken in regards to stray magnetic fields as other electronics around the magnetometer can skew its readings. Due to its wide use a magnetometer provides accurate heading readings for a relatively simplistic design at a low cost.

A GPS can also obtain a heading reading. Though it is less affected by surrounding electronics commercial GPS has an error of $\pm 6\text{ ft}$ and so is a poor choice for precise heading adjustments. GPS also takes significantly longer to update, this is not optimal when time is a driving constraint. GPS will add some superfluous complexity and cost to the attitude determination system.

An infrared proximity sensor is a promising alternative as it provides a median cost between the magnetometer and GPS. The major drawbacks of an infrared range finder occur in its implementation and added complexity. In order to provide proper readings the infrared sensor would have to be externally mounted, a contradiction to a robust design. Additionally, the infrared measurements are skewed by haze, mountains, and buildings. Since the vehicle is to be deployed in a variety of environments, infrared would not be the optimal choice.

The final option is three separate GPS units located on the vehicle. The primary deficit with this option is that the error of each GPS is larger than the vehicle itself. This setup would provide erroneous attitude data that is primarily useless and so is not a viable option for this small application.

Table 48 presents a grading breakdown and Table 49 lists the scores for each attitude sensor suite. At the bottom of Table 49 the weighted score of each attitude determination subsystem is listed. Despite electrical interference problems the 3-axis accelerometer, 3-axis gyroscope, and magnetometer sensor suite is the clear winner as it provides accurate data at a cheap cost and with user simplicity.

3.2.5.2 Altitude Determination

Metric	Weight	Description
Accuracy	30%	The vertical determination sensors shall be able to accurately provide altitude data of the vehicle.
Range	30%	The vertical determination subsystem must provide accurate readings at an altitude of 400ft.
Usability	25%	The components must be simple enough to be integrated electrically into the rest of the navigation system.
Cost	15%	The cost of the vertical determination suite shall be minimized but bounded to the quality of the sensors.

Table 50. Positional Determination Metric Description

Metric	1	2	3	4	5
Accuracy	>3 feet	<3 feet	<2 feet	<1 feet	<0.5 feet
Range (AGL)	<50 feet	<100 feet	<200 feet	<400 feet	>400 feet
Usability	Federally restricted	Federal limitation	Mission limiting	Developmental stage	College level
Cost	> \$100	< \$100	< \$50	< \$30	< \$10

Table 51. Attitude Determination Metric Point Assignment

	Barometer	Sonar Proximity Sensor	Laser Proximity Sensor
Accuracy	3	5	5
Range	5	1	5
Usability	5	3	3
Cost	4	4	1
Final Score	4.25	3	3.9

Table 52. Attitude Trade Table

Altitude Determination Trade Discussion

Not only is it critical to know the vehicle's precision attitude but also its position. Both the attitude and position of the vehicle must be known for RAPTR to be capable of returning the coordinates of a target to a user. GPS will be used to determine the vehicle's position in the vehicle's X and Y plane very accurately; however, GPS lacks precision in the vehicle's Z-axis (altitude above ground). To determine the sensor suite most fit for deciphering the vehicle's altitude Table 50 lays out key traits of the sensor suite. A trait to note, that has not been aforementioned, is range. The altitude determination sensor must be able to provide accurate altitude measurements to the user while at 400ft AGL.

Table 50 graphically lays out the metric criteria for the altitude determination sensor suite. The range requirement almost immediately disqualifies the sonar proximity sensor with a maximum range of around 30ft. The laser proximity provides a more accurate altitude reading at the same range as a barometer. The laser proximity sensor is cast aside due to a project constraint on the portability of RAPTR. Laser range finders, though accurate, are far more bulky and heavy than a barometer. Increasing the size of the sensors means increasing the size and capabilities of the vehicle which will cause a skyrocket in price. The barometer provides an altitude reading under 2ft which will be sufficient for RAPTR. Table 52 depicts the winner of the altitude determination suite as a barometer.

3.2.5.3 Autopilot Subsystem

Metric	Weight	Description
Hardware Support	10%	The hardware that is supported by the autopilot platform will affect the possibilities for what kind of peripherals and sensors can be used in the mission.
Mission Capabilities	25%	The autopilot must be very customizable as the RAPTR vehicle will be flying a very unique mission. The autopilot must be able to deal with unique scenarios
Extras	25%	Choosing an autopilot platform is difficult to do with standardized metrics so this metric will allow for any unique features to be accounted for in the trade study.
Development Resources	30%	The autopilot controls for this project must be developed rather quickly so having a plethora of available resources to help development is a must.
Development Learning Curve	10%	Similar to the development resources, it is important that the autopilot platform chosen is easy to learn so that development may start as soon as possible.

Table 53. Autopilot Metric Description

Metric	1	2	3	4	5
Hardware Support	Supports very few boards that are difficult to obtain	Supports very few boards that are easy to obtain	Supports a medium amount of boards that are somewhat difficult to obtain	Supports medium amount of difficult to obtain boards with some support of more popular boards	Supports most or all of the most popular boards
Mission Capabilities	Platform has minimal mission design capabilities	Platform has some mission design capabilities but is missing many advanced features	Platform supports some advanced mission design features	Platform has many advanced mission design capabilities	Platform has most advanced mission design capabilities that would be needed for this project
Extras	Extra features are not relevant to this project	Extra features are slightly relevant to this project	Extra features are somewhat relevant to this project	Extra features are relevant to this project	Extra features are very relevant to this project
Development Resources	Only resource is online documentation	Resources include documentation and some way to contact the platform's developers	Resources include documentation and some online community for the platform	Resources include documentation, an online community, and some way to contact the developers	Resources include documentation, one or more online communities, and several ways to easily contact developers
Ease of Use	Platform is extremely difficult to learn	Platform is somewhat difficult to learn	Platform can be learned in a timely fashion	Platform can be learned quickly	Platform can be learned very quickly

Table 54. Autopilot Platform Metric Point Assignment

	Ardupilot	PX4	Paparazzi
Hardware Support	5	2	4
Mission Capability	4	3	5
Extras	2	3	4
Development Resources	5	4	1
Development Learning Curve	4	5	2
Final Score	3.9	3.65	3.15

Table 55. Autopilot Trade Table

Autopilot Trade Discussion

The trade study of options for autopilot platform may be seen in Table 55, and a description of the metrics on which the options were compared may be found in Table 53 with a description of each grade in Table 54.

The first metric considered is also one of the easiest to determine, that being the hardware supported by each

autopilot platform. This metric is easy to determine because all autopilot platforms have a list of all supported hardware that is not hard to find and is much less subjective than the other metrics. Hardware support will be a limiting factor when it comes time to start buying flight control boards but most boards have similar capabilities so the most important differentiating factor is how difficult it will be to obtain the boards, which is why hardware support has the lowest weight of any metric. The ArduPilot platform easily has the most widespread support of any platform being considered, with the ArduPilot being one of the most popular autopilot platforms for hobbyists. Because of this the ArduPilot has support for most of the more popular flight control boards. The PX4, on the other hand, was created almost specifically for the Pixhawk micro-controller board. PX4 does have support for other boards but many of them are specifically for racing or for quadcopters so as far as this project is concerned, the Pixhawk is the only supported board. Thankfully, the Pixhawk is a very capable and easily available so this is not a large hindrance. The Paparazzi platform is somewhere in the middle with most of the supported hardware being more obscure and difficult to obtain boards but recently has begun supporting the Pixhawk board.

The next metric considered is mission capability. Mission capability is considered to be the possibilities of mission design that are available out of the box for the platform. Since this project is on a small time scale, it is preferable to spend as little time as possible building custom mission profiles so that all effort can be spent on the control system itself. The ArduPilot platform being very popular is very helpful because it has had many people iterate on the open source project, leading to a plethora of modules to help design a mission profile. The PX4 is very similar to ArduPilot but is missing certain capabilities that make it slightly less qualified than the ArduPilot. The Paparazzi is the most technical autopilot platform of the alternatives being considered and it was also created with fully automatic flight in mind. Because of this it has the most robust mission design capabilities of all the alternatives.

The extras metric allows for the asymmetric design of these autopilot platforms to be considered in the trades study. The most important extra to be considered for the ArduPilot platform is its ability to natively control a camera for stabilization and shutter control. The only problem is that this may not be relevant since the camera used for this project may not be compatible with the ArduPilot firmware but this extra should still be accounted for in the trade study. The extra being considered for the PX4 is the software license it uses. One of the major differences between the ArduPilot and PX4 platforms is the software licenses that each use. The license that ArduPilot uses requires that any changes made to the software be made public, while the software license of the PX4 allows for one to make changes to the source code and keep the changes private if they so choose. This is somewhat relevant as this project is being contracted by a private company so being able to own the IP for the autopilot code is important. The extra feature being considered for the Paparazzi platform is the fact that it is a platform primarily focused on fully automatic flight, as opposed to the other alternatives which are at least equally focused on manual flight. This allows for greater mission capabilities which have already been accounted for in this trade study but more importantly this means that, while the development resources are not that great, the developers of the Paparazzi platform will be very knowledgeable on fully automatic flights. This will allow for better help even if there is not as great of access to the development resources.

Development resources is a measure of how many resources there are to help troubleshoot problems and learn how to develop an autopilot system on a given platform. ArduPilot has fantastic resources available online with a user forum and several ways to contact the primary developers of the platform. Similarly, PX4 also has some fantastic resources with a user forum and a slack channel for contacting developers. Paparazzi, on the other hand, does not have great resources with the largest problem being the lack of a user forum. The only way to contact the developers is through a chat system on the Paparazzi wiki or github which is not ideal.

The final metric to be considered for the trade study on autopilot platforms is development learning curve. ArduPilot being very popular helps greatly with the learning curve but there is still plenty of advanced capabilities that may take some time to get acquainted with. The PX4 is very similar to the ArduPilot but with some simplifications that will make it easier to pick up. Paparazzi is the most technical of all the alternatives considered so it has the most difficult to learn development.

3.2.5.4 Imaging Subsystem

Metric	Weight	Description
Meeting Resolution Requirements	15%	The imaging system must meet the minimum resolution requirements for object detection, recognition, and identification from 400 ft altitude.
Size of Field of View	20%	With a larger width of field of view, there is a higher likelihood the target will be detected for a constant gimbal angle.
Ability to Image in Poor Visibility	25%	This measures the capability of the imaging suite to image in poor visibility and around objects.
Mechanical Complexity & Power Draw	15%	This measures the total complexity of integrating the imaging suite to the vehicle, as well as allocating power, data, and communication streams
Cost, weight, and data collected	25%	This measures the financial price, size and weight, and data sent for the imaging suite to function.

Table 56. Imaging Suite Metric Description

Metric	1	2	3	4	5
Resolution Requirements	Object won't be able to be detected	Object may be able to be detected with high contrast	Object can be easily detected even with non ideal conditions	Object can be recognized as a certain shape	Object can be identified as a certain kind of object, vehicle, etc.
Field of View	Fixed FOV and <200 ft width	Fixed FOV and <400 ft width	Fixed FOV and <600 ft width	Fixed FOV and <1000 ft width	Adjustable FOV
Poor Visibility Imaging	Object can't be detected in low lighting	Object can't be detected through smoke, fog, or other visual impediments	Object can't be detected at night	Object can be detected in all lightings and environmental conditions	Object can be detected through trees and other obstacles
Complexity & Power draw	Requires significant wiring and integration configurations	Requires complex mounting or has a large power draw	May require a slightly more complex integration or has a slightly larger power draw	Optimal in being either very mechanically simple or has a very low power draw	Is very simple to integrate and has a low power draw
Cost, Weight, and Data	Has a large cost, is very heavy, and requires a massive data stream to the ground station	Has significant drawbacks in two of cost, weight, and data stream	Has a drawback in either cost, weight, or data stream	No significant drawbacks, and excels in at least one metric	No significant drawbacks, and excels in at least two metrics

Table 57. Imaging Suite Metric Point Assignment

	Single Camera	Multiple Cameras	Camera and Thermal Sensor Together	LIDAR Scanner
Resolution	5	5	1	3
Field of View	3	4	3	5
Visibility	2	2	4	5
Complexity/Power	5	3	4	1
Cost/Weight/Data	5	3	4	1
Final Score	3.85	3.25	3.35	3.1

Table 58. Imaging Trade Table

Imaging trade Discussion When considering different imaging suite options, five different criteria were selected for weighing the merits of each option and the feasibility for implementation into the mission of RAPTR. These were: meeting the resolution requirements found in the derived requirements section, the width of the image plane field of view and its capability for adjustment, the visibility conditions required for imaging, the mechanical complexity and power draw needs, and the cost, weight, and amount of data being sent to the ground station. These were selected as the critical metrics of each design since they each relate either to the requirements of the mission, the total capability of the imaging suite, or the feasibility of integration.

The metrics were assigned a score based on either certain specific performance parameters, or based on a relative scale when compared to the options. The resolution, field of view, and visibility metrics fall into the former category, while the complexity/power and cost/weight/data metrics were scaled with the best option receiving a five and the worst option receiving a one. The weights assigned to each option are based on the importance to meeting the functional requirements of the mission. The resolution and complexity/power metrics had the lowest weight since both metrics could be easily improved with better hardware or with more time spent on accommodating the sensor. The poor visibility imaging and cost/weight/data metrics consequently have the highest weight, since RAPTR may frequently be used in these visibility conditions and cost/weight/data of the sensor can be prohibitive to the overall function of RAPTR as a whole. The field of view metric falls into a similar boat as the resolution and complexity/power metrics in that it can be more easily mitigated, however it carries a slightly higher weight since it can make the mission a failure if not properly accounted for.

The single camera baseline design scored the highest in the trade study, and it excelled particularly in the resolution, complexity/power, and cost/weight/data metrics. Since the camera is expected to have 4K resolution, it will be able to meet the highest level identification requirements without issue. Additionally, since the camera is the only image sensor, it will be the easiest to integrate with the vehicle as it won't have to battle with vision or power issues from another sensor. The Single camera will be the most cost effective by itself, will trivially have the lowest weight out of the options, and has the least amount of data to transmit to the ground station without any overlap from other sensors. The only two issues with the single camera approach are the minimal field of view offered and the necessity of good visibility conditions to image, where it ties for the worst option in both cases. To meet the resolution requirements, the single camera has a limited field of view, which may necessitate either camera gimbaling or a scanning motion from the vehicle to allow for the camera to spot the target. Additionally, since the camera is dependent on the lighting and environmental visibility conditions, it won't be able to meet the mission requirements if operated at night or if these condition are poor.

The second option considered was the multiple camera approach, which came in third place in the trade matrix. The only advantage to using multiple cameras instead of a single one is the expanded field of view, which increases the likelihood that a target would be detected over a wider search path. The resolution and visibility constraints will be equal to the single camera, however employing multiple cameras would result in impactful drawbacks in the complexity/power and cost/weight/data metrics. Utilizing multiple cameras would require more difficult mounting to make sure that there is no image plane overlap, and that each camera has a clear line of sight with no other cameras in the way. On top of this, the power, weight, cost, and data sent would all increase by a factor of how many cameras are added.

The third option of using a thermal sensor along with a digital camera finished in second place in the trade matrix, where it excels in visibility and struggles in image resolution. Common thermal sensors used in industry and within the project budget have a much lower resolution than digital cameras, wherein these resolutions are too low to be able to detect a target from 400 feet altitude. The field of view would be the same as the single camera, and the complexity/power and cost/weight/data metrics would all be better than using multiple cameras but not as ideal as

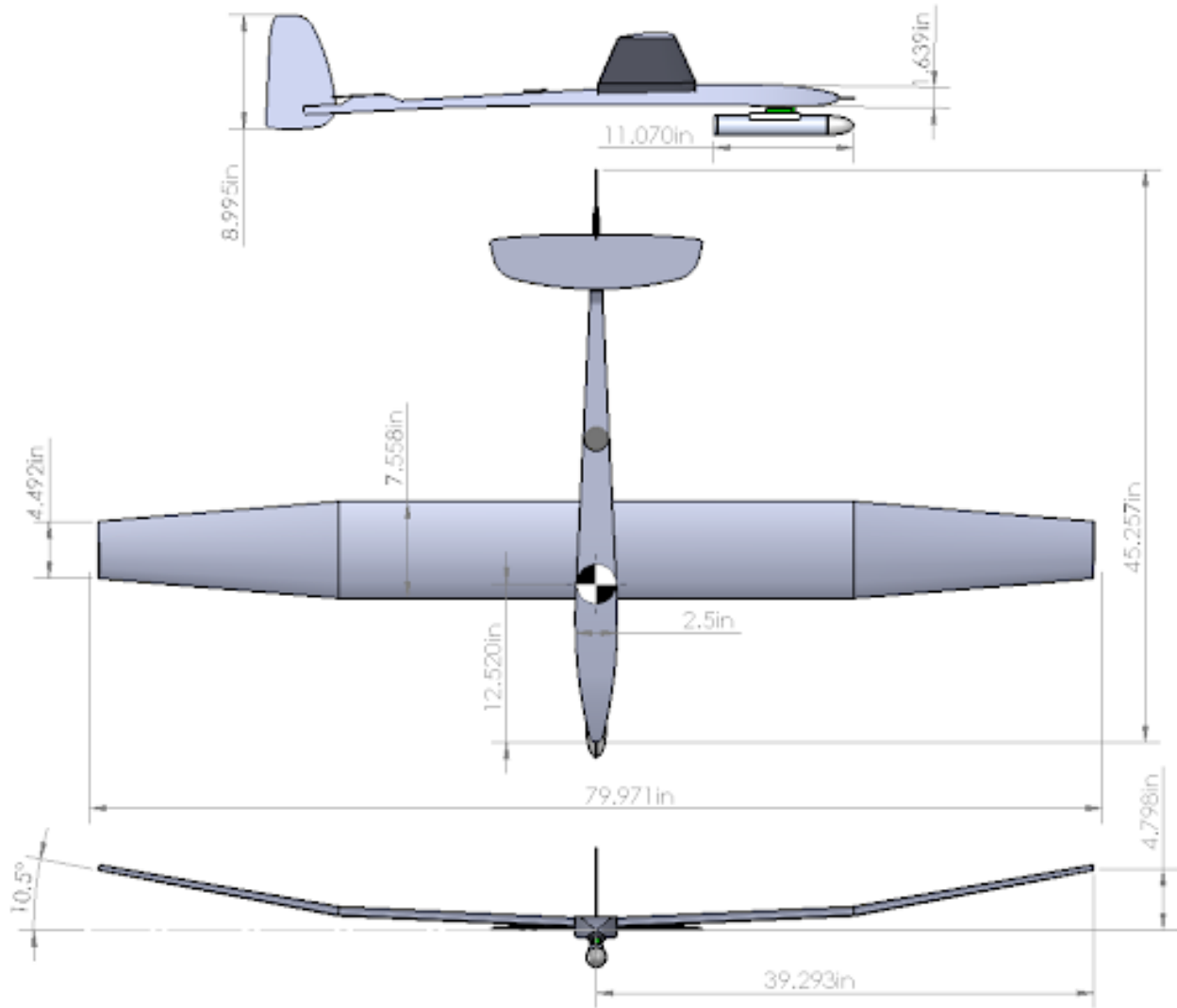
using a single camera. The uniqueness of the thermal sensor lies in its ability to image through poor lighting and environmental conditions, since it is only dependent on the heat signatures of the objects in its field of view. This benefit did not prove significant enough in the end, however, as the drawbacks from the other areas proved too costly.

The final option considered was a LIDAR scanner, which finished last in the trade matrix due to a few very costly drawbacks. The LIDAR will offer only enough resolution to be able to detect and potentially recognize the object, which doesn't satisfy the highest level of success of target identification that the camera options do. The LIDAR system additionally fails in its extreme complexity and power draw requirements, as well as in cost, weight, and data size. The LIDAR system would be many times heavier than any other payload option, and it would be extremely expensive to find a LIDAR scanner that can operate at the desired mission range. The primary benefit to employing such a system would be in its ability to easily scan a wide area in search of the target, as well as in its ability to find targets through foliage or through other objects that a camera or thermal sensor wouldn't be able to image through.

3.3. Baseline Design

The final design of RAPTR, including its dimensions, is shown in figure 30. The system is composed of three primary subsystems: the air-frame, the propulsion system, and the navigation and control system. The air-frame is a COTS Hyperflight Andreas glider² with a widened fuselage to host the internal components. The propulsion system is a Cesaroni I-class solid rocket motor⁵ mounted under the fuselage near the nose along a linear bearing designed to allow the motor to fall off after use. The navigation and control is handled by a Pixhawk flight controller²⁵ interfacing with a suite of sensors for attitude and position data and two servos for elevator and rudder control.

The commands and telemetry will be communicated to and from a ground station. This is a laptop computer connected to the pixhawk's receiver. The ground station will also process the captured images. The aero team's software geolocates the images based on vehicle telemetry and then runs a target recognition algorithm to detect the presence of targets in the image. This data is then passed into the EE's software to classify the targets within the image.

**Figure 30. Baseline Design of RAPTR**

The masses of the three subsystems and the EE payload are given in table 59.

Component	mass [lb]
Air-frame	1.14
Motor and Mount	1.50
Electronics	0.48
Payload	1.10
Total	4.22

Table 59. Subsystem Weight Breakdown

The vehicle will launch from a rail as the motor is ignited. A pilot will control the flight until the motor is exhausted and jettisoned. At this point, the pixhawk will take control of the flight and guide the vehicle along the programmed heading. It is during this glide phase that the primary mission occurs; images will be taken and transmitted by the EE payload as the vehicle flies over the target corridor.

4. Requirements Development

Author: Aubrey McKelvy, Logan Thompson, Zach Donovan, Anna Tiberi, Greg Clements, Austin Abraham, Everett Hale, Thad Gleason, Nick Carvo, Jeremiah Lane, and Tyler Faye

4.1. Requirements Flow Down

The following tables detail the requirements flow down of the project. The team first developed the functional requirements listed in table 60 based upon the customer project presentation. Next the functional requirements were broken down into derived requirements meant to guide the design.

Requirement	Description
1	The system shall survey a 2,000 foot long and at least 400 foot wide corridor beginning 2,000 feet from the user and aligned with a user defined heading.
2	The system shall be man portable.
3	The system shall transmit images and telemetry data to a ground station.
4	The system shall identify and geo-locate targets present in the captured images
5	The system shall complete its mission (launch to images processed) within 3 minutes.
6	The system shall comply with all federal and state laws regarding testing and functionality.

Table 60. Functional Requirements

Functional Requirement 1: The system shall survey a 2,000 foot long and at least 400 foot wide corridor beginning 2,000 feet from the user and aligned with a user defined heading.		
Derived Requirement	Description	Verification & Validation
1.1	The vehicle shall be capable of navigation to and along the corridor from a launch heading error of up to 25 degrees.	Verification Flight Testing
1.1.1	The vehicle shall be capable of turn radius of 350 feet	Verification Flight Testing
1.1.2	The vehicle shall be autonomously controlled during the glide phase	Verification Flight Testing
1.1.3	The vehicle shall be capable of navigation and control along specified GPS waypoints	Verification Flight Testing
1.1.4	The vehicle shall be manually controlled during the ascent phase	Verification Flight Testing
1.1.5	The vehicle shall be capable of receiving manual user control inputs	Controls Verification Testing
1.1.6	The vehicle shall be capable of maneuvering control surfaces to achieve both autonomous and manual control	Controls Verification Testing
1.2	The vehicle shall achieve a glide slope less than or equal to 5.7 degrees	Wind Tunnel Verification Testing
1.2.1	The Vehicle shall have a Lift to Drag ratio of at least 10	Wind Tunnel Verification Testing
1.2.2	The Vehicle shall be capable of maintaining an angle of attack	Wind tunnel Verification Testing
1.3	The vehicle shall utilize an unpowered glide to survey the corridor	Acceptance Testing
1.3.1	The vehicle shall attain an altitude of at least 700 feet	Verification Flight Testing
1.3.2	The vehicle shall attain a speed of at least 100 feet per second	Verification Flight Testing
1.4	The vehicle shall withstand the forces of the launch and glide phases	Structural Verification Testing
1.4.1	The motor mount shall withstand the force generated by the motor at maximum thrust	Structural Verification Testing
1.4.2	The wings shall withstand the additional weight of the payload and electronics during the glide phase.	Structural Verification Testing
1.4.3	The wings shall withstand the aerodynamic loading experienced during maximum speed	Structural Verification Testing
1.5	The vehicle shall be able to house the payload and other essential electronics components	Acceptance Testing

Table 61. Derived Requirements From Functional Requirement 1

Functional Requirement 2: The system shall be man portable.		
Derived Requirement	Description	Verification & Validation
2.1	The deployment system shall collapse to a fit within a 4'x2'x2' envelope.	Acceptance Testing
2.2	The system shall weigh no more than 10 pounds.	Acceptance Testing

Table 62. Derived Requirements From Functional Requirement 2

Functional Requirement 3: The system shall transmit images and telemetry data to a ground station.		
Derived Requirement	Description	Verification & Validation
3.1	The system shall simultaneously down-link image data and telemetry data to the ground station over the ISM band frequencies of 915 MHz and 2.4GHz	Acceptance Testing
3.1.1	All separate transmitters and receivers shall not interfere with each other.	Communications Verification Ground Testing
3.2	The system shall transmit image and telemetry data at least 4,000 ft to the ground station in real time	Communications Verification Ground Testing
3.2.1	Transmitting antenna will have a gain of at least 10dB	Acceptance Testing
3.2.2	Transmitting power will be at least 20 dBm (TBR)	Acceptance Testing
3.3	The vehicle system shall be radio transparent	Communications Verification Ground Testing
3.3.1	No material on the vehicle shall inhibit the operation of the antenna	Acceptance Testing
3.4	The system shall down-link data to the ground station at a data rate of no less than 64Kbps	Acceptance Testing

Table 63. Derived Requirements From Functional Requirement 3

Functional Requirement 4: The system shall identify a distinctly colored target and relay the target's latitude and longitude.		
Derived Requirement	Description	Verification & Validation
4.1	The ground station shall output a bounding box over potential targets to the EE software for classification as target or non-target	Software Verification Testing
4.2	The ground station shall compute local relative coordinates of the target as well as global latitude and longitude of the target	Software Verification Testing
4.2.1	The vehicle/payload shall utilize a sensor suite to quantify its location and attitude	Acceptance Testing
4.2.2	The vehicle shall collect payload look angle as telemetry data	Acceptance Testing
4.2.3	The ground station shall compute the coordinates of the center of the target to within 150 ft	Software Verification Testing

Table 64. Derived Requirements From Functional Requirement 4

Functional Requirement 5: The system shall complete its mission (launch to images processed) within 3 minutes.		
Derived Requirement	Description	Verification & Validation
5.1	The vehicle shall go from storage to mission completion within 15 minutes	Acceptance Testing
5.2	The vehicle shall take 20 seconds to travel 2000 ft laterally and 600 ft vertically.	Verification Flight Testing.
5.2.1	The vehicle shall achieve a speed of at least 100 ft/s	Verification Flight Testing
5.2.2	The vehicle shall utilize a solid rocket propulsion system for launch	Acceptance Testing
5.2.2.1	The vehicle shall be protected with thermal heat shielding tape	Thermal Verification Testing
5.2.2.2	The propulsion system shall detach from the vehicle after burning and parachute to the ground	Verification Flight Testing
5.3	The ground station shall receive and process an image within 60-90 seconds of capture	Verification Ground Testing

Table 65. Derived Requirements From Functional Requirement 5

Functional Requirement 6: The system shall comply with all federal and state laws regarding testing and functionality of the system.		
Derived Requirement	Description	Verification & Validation
6.1	The vehicle shall fly with the National Association of Rocketry and the Tripoli Rocketry Association	Acceptance Testing.
6.1.1	The vehicle shall fly under the supervision of the Northern Colorado Rocketry club, led by Mr. Joe Hinton.	Acceptance Testing.

Table 66. Derived Requirements From Functional Requirement 6

5. Detailed Design

Author: Aubrey McKelvy, Logan Thompson, Zach Donovan, Anna Tiberi, Greg Clements, Austin Abraham, Everett Hale, Thad Gleason, Nicholas Carvo, Jeremiah Lane, and Tyler Faye

5.1. Structures

There are two derived requirements that apply to the structure of the RAPTR vehicle. The first is DR 1.4 stating "The vehicle shall withstand the forces of the launch and glide phase." This requirement has three children that also apply to structural component of the project. The second is DR 1.5 stating "The vehicle shall be able to house the payload and other essential electronics components."

Derived requirement 1.4 and its children will be examined first. This requirement has to do with the structural integrity of the RAPTR vehicle. The first child requirement is 1.4.1 which states "The motor mount shall withstand the forces generated by the motor at maximum thrust." The motor mount, shown in Figure 31, is made out of 60% infill 3D printed Polylactic Acid (PLA) plastic. The motor mount is an integral component on the motor assembly shown in Figure 32.

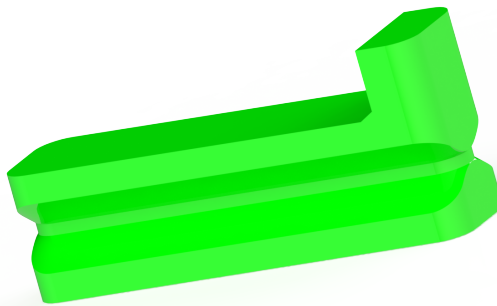


Figure 31. Motor mount

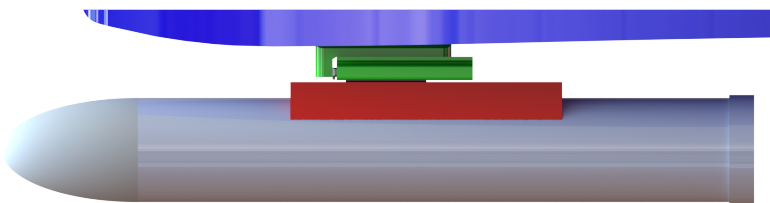


Figure 32. Motor assembly

5.1.1. Detachable Engine Mechanism Design

The motor assembly is broken down in further detail in Figure 33. The purpose of this assembly is to secure the motor to the vehicle pre-launch and during the thrust phase, and then allow the motor to separate from the vehicle and parachute back to the ground after it burns out. The motor assembly has six components. The first three, the motor mount, bearing rail, and torsion spring, will be permanently fixed to the vehicle. The motor mount will be bonded to

a board within the vehicle using epoxy and then protrude through the underside of the vehicle. The COTS bearing rail will then be epoxied to the underside of the motor mount. The torsion spring will be integrated into the aft part of the motor mount. The other three components, the bearing carriage, motor adapter, and motor, will also be epoxied together and will separate from the vehicle after the motor has burnt out.

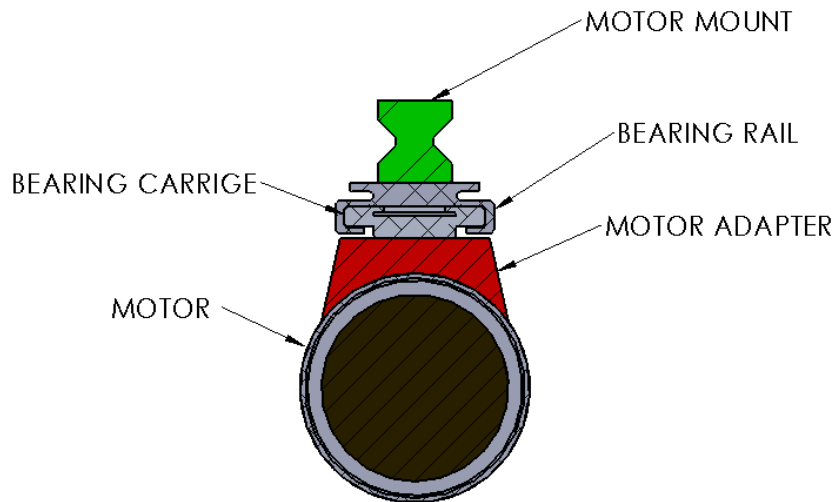


Figure 33. Motor assembly drawing

The functionality of the motor assembly is depicted in Figures 34, 35, and 36. Figure 34 shows the assembly pre-launch when the vehicle is vertical on the launch stand. The torsion spring in the deployed state and is pushing against the bearing carriage ensuring the motor doesn't separate from the vehicle prematurely. Once the motor is ignited and begins to produce thrust, it enters the state depicted in Figure 35. At this point, the thrust of the motor has brought the bearing carriage up against the tab on the motor mount. This movement of approximately half an inch gives the spring room to retract. The assembly will remain in this state throughout the burn phase of the mission held in place by the thrust of the motor. Once the motor has burnt out, the assembly moves to the state shown in Figure 36. With the motor no longer producing thrust to hold the bearing carriage against the motor mount tab and the spring retracted, the motor slides down the rails and separates from the vehicle to parachute back to the ground.

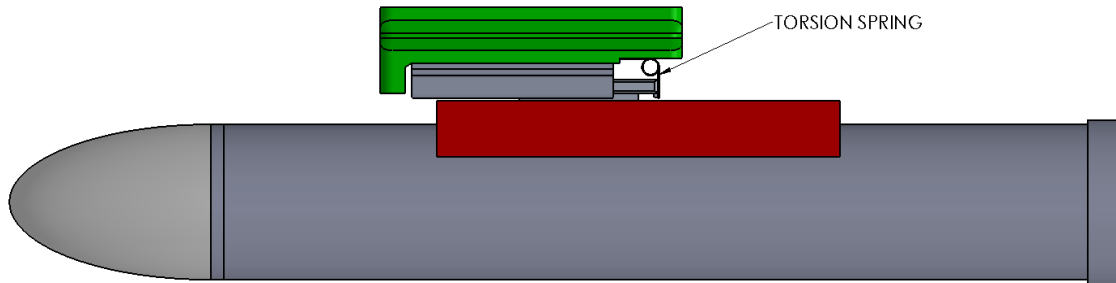
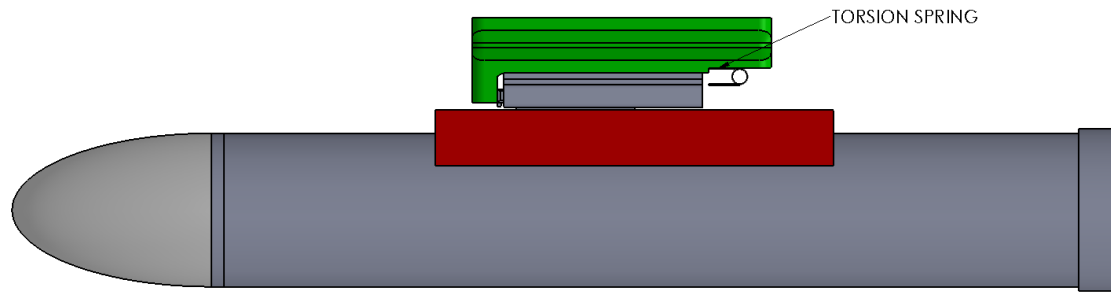
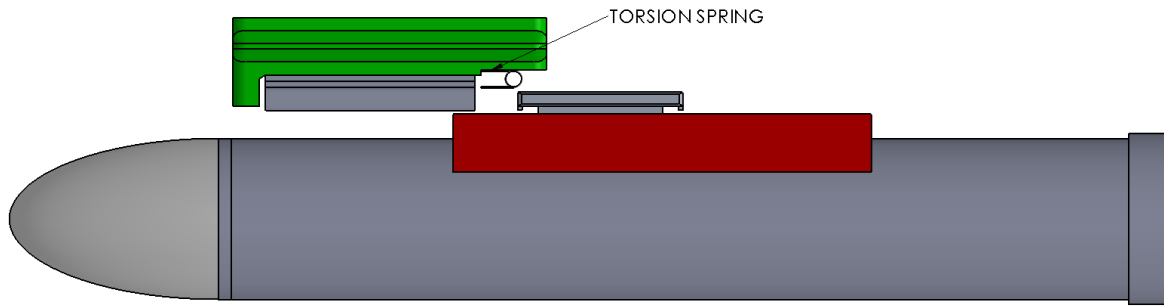


Figure 34. Motor separation, pre-ignition

**Figure 35. Motor separation, ignition****Figure 36. Motor separation, post-burnout**

5.1.2. Engine Mount Structural Analysis

The tab on the motor mount is how the thrust from the motor is transmitted to the vehicle, so it is crucial that it doesn't fail on launch. To verify the structural integrity of this part, the SolidWorks model was brought into Ansys mechanical for analysis. Once the geometry was in Ansys, the correct material was assigned and the mesh was generated. Next, a fixed support was added on the face opposite the tab to simulate the mount being epoxied to the board inside of the vehicle. Then, the maximum thrust of the motor was simulated by applying a force of 21.132 lbf to the face of the tab. It should be noted that this is an ultimate worst case scenario being modeled. Due to the static analysis, this is the equivalent of the vehicle being stationary and the motor firing at full speed which will never actually happen. However, even in this worst case scenario, the motor mount will remain structurally sound. As seen in Figures 37 and 38 the Ansys results show a maximum stress of 1,166.2 psi. As seen in table ?? this provides a factor of safety of 5.20 with the chosen material of PLA plastic. If it is decided that more strength is required after further testing, 3D printed onyx plastic with carbon fiber can be used to provide a factor of safety of 87.06. The other potential failure point is the epoxy; however, our chosen epoxy is rated at 3,400 psi, so given this analysis it will remain sound. Through this analysis, it can be seen that derived requirement 1.4.1 is satisfied.

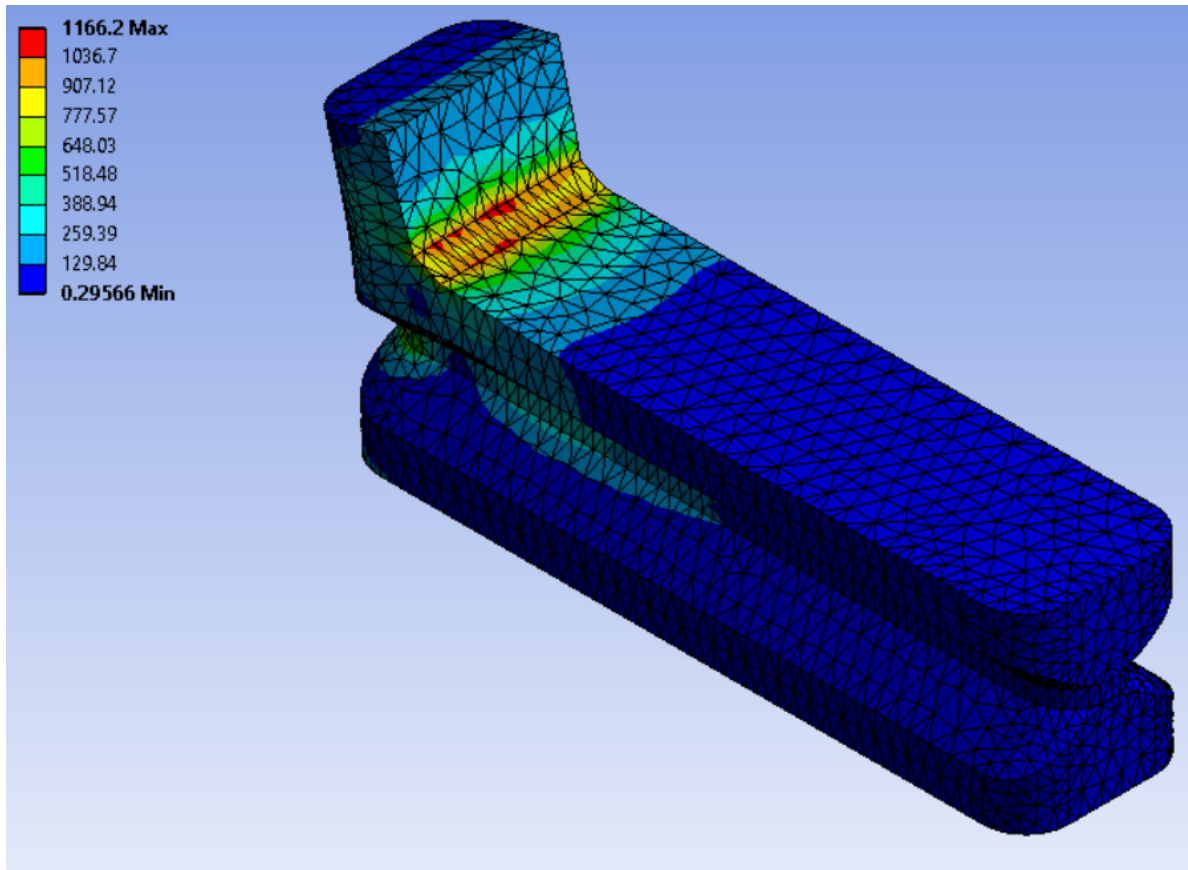


Figure 37. Motor mount Ansys analysis, view 1

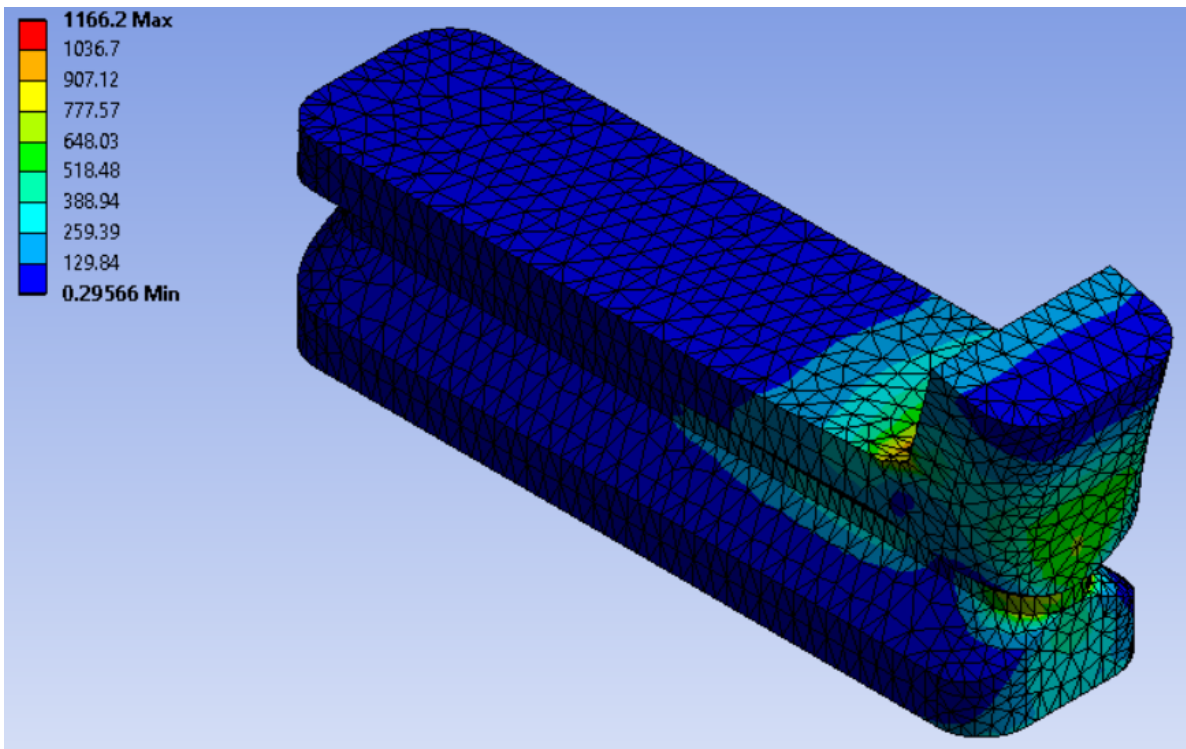


Figure 38. Motor mount Ansys analysis, view 2

Material	Tensile strength [psi]
ABS	5,656.47
PLA	6,066.23
Onyx with carbon fiber	101,526

Table 67. Potential motor mount material tensile strengths^{14 13 11}

5.1.3. Analytic Wing Bending Model

Now that there was a feasible way for the rocket to deliver its force on to the aircraft we became worried with how fast this glider would end up going. The two meter span of the aircraft and its cambered airfoil means high relative lift forces on the vehicle at all times of the flight, even when at a zero angle of attack. These large wings are made of balsa ribs and spars shrink wrapped with a plastic Monokote material making them a very strong, flexible, and lightweight, composite lifting surface. The point of concern with these wings though is where they connect to the fuselage because this is mainly where the highest shear and bending moment stresses will arise. This connection is made by a ten inch long, quarter inch diameter, carbon fiber rod that threads through a brass bushing mounted in the fuselage and then five inches into both wings.

Figure 39. AndREaS glider²

In order to get an approximation of what will happen during flight at this critical junction an analytic model for wing bending was constructed in Matlab. This model started by formulating an elliptical load distribution for the wing using the equation $q(x) = ka\sqrt{L^2 - x^2}$ where ka is the lift profile coefficient, L is the length of the wing, and x is the distance along the wing. By integrating the equation above along the length of the wing one can get an expression for ka in terms of lift, and thus an expression for ka in terms of the load factor $n = \frac{\text{lift}}{\text{weight}}$. Using results from CFD analysis, Solidworks, and propulsion model estimates, we were able to find an estimate for the worst lift the wings would experience. By plugging in $\rho = 0.002377 \text{ slug}/\text{ft}^3$, $v_{max} = 162 \text{ ft}/\text{s}$, $S = 1.824 \text{ ft}^2$, and $C_{L,\alpha=0} = 0.4$ to the lift equation, an approximate lift was found of 22.75 lbs. This number was used along with the total weight ($W_{tot} = 3.5 \text{ lbs}$) to get a load factor $n = 6.5$. Finally, this load factor was converted back into a value for ka and then ultimately into an approximate load distribution for our thrust phase. (Figure 40)

Once the correct, representative load distribution was found the procedure became much more straight forward. To get shear force from a distributed load one must find the negative integral of the distributed load from wing root to wing tip. Then boundary conditions are added to represent the zero shear force seen at the wing tip. This shear force $V(x)$ is then integrated with boundary conditions at the tip to find the bending moment $M(x)$ along the wing. Shown below are the governing equations for this process as well as the plots for shear force and bending moment along the wing span.

$$V(x) = - \int q(x)dx \rightarrow \text{ where } V(L) = 0 \quad (1)$$

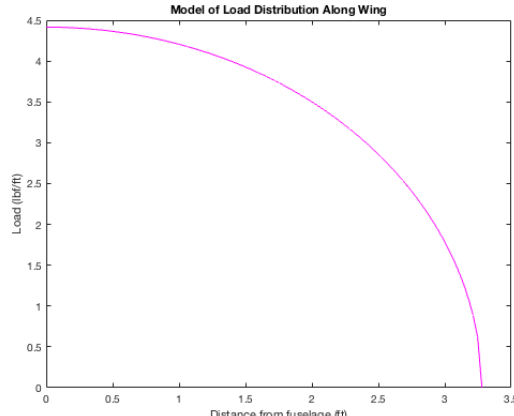


Figure 40. Model of distributed load during thrust.

$$M(x) = \int V(x)dx \rightarrow \text{ where } M(L) = 0 \quad (2)$$

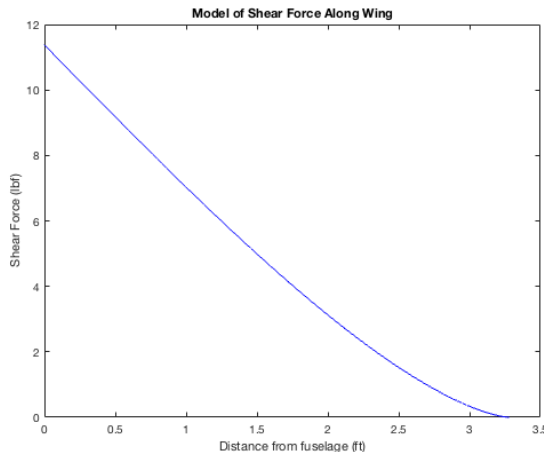


Figure 41. Model of shear force during thrust

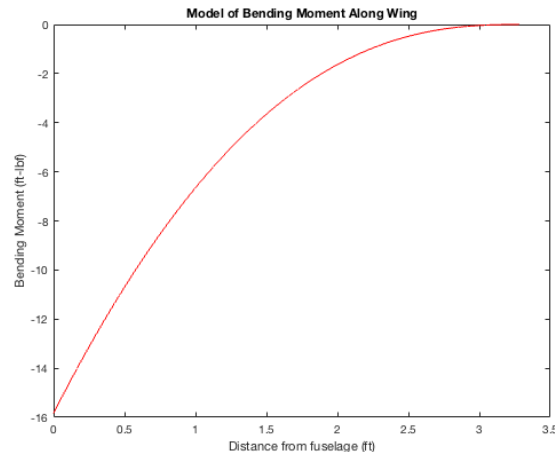


Figure 42. Model of bending moment during thrust

From these plots one can see that the boundary conditions were applied successfully to the shear and moment equations as they have values of zero where the wing ends. Also one can see the points where maximum shear stress and bending stress are derived from. In figure 41, notice the maximum shear force of 11.37 lbf at the wing root, which when applied to the circular cross section of a 0.25 inch diameter rod gives a max shear stress of $\tau = 231.8$ psi. When looking at bending moment one can see from the graph that its maximum also occurs at the wing root as expected. This maximum bending moment is -15.83 lbf-ft which doesn't seem like a lot at first, but when this bending moment is plugged into the flexure formula ($\sigma_{max} = \frac{M_d}{I}$) it gives a maximum stress of $\sigma_{max} = 61.9$ ksi. Listed in the table below (table 68) are the tensile strengths of the different materials that were considered for the main wing spar. The steel rod that comes with the glider would not fail at our projected maximum speed with a factor of safety of 2.25, but leaves little room for unexpected perturbations like wind gusts or quick changes in angle of attack. Also steel can get heavy very quickly so lighter alternatives like aluminum and carbon fiber were researched. In the end, pultruded carbon fiber was decided upon for RAPTR because of the high factor of safety coupled with its relatively low weight. From this analysis one can see that derived requirements 1.4.2 and 1.4.3 have been satisfied.

Material	Yield Strength	Tensile Strength	FOS
Aluminum 6061-T6	40 ksi	45 ksi	0.72
1080 Hot Rolled Steel	85 ksi	140 ksi	2.25
Pultruded Carbon Fiber	N/A	710.6 ksi	11.46

Table 68. Strengths of potential wing spar materials^{34 35 36}

5.1.4. Modifying Fuselage for Flight Hardware

The RAPTR vehicle will be constructed from a Hyperflight AndREaS glider kit. This comes from Germany and consists of a few hundred laser cut balsa and plywood pieces that are put together with CA glue, wood glue, and epoxy. This kit, shown in Figure 39, fits all the needs for the RAPTR mission except DR 1.5, "The vehicle shall be able to house the payload and other essential electronics components." The unmodified glider has a fuselage width of about 1.5 inches. This is too thin to house the electrical engineering teams payload and the Pixhawk 4 flight controller. The payload has a width of 2.5 inches and the Pixhawk is about 1.75 inches wide. To accommodate these components, the fuselage of the glider will be widened by an inch. The dimensions of the RAPTR vehicle made from the modified AndREaS can be seen in Figure 43. The vehicle has a wingspan of 79.97 inches, length of 45.26 inches, and maximum width of 2.5 inches. With these dimensions, DR 1.5 is satisfied.

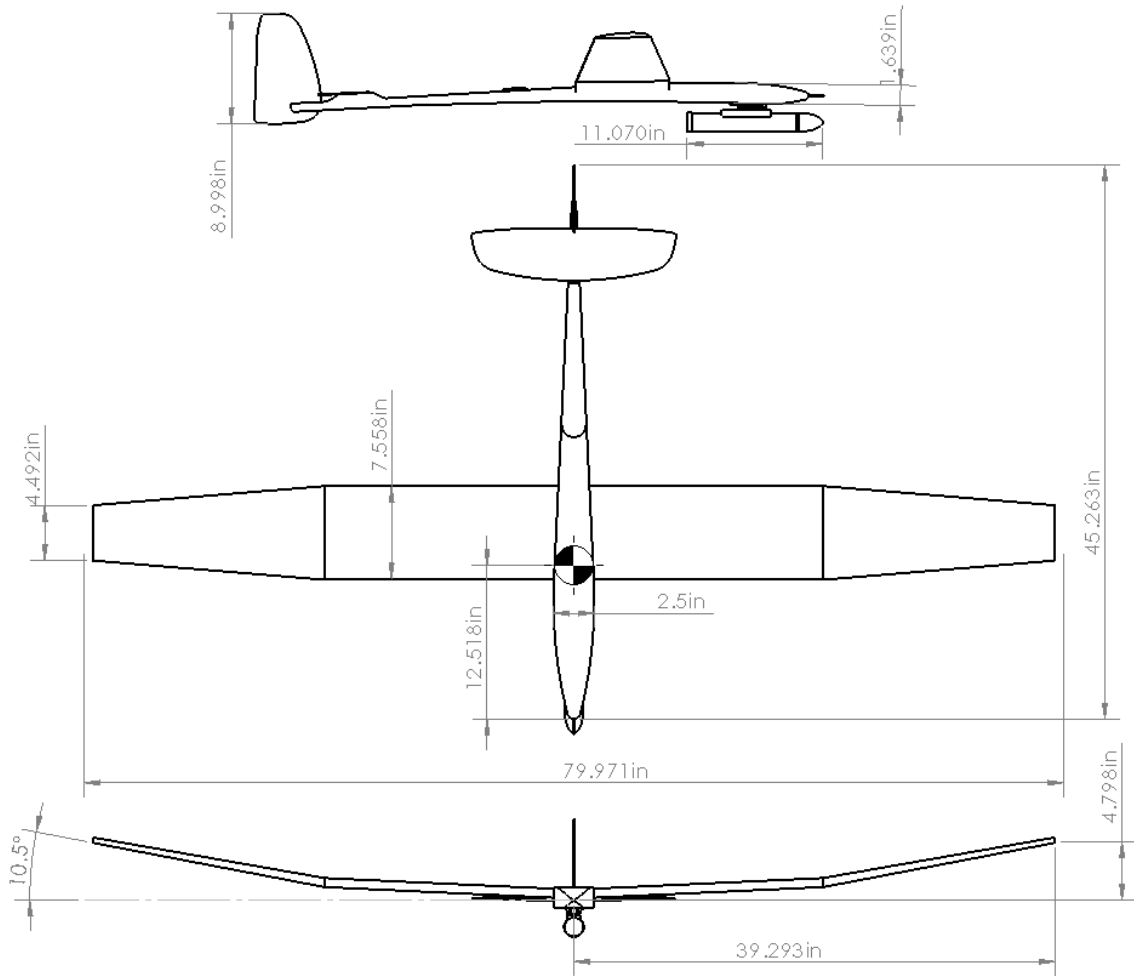


Figure 43. RAPTR vehicle three view

In order to actually make the wider bulkhead pieces we had to recreate the original pieces (Figures 44 and 45) in CAD using careful measurements from calipers. Once the pieces are in CAD it should be relatively trivial to extend their width by an extra inch. Once the pieces are modified in CAD we simply have to find the same thickness of plywood that the originals were cut from and cut out the modified bulkheads using a laser cutter and our CAD sketches. To widen the upper and lower fuselage pieces we will have to trace the outline of the fuselage onto 1/16 inch thick balsa sheet and cut out the pattern. The bottom will be mostly one glued on sheet, but the top will be half glued on sheet and half removable maintenance hatch. This hatch will be made of the same balsa sheet as the rest of the upper fuselage but will need flanges and extra structure added to help keep it in place during flight. With all of this being said, these modifications seem extremely plausible to perform and should not add much extra manufacturing time to building RAPTR.

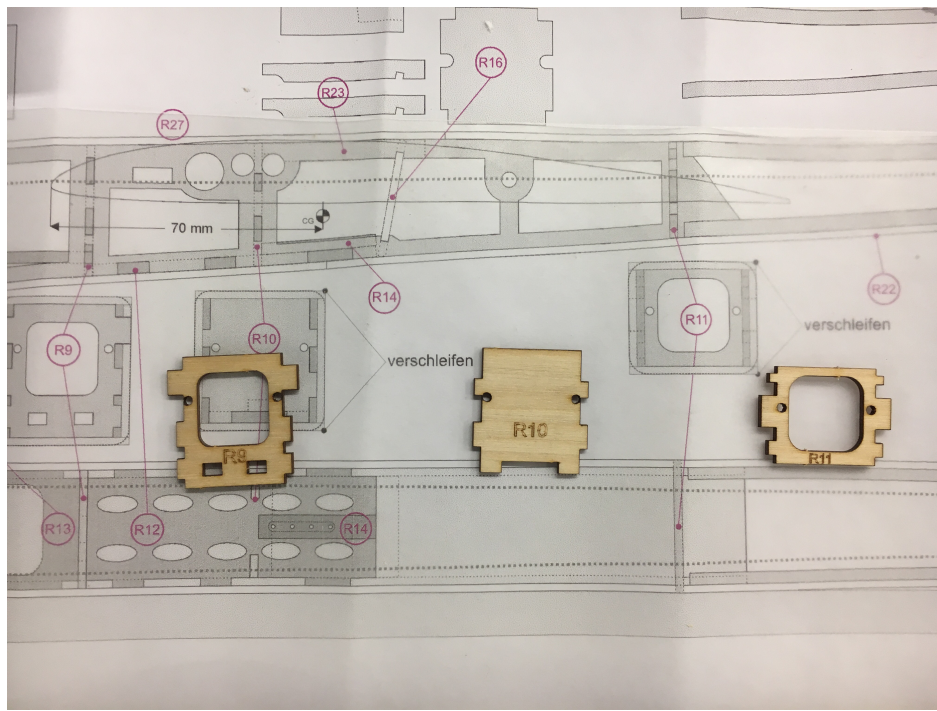


Figure 44. Some of the bulkheads that will be modified

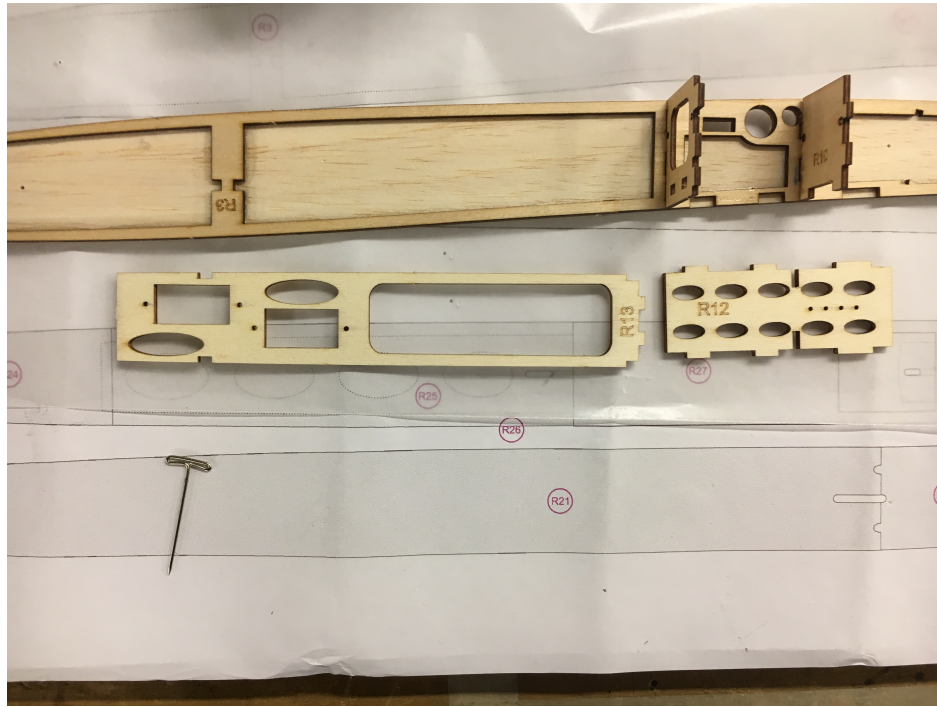


Figure 45. Some of the bulkheads that will be modified

Final SolidWorks renderings of the RAPTR vehicle can be seen in Figures 46 and 47. This SolidWorks model is used for CFD analysis, initial PID gain calculations, fuselage layout, and as a basis for the CAD model used for propulsion simulations.

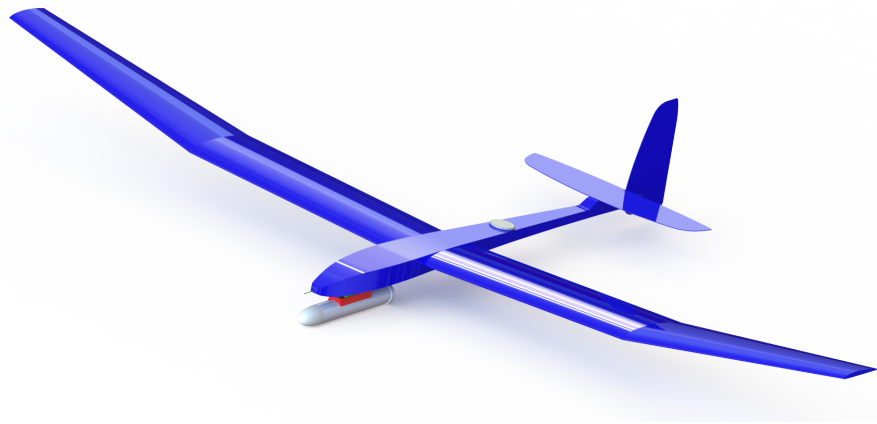


Figure 46. RAPTR Vehicle, View 1



Figure 47. RAPTR Vehicle, View 2

5.1.5. Vehicle and Payload Integration

The integration of the electrical engineering payload with the aerospace engineering teams vehicle is a crucial element of the RAPTR mission. Since there are no shared electrical components, the only interface between the two components is mechanical. The payload is restricted to 6 x 2.5 x 1.5 inches and 1.5 pounds. The location of the payload in the fuselage is shown in Figure 48. The components of the payload will be bolted to the board running through the fuselage. Additionally, there will be a hole cut in the bottom of the fuselage for the camera to have a clear field of view of the target area. The exact location of the camera hole and mounting holes will be finalized when the electrical engineering team has completed their final hardware design.

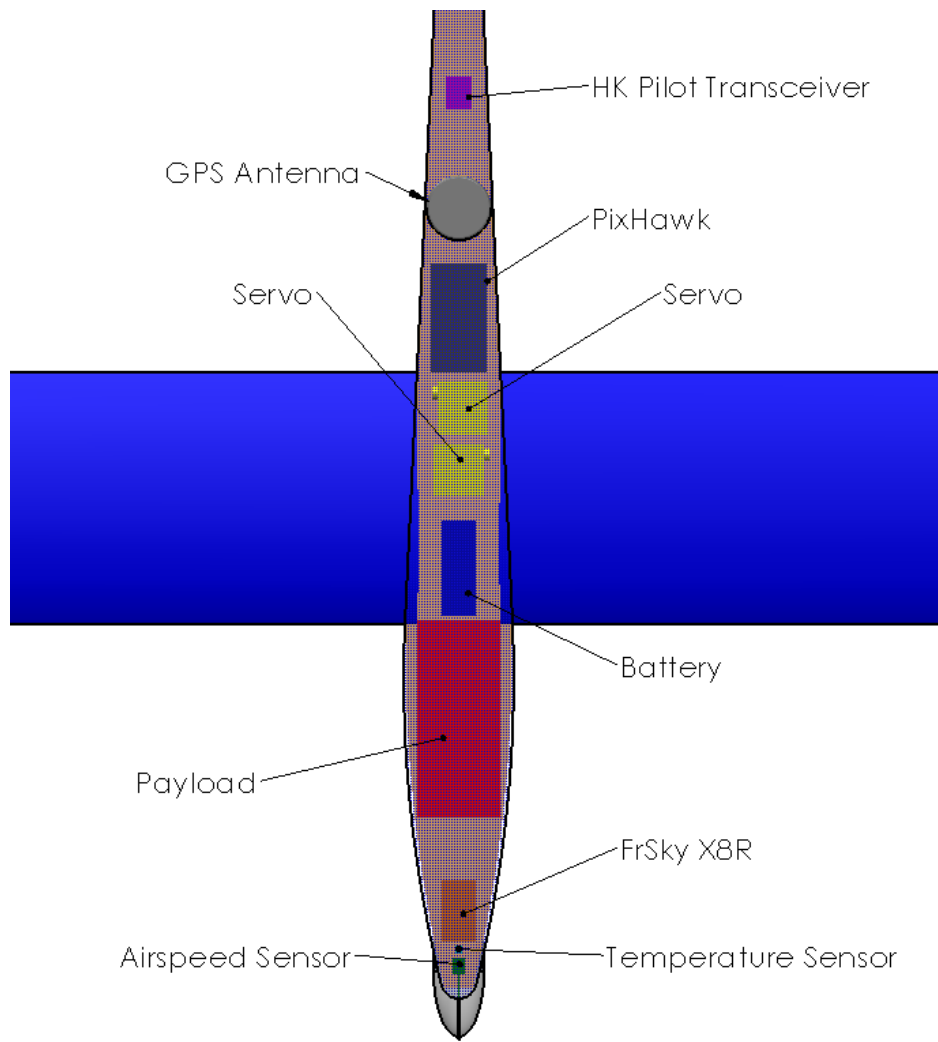


Figure 48. RAPTR Fuselage Layout

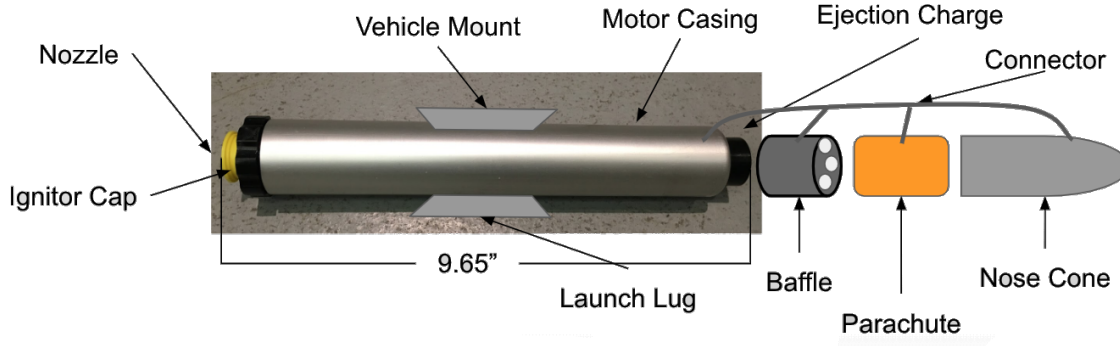
5.2. Propulsion

The propulsive phase of the mission satisfies requirements concerning distance, speed, and altitude that are necessary for mission success. The requirements the propulsion system must satisfy are outlined in Table 69. The main requirement is derived requirement 5.2.2 which states that "The vehicle shall utilize a solid rocket propulsion system for launch." This requirement is a derived requirement that ultimately is dictated by the customer, Lockheed Martin, who stated they desired a rocket propulsion system be used to complete the mission in a 3 minute time period.

Derived Requirement	Description
1.3.1	The vehicle shall attain an altitude of at least 700 feet
1.3.2	The vehicle shall attain a speed of at least 100 feet per second
2.1	The deployment system shall collapse to a fit within a 4'x2'x2' envelope.
2.2	The system shall weigh no more than 15 pounds.
2.3	The deployment system shall be able to launch from variable terrain.
5.1	The vehicle shall go from storage to mission completion within 15 minutes.
5.2	The vehicle shall take 20 seconds to travel 2000 ft laterally and 600 ft vertically.
5.2.1	The vehicle shall achieve a speed of at least 100 ft/s.
5.2.2	The vehicle shall utilize a solid rocket propulsion system for launch.
5.2.2.1	The vehicle shall be protected with thermal heat shielding tape.
5.2.2.2	The propulsion system shall detach from the vehicle after burning and parachute to the ground.
FR6	The vehicle shall comply with all state and federal laws concerning testing.
6.1	The vehicle shall fly with the National Association of Rocketry and the Tripoli Rocketry Association.
6.1.1	The vehicle shall fly under the supervision of the Northern Colorado Rocketry club, led my Mr. Joe Hinton.

Table 69. Derived Requirements Relating to the Propulsion Subsystem

The full design chosen for the propulsive system of RAPTR is shown in Figure 49 below.

**Figure 49. Propulsive System Design**

5.2.1. Engine Choice and Design Parameters

To meet all of these requirement a class I engine was chosen. The engine chosen is an I55-9 engine. The I classification of the engine indicates it has a total impulse, or I_{tot} , between 71.9 and 144 $lb\cdot sec$. The characteristics of the rocket engine are as follows⁴⁵. The values from the Thrust Curve organization were certified by the Canadian Association of Rocketry on 17 June 2014. Figure 51 shows the thrust curve of the I55 engine, experimentally found. The manufacturer of this engine is Cesaroni Technology. The manufacturer's name for the engine is the Cesaroni P38-3G Mellow,

however in this document it will be referenced as an I55-9 engine, because this is the international standard name for an engine of this classification. Figure 50 shows what a fully integrated engine (not including the nose cone attachment, motor mount, or launch lug) would look like.



Figure 50. Fully Integrated Engine

Characteristic	Associated Value	Units
Motor Length	9.65	in
Burn Time	7.25	sec
Ejection Charge Delay	2-9	sec
Diameter	1.50	in
Total Weight	15.41	oz
Propellant Weight	7.90	oz
Average Thrust	12.41	lb_f
Maximum Thrust	21.24	lb_f
Total Impulse (I_{tot})	88.71	$lb_f \cdot sec$
Specific Impulse (Isp)	180	sec
Propellant	Cesaroni Mellow	

Table 70. I55-9 Engine Characteristics

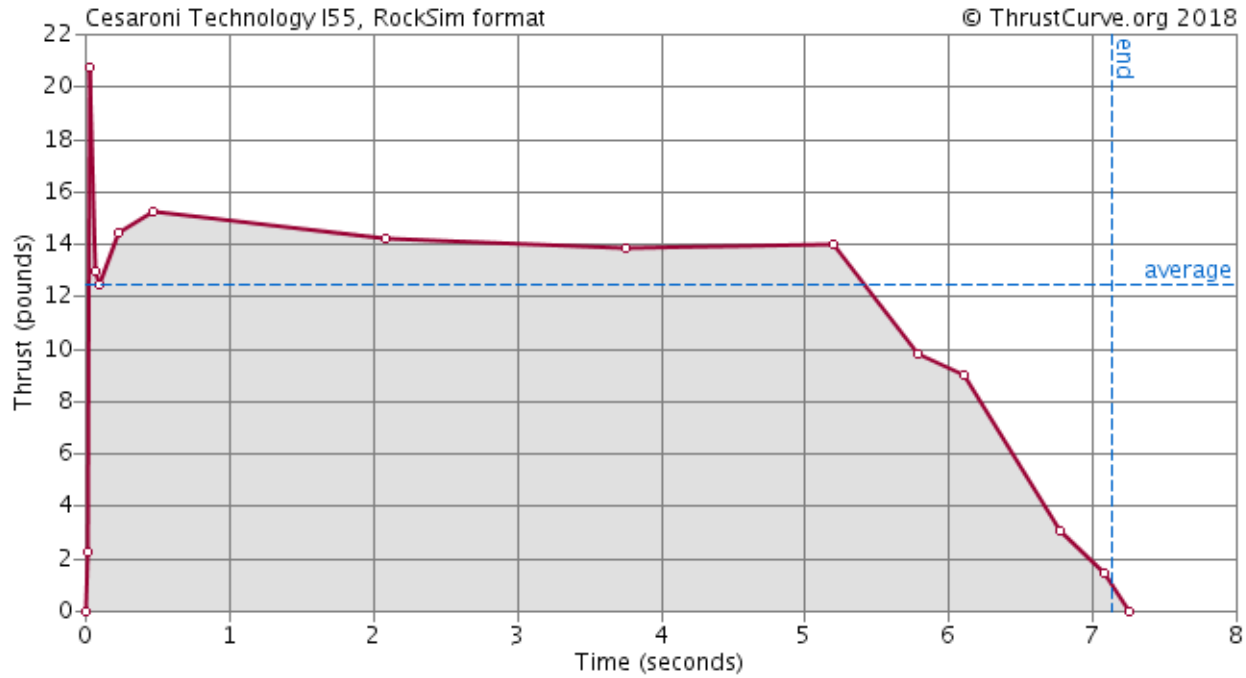


Figure 51. Experimental Thrust Curve from ThrustCurve.org

The engine is composed of two main components - the engine itself and the casing. The casing is a Cesaroni

3-Grain Casing, as the engine holds three propellant grains (this is the determining factor of the length of a rocket engine). Figure 52 shows what the propellant grains (Cesaroni Mellow propellant) look like. These grains reside in the black casing of the engine. Figure 53 shows these two components side-by-side - on the left side of the image is the engine containing (from bottom to top) the igniter cap (yellow), the nozzle (inside of the igniter cap), the propellant grain (inside of the black ablative casing), general engine casing (black ablative material), and the ejection charge (top extension of the engine). On the right of the image is the aluminum engine casing with an opening at the top for the ejection charge, and threads at the bottom of the image that screw into the engine.



Figure 52. Engine Components - Engine and Propellant Grain



Figure 53. Engine Components - Engine and Case

The launch angle the vehicle will be launched from will be fixed for the user between 0 and 20 degrees from vertical. This allows a wide range of possible altitudes and lateral distances achievable during the propulsive phase of the mission. Figure 54 shows what the model of the full vehicle including the propulsive phase looks like (the model will be discussed further in depth in a later section). 20° from vertical is the maximum the Northern Colorado Rocketry club is allowing RAPTR to launch at, which is 15° greater than the nationally allowed 5° from vertical. By launching at either 0° or 20° from vertical it can be seen on the left plot that in both scenarios the vehicle reaches well above the minimum altitude set by D.R.1.3.1 and D.R.5.2. The lateral distance covered by the vehicle in each situation is one element that will be looked into further with testing of the vehicle. If the vehicle is launched at 20 degrees vertical in a nominal situation (i.e. no wind and no launch angle error), it will cover a lateral distance of approximately 1400 feet from the launch site, at which point it will be at an altitude of approximately 1300 feet. D.R.5.2 states that the vehicle shall travel 2000 feet vertically in 20 seconds, however the burn time and therefore the propulsive phase of the mission only accounts for 7.25 seconds of this time line, therefore the vehicle must reach the minimum altitude but is not necessarily required to reach the full lateral distance in that time, as the glide phase of the mission will account for the majority of the lateral distance covered. Ideally RAPTR would be launched 20° from vertical, however this causes concern with the speeds achieved by the vehicle. This concern will be explored more in depth in a later section.

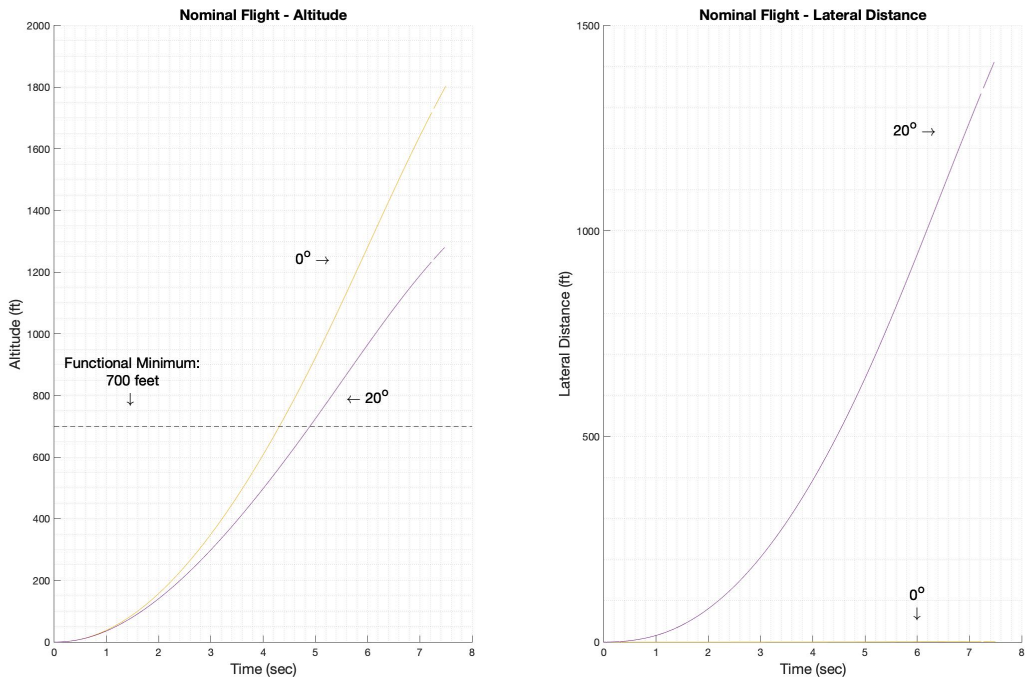


Figure 54. Nominal Flight Path - Propulsive Phase

5.2.2. Propulsion Models

5.2.2.1 RockSim

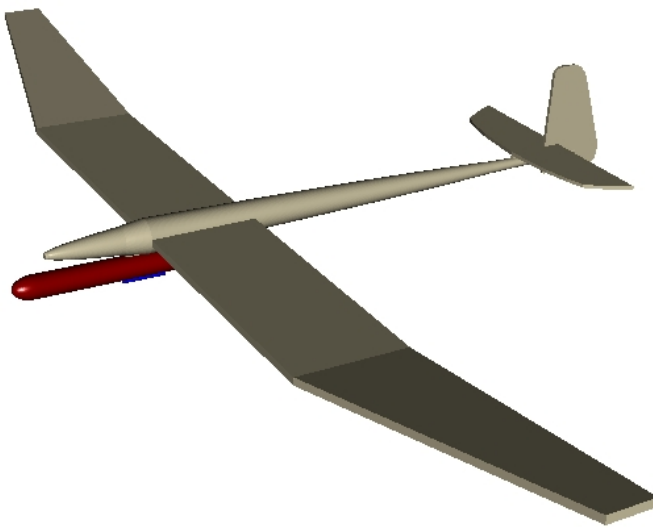


Figure 55. RockSim 3D CAD Model Input

Please note this model was NOT used for data, simply to achieve a high fidelity CAD model which could then be modified slightly to be used by the OpenRocket software. Figure 55 shows the simplified 3D CAD model that was input into the RockSim software. RockSim is "a model rocket design and flight simulation system."¹⁰ The equations used in simulation are widely used for all aerodynamics and ballistic modeling, for example the model for the drag force. The program calculates the drag coefficient for each time increment based on the inputted 3D model. This program is very sophisticated: it calculates the center of gravity and center of pressure. Any wind direction and force can be input into the program and it also accounts for angular acceleration, the corrective moment coefficient, the damping moment coefficient, cross wind drag and lift, damping ratios, and longitudinal and radial moments of inertia. However this program was not used for two main reason: the first being that the model input was unable to run in the simulation because it was too advanced of a CAD model. This program is advanced at modeling but is not normally used for a glider. The second limiting factor was the cost, which was \$123.60. Again, please note this model was NOT used for verification with other data - but simply used as a basis for the level of sophistication for the OpenRocket model which was used.

5.2.2.2 OpenRocket

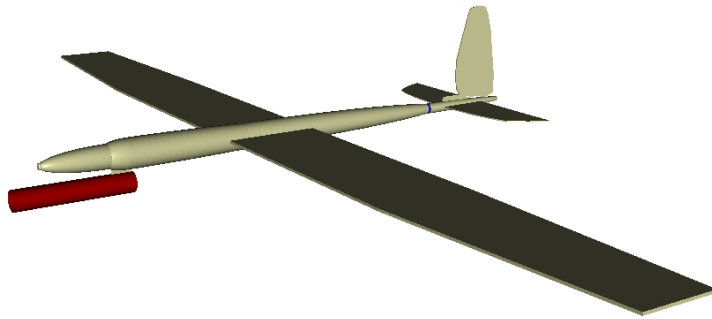


Figure 56. OpenRocket 3D CAD Model Input

Figure 56 shows the 3D CAD model that was the input design for the simulation. This CAD model is very simplified compared to the full structural model from the structures section of this report. It is also taken from the RockSim 3D CAD model, which has a high degree of fidelity, and simplified so the program could take it as an input. This is a very important model, despite any differences between this model and the true structural model, because this model takes into account the effects of the large surface due to the wingspan that a normal model rocket does not have. Even though this 3D CAD model is not 100% true to the real structure of the vehicle, it provides a more in depth analysis of the ballistic phase of the mission than a point-mass model would. The OpenRocket model is used because of this higher degree of fidelity than a point-mass model and the consideration of the wingspan, control surfaces, extended fuselage area, and rocket mounting location.

OpenRocket is an open-source rocket simulation software that was originally developed as a master's thesis by Sampo Niskanen entitled, *Development of an Open Source model rocket simulation software*¹². It is a simulation environment written entirely in Java. The software makes the stability of the rocket the central priority of the simulation and it is "deemed statically stable if its center of pressure (CP) is aft of its center of gravity (CG)." ¹² Center of gravity for our simulation was given by the structural team on RAPTR and put in as an override for the program so OpenRocket did not calculate the center of gravity from the simplified model. SolidWorks calculated the center of gravity with the full-fidelity CAD model. In order to determine the center of pressure on the rocket the Barrowman Method is used (originally presented at a NASA conference in 1966).¹² This program does not use a CFD analysis for the aerodynamics of the model, instead using discrete calculations.

OpenRocket operates in both incompressible and compressible flow regions based on Mach and Reynolds number as well as the Prandtl factor, which "corrects subsonic force coefficients for compressible flow."¹² The equation for the Prandtl factor can be seen below.

$$P = \frac{1}{\sqrt{1 - M^2}} \quad (3)$$

Figure 57 shows the steps OpenRocket completes the calculate all elements of the simulation. The numerical integration is performed using a 4-th Order Runge-Kutta approximation. The orientation of the vehicle at each time step is stored within a quaternion that transforms the values between world and rocket coordinates.

The process of simulating rocket flight can be broken down into the following steps:

0. Initialize the rocket in a known position and orientation at time $t = 0$.
1. Compute the local wind velocity and other atmospheric conditions.
2. Compute the current airspeed, angle of attack, lateral wind direction and other flight parameters.
3. Compute the aerodynamic forces and moments affecting the rocket.
4. Compute the effect of motor thrust and gravity.
5. Compute the mass and moments of inertia of the rocket and from these the linear and rotational acceleration of the rocket.
6. Numerically integrate the acceleration to the rocket's position and orientation during a time step Δt and update the current time $t \mapsto t + \Delta t$.

Figure 57. OpenRocket Simulation Calculation Steps¹²

The following simplifying assumptions are made in the model¹².

Simplifying Assumption	Accuracy Analysis for RAPTR
The angle of attack is very close to zero.	All fins and wings have an angle of attack of zero so this will be accurate for our scenario.
The flow around the body is steady and non-rotational.	Because our vehicle will only be subsonic and is also smooth this is an accurate approximation.
The rocket is a rigid body.	RAPTR is a rigid body, however this does ignore the effects of wing bending perpendicular to the thrust vector and flutter, which are assumed to be negligible during the thrust phase.
The wings are flat plates.	A close approximation as our wings have a very slight airfoil profile.
The center of pressure location is primarily affected by the fins.	This approximation is taken from the Barrowman Thesis and is assumed to be correct for our situation.
Normal force and pitching moments produced by the body are assumed to be equal at subsonic and supersonic speeds.	Because we will not be going at supersonic speeds this will not affect RAPTR.
Mach cone effects are ignored.	This will not affect us as the vehicle will be subsonic for the entire flight.
The boundary layer is assumed to be fully turbulent in all cases.	This is a close approximation that will not affect our flight.
The surface is smooth and the surface roughness is completely submerged in a thin, laminar sublayer.	The surface of our vehicle will be covered in Monokote, which is very smooth.
Coriolis effect is ignored.	Considering we are not traveling very far laterally or very high compared to other high powered rockets this assumption is a good approximation.

Table 71. OpenRocket Simplifying Assumption and Analysis for its use for RAPTR¹²

OpenRocket is a very reliable software that is used by many model rocketry enthusiasts. OpenRocket outputs 53 different variables from the simulation, including total acceleration, total velocity, lateral distance, altitude, and many more. The simulation accounts for the launch environment, wind inputs, drag, lift, normal and axial moments, moments of inertia, center of gravity and pressure on the vehicle, and any instability that could be caused during

flight. It also intakes the entire thrust curve of the rocket engine and uses this instead of a constant thrust the entire flight. OpenRocket is the simulation used for all of our propulsive phase values, and it is backed up by data from the MATLAB simulation.

5.2.2.3 MATLAB

To further assist with the design of the propulsion system, a MATLAB code was developed to simulate the trajectory and speed of the vehicle during its ascent. The code utilized the function "ode45" to solve the differential equation, $\frac{dV}{dt} = \frac{F}{m}$, at each time step. This acceleration was used to solve for the velocity and position of the vehicle. The forces acting on the vehicle used in this simulation were gravity, thrust, and drag. Since the vehicle is intended to maintain a zero angle of attack during ascent, the lift force acting on the vehicle will be relatively low and was neglected, along with the rotational accelerations. An experimentally determined thrust curve for the motor was loaded into the simulation and interpolated at each time step to determine the thrust force acting on the vehicle. The direction of this thrust force was assumed to be tangent to the vehicle trajectory after it leaves the launch stand. While still on the launch stand, this thrust direction was restricted to the launch angle. The drag force was computed at each time step using the equation;

$$D = 0.5\rho V^2 C_D A \quad (4)$$

where ρ is the density of air, V is the total velocity of the vehicle, C_D is the coefficient of drag for the vehicle, and A is the cross sectional area. The density of air was inputted as a constant sea level value. The cross sectional area was computed using the known geometry of the vehicle. This total drag force was split into x and z components so that it acted opposite to the vehicle's trajectory. The gravity acting on the vehicle was assumed constant and acting straight down throughout the ascent. Below is a table summarizing all of the inputs and assumptions used for the simulation.

Variable	Value
Launch Rail Length	8 ft
Launch Angle	90 deg
Density of Air	2.377e-3 slug/ft ³
Cross Sectional Area	0.081 ft ²
Mass	4.409 lbs
Gravity Constant	32.185 ft/s ²
Cd	0.33

Table 72. MATLAB Simulation Parameters used in the Simulation

Assumption	Accuracy
Zero rotational acceleration	The vehicle will be stable in roll, pitch, and yaw. Additionally, the vehicle will be manually controlled during ascent to prevent rotational accelerations
Constant air density	The vehicle will reach a maximum altitude of no more than 1000ft. The change in density at this altitude will only be about 0.6 psi
Thrust/Drag force tangent to trajectory	The angle of attack of the vehicle will be held constant at 0 deg during launch. This means this assumption is quite valid.
Lift force is zero	Because the angle of attack of the vehicle will be held at 0 deg, the lift force will be close to zero. Additionally, the lift force acting on the vehicle will be counteracted with the elevator so that it maintains a straight flight path.
Mass of rocket is constant	The total weight of the propellant is about 223 g which is about 10% of the total vehicle weight without any additional mass. This will certainly add some error to the simulation, however, it will still be relatively accurate.

Table 73. MATLAB Simulation Assumptions and Accuracy

The primary output of the MATLAB simulation is the position, speed, and acceleration of the vehicle throughout the thrust/ascent phase. Having these relatively accurate outputs aided in selecting a motor that will satisfy the relevant

design requirements.

5.2.2.4 Expected Sources of Error During Launch

Using the OpenRocket software, two different Monte-Carlo scenarios were run to look at compliance with the requirements for the propulsive phase of RAPTR's mission. On launch day there are two expected variations from nominal conditions: wind and launch angle error. For all simulations, the plots only go through burnout of the rocket at approximately 7.25 seconds as this is the end of the propulsive phase of the mission.

Wind Monte-Carlo The Northern Colorado Rocketry club, with whom we are launching, has a maximum of 15mph sustained wind that they are able to launch in. However, because RAPTR has a much greater surface area than most model rockets we modeled linearly through 10mph sustained winds. The winds modeled vary from no wind up to 10mph sustained wind varying from a headwind to a crosswind. These are the conditions expected on a launch day as we will be launching in the Northern plains of Colorado, where the wind comes from the North and down from the front range of the Rocky Mountains with great enthusiasm. Looking at both velocity and altitude for the varying wind situations the plots in Figures 58 and 59 show how the vehicle's altitude and total velocity respond to wind variation. In both situations it can be clearly seen that the required functional minimums are exceeded with no problems, with a functional minimum of 700 feet altitude and 100 feet per second at the end of the burn phase. In both scenarios for all cases of wind these minimums are exceeded.

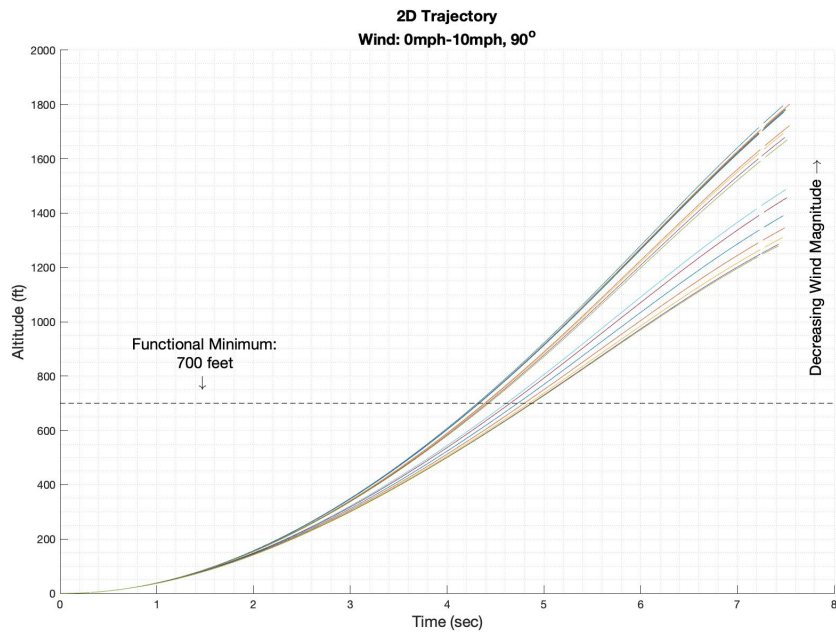
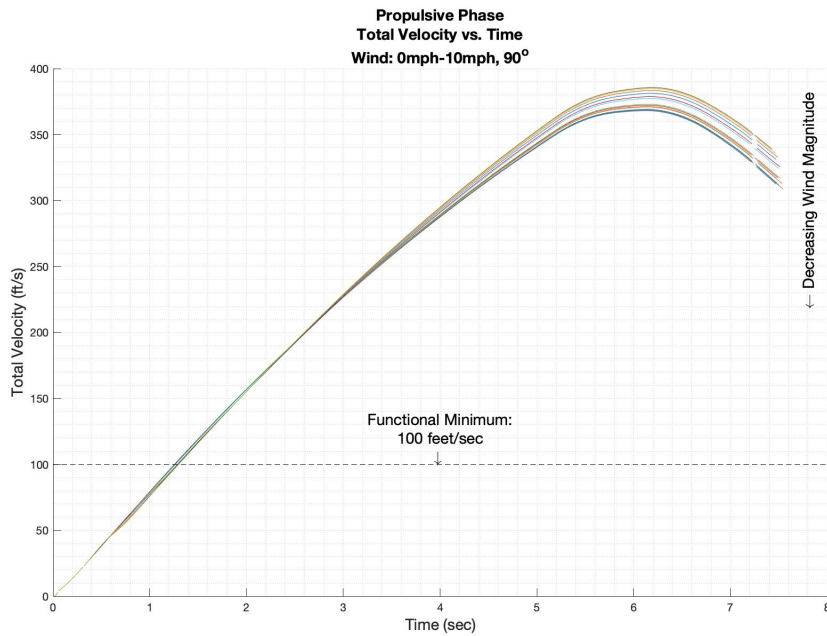
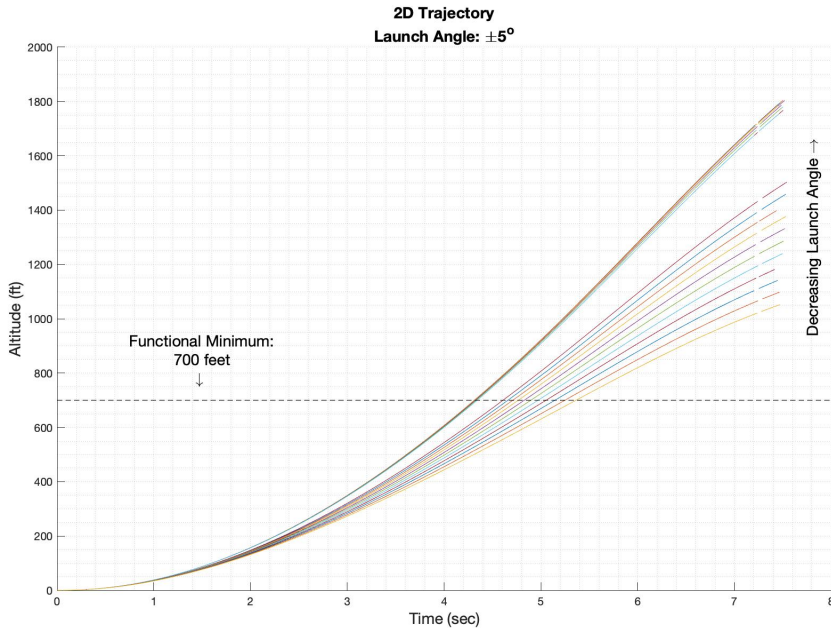


Figure 58. OpenRocket Monte-Carlo Simulation: Wind and Altitude

**Figure 59. OpenRocket Monte-Carlo Simulation: Wind and Velocity**

Launch Angle Error Monte-Carlo The vehicle will be launched from an angle between 0 and 20 degrees from vertical. The Monte-Carlo for the Launch angle varies $\pm 5^\circ$ from the maximum and minimum possible launch angle, therefore it goes between -5° to $+5^\circ$ from vertical and 15° to 25° from vertical. These launch angle errors were put into the OpenRocket software and the Monte-Carlo simulation was created. Figures 60 and 61 show that even with expected variation in launch angle the vehicle will always exceed the functional minimum altitude and the functional minimum velocity.

**Figure 60. OpenRocket Monte-Carlo Simulation: Launch Angle Error and Altitude**

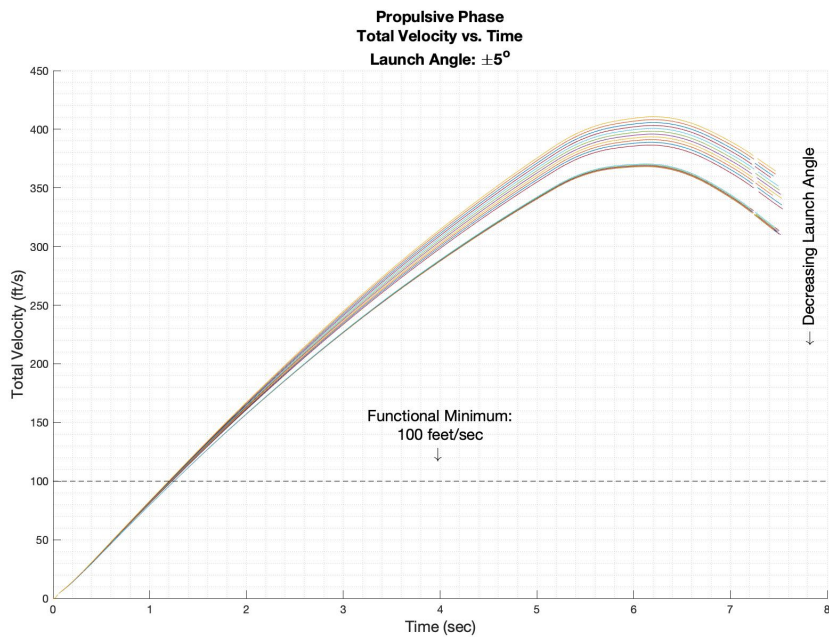


Figure 61. OpenRocket Monte-Carlo Simulation: Launch Angle Error and Velocity

5.2.3. Maximum Velocity and Weight Considerations

Looking at the plots above it can be observed that the vehicle will reach a very high total velocity, over 400 ft/sec. Because this velocity is so high it is unclear if every component would survive this velocity, so there are several off-ramps from the current design to ensure mission success in every possible launch and flight condition. Several options are: electric propulsion system, lower class engine, and increase the mass of the vehicle. An electric propulsion system would not meet customer requirements as they dictated their desire for a rocket powered system. A lower class engine would not give the thrust characteristics we are looking for - primarily the long burn time and low accelerations experienced. In addition the larger engine gives us room for error in the weight calculations, especially for the electrical engineering payload uncertainty. Figure 62 shows the effects of increasing the mass of the vehicle. The current vehicle design mass is 67.65 ounces, however at this mass the vehicle exceeds the maximum velocity. An ideal mass would be 105 ounces, which would meet the functional minimum of 700 feet for the altitude and the potential maximum of 162 feet per second, derived as the maximum from the controls team. The additional weight would be evenly distributed along the vehicle, specifically aft of the rocket engine to increase the stability of the vehicle during the thrust phase of the mission. Therefore, this plot proves it would be possible to decrease maximum velocity and increase vehicle mass if required. This will be finalized early next semester after more analysis.

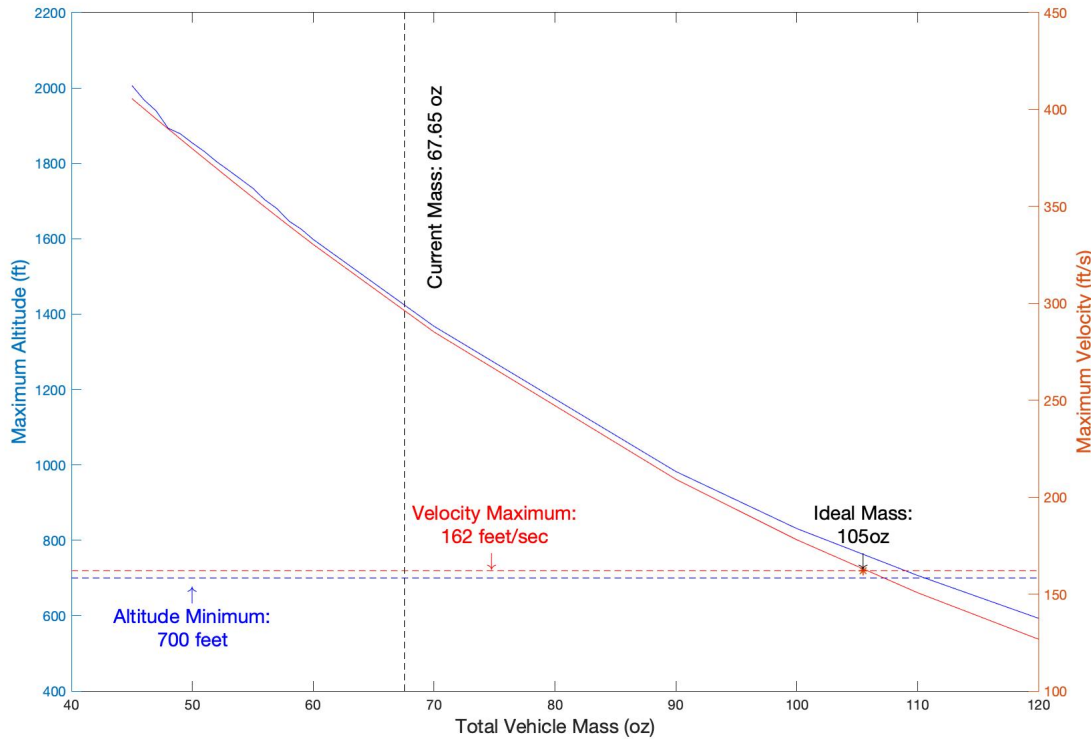


Figure 62. OpenRocket Weight Design Point Plot

5.2.3.1 Thrust Curve Error

Deviation from the experimental thrust curve provided by the Canadian Association of Rocketry is expected to vary by a small percentage for every rocket propellant grain created for model rocketry. For this reason the thrust curve was varied, in its entirety, between 95% of the claimed values and 105% of its claimed values. Table 74 below shows the percent error in the thrust curve with the altitude at motor burnout and the maximum speed. Due to the nature of the OpenRocket software it is not possible to stray from the given thrust curve, however in the MATLAB simulation it was possible to obtain three different plots for these variations, not enough for a full Monte-Carlo but enough for a performance plot. Figure 63 shows the total velocity and altitude of the vehicle through burnout with the addition of the extra weight and the thrust curve variation. For both altitude and velocity with the variation in thrust and the increased weight of the vehicle the requirements for functional minimums are satisfied, and the possible maximum velocity of 162 ft/s is also met. Figure 64 is a performance plot that shows how burnout altitude and maximum velocity respond to thrust deviation. These curves can be extrapolated if necessary to look at even greater variations in thrust, but was not at this point in time because we do not believe there will be more than a 5% variation in the thrust performance.

Percent Error (%)	Maximum Altitude (ft)	Maximum Velocity (ft/s)
0	801	177
-5	738	159
+5	873	194

Table 74. Thrust Curve Error Simulation Results with Increased Weight

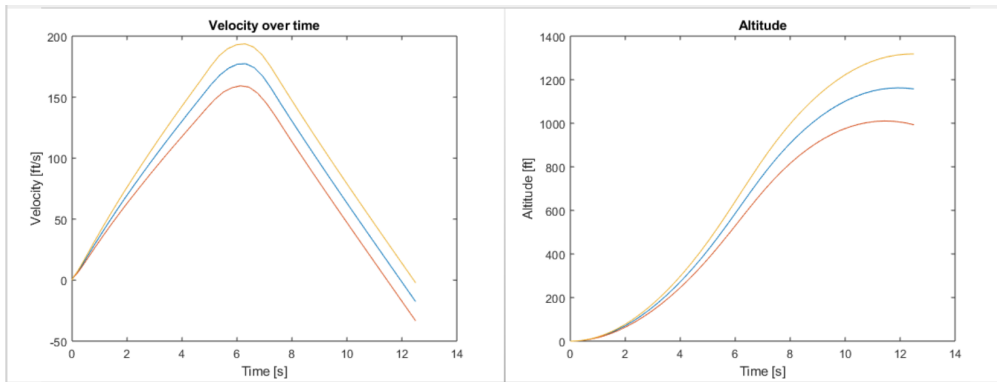


Figure 63. Increased Weight MATLAB Simulation: Thrust Curve Error Plots

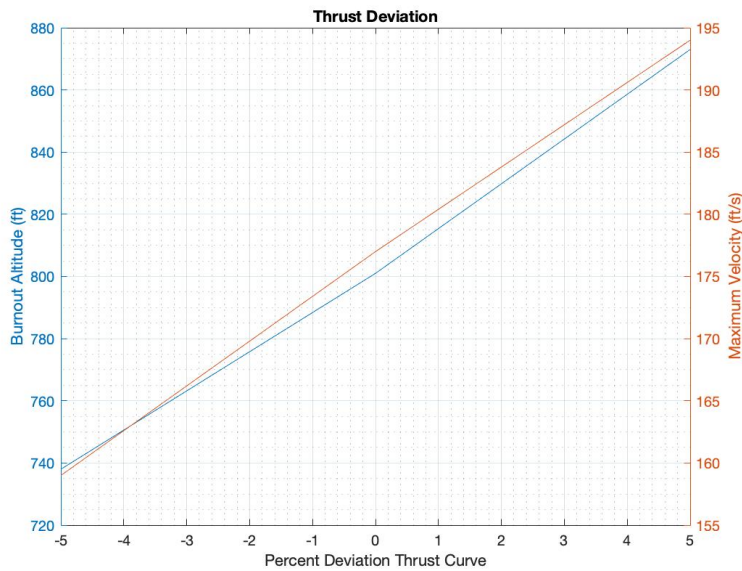


Figure 64. Increased Weight MATLAB Simulation: Thrust Curve Error Performance Plot

5.2.4. Parachute and Nose Cone

After the burn phase of the mission, drag and gravity of the vehicle, which will still be moving upwards, will cause the rocket (attached to the main vehicle via the motor mount discussed in the structures section of this paper) will fall off. Nine seconds after ignition, the black powder ejection charge will blow the nose cone off the engine casing, freeing the parachute. At the end of the mission the engine and all attached components will be retrieved. It should be noted this ejection charge can be changed from any where between two and nine seconds, however we are intending to keep the nine second ejection charge delay due to the time line of our mission and long burn time of our engine. Per The National Association of Rocketry and Tripoli Rocketry Association regulations, because our engine will be detaching from the main vehicle, the rocket is required to have either a parachute or a streamer to ease retrieval. Figure 49 shows the full set up of the engine, including the nose cone, parachute, baffle, and connector. The nose cone will be 3D printed from heavy duty PLA and will resemble the nose cone seen in Figure 65.

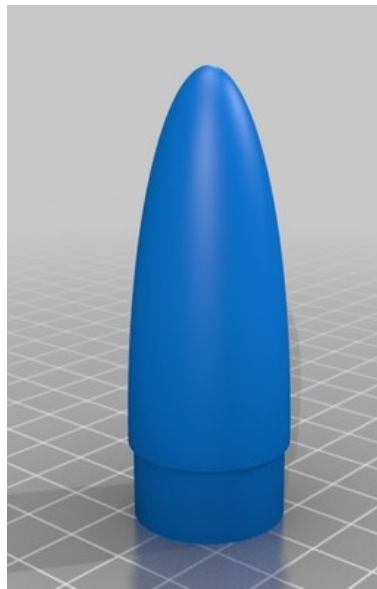


Figure 65. Nose Cone General Shape¹⁵

The nose cone was chosen to be more oblique than ogive to allow more packable room for the parachute and its thermal protection. The nose cone will have a shoulder that attaches to the motor casing and will contain thermal protection for the parachute, the parachute, and a connecting strap between these elements and the rocket itself. This connecting strap will most likely be a Kevlar strap attached to the engine casing, the thermal protection (if it is reusable), the parachute, and the nose cone. The strap will be attached using a heat resistant epoxy.

Due to the extreme temperatures experienced at the nose of the rocket engine and the black powder ejection charge which will blow the nose cone off the engine nine seconds after ignition. In order to protect the parachute from this ejection charge and the thermal effects at the nose of the engine, a baffle or other thermal wadding will have to be used. A baffle provides the same protection as wadding but depending on the material may be reusable. At this point it is not critical to decide which method we will use for parachute protection and this will be decided early next semester as both of these methods are cost-effective and provide protection to the recovery system.

$$D = \sqrt{\frac{8mg}{\pi\rho C_D V_g^2}} = \sqrt{\frac{8 \cdot 0.2521[kg] \cdot 9.81[m/s^2]}{\pi \cdot 0.975[kg/m^3] \cdot 1.5 \cdot (5[m/s])^2}} = 0.415[m] = 41.5[cm] = 16.34[in]$$

Figure 66. Parachute Size Calculation¹⁶

The parachute will be an 18 inch diameter parachute that is light weight and packs to a small enough size to fit inside of the nose cone. Figure 66 shows the calculation done to determine the size of the parachute required. In the calculation the coefficient of drag of the parachute was assumed to be 1.5, which is reasonable for a parachute of the material we are looking at. The velocity at which the engine will hit the ground, V_g , is a recommended velocity for an engine to be successfully reused from the National Association of Rocketry. An 18 inch diameter parachute was chosen to ensure a higher factor of safety for the retrieval of the engine elements. If necessary a 24 inch diameter parachute could also be used if the 18 inch fails in an unforeseen way. Figure 67 shows an example of a COTS 18 inch diameter parachute.



Figure 67. Parachute Example

It should be mentioned that if the parachute does not deploy as expected we will not have mission failure - it can be considered a streamer and will still comply with all test-site regulations and easy to find. It will mean a slightly bumpier landing for the reusable elements of the engine design and a possible replacement of the engine casing depending on its condition upon retrieval.

5.2.5. Launch Stand and Interface

The vehicle will interface with a launch stand using a launch lug epoxied to the side of the engine casing with thermal resistant epoxy. The launch lug will be a 1010 conformal rail guide, such as the one see in Figure 68. The launch lug will slide into the launch rail and slide out during launch.

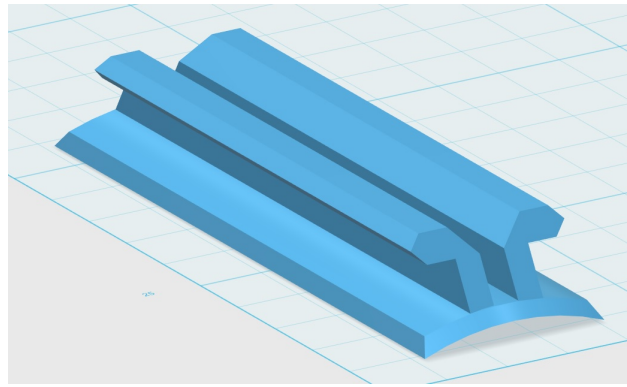


Figure 68. Launch Lug Example

The launch stand and rail must conform to derived requirements 2.1, 2.2, 2.3, and 5.1. The launch stand will be a Knight Manufacturing FLP-48 Model. This launch stand has a 48x45 inch footprint. The stand comes with a high temperature resistant 12 gauge steel blast deflector. The launch stand allows for a pivoting launch rod to the launch angle can be adjusted with a high degree of freedom, allowing launch stand corrections for variable terrain. This launch stand weighs approximately 12 pounds and collapses down, which allows it to be man portable. The launch stand can be seen in Figure 70.



Figure 69. Launch Stand²⁰

The launch rail will be a standard 1x1 inch Aluminum rail from Apogee Rockets that will attach to the launch stand.

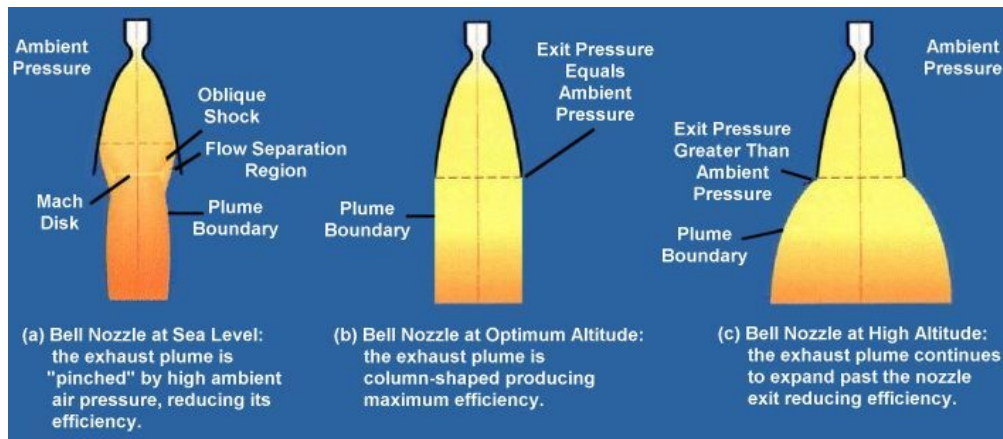


Figure 70. Close-Up Of Launch Rail²⁰

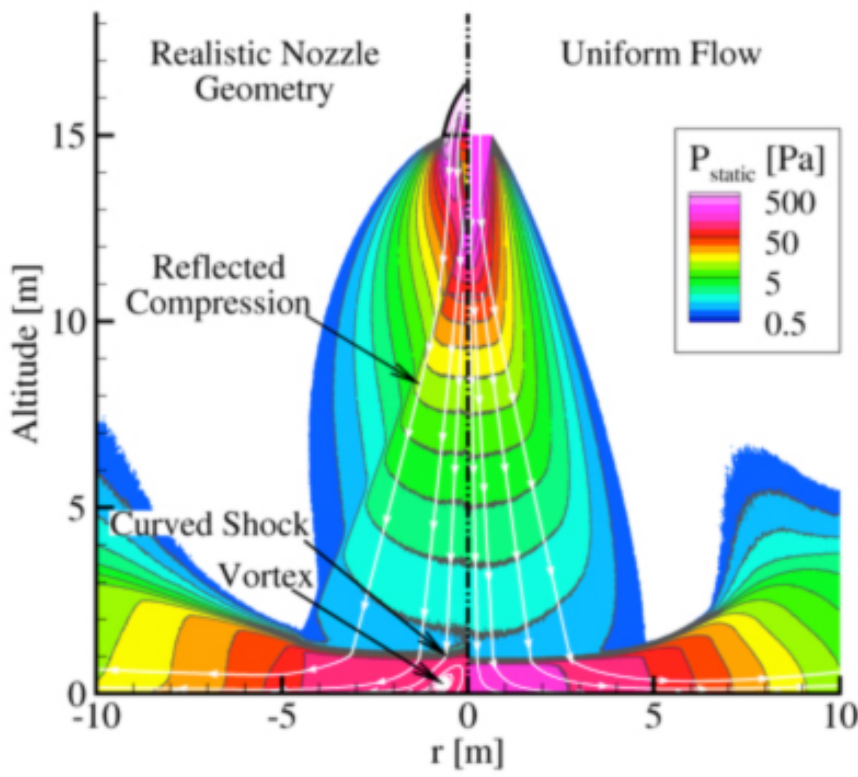
5.2.6. Exhaust: Thermal Effect and Plume Characteristics

The thermal effects of the rocket engine exhaust are the most critical project element at this point in time. Unfortunately every attempt to model the plume characteristics and thus gauge the temperature the vehicle will experience was unsuccessful. This is due to the complexities of solid rocket exhaust plume, which will be explained in detail in this section.

Dr. James Nabity, a professor in the Ann and H.J. Smead Aerospace Department who teaches undergraduate level propulsion and does research in propulsion systems, was the first source in the attempt to model the solid rocket thermal characteristics. Dr. Nabity was incredibly helpful, but unfortunately came to the conclusion that not enough was known about the propellant, the chamber, or the nozzle to determine any thermal properties. However he did point out that this rocket was designed for sea level and therefore, because Colorado is at a higher elevation the ambient pressure is less than at sea level. For this reason, the nozzle will be in an under-expanded state meaning the plume of exhaust from the rocket will expand more radially than it would at a lower altitude. This phenomenon can be seen in Figure 71 below.

Figure 71. Bell Nozzle Plume Expansion and Altitude Compensation³¹

A second attempt to model the thermal characteristics followed a NASA publication from 1966. This model would have been able to provide with plume diameter, but not temperature³². Unfortunately all of the elements needed to calculate the plume diameter required a static test firing of the engine to determine the characteristics. This static test firing will take place in January or February of 2019 - early next semester. A final factor that made it challenging to model the thermal and plume dynamics of the rocket engine was the oversimplification of most models. Figure 72 shows the complexity of plume dynamics and why they are near impossible to model analytically.

Figure 72. Realistic Nozzle Geometry versus Uniform Flow Simplification³¹

The thermal effects on the rocket and entire system could be catastrophic - for this reason there are several heat shields that will be considered and tested. The first method being tested during static thermal testing is aluminum tape coated with glass cloth. This aluminum tape being considered is rated for up to 600K of continuous heat and is the cheapest option. If this heat shield material is unable to effectively shield the vehicle from the motor exhaust during

testing, a "Lava Heat Shield" will then be tested. This type of heat shield is made of volcanic rock and is capable of shielding 80% of radiant heat. It is able to withstand direct temperatures up to 1400K. This method would be much more expensive but may prove to be necessary. Because the temperature of the exhaust is a maximum of 1700K right at the nozzle, there is a high confidence that this heat shield could effectively protect the vehicle from the exhaust. The motor exhaust will not be directly aimed at the vehicle and there will be a couple of inches between the nozzle and the vehicle. This means the exhaust will cool down significantly before interacting with the heat shield. Of course, this will all need to be verified during thermal testing.

5.2.7. Launch Regulations and FAA Compliance

For the vehicle to be tested, it must comply with a set of regulations and safety codes. The regulations pertaining to high powered rockets and unmanned aerial systems are enforced by the Federal Aviation Administration (FAA), National Fire Protection Agency (NFPA), and Academy of Model Aeronautics (AMA). The most important of these regulations that drove the design of the vehicle are tabulated below along with the specific code or regulation that they are derived from.

Requirement	Derived From
A member at launch shall have a level 1 certification for high powered rockets	NFPA Code 1127
Rocket shall be launched no greater than 20 degrees from vertical	NFPA Code 1127
Shall be launched through a NAR certified rocketry club at an approved launch site	NFPA Code 1127
Unmanned and does not create a hazard to any persons, property, or other aircraft	14 CFR Part 101.23
Operating requirements defined in Part 101.25	14 CFR Part 101.25
Proper notification is given to FAA as defined in Part 101.27	14 CFR Part 101.27
Aircraft shall be capable of manual controls override	AMA Doc #560
Vehicle shall weigh less than 55 lbs	14 CFR Part 101.41

§ 101.25 Operating limitations for Class 2-High Power Rockets and Class 3-Advanced High Power Rockets.

When operating *Class 2-High Power Rockets* or *Class 3-Advanced High Power Rockets*, you must comply with the General Operating Limitations of § 101.23. In addition, you must not operate *Class 2-High Power Rockets* or *Class 3-Advanced High Power Rockets* –

- (a) At any altitude where clouds or obscuring phenomena of more than five-tenths coverage prevails;
- (b) At any altitude where the horizontal visibility is less than five miles;
- (c) Into any cloud;
- (d) Between sunset and sunrise without prior authorization from the [FAA](#);
- (e) Within 9.26 kilometers (5 nautical miles) of any [airport](#) boundary without prior authorization from the [FAA](#);
- (f) In [controlled airspace](#) without prior authorization from the [FAA](#);
- (g) Unless you observe the greater of the following separation distances from any [person](#) or property that is not associated with the operations:
 - (1) Not less than one-quarter the maximum expected altitude;
 - (2) 457 meters (1,500 ft.);
- (h) Unless a [person](#) at least eighteen years old is present, is charged with ensuring the safety of the operation, and has final approval authority for initiating high-power [rocket](#) flight; and
- (i) Unless reasonable precautions are provided to report and control a fire caused by [rocket](#) activities.

[§ 74 FR 38092, July 31, 2009, as amended by Amdt. 101-8, 74 FR 47435, Sept. 16, 2009](#)

Figure 73. Operating Requirements for High Powered Rockets

§ 101.27 ATC notification for all launches.

No person may operate an unmanned rocket other than a Class 1 - Model Rocket unless that person gives the following information to the [FAA ATC](#) facility nearest to the place of intended operation no less than 24 hours before and no more than three days before beginning the operation:

- (a) The name and address of the operator; except when there are multiple participants at a single event, the name and address of the person so designated as the event launch coordinator, whose duties include coordination of the required launch data estimates and coordinating the launch event;
- (b) Date and time the activity will begin;
- (c) Radius of the affected area on the ground in nautical miles;
- (d) Location of the center of the affected area in latitude and longitude coordinates;
- (e) Highest affected altitude;
- (f) Duration of the activity;
- (g) Any other pertinent information requested by the ATC facility.

[Doc. No. [FAA-2007-27390](#), [73 FR 73781](#), Dec. 4, 2008, as amended at Doc. No. [FAA-2007-27390](#), [74 FR 31843](#), July 6, 2009]

Figure 74. Notification Requirements

After speaking extensively with the president of the closest National Rocketry Association and Tripoli Rocketry Association supported club, Mr. Joe Hinton of the Northern Colorado Rocketry club, the following dates were requested. Bureau of Land Management has agreed to let NCR use the land for these dates and Mr. Hinton is waiting on approval from the FAA, which will not prove to be any issue. This satisfies FR6. All of the dates listed in Figure 75 are available for RAPTR to launch on, with the full support of the rocketry club.

PROPOSED LAUNCH SCHEDULE 2019

Date(s)	Launch Site	Misc Info/Comments
Sat. Jan 5	Atlas	
Sat. Jan 12	Atlas	CU/CSU Senior Projects
Sat. Feb 2	Atlas	
Sat. Feb 9	Atlas	CU/CSU Senior Projects
Sat. March 2	Atlas	
Sat. March 9	Atlas	CU/CSU Senior Projects
Sat. March 30	Atlas	CU/CSU Senior Projects
Sat - Sun April 6 - 7	North	
Sat - Sun April 13 -14	North	CU/CSU Senior Projects
Fri-Sun May 3-5	North	Space Race Celebration
Fri-Sun May 31-June 2	North	Mile High Mayhem
Fri-Sun July 5 -7	North	High Skies in July
Sat – Sun August 3 -4	North	
Sat –Sun Sept 7 -8	North	
Fri – Sun Oct 4-6	North	Oktoberfest
Sat – Sun Nov 2 -3	North	
Sat Dec 7	Atlas	

Figure 75. Requested Launch Schedule with Northern Colorado Rocketry Club

5.3. Aerodynamics

5.3.1. Aerial Vehicle Design

For our aerial vehicle design, we needed to address 3 of our derived requirements. First we took a look at DR 1.1.5 which states "The vehicle must exhibit natural stability in all phases of flight." This requirement ensures that during the manual control phase, we are able to keep the vehicle under control and get it to where it needs to be. This also ensures that we are able to have an automatic control system that is able to control the vehicle using just the rudder and the elevator. Second was DR 1.1.2 that states "The vehicle must be capable of performing a turn with a radius of 350 feet." The purpose of this requirement was to account for any error in setting up the launch stand or in the manual control. This requirement stems from our maximum error in heading of 25 degrees. Given that our controller will engage with around 1000 feet of glide before we begin our imaging corridor, we are able to calculate the radius of the required turn. This was found to be 350 feet. Lastly, DR 1.2 states that the vehicle needed to achieve a glide slope of 5.7 degrees. This requirement ensures that after our glide of 3000 ft, we don't lose more than 300 ft of altitude.

The first task completed was CFD analysis of our vehicle of choice. To start, the SolidWorks model was imported into ANSYS. In order to facilitate the meshing process, gaps had to be filled and surfaces had to be refined. ANSYS' CAD modelling program has built in functions to refine the surfaces and simple extrusions could be used to fill the gaps in the model. After the model was refined, the model could be built into an enclosure. For the flow to be properly oriented when it interacts with the structure, the inflow wall had to be hemispherical with the end of the vehicle at the center. This was then followed by a large cylindrical tunnel in which the fluid was able to return back to its steady-state condition. Lastly was the outflow wall which was simply a plane. After this fluid volume was created, the vehicle could be subtracted from the interior leaving one more surface boundary, the vehicle. Figure 76 shows how this fluid volume looks.

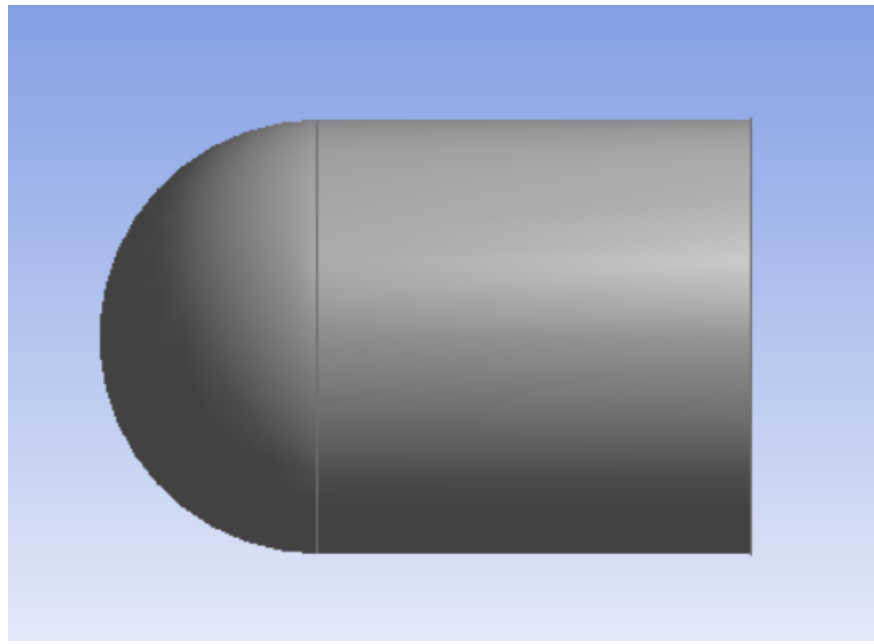


Figure 76. Fluid volume used for CFD analysis

The next step was to import this volume into the meshing program. Throughout much of the volume, we desired the mesh size to be rather large. This was done for two purposes. First it would decrease the computational cost and therefore decrease the time each simulation would take. Another reason was because we were limited to the educational version of this software which limits the number of elements to 500,000. Given our large vehicle and therefore large boundary this limit would've been easily reached otherwise. Near the vehicle is where we needed the elements to decrease in size to capture the details of the geometry as well as the rapidly changing fluid behavior in these regions. To be sure that we were in fact capturing most of the detail of the vehicle and not creating bad elements, some of the other specifications such as defeature size and element skewness were adjusted. The mesher was then able to be run and returned the mesh used for the stability simulations. Figures 77 and 78 show the mesh on the boundary surfaces of our volume and a wireframe of the mesh. We can see from this image that the mesh becomes much finer

on the boundary of the vehicle.

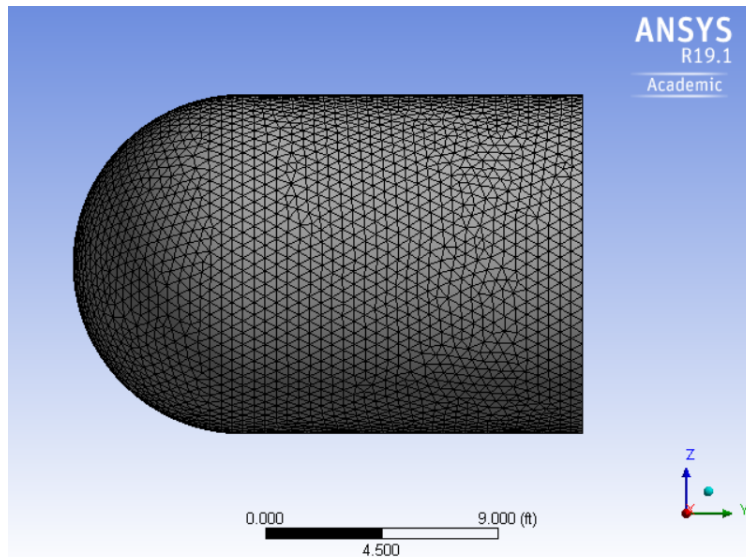


Figure 77. Mesh on the exterior boundary of the interior fluid volume

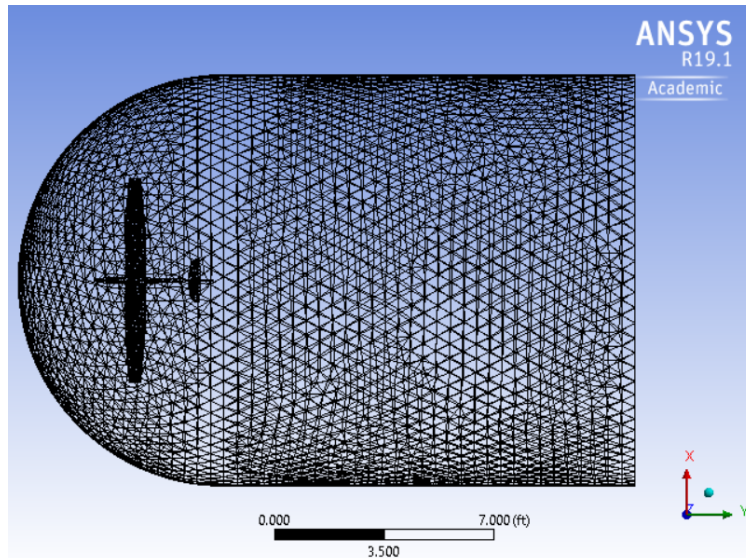


Figure 78. Wireframe view of the mesh generated

Once the mesh was created, we were able to bring it into Fluent to begin the simulation. The first thing to do was to define our models. Since we are operating in the incompressible regime, we do not need to define a method to solve for energy or temperature and we can leave density as a constant. Since we were interested in the turbulence generated by our model, we had to change our viscous model from laminar. For simplicity we chose a Spalart-Allmaras RANS model. RANS has an advantage in stability by introducing the eddy viscosity which increases overall viscosity in the solution. This allows us to visualize an averaged turbulence and due to the increased viscosity, increases the stability of the method. We then defined the boundary conditions on the surfaces we created earlier. The inflow was set to a Dirichlet inflow with a set velocity magnitude and direction. The vehicle boundary was also set to a Dirichlet boundary with zero velocity to strongly enforce no slip and no penetration. The wall was set to a Neumann boundary with zero flux normal and tangential. This confined the flow to the boundary but allowed it to flow as it would in the freestream. Lastly, the outflow was set to a Neumann outflow with a flux equal to the amount of flow through the system. Next we defined the solution method for our simulations. Due to the complex geometry of our vehicle, a simplified method

would not converge. For this vehicle, a coupled solution must be used. The solution was run with second order basis functions using an upwind method in velocity and second order basis functions in pressure. This higher order method serves to provide a quicker convergence rate with higher accuracy than a linear solver but takes more time per iteration. Since we were most interested in the accuracy, the second order methods were chosen.

With the setup for the simulations done, we were able to setup the reports for each simulation and run each case. We defined force reports in the x, y, and z directions and moments about each acting at the center of gravity. After these were defined, we could initialize the solver and run the solution. The solution was run until the system had converged, then the forces and moments were recorded for that state. The state was changed and the solution run again. Since we were interested in the vehicles behavior through stall, the angle of attack was varied from $\alpha = -22^\circ$ to $\alpha = 22^\circ$. This gave us our information about stall as well as in the linear region for stability analysis. Since we were only concerned with sideslip angle as it pertained to stability, we only varied sideslip angle from $\beta = -4^\circ$ to $\beta = 4^\circ$. Changing these angles was simply a matter of changing the components in each direction leaving the magnitude of velocity constant. The same was true about velocity and therefore was varied from $u = 130 \text{ ft/s}$ to $u = 140 \text{ ft/s}$. Changing the inflow velocity was simply done by changing the value of velocity magnitude leaving relative components constant. These simulations gave us the required information to calculate most of our stability derivatives.

In order to calculate the stability derivatives, the results from the CFD simulations were plotted vs their respective independent variable. Examples of this can be seen by figures 79 and 80. Because we are interested in the stability about our trim state, we performed a linear regression best fit in the linear region of these plots: $\pm 4^\circ$ about 0° . This same task was completed for all of the coefficients calculated during the CFD simulations. Because we are unable to add an angular velocity in the CFD simulations, we had to settle for the analytically calculated values for these stability derivatives. Although we were unable to directly back these out of simulation data, we were able to improve these results from the results from CFD. This improvement comes from some of the values that these stability derivatives depend on.

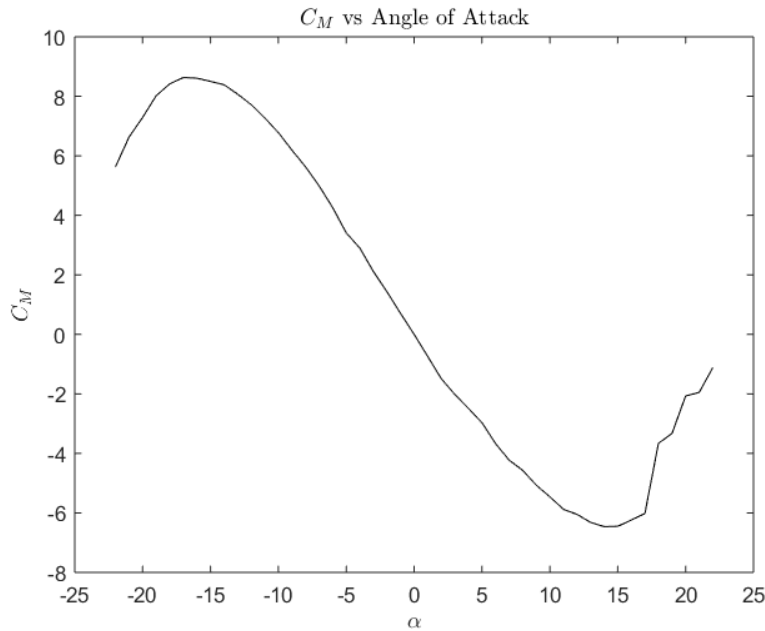
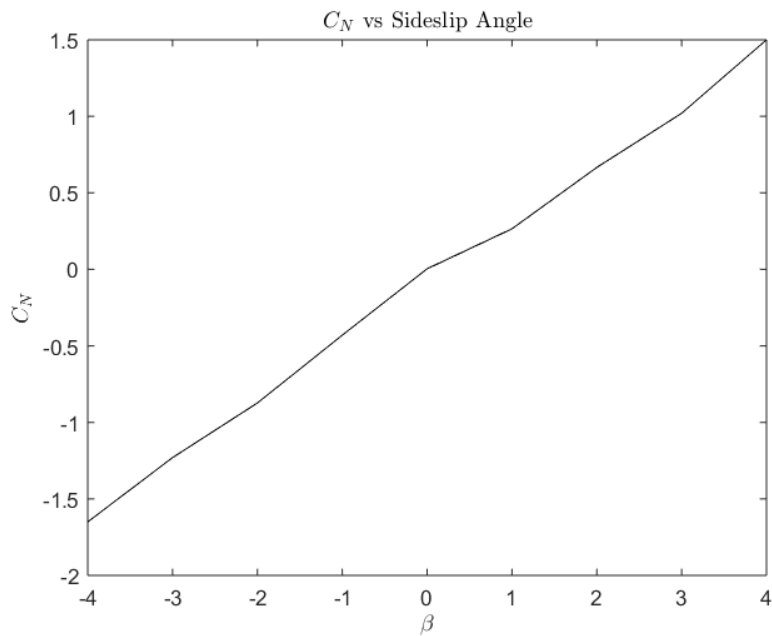


Figure 79. Coefficient of pitch moment vs angle of attack

After the completion of the CFD analysis and stability derivative improvement, we obtained the following stability derivatives given by tables 75 and 76. Note that these derivative are in English units and angles are in radians.

**Figure 80.** Coefficient of yaw moment vs sideslip angle

	C_x	C_z	C_m
u	$-4.58 \cdot 10^{-4}$	-0.0062	$-6.38 \cdot 10^{-4}$
α	0.1559	-4.0189	-0.4143
$\dot{\alpha}$	0	-1.4944	-5.1164
q	0	-4.9263	-16.866

Table 75. Longitudinal stability derivatives found in CFD analysis

	C_y	C_l	C_n
β	-0.7589	-0.1326	0.0248
p	-0.0124	-	0.0045
r	1.9344	0.0045	-0.0178

Table 76. Lateral stability derivatives found in CFD analysis

In order to confirm the behavior found in the CFD analysis, another method was used to find the stability derivatives. The second method used was a program called Digital Datcom. This was a program developed by the United States Air Force and completed in 1978. Datcom stands for Data Compendium and is used to calculate most of these stability derivatives. The input to this program is a text file with geometric data of the vehicle as well as flight conditions such as altitude and freestream mach number. This data includes the cross sectional area at various points along the vehicle as well as data for the wing such as airfoil shape, chord length, wing span, and dihedral angle. After the input file was typed up, the program could be executed and the output file created. In this output file contains the stability derivatives that can be seen in tables 77 and 78.

	C_x	C_z	C_m
u	$-4.58 \cdot 10^{-4}$	-0.0062	$-6.38 \cdot 10^{-4}$
α	0.1559	-5.8041	-1.6604
$\dot{\alpha}$	0	-2.3715	-8.0042
q	0	-8.6001	-24.3335

Table 77. Longitudinal stability derivatives found in Datcom analysis

	C_y	C_l	C_n
β	-0.1112	-0.0019	0.0347
p	-0.0139	-0.5091	-0.018
r	1.9344	0.0386	-0.0296

Table 78. Lateral stability derivatives found in Datcom analysis

These stability derivative were used to solve for vehicle stability using a eigenvalue locus plot and it was found that the vehicle exhibits natural stability during its glide phase. The next task was to ensure that during the thrust phase of the vehicle's mission we are also naturally stable. Since we are attaching the rocket motor fore of the vehicle's center of gravity, our system's center of gravity is shifted forward. Using simple calculations accounting for this shift in center of gravity we find that the vehicle is more stiff during the launch phase of the mission. We again choose to look at the pitch stiffness and yaw stiffness most heavily when determining our vehicle's stability as they have the largest effect. As can be seen in tables 79 and 80 our vehicle does, in fact, become more stable during the trust phase due to our rocket motor.

	C_{m_a}
Glide	-0.4267
Thrust	-2.7905

Table 79. Pitch stiffness during thrust and glide phases

	C_{n_β}
Glide	0.0248
Thrust	0.0283

Table 80. Yaw stiffness during thrust and glide phases

From the previous analysis, we can see that our vehicle will exhibit natural stability during both phases of flight and therefore satisfies derived requirement DR 1.1.5.

Using the data found for the forces in the x and z directions during the CFD simulations, we are able to create the coefficient of lift and coefficient of drag vs angle of attack plots for our vehicle using equations (5) and (6).

$$C_L = C_X \cos(\alpha) - C_Z \sin(\alpha) \quad (5)$$

$$C_D = C_X \sin(\alpha) + C_Z \cos(\alpha) \quad (6)$$

After the coefficients of lift and drag were found, they too were plotted vs angle of attack. These two plots can be seen in figures 81 and 82.

Possibly the more important result from the coefficients of lift and drag is the lift to drag ratio. This was needed in order to find this vehicles optimum angle of attack and its glide slope at each angle of attack. To find this was simply a matter of dividing the coefficient of lift by the coefficient of drag at each angle of attack. This, again, was plotted against angle of attack and can be seen by figure 83.

Moving on to derived requirement DR 1.2, we now have the required information in order to calculate the optimum glide slope angle for our vehicle. The equation to calculate this angle is given by equation (7).

$$\gamma = \tan^{-1} \left(\frac{1}{L/D} \right) \quad (7)$$

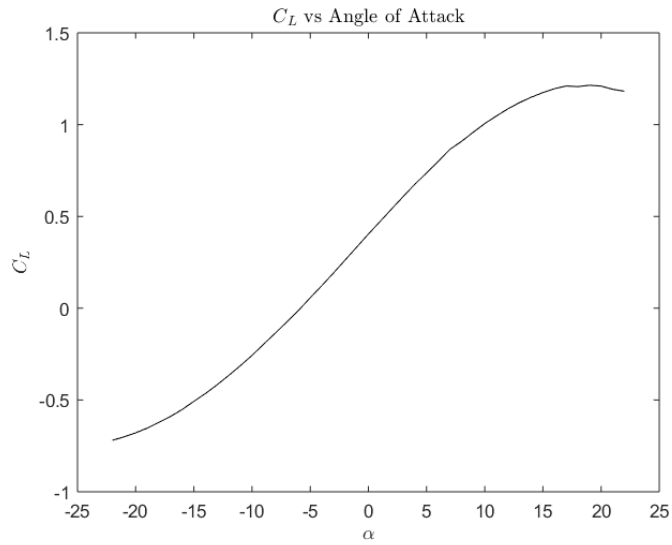


Figure 81. Coefficient of lift vs angle of attack

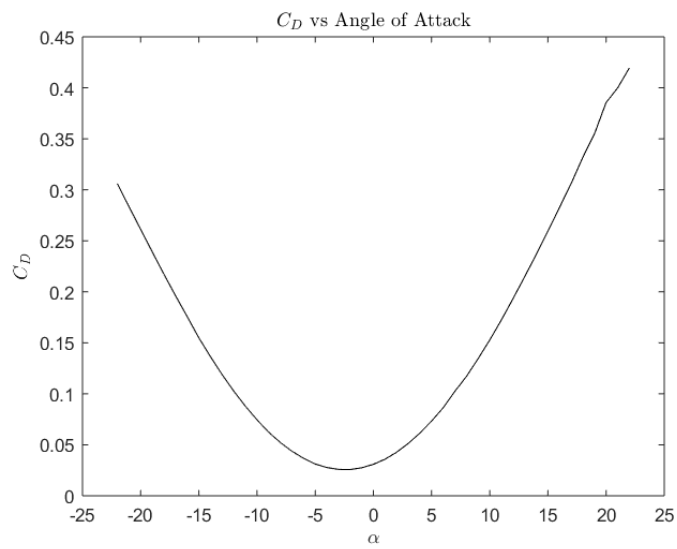


Figure 82. Coefficient of drag vs angle of attack

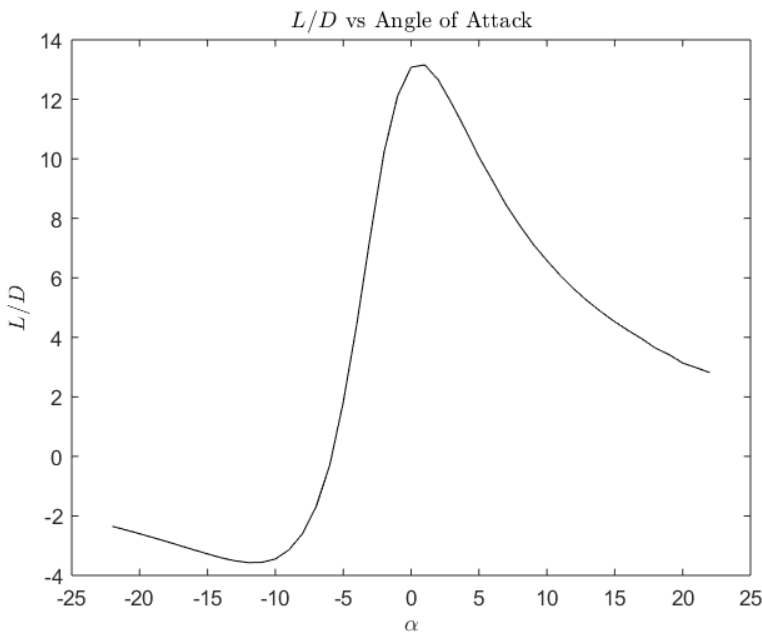


Figure 83. Lift to Drag ratio vs angle of attack

To find our minimum glide slope angle, we needed to find the maximum lift to drag ratio. This was done by finding the peak on the plot of lift vs angle of attack and was found to be 13. Plugging this value into equation 7, we found that we can achieve a glide slope angle of 4.4° . This is less than our required value of 5.7° and therefore satisfies derived requirement DR 1.2.

The last requirement we were to address was DR 1.1.2. This was the requirement stating that we must be able to perform a turn with a radius of 350 feet. This requirement was made to ensure that we would be able to correct for an error during launch. We used our maximum allowable launch angle of 25° and our estimate that we would burn out with 1000 feet before our imaging corridor. We were able to take these numbers and plug them into equation (8) in order to get our maximum radius turn to correct back to our planned flight path. This trajectory is shown in figure 84.

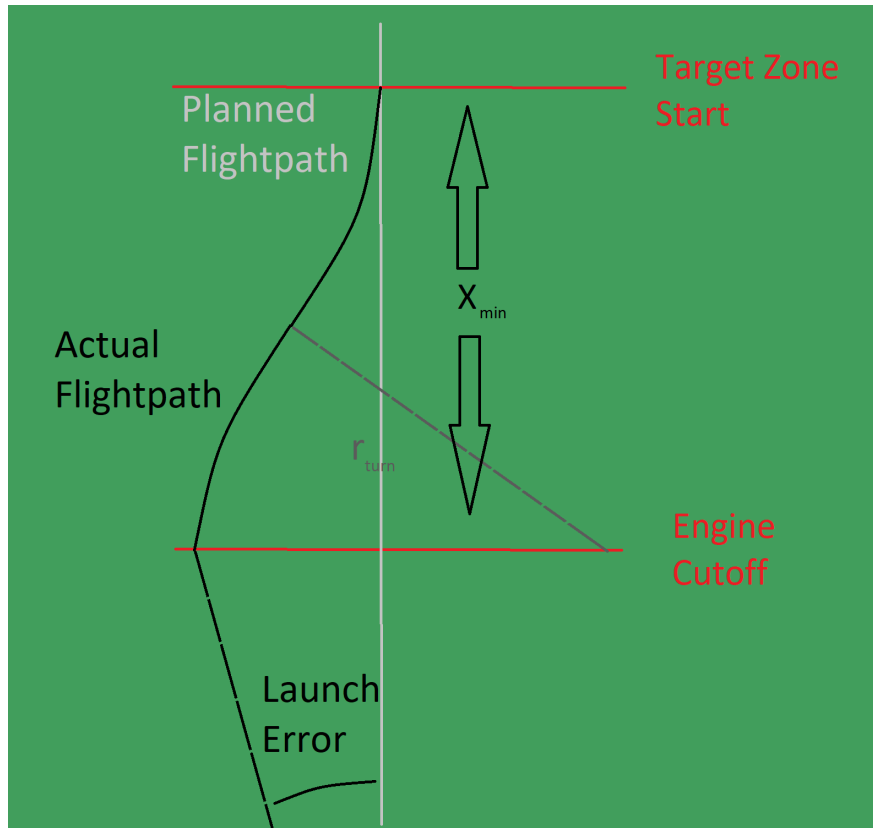


Figure 84. Course Correction Flight Path

The turn radius required to make this maneuver is the important factor for determining loading on the vehicle and quantifying performance limitations. The expression for the turn radius given the information shown in figure 84 was derived and is given in equation 8.

$$r_{turn} = X_{min} \left(2 \sin \left(\tan^{-1} \left(\frac{1000 \tan(\sigma_{launch})}{X_{min}} \right) \right) \right)^{-1} \quad (8)$$

To determine the feasibility of this maneuver given our design and flight conditions and to better describe the design requirements, we created a performance plot for the mission. This plot is shown in figure 85. The axes of the plot show wing loading (cruise weight divided by wing area) along the x axis and thrust to weight ratio on the y axis. For conventional aircraft, this is all there is, but RAPTR will only have thrust for a portion of the flight and after that portion the weight changes. To keep the performance plot sensible, these changes necessitated a scaling of the axes. The solution is to have the weights be the same. To do this, the y axis was scaled by a factor of take-off weight divided by cruise weight. This scales the value up, which makes sense because the thrust to weight ratio needs to be higher to equate the same thrust for a lower weight.

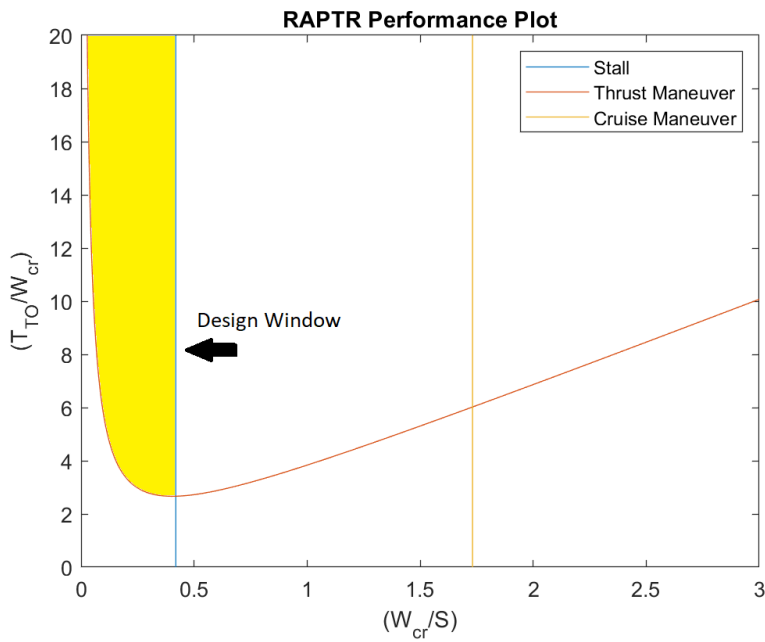


Figure 85. RAPTR Performance Plot

There are three lines plotted. The two most critical are the stall and thrust maneuver lines. These two bound the design window, highlighted in yellow. The stall line is set by picking a stall speed and making an assumption for the lift coefficient. The thrust maneuver line is defined by a circular ascent and turn to end up straight and level at 800 feet of altitude, it constricts both wing loading and thrust to weight ratio. The third line plotted is the cruise maneuver and relates to executing the turn described in figure 84. It is clear that this is not a very constricting mission requirement.

The vehicle must fit in the design window to be able to fly the mission. The Hyperflight Andreas' design point was computed and overlaid onto the design plot. This is shown in figure 86.

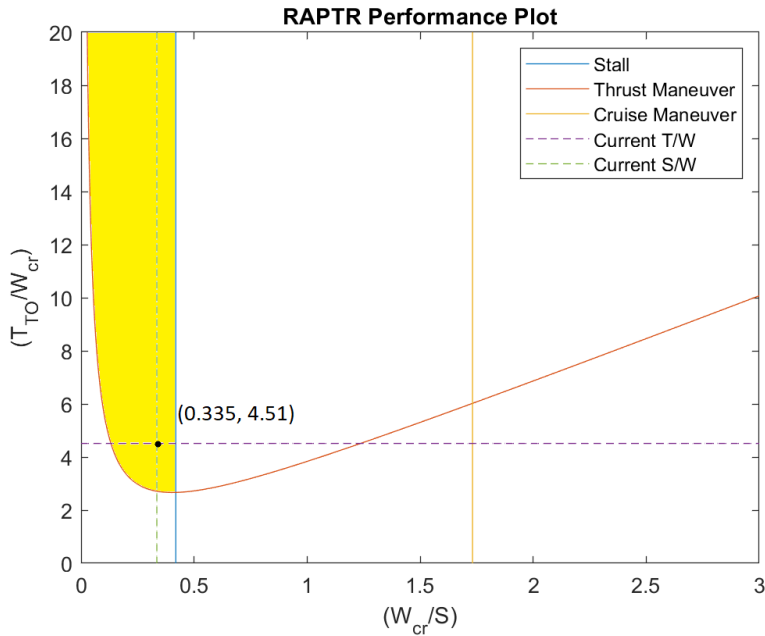


Figure 86. RAPTR Performance Plot overlaid with Andreas Design Point

It is clear that the Hyperflight, with a scaled thrust to weight ratio of 4.51 and a cruise wing loading of 0.335, fits

within the design window and will satisfy the mission requirements .

5.4. Electronics and Controls

The electronics are the nervous system and the controls are the brain of RAPTR. Both represent the median between the user's inputted mission objectives and the method through which RAPTR inevitably returns a geolocated target to the user. Electronics and controls work simultaneously to accomplish FR 1 stating that the system shall survey a 2,000 foot long and 400 foot wide corridor beginning 2,000 feet from the user and aligned with a user defined heading and FR 4 saying that the system shall identify a distinctly colored target and relay the target's latitude and longitude. Upon manual control of RAPTR during ascent the, the user switches to autopilot mode. The control system passes correction, servo outputs allowing RAPTR to glide along the user designated flight trajectory. RAPTR continually relays vehicle telemetry information to the ground station. This telemetry data is parsed to find the target's latitude and longitude.

5.4.1. Vehicle Electronics

5.4.1.1 Full Parts List

Table 81. Electrical components used in RAPTR.

Electrical Component	Weight	Dimensions	Voltage	Current
Turnigy Graphene Panther	0.110 lb	2.87x1.02x0.63 in	7.4 V (supply)	71.25 A (supply)
COTS Power Module	0.037 lb	0.98x0.83x0.35 in	5.37 V (supply)	2.25 A (supply)
Custom Power Board	0.04 lb	1.5x1.5x0.25 in	5/6 V (supply)	1/6 A (supply)
Pixhawk	0.088 lb	3.31x1.73x0.47 in	4.9-5.5 V	175 mA
Holybro GPS/Compass	0.045 lb	1.5x1.5x0.43 in	5 V	60 W
Airspeed Sensor	0.026 lb	0.94x0.67x0.39 in	5 V	25 mA
YKS 3DR Telemetry Radio	0.025 lb	2.20x1.07x0.55 in	5 V	100 mA
FrSky X8R	0.037 lb	1.85x1.06x0.55 in	5 V	125 mA
Futaba S3152	0.090 lb (x2)	1.57x1.50x0.79 in (x2)	4.8-6 V (x2)	10-1,000 mA (x2)

Overview

The vehicle electronics can be easily divided into four main categories: the power system, the Pixhawk, the peripherals, and the servos. These four groups of components work together to accomplish functional requirements 3 and 5, in addition to derived requirements 1,1,2, 1.1.3, 1.1.4, 1.1.5, 1.1.6, 4.2.1, 4.2.2, and 6.3.

Power System

The power system facilitates the completion of all objectives by providing necessary current to the other 3 modules of the vehicle. This power system is comprised of a custom board with 5V and 6V outputs and a power management board shipped together with the Pixhawk 4.



Figure 87. Turnigy Graphene Panther 2S LiPo Battery²².

The battery chosen to supply RAPTR's vehicle components with power is the Turnigy Graphene Panther two cell Lithium Polymer battery. This battery has a capacity of 950mAh which provides for an estimated idle battery life of 1.7 hours and operating battery life of 1.3 hours based on the current draw of all connected components. The 7.4V provided by this battery, while higher than what is required or desired by any individual component, provides appropriate headroom for voltage drops that may occur during current spikes. This prevents component "brown-out" situations where malfunctions can occur due to lower than required voltages being provided. The 7.4V supplied is stepped down to more appropriate levels before power is passed to the attached devices within the RAPTR vehicle. The maximum continuous discharge current of this battery is rated at 71.25A, far exceeding the approximate maximum current draw of all components at only 2.585A, meaning that no component should ever be current-starved during the duration of the mission. (DR 6.3)

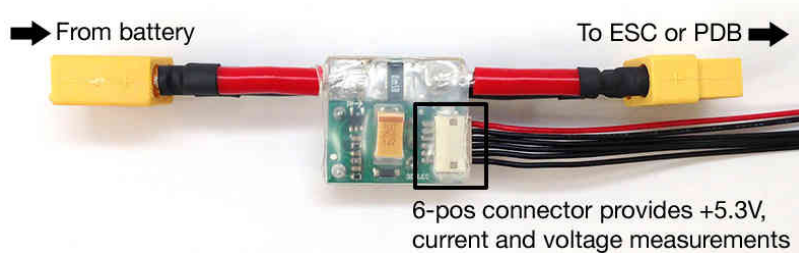


Figure 88. Pixhawk Common Power Module²³.

The COTS power management board provides primary power for the Pixhawk controller in addition to a measurement of the current battery voltage. This allows the current battery level to be displayed on the Mission Planner software at the ground station. It also provides current monitoring capability to assist in accurately compensating for interference with the compass (both internal and peripheral) from other devices. The COTS power management has a 2-pin connector that attaches directly to the JST-SYP discharge plug of the selected battery, a second 2-pin connector to provide unmodified battery power to our custom board, and a 6-pos connector to be plugged directly into the main Pixhawk power port. This 6-pos connection supplies the Pixhawk with a stable 5.37V power supply limited to a maximum current of 2.25A so long as the battery power source is capable of supplying this voltage and the current demanded by the Pixhawk. (DR 6.3)

The custom board includes a diode and a voltage regulator chip, as well as connection points for input battery power and output servo rail and supplemental Pixhawk power. The input power connection is wired to the COTS power management board's unmodified battery power output connector using 20-gauge single core wire with a maximum

current capacity of 6A. The servo rail power output will be connected to the Pixhawk servo rail power connection, also utilizing 20-gauge single core wire. The supplemental Pixhawk power output will be connected to the Pixhawk's USB power input pins utilizing a lighter single core 24-gauge wire capable of safely carrying 3.5A of current. (DR 6.3)

The custom board's diode has a forward voltage drop of 1.4V, allowing us to convert the 7.4V battery output down to the desired 6V for the Pixhawk servo rail. The maximum current rating of the chosen diode is 6A, far exceeding the approximate 2A current requirement from two stalled servo motor. It is important to note that the Pixhawk and its peripherals will be unable to use the servo rail input as a third power source since the maximum servo rail input voltage for this use case is 5.7V. Consequently, the zenar diode required to use the servo rail as an additional source of power will not be added. (DR 6.3)

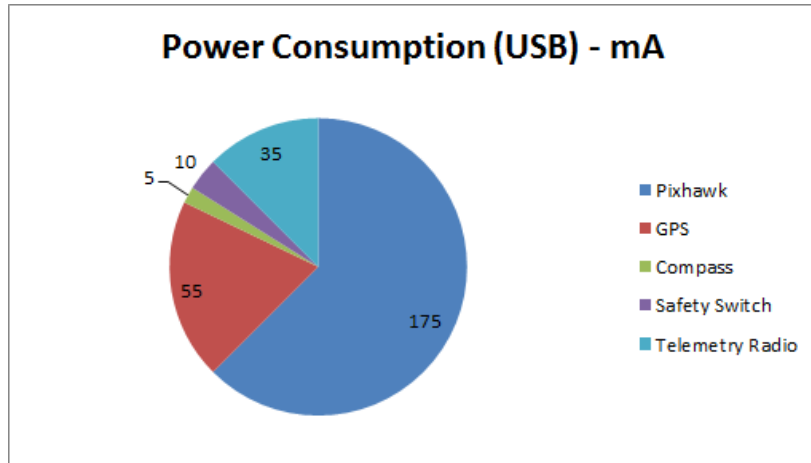


Figure 89. Pixhawk USB Power Consumption²⁴.

The maximum current draw of the Pixhawk over USB power, combining measured USB power draw (Figure 89) with the maximum 125mA current rating of the FrSky X8R, is approximately 405mA. The Pixhawk and its connected peripherals may be powered from the Pixhawk USB power input with a source ranging from 4.1-5.7V. The voltage regulator provides a steady 5V output with a maximum sustained current rating of 1A, making it an ideal backup power source with appropriate voltage and adequate current headroom to ensure seamless power delivery in the event of the (DR 6.3).



Figure 90. Pixhawk 4 Flight Controller²⁵.

Pixhawk 4 Flight Controller

The Pixhawk 4 flight controller acts as the "brain" of the entire system, controlling the power and signal sent to various connected devices. All of the calculations are controlled by a 32-bit Arm Cortex-M7 processor running at 216 MHz with 512 kilobytes of RAM and 2 megabytes of memory. All communications protocols are handled by a separate processor, an Arm Cortex-M3 running at 24MHz with 8 kilobytes of SRAM available. The Pixhawk 4 also includes several onboard sensors such as a pair of inertial measurement units with accelerometer and gyroscope, a magnetometer, and a barometer. These two IMUs aid the ground station geolocation software by providing critical information about the vehicle attitude at the time a photograph was taken. (DR 4.2.2)

Peripheral Devices

The third primary portion of the vehicle electronics is all of the peripheral devices connected to the Pixhawk controller, which includes the following items: GPS/Magnetometer, Safety Switch, Buzzer, Airspeed/Temperature, Telemetry Radio, and RC Radio.



Figure 91. Holybro GPS Module²⁶.

The GPS/Magnetometer unit is comprised of a NEO-M8N GPS/GLONASS receiver with integrated IST8310 magnetometer. This is connected via the included and attached cable to the Pixhawk's GPS port. This allows the user to determine the location of the vehicle to within 8.2 feet in addition to velocity within 0.164 ft/sec and magnetic heading to within 0.3 degrees. This data is used alongside that from the integrated Pixhawk IMUs to provide critical reference information for the ground station's geolocation software. (DR 4.2.1)

The Pixhawk requires both a safety switch and a Buzzer for operation. Both are included within the Holybro GPS Module selected for use in the RAPTR vehicle, and utilize the same connections. The safety switch is used to enable and disable all of the commands sent from the Pixhawk to the motors or servos attached via the servo rail. It also disables motor and servo outputs via the CAN bus, but this is not applicable to our project. This serves to ensure control surfaces are not unintentionally active. When the Pixhawk status light blinks intermittently the servo output is disabled, however once the safety switch has been pressed the status light remains on continuously to indicate servo and motor outputs have been enabled. The buzzer allows the Pixhawk to play tones in response to user commands or changes in mode. This assists the user when setting up the Pixhawk for first time flight, allowing for faster deployments to meet the 3 minute time limit. (FR 5)



Figure 92. Airspeed and Integrated Temperature Sensor²⁷.

The airspeed and temperature sensor provides necessary information for the Pixhawk flight controller's autonomous control software. This will be connected to the I2C input port of the Pixhawk using the included cable and a cable extension (if necessary). The sensor will be mounted such that the metal tube protrudes from the tip of the vehicle, with rubber tubing providing a more flexible connection to the pressure sensor itself. Using the airspeed information, combined with vehicle attitude and location data, the Pixhawk can adjust the glider's attitude to keep it on course within our flight corridor without leaving user set bounds for altitude (minimum and maximum) or minimum velocity. The temperature sensor specifically allows for corrected from measured pressured to true airspeed based on the changing density of air with respect to temperature. With these corrections applied the airspeed sensor is accurate to within +/-3.28 ft/s, allowing for accurate and precise measurement of airspeed. (DR 4.2.1)



Figure 93. 3DR Radio Telemetry Set²⁸.

The YKS 3DR telemetry radio module operates on the 915 MHz band to relay telemetry data from the vehicle back to the ground station and receive navigation commands intended for the Pixhawk from the ground station. It consists of a pair of combination transmitter/receivers, a ground module and an air module each with their own antenna. The ground module directly plugs into the ground station computer with its attached USB connector, while the air module connects to the Pixhawk's "TELEM1" port through the included cable. The maximum transmission power of each module is 20dBm (100Mw), and the paired modules can communicate wirelessly at a data rate of up to 250Kbps. They will be configured within the Mission Planner software on the ground station to transmit with the full 20dBm of power at a data rate of 64Kbps to maximize the communication range. The maximum duty cycle of the transmission will be set to 100% to avoid limiting the bandwidth, and the communications protocol will be set to MAVLink with a maximum transmission length of 33 milliseconds to minimize latency. Standard 3DR communication modules retain greater than 40% of their original signal strength at ranges of up to 8,200 feet, but if deemed necessary during initial communications testing the telemetry radio may be replaced with a RFD900 transceiver set which retains greater than 97% original signal strength at distances of 10,000 feet. The Mission Planner software on the ground station will utilize this telemetry radio pair to transmit GPS waypoints and communicate other relevant navigation and telemetry information. The 915MHz band is not utilized by any other radio present on the vehicle, eliminating communication interference concerns. (DR 1.1.2, 1.1.3, 3.1, 3.2, and 3.4)



Figure 94. FrSky X8R RC Transceiver²⁹.

The FrSky X8R transceiver serves as both a method for manual control during the ascent phase and as a backup in the event that MAVLink radio communications have been lost. The X8R communicates directly with a handheld remote controller such as the FrSky Tanaris X9D and relays control commands in addition to information on battery pack voltage, instantaneous current consumption, total current consumption, and GPS status. The X8R module present on the vehicle directly plugs into the Pixhawk TELEM2 port using a Pixhawk to FrSky telemetry cable. The antenna included with the X8R is printed directly onto a circuit board to help increase range and reduce size, allowing for a specified operating range of greater than 4,920 feet. This radio operates on the 2.4GHz band with the ability to select any channel within this band to eliminate interference. The X8R also supports the option to include a user-defined failsafe maneuver in the event that communications are lost completely. (DR 1.1.5, 1.1.6, 3.1.1, and 6.3)



Figure 95. Futaba S3152 Servo Motor³⁰.

Servos

The final electrical components of the RAPTR vehicle are the two Futaba S3152 servo motors, designed for high torque, high speed applications. Figure below shows the required torque to achieve maximum deflection of both the elevator and rudder as a function of the vehicle's speed, along with a reference point for the maximum torque output of the S3152 motors when supplied with 4.8V power.

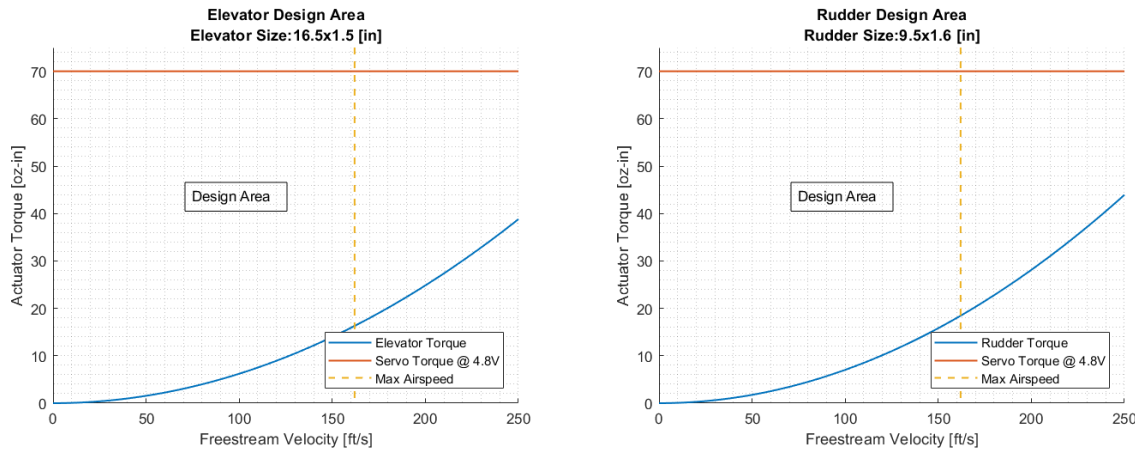


Figure 96. Airspeed vs Control Surface Torque.

Despite the clear capabilities of the servo when powered with 4.8V, the S3152 motors onboard the RAPTR vehicle will be provided with 6V from the Pixhawk servo rail. This allows adequate overhead to account for both increased airspeed over the control surfaces while the motor burns and mechanical losses present in any system. When provided with a 6V power source the S3152 motors can generate up to 87 oz-in of torque, more than four time larger than the required torque for full control surface deflection at our maximum airspeed.

The servos will be connected utilizing standard PWM cables, utilizing PWM male/female connectors and 22-gauge single-core wire, from the Pixhawk servo rail output connections. This cable is capable of carrying a maximum of 5 amps of current, providing significant overhead for the approximate 1-3A stall current of the servos. This cable's third wire provides the pulse-width modulated control signal that instructs the servo of the desired direction and speed of motion. The servo output shafts will be connected to the control surfaces by means of small steel cables contained within special channels in the airframe to avoid interference with electrical wiring. The servos are capable of rotating at 64.8 RPM, or 0.18 seconds per 60 degrees of motion, allowing for rapid response to control inputs and outside influences while traveling at high speeds. (DR 1.1.6)

5.4.1.2 RAPTR Electronics Diagrams

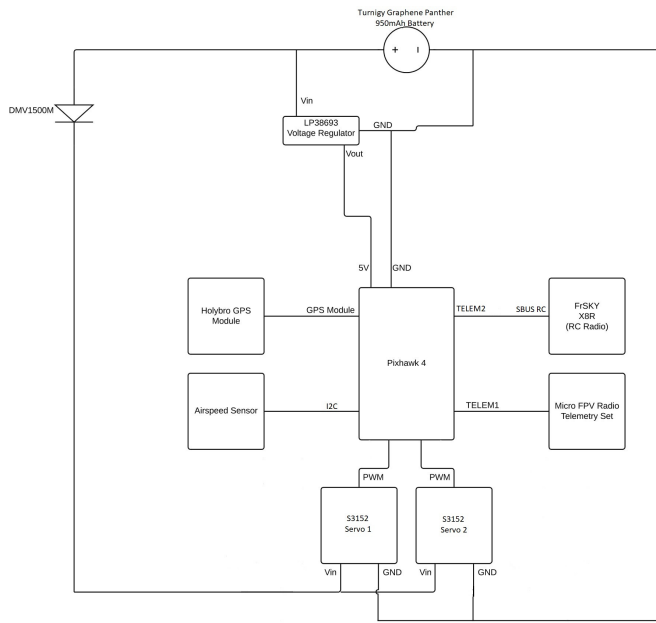


Figure 97. RAPTR Circuit Diagram.

Circuit Diagram

The fundamental circuit diagram for the RAPTR vehicle's electronics is shown above in Figure 97, with several items of importance that need to be highlighted.

The servo Vin and GND inputs are shown as direct connections to the diode on the custom power management board, while the physical wiring will pass this connection through the Pixhawk servo rail. It was drawn in this fashion to avoid confusion with the power sources for the Pixhawk itself and to more clearly indicate that the power passing through the diode is supplied only to the servo motors and not to any other device on the RAPTR vehicle.

The connection from the Pixhawk to the FrSky X8R contains two labels, TELEM2 and SBUS RC, to indicate the names of the connected ports on both the Pixhawk and the X8R. The other connections are labeled only once because the wires are either permanently attached to the peripheral module or there is only one unlabeled port available on the peripheral module for connections.

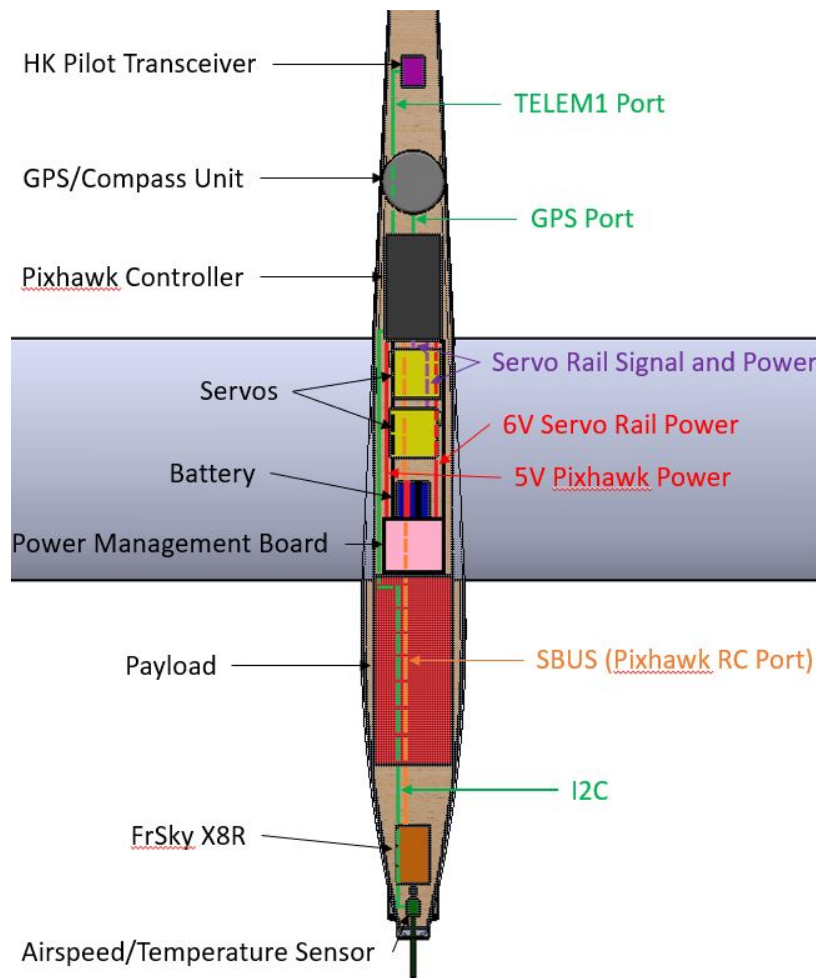


Figure 98. RAPTR Wiring Diagram Overlay.

A wiring diagram for the electronics overlaid onto the fuselage of the RAPTR vehicle is shown above in Figure 98 labeled with important devices and connections. There are a few key takeaways from this diagram.

The first is that the servos are placed as far away from communication devices as possible to minimize the noise they produce. Servos are notoriously noisy devices, a consequence of their high current draw and PWM controlled operation. While the telemetry radio (HK Pilot Transceiver) and RC transceiver (FrSky X8R) are robust devices, the magnetometer contained within the GPS/Compass module is more susceptible to the effects of nearby electromagnetic interference. For this reason the GPS/Compass module was placed on the surface of the vehicle and in the largest gap available between RF generating devices including the payload. The skin of the vehicle, while radio transparent, will help attenuate some small amount of noise and the unobstructed view of the sky will assist with GPS accuracy and reliability.

The battery and servo motors are placed as near to the vehicle's center of gravity as is possible owing to the fact that they are the heaviest individual components. Should a mounting solution for these components fail, it's imperative that the changing moment created by any movement of them within the airframe be minimized by shortening the moment arm as much as possible without interfering with the space allocated for the payload. Their slightly rearward position also aids in moving the vehicle's center of gravity slightly closer to the center of lift, especially during the ascent phase when the rocket motor is still attached.

5.4.2. Pixhawk IMU Uncertainty

Since the Pixhawk weights each sensor measurement based off of that sensors error, a system error is difficult to model. Instead the physical hardware is tested and the results are observed. The Pixhawk was placed on a level surface so that reference point was zero roll and zero pitch. After approximately 1 minute the Pixhawk was taken through

various extreme rotations and vibrations in an attempt to disrupt the IMU readings. These motions are depicted on the right hand side of Figure 99 and Figure 100. The Pixhawk was then left to rest on the level surface once more for approximately ten minutes. The left hand side of Figure 99 and Figure 100 depicts the full test. The mean value of the first and last thirty seconds is computed to demonstrate no significant deviation from nominal. The roll data deviates a maximum of 0.95° and the pitch data deviates a maximum of 1.782° .

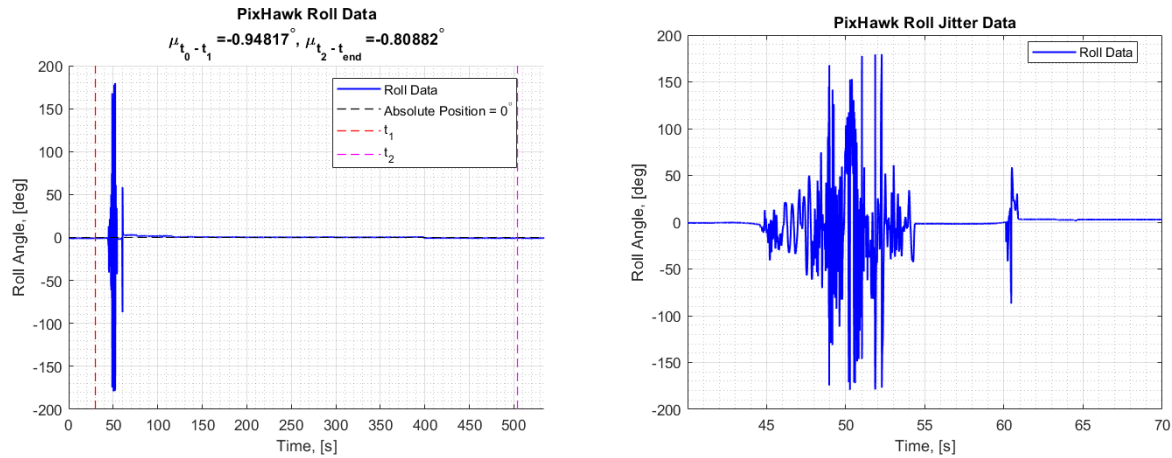


Figure 99. Experimental Pixhawk roll test data.

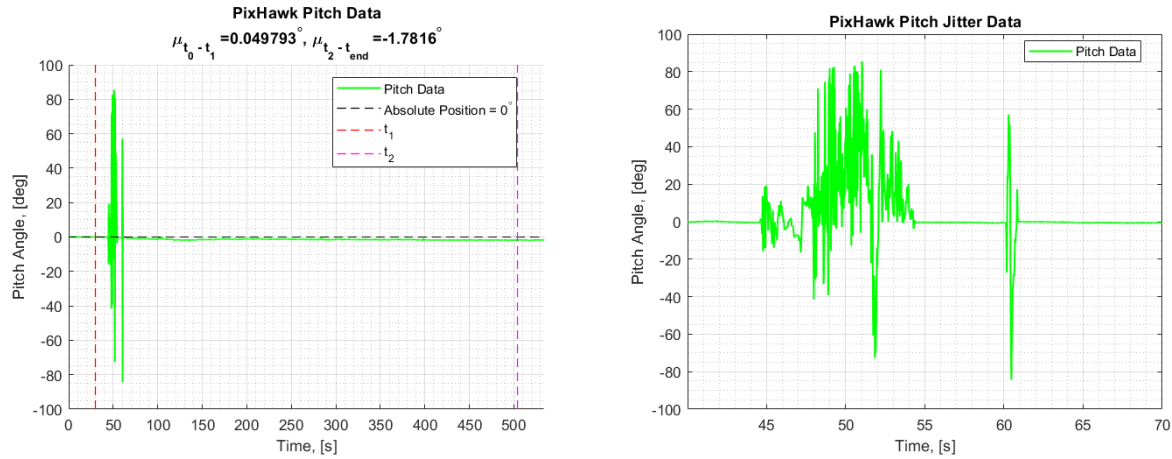


Figure 100. Experimental Pixhawk pitch test data.

5.4.3. Transmission and Reception

A key component in the mission success of RAPTR lies in effective communication between the ground station and the payload or vehicle. RAPTR must be able to transmit and receive the following information:

- GPS navigation waypoints from the ground station for the Pixhawk's ArduPilot autopilot software (DR 1.1.3)
- Manual control commands from an RC controller for the X8R RC transceiver (DR 1.1.5)
- Telemetry data from the vehicle for the ground station software (FR 3)
- Image data from the payload for the ground station software (FR 3)

While the transmission of image data from the payload will be handled by the ECE Team as part of their payload requirements, the transmission of all telemetry data and control inputs will be handled by the AE Team. As a result there will be three different communications devices present onboard the vehicle as seen in Figure 82, with two falling within the vehicle electronics described above and one integrated into the imaging payload provided by the ECE Team.

5.4.3.1 TX/RX Hardware

Table 82. Electrical components used in RAPTR.

TX/RX Component	Device's Team	Transmission Frequency
YKS 3DR Telemetry Radio	AE Team	915 MHz
FrSky X8R RC Transceiver	AE Team	2.4 GHz
Payload Transceiver	ECE Team	2.4 GHz

The primary concern with these communications methods is the potential for interference between the two 2.4GHz band transceivers onboard the vehicle, the X8R and the payload itself. To explain the process of eliminating the interference potential it is first necessary to provide some background on the 2.4GHz communication band.

The ISM 2.4GHz band is not just one frequency of communications at the 2.4GHz frequency, but a range of frequencies beginning at 2,400MHz and ending at 2,500MHz. This range of frequencies is subdivided into a total of 14 different channels (11 allowed within the US), with each channel having a lower frequency, upper frequency, and center frequency. Each of these channels is 22 MHz wide from lower frequency to upper frequency, with the transmitter and receiver for a given channel tuned to that channel's center frequency by means of a band-pass filter with a matching center frequency. These channels begin with a center frequency of 2,412MHz and continue in 5MHz increments - 2,412, 2,417, 2,422, etc. - all the way up to channel 11 at 2,462Mhz (the highest US-legal channel) and beyond to channel 14 at 2,484MHz (the highest 2.4GHz channel frequency worldwide).

Band-pass filters, however, are unfortunately limited in how narrow a frequency band they can transmit due to the physical properties of inductors and capacitors. An ordinary band-pass filter will have peak transmission at its center frequency with an exponential decrease in signal intensity as the frequency moves away from the center frequency. This signal attenuation behavior can be graphed as a measure of signal power (dBm) across a frequency spectrum, as seen in Figure 101. When graphed in this fashion a band-pass filter's output will appear as a bell curve centered on the filter's center frequency.

Standard 2.4GHz band band-pass filters are capable of completely filtering signals with a frequency 11MHz faster or slower than the filter's center frequency. This means that with an effective channel with of 22MHz and channels running from 2,412MHz to 2,462Mhz there can be a maximum of 3 different channels simultaneously transmitting and receiving with no interference from one another - channels 1, 6, and 11. If one transceiver pair communicates on channel 1 and a second communicates on channel 11 within the 2.4GHz band there will be no overlap between the two frequencies. This allows for both 2.4GHz transmissions to operate at maximum bandwidth without experiencing any interference from the other.

The most common application, by far, of the 2.4GHz band and its associated channels is for use in Wi-Fi networks across the globe. Every wireless router on the planet has the ability to transmit on these channels, and it's common to have multiple routers operating in close proximity such as in apartment or office complexes. An example of a Wi-Fi spectrum graph displaying local 2.4GHz networks and their associated channels and signal strengths may be seen below.

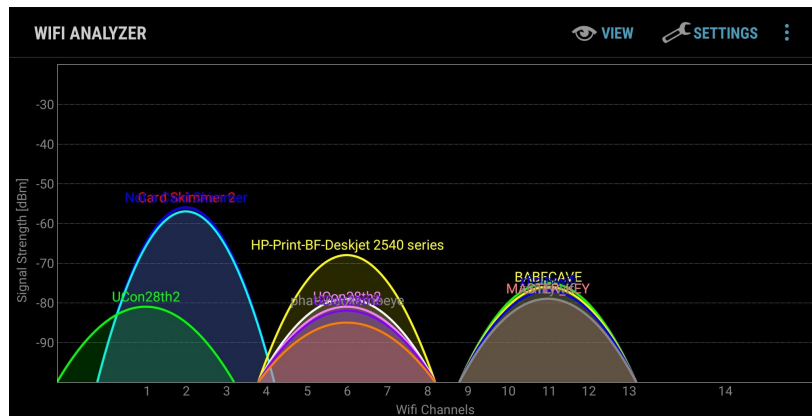


Figure 101. Example of a Wi-Fi Spectrum Analyzer Output.

Similar to the Wi-Fi networks visible in the above figure, the two 2.4GHz communications devices onboard the RAPTR vehicle will be able to select different channels from one another to eliminate interference concerns. You can see, by looking at the signal strength of the green, salmon, and brown networks, that these three channels are capable of operating simultaneously without interference. During communications testing the AE Team and the ECE Team will work together to determine which channels will be utilized. The current planned solution is to simply utilize channels 1 and 11 to avoid confusion, which will be more than sufficient to ensure there is no overlap between the two signals. This will allow both the ECE Team and the AE Team to transmit and receive their necessary data without interference in accordance with derived requirement 3.1.1.

5.4.4. RAPTR Control via Pixhawk

Though control is divided into manual user control during ascent and autonomous control during glide, both these phases of flight utilize the same control principles. RAPTR's control system breaks down FR 1 to accomplish the following components of DR 1.1 as depicted in Table 83. Holistically, the controls primary objective is to command RAPTR to the user's specification. The Pixhawk accompanied by ArduPlane comprises the controls hardware and firmware platform, respectively. The controls sub-team focused on the following objectives this semester with the purpose of understanding and deriving all information necessary to create a successful control architecture next semester.

1. Research of Pixhawk control code
2. Understanding of Pixhawk control architecture
3. Development of RAPTR control dynamics to include PID gain approximations

Functional Requirement 1: The system shall survey a 2,000 foot long and at least 400 foot wide corridor beginning 2,000 feet from the user and aligned with a user defined heading.		
Derived Requirement	Description	Verification & Validation
1.1	The vehicle shall be capable of navigation to and along the corridor from a launch heading error of up to 25 degrees.	Verification Flight Testing
1.1.2	The vehicle shall be autonomously controlled	Acceptance Testing
1.1.3	The vehicle shall be capable of navigation and control along specified GPS waypoints	Verification Flight Testing

Table 83. Derived Requirements From Functional Requirement 1

5.4.5. ArduPlane Control Code

At a high level, the ArduPlane control code is a software outline malleable to a variety of fixed wing aircraft designs. The purpose of discussing the ArduPlane's control code is not to layout the code implemented in RAPTR but to demonstrate a high level understanding of Arduplane. The primary control focus of next semester is the development of this code. An in-depth description of ArduPlane's code is not discussed in detail throughout this report but may be found on ArduPlane's website¹.

The AndREaS glider is a fairly conventional design which significantly simplifies the process of fusing the AndREaS glider with the Pixhawk. RAPTR's three design variances from a traditional fixed wing aircraft are the addition of a solid rocket motor, polyhedral wing, and absence of ailerons. The solution to dealing with a solid rocket motor was addressed earlier through implementing high-speed/high-torque servos. A polyhedral wing and absence of ailerons are linked design deviations from traditional designs. Again, as mentioned in section 5.3, the AndREaS is able to initiate a coordinated turn simply by manipulating the rudder because of its polyhedral design. Though this is not a conventional turning method with ailerons, the Pixhawk's control surface manipulation may be adjusted accordingly to compliment the AndREaS model.

Figure 102 depicts another RC model glider aircraft that utilizes only elevator and rudder control. It should be noted that this example is not the airframe that will be used for RAPTR but merely provides an example of a similar glider aircraft, sporting an elevator/rudder configuration, capable of being controlled through ArduPlane with the Pixhawk. This configuration is common among gliders and possesses heritage among RC aircraft as well. ArduPlane is capable of roll control through the rudder by mixing the roll and yaw state inputs and adjusting the rudder accordingly. The

mixing amount is scalar variable that weights how much rudder deflection is necessary to induce a given roll. Next semester will consist of experimentally testing RAPTR with various glide tests to tune this value precisely.



Figure 102. UMX Radian BNF remote control glider³.

Another essential area of research this semester and development next semester is the ArduPlane's autonomy through following user defined GPS waypoints. For a bit of background, ArduPlane displays mission critical information in a GUI called Mission Planner. Figure 103 depicts Mission Planner and functions similar to a heads-up display. This image is presented not to explain the coding necessary for RAPTR's mission but to give the reader a visual picture of the firmware being worked with.



Figure 103. Visual of ArduPlane's Mission Planner GUI.

Similarly, Figure 103 serves a similar purpose in presenting the definition of the GPS waypoints in ArduPlane. The GPS waypoint configuration defined in Figure 104 is more complex than RAPTR's mission profile as RAPTR's trajectory is merely along a given heading.

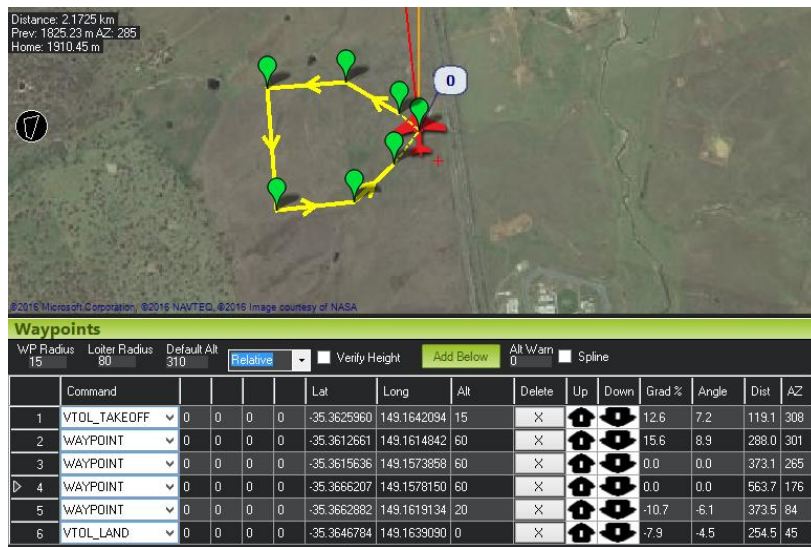


Figure 104. Visual of ArduPlane's Mission Planner GUI.

Table 84 lists the spacial inputs necessary to define RAPTR's trajectory through GPS waypoints. All other flight characteristics, such as gradient %, distance, and azimuth are computed from the spacial waypoints. It is crucial to note that if the vehicle is displaced from its planned trajectory then the vehicle will turn back toward the designated path to right itself. This is particularly important as some heading variability will occur on launch but this variability will be corrected by the autopilot and within the limitations of the vehicle (see section 5.3). **Implementation of the Pixhawk autopilot satisfies DR. 1.1.3**

Table 84. ArduPlane's autonomous GPS waypoint interface.

GPS Waypoint Inputs
Latitude
Longitude
Altitude

5.4.6. Pixhawk Control Architecture

The Pixhawk is a complicated IMU performing an exceptional amount of measurements, calculations, and verifications at a high frequency rate in order to keep the vehicle it controls aloft. Due to the Pixhawk's complexity, it is very difficult to appropriately model the Pixhawk system, even subsystems, as a whole. Though a comprehensive model is beyond the time constraints of this class, it is nevertheless extraordinarily beneficial to understand how the Pixhawk works to properly format the Pixhawk to RAPTR next semester. Figure 105 graphically depicts the Pixhawk control architecture.

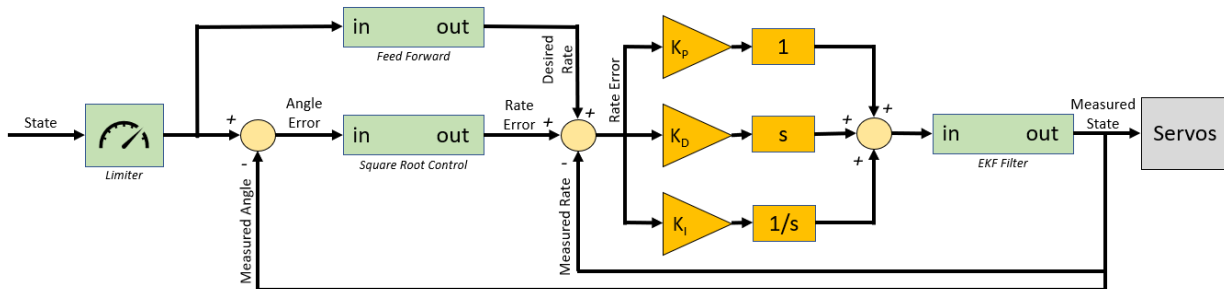


Figure 105. Functional block diagram of the Pixhawk control architecture.

The above control architecture is uses telemetry gathered by the Pixhawk's IMU and external sensors to interpret the current flight conditions of the aircraft, compare the desired flight conditions to the measured flight conditions, and command the servos attached to the rudder and elevator accordingly. This process begins with the Pixhawk accepting an inputted, desired state, shown on the left side of Figure 105. For simplicity, consider the case where the Pixhawk is attempting to determine only the vehicles attitude and not position. In this instance the state is composed of the roll angle, pitch angle, and yaw angle. This state is first passed through a limiter. The limiter consists of any user or system imposed restrictions on the state. These restrictions may include bank angle limits, pitch limits, etc. but are more geared toward the positional limits (such as a user defined bounding volume for the vehicle).

The Pixhawk then passes this desired state in two separate directions. The first direction is through a Feed Forward for later use and in the second direction the difference between the desired state and measured state is computed. This difference is referred to as error. This angle error is passed through a square root controller to yield the rate error. The rate error is used to limit the attempted rate of change to keep the vehicle under certain acceleration levels to prevent damage. The square root controller's output, desired rate, and measured rate is computed and passed into the Pixhawk PID. The resulting state is passed into an Extended Kalman Filter (EKF).

It is important to note that the EKF is passed current state and associated error information for all external sensors and the IMU. Figure 106 depicts a graphical FBD of the Pixhawk EKF. The EKF begins by using the IMU to predict the aircraft's state. The measured angular rate, obtained from the two 3-axis gyroscopes, is integrated for angular position. This angular position yields the body coordinate frame of the vehicle, $\langle X, Y, Z \rangle$. Acceleration data is then obtained from the accelerometer. Since gravity always acts toward the center of the Earth (ie. its direction is considered absolute), the accelerometer data coupled with the angular position of the vehicle is used to transform the acceleration in the body frame, $\langle X, Y, Z \rangle$, into the acceleration of the world frame, $\langle N, E, D \rangle$. This position is integrated twice to find the vehicles position in the $\langle N, E, D \rangle$ world frame. This position is combined with the measured GPS position yielding the innovation (error) between the new measurements. As mentioned earlier, the GPS error and respective IMU error is computed and passed into the EKF. This sensor error dictates how heavily each measurement is weighted. For instance if the GPS error is greater than the error of the IMU, then the IMU measurement has more significance, hence is weighted more, than the GPS measurement. The EKF finally returns a state correction to the Pixhawk system.

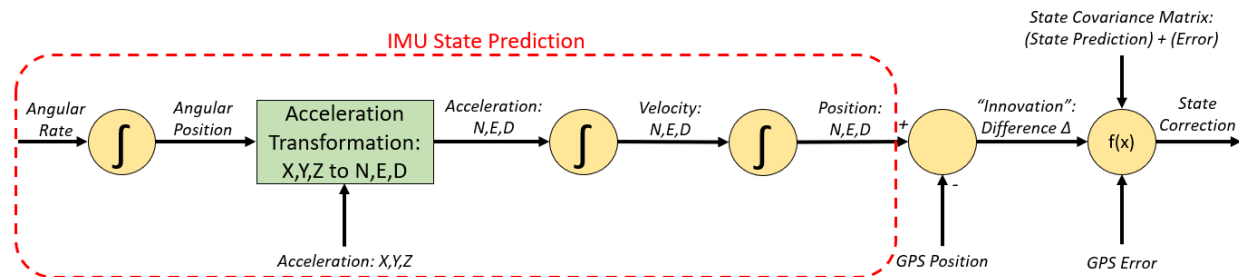


Figure 106. Functional block diagram of the Pixhawk Extended Kalman Filter.

The measured state, comprised of the measured angle and measured rate, is fed back into the system for further iteration. The correction state is passed into the servos to control their position and adjust the orientation of RAPTR.

5.4.7. PID Gain Approximation

5.4.7.1 Problem Statement

Due to the complexity of the Pixhawk, it is not feasible to model the entire system's architecture. The problem arises that for the Pixhawk to effectively control the vehicle it must know how much effect a given rudder or aileron deflection will change the vehicles orientation. If the control surface deflection affects the system too much the aircraft will lose control. If the control surface deflection is too small the aircraft will not be maneuverable enough to be of any use. The control surface gains, PID gains, dictate the under and overshoot of the control surfaces and hence of the entire aircraft. Figure 107 depicts the PID input in ArduPlane. Again RAPTR is only equipped with an elevator and rudder so these are the only PID gains that need to be computed as the servo roll PID is irrelevant. The integral gain serves to reduce any steady state error that may occur but is not critical to push a measured state toward a desired one and so the integral gain is assumed to be zero.

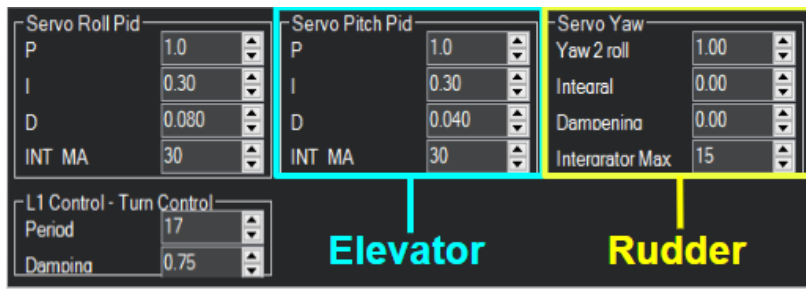


Figure 107. PID gain input in ArduPlane.

5.4.7.2 Problem Approach

The Pixhawk PID control architecture is depicted in Figure 108. In the control block diagram, the error between demanded state and the measured state is pushed through a PID controller and then applied to the natural dynamics of the system (plant) before returning the aircraft's state. The equations for the PID controller and plant in the frequency domain are given by Equation 9 and Equation 10.

$$K(s) = K_P + K_D s + K_I \frac{1}{s} \quad (9)$$

$$X(s) = C(sI - A)^{-1} B \vec{u} \quad (10)$$

To control the system, the natural behavior of this system must first be understood. An approximation of RAPTR's plant is created first before attempting to control the dynamics.

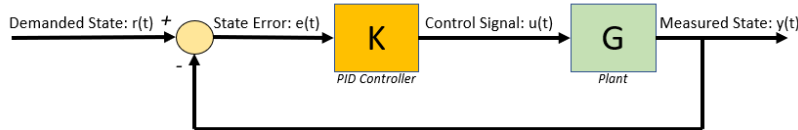


Figure 108. Control block diagram of the PID approximation of the Pixhawk.

Natural Dynamics

The longitudinal and lateral dynamics of RAPTR are approximated by the first-order Equation 11. Longitudinal and lateral dynamics were decoupled and linearized from the assumptions in Table 85. Equation 12 is used in Equation 10 to extract the dynamics for a particular variable of interest.

$$\dot{\vec{x}} = A\vec{x} + B\vec{u} \quad (11)$$

Table 85. Longitudinal and lateral decoupling and linearization assumptions.

Longitudinal Assumptions	Lateral Assumptions
Existence of a plane of symmetry	Linearization of equations
Absence of rotor gyroscopic effects	Absence of rotor gyroscopic effects
	Neglect aerodynamic cross-coupling

$$y = C\vec{x} + D\vec{u} \quad (12)$$

The state vectors for the longitudinal and lateral system are given by Equation 13 and Equation 14 respectively. The A and B matrices are system matrices composed of the aerodynamic, inertial, and dimensional qualities of RAPTR. All dimensionless aerodynamic coefficients are computed in section 5.3 and the inertial and dimensional parameters are computed using the Solidworks model from section 5.1. The dimensionless control coefficients are approximations from general aviation aircraft as a CFD model could not be run on time for comprehensive results. Due to RAPTR's large elevator and rudder, the current control coefficient approximations are underrepresentative of RAPTR's control authority.

$$\vec{x}_{lon} = [u \quad w \quad q \quad \theta] \quad (13)$$

$$\vec{x}_{lat} = [v \quad p \quad r \quad \phi \quad \psi \quad y^E] \quad (14)$$

Figure 109 depicts the behavior of the longitudinal open-loop system due to a disturbance in pitch. Figure 110 depicts the behavior of the lateral open-loop system due to a disturbance in yaw. Obviously, there are a variety of other disturbances that may be modeled; however, these disturbances directly in line with the PID gains for pitch and yaw and so are displayed here.

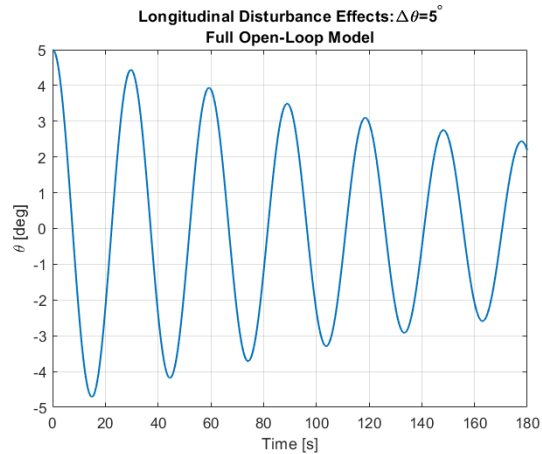
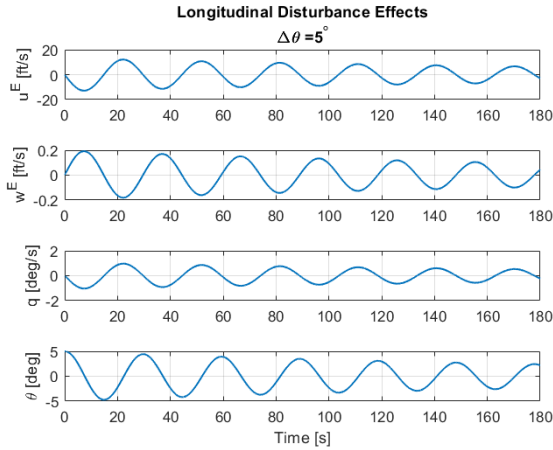


Figure 109. Longitudinal open-loop dynamics due to a pitch disturbance.

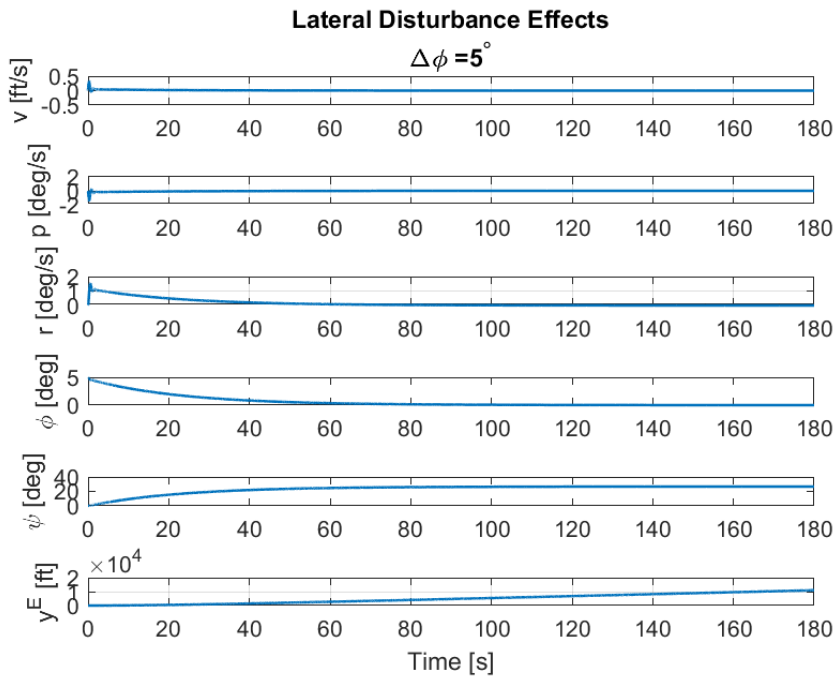


Figure 110. Lateral open-loop dynamics due to a yaw disturbance.

Control Dynamics

Before a control system is tuned, a benchmark of the control system's behavior must first be formulated. Table 86 displays these benchmarks. Damping ratios ≥ 1 are not chosen as this infers that the system is critically damped or overdamped. An overdamped system decreases the response time and so is not desired. Similarly, lower damping ratio's are chosen, with particular reference to the lateral dynamics, to expedited the speed at which the dynamics approach equilibrium. Conservative time constants are chosen to avoid excessively quick movements by the aircraft. Figure ?? graphically displays the longitudinal and lateral target zone.

Table 86. Longitudinal and lateral target zone specifications.

	Longitudinal	Lateral
Damping Ratio Range	$0.85 \leq \zeta \leq 0.3$	$0.95 \leq \zeta \leq 0.99$
Time Constant Range	$2 \leq \tau \geq 10$	$2 \leq \zeta \geq 30$

Selecting the proportional and derivative control gains is a three step process. The first step begins in Figure 111 for proportional gain. A range of proportional gains is iterated through until a gain within the target zone is acquired. The second step is shown in Figure 113. In this step, the proportional gain is found in step one is held constant while a range of derivative gains is iterated through until the desired gain is discovered. Figure 114 depicts both iterations of the proportional and derivative gain as well as the selected design point. The numerical values of the chosen PD gains are listed in Table 87.

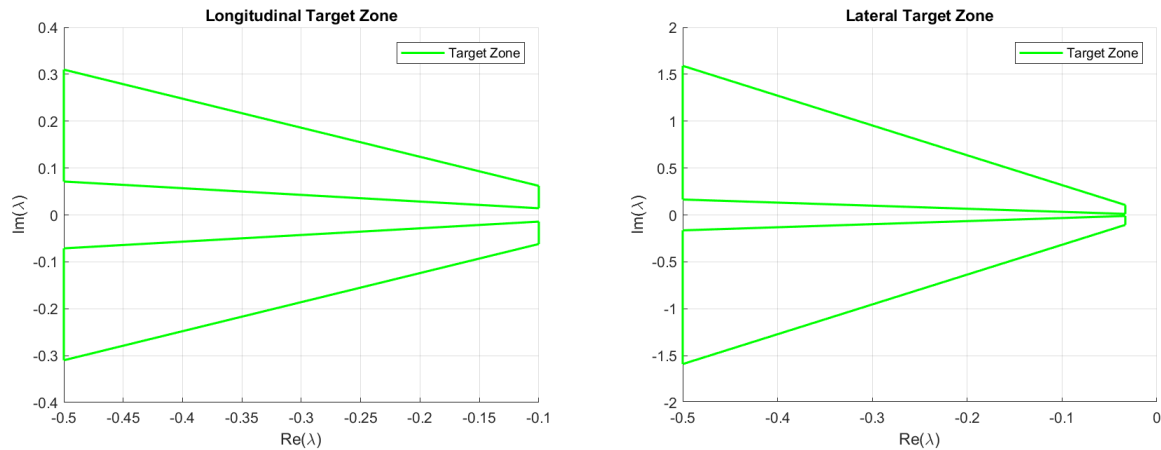


Figure 111. Longitudinal and lateral target zones.

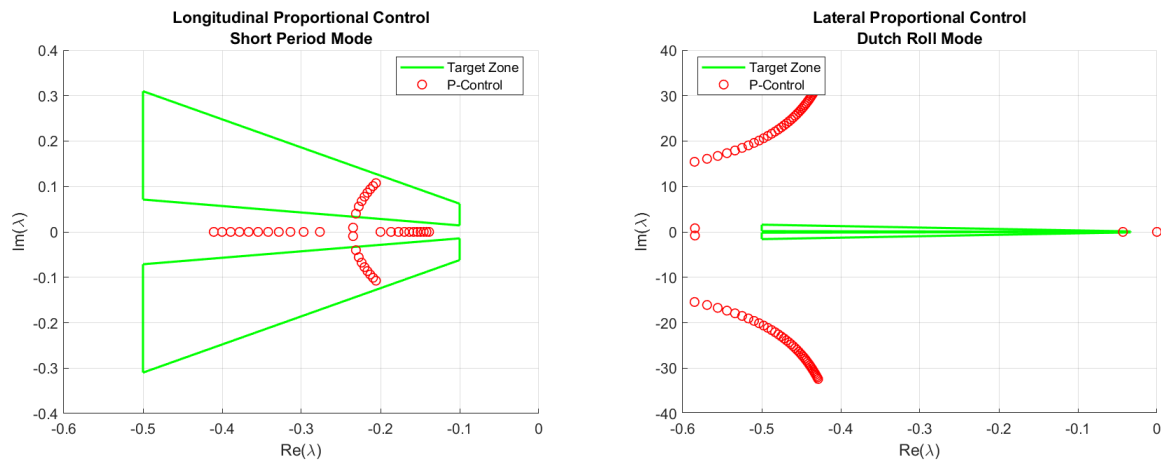


Figure 112. Longitudinal and lateral P control locus plot.

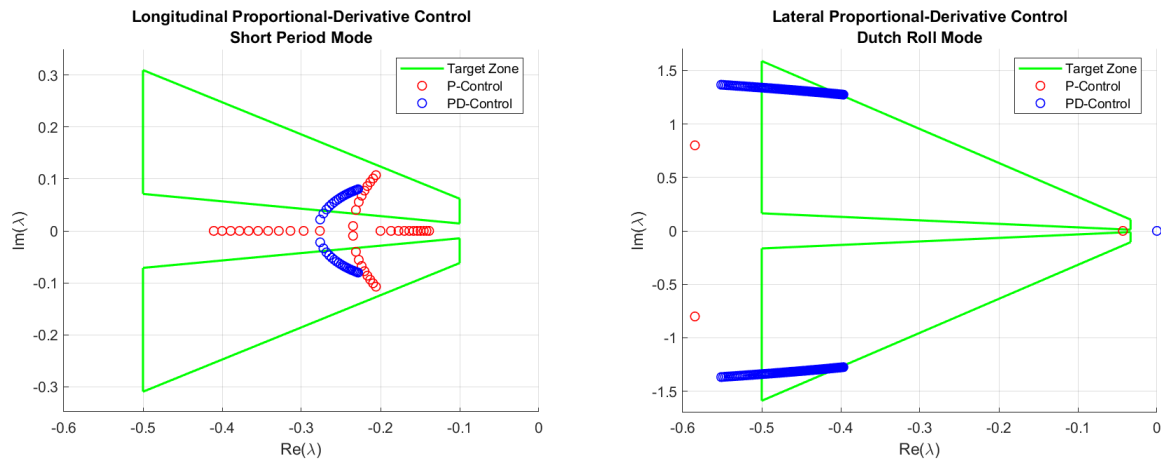


Figure 113. Longitudinal and lateral PD control locus plot.

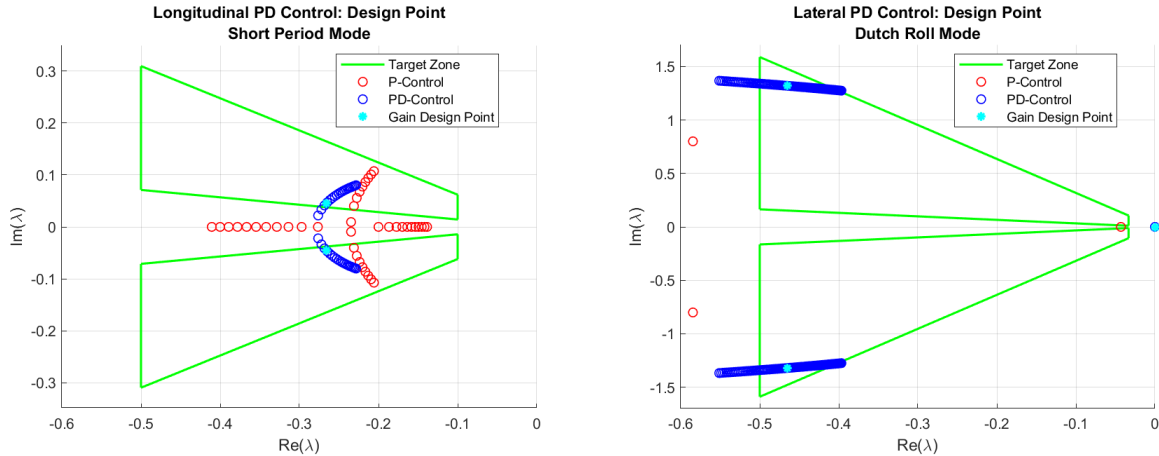


Figure 114. Longitudinal and lateral design point locus plot.

Table 87. Longitudinal and lateral PD gains.

	Longitudinal	Lateral
Proportional Gain	0.0158	0.178
Derivative Gain	0.018	0.075

Once the design point is determined, the PD gains are implemented back into the dynamics system. Figure 115 depicts the longitudinal pitch response with associated PD damping. Figure 116 depicts the lateral yaw and roll response with associated PD damping. The roll response initially increases before returning to zero as a yaw induces a roll right before both are damped out by the control system. These plots demonstrate how the control system uses the determine PD gains to damp the system. **This analysis proves feasibility for DR 1.1.2.** It is important to note that though these gains produces the general desired behavior, adjustments to these gains must be made to decrease the system's time constant.

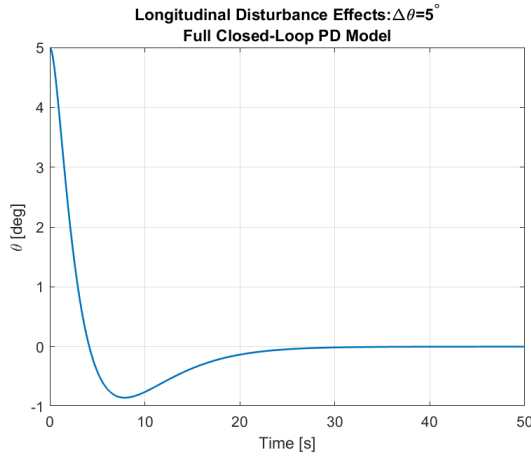


Figure 115. Longitudinal closed-loop effects on pitch angle.

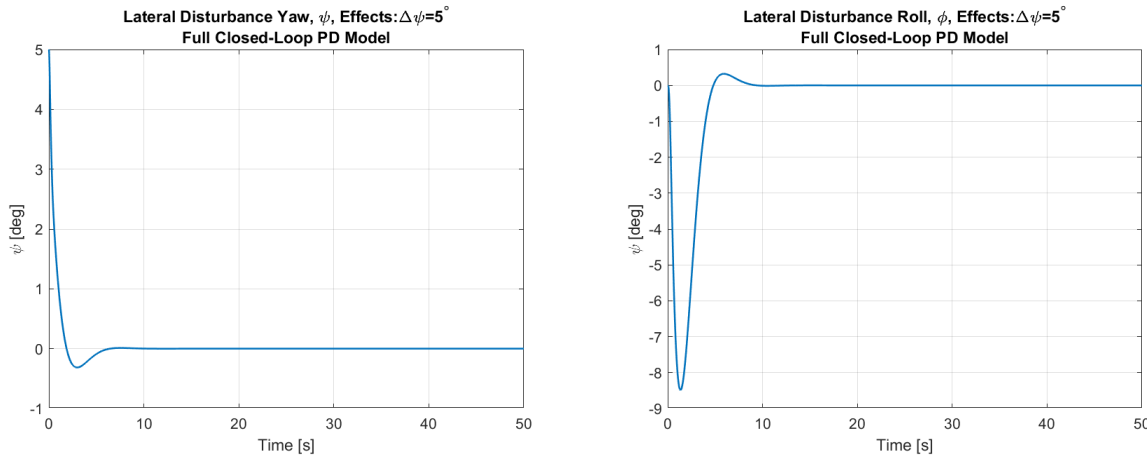


Figure 116. Lateral closed-loop effects on pitch angle.

5.5. Software

When designing the ground station software, Functional Requirement 4 (FR 4) and the overall project purpose guided the design decisions and algorithm development. FR 4 states that the ground station software must be capable of identifying a distinctly colored target and relay its latitude and longitude to the user, from which two subsequent derived requirements are established to separately require the outputting of a bounding box over potential targets and to compute local, relative world coordinates along with the target's latitude and longitude within 150 ft of its true location. This division naturally necessitates two separate but interdependent design solutions to expound: target recognition and target geolocation. Figure 117 provides an overview for the functions of the ground software, as well as a current flowchart detailing the code:

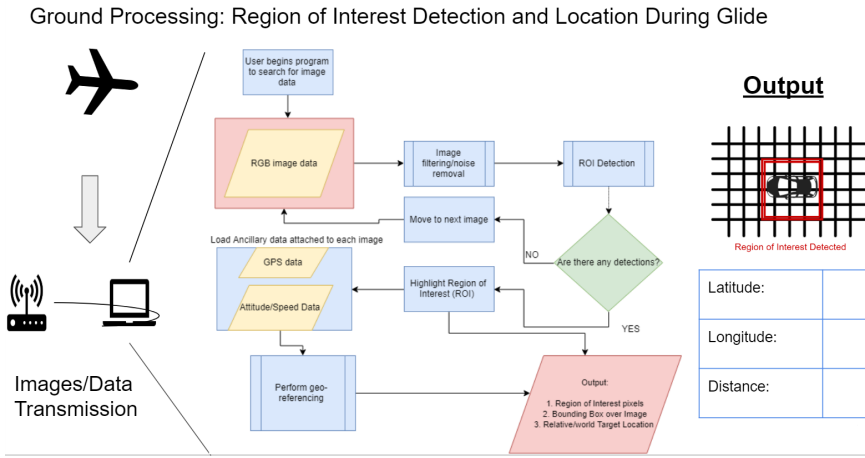


Figure 117. Software CONOPS and Flowchart

5.5.1. Target Recognition Software

The design of the target recognition software was driven by DR 4.1 and FR 5, which both state that the software must output a bounding box over potential targets, and that the entire mission must be completed within three minutes from launch to images processed. To complement these requirements, multiple assumptions were made about the nature of the targets that the software will be detecting; namely, that the target size is known to be 5x5x5 ft and that the target is distinctly colored relative to its background. Since the requirements for the aerospace engineering team's portion of the software don't require target classification and only require target detection, the driving factor for what detection algorithm was chosen was primarily decided by speed and simplicity. One of the more simple and quick methods of image detection is to background subtraction to separate potential targets from the background. This method depends

on differing image intensity to detect a distinction between potential target and background in order to detect the potential target. This is where the assumptions made for this project come in to play as having a distinctly colored target will greatly help with this method of detection. Since the only requirement for the aerospace engineering team is to detect potential targets and not classify, there is no training data required as an input making the development of the software much faster. This method only requires the size of the target as an input to be able to detect it, making it perfect for this project.

This detection algorithm utilizes a triple sliding window method, which compares the sample statistics of the pixel intensities between the inner and outer windows. The inner most window is a square with side length approximately equal to 90% of the pixel length of the target, and the square defining the inner perimeter of the outer window annulus has a length approximately equal to 110% of the pixel length of the target. With the geometry of the inner and middle windows defined, the square constraining the outer perimeter of the outer window annulus is defined such that the total number of pixels within this window are equal to those in the inner most window. The purpose of this geometric configuration is to provide a sample that will entirely consist of pixels of the target in the inner window, and a sample that consists entirely of the background in the outermost window. The middle window serves as a buffer between the inner and outer windows where no pixels are analyzed. Figure 118 provides a visual for how the sliding window operates over an image:

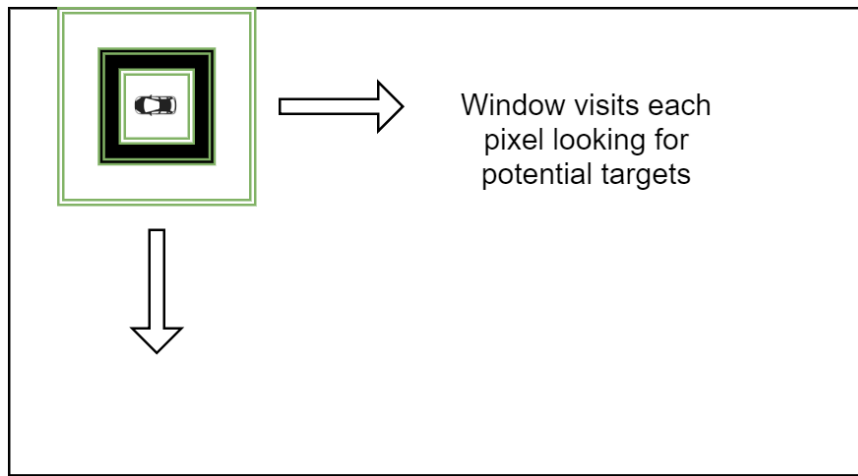


Figure 118. Sliding Window Over a Target With a Blank Background

Table 88 defines the geometry of each of the windows:

Window	Side Length
Inner	90% of Target Pixel Length
Middle	110% of Target Pixel Length
Outer	$\sqrt{Length_{inner}^2 + Length_{middle}^2}$

Table 88. Window Geometry

This sliding window operates on each pixel in the image, starting from the top left and moving each column in each subsequent row. If processing time must be decreased based on mission modifications or processing needs of the EE team, then the spacing between analyzed pixels can be increased such that the window will not be perfectly centered on the target but will still capture most of the target pixels. Since the geometry of the sliding window cannot be nominally structured at the edges of processed images, the algorithm ignores pixels that within the length of the outer window from the edge of the image. This is to enforce consistency in the analysis of all pixels visited by the window, and will not present a problem due to the wide field of view relative to the target size.

At each pixel visit in the sliding window, the algorithm computes a test statistic which compares the sample means and variances between the inner and outer windows. The test statistic works to provide a measure of how different the two pixel distributions are based on the differences between their sample means and the variance in the outer window distribution. This can be thought of as a pseudo-hypothesis test that compares a null stating that the the

sample means between the two windows are the same to an alternative that states that they are different. This is not a true hypothesis test, however, since all the computed test statistics are compiled and the decision to reject the null is based on the largest test statistics compiled and where their corresponding pixels are located within the image. Additionally, the test statistics used can be heuristically developed to maximize the likelihood of correct detection. For example, only the outer window variance may be analyzed since the variance of the target pixels is highly unknown and irrelevant compared to the background. As such, this can be thought of more as an exercise in determining what statistical measures can be utilized from each distribution to most optimally determine if a properly sized target is contained within the inner window. An example of one possible test statistic that compares the sample means is given in equation 15, where \bar{X} and s are the sample mean and sample standard deviation, respectively; and the subscript 1 denotes the inner window and the subscript 2 denotes the outer window³⁷:

$$T = \frac{\bar{X}_1 - \bar{X}_2}{s_2} \quad (15)$$

This is a relatively simple test statistic, and has been the one used in all preliminary verification and validation with test images. There is a wide range of test statistics that may be used, including F-test statistics to strictly compare sample variances, and a Kolmogorov-Smirnov Test to determine if the two samples are drawn from the same distribution, both given in equations 16 and 17, respectively:

$$F = \frac{s_1^2}{s_2^2} \quad (16)$$

$$D = \sup_x |F_1(x) - F_2(x)| \quad (17)$$

Further test statistics can be used based on edge detection within the sliding window, which will be further explored in the software development and optimization slated for next semester. A large portion of this software testing and development will involve determining which tests provide the most useful information about differentiating the target from its background and how to utilize the test statistics to inform decisions about where the target is located.

As mentioned previously, the appropriate test statistic is calculated at each pixel the window visits, and these test statistics are compiled into a vector after the window has finished looking at the pixels. One of the most challenging aspects of the detection portion of the software, accordingly, is utilizing this information to determine if a target is located in the image, and if so, where. Currently, it has not been decided the exact course of action to take at this stage; however, based on heuristic testing of the detection software and a hybrid between a constant false alarm rate and a cluster analysis approach, the software has been successful in detecting a single target in an example test image. One of the example images used in the detection software development is shown in figure 119, which was used based on the high contrast between the target (person laying) and the background:



Figure 119. Example Image of a Target with High Contrast with Background

To detect the person laying, the user inputs the size of the target in pixels, assuming a square shape around the entirety of the target. In the actual implementation of the detection algorithm used in full system testing, this pixel

size will be a function of altitude, and will require altitude data associated with each image to transform the target's spatial dimensions into pixel lengths. This transform is described in equations 18 and 19, where P_{target} is the length of the target in pixels, L_{target} is the length of the target in feet, P_{image} is the number of total pixels in the image in either the horizontal or vertical direction, FOV is the field of view in feet, a is the camera altitude, and iFOV is the angular field of view of the camera.

$$P_{target} = \frac{L_{target} P_{image}}{FOV} \quad (18)$$

$$FOV = 2a \tan\left(\frac{iFOV}{2}\right) \quad (19)$$

With the target size in pixels properly defined, the image is then converted to grayscale or to a saliency map, which reduces the image pixel matrix from three dimensions to two and in the case of the saliency map heightens the intensity of unique pixels relative to their surroundings. Figure 120 provides an example of a saliency map of the original test image:

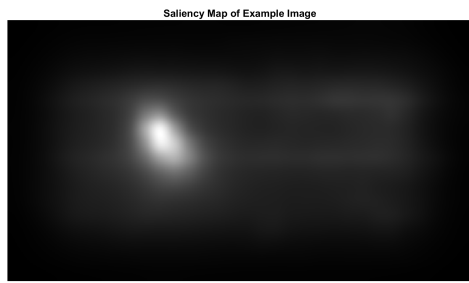


Figure 120. Saliency Map of Example Image

the sliding window is then run over the target, operating on the individual pixel intensities, and test statistics defined in equation 15 are calculated for each pixel visited by the window. From here, the algorithm must determine which pixels are considered target pixels. This is done by taking the maximum test statistic values equal to the square of 10% of the target's length. This seemingly arbitrary number represents the pixels in the very center of the target, which works to define the bounding box over the target to be output to the user and the EE team software. Figure 121 shows these target pixel "hits" overlaid on top of the target:



Figure 121. "Target" Hits Overlaid on the Example Image

In this case, all of the "hit" pixels are directly on the target, however it is very possible that there is a small region that may have a large test statistic and will fall within the maximum region defined above. In this case, if more than

50% of the hit pixels are clustered within a square region the size of the target, then software will output a bounding box over the mean coordinates of the cluster of hit pixels equal to the size of the outer perimeter of the outer box of the sliding window. Figure 122 shows the output of a bounding box over the target, wherein the region of interest (ROI) is defined and this ROI can be cropped and output to the EE team for classification.

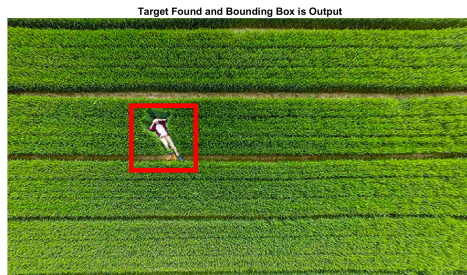


Figure 122. Bounding Box Over the Target

For next semester, the bulk of the work involving software development entails optimization with many of the heuristic approaches introduced previously, as well as validation with separate drone tests along with full system testing. Specifically, determining which test statistics to use and how to optimally use their provided information to inform the presence of a target along with refining the spacing between pixels which the sliding window operates over. Additionally, complementary approaches to the current detection scheme will be explored, all with the motivation to increase capability of target detection while balancing processing time.

5.5.2. *GeoLocation Software*

With the target detection and regions of interest defined, the geolocation portion of the ground software can now be performed to locate potential targets in both local and geodetic frames. As stated previously, the geolocation software was written to meet Derived Requirement 4.2 which states the ground station software must be able to calculate the location of a potential target to within 150ft of the true location. This process requires knowing three pieces of information, which include the pair of pixel coordinates corresponding to the center of the region of interest defined in the target detection output and the camera altitude from which the image was taken. From these three pieces of information, three unknown pieces of information are sought after; the North, East, and Down (NED) world coordinates of the target, along with the target latitude, longitude, and elevation. In order to derive the location of the target in the NED world coordinates two important problems must be solved: transforming the target pixel coordinates into the camera frame, and subsequently transforming the camera coordinates to a local world and geodetic coordinate system. A visualization of the pixel and world coordinate frames can be seen in Figure 123. The range defined in the left-hand side vector is the Z coordinate distance from the target to the camera in the camera frame, which extends outward from the camera and is normal to the camera plane.

Pixel to World Transformation

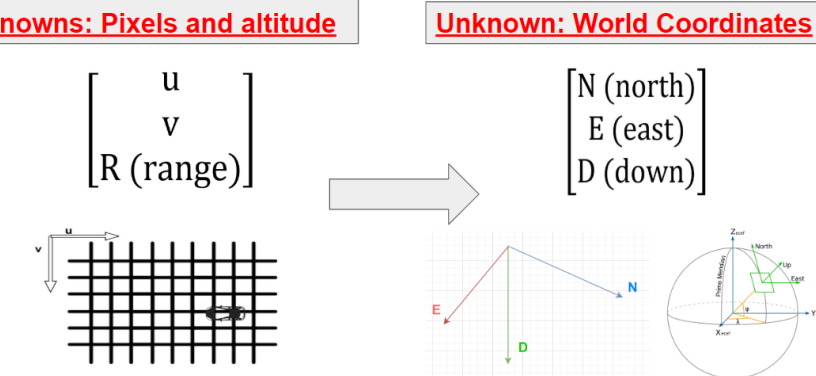


Figure 123. The Known Pixel Coordinate Frame and the Unknown World Coordinate Frame

With the problem of transforming between pixel coordinates and world coordinates well defined, a governing function must be derived which takes as an input the target pixel values and altitude, then is able to output the associated world coordinate values of the target. The problem approach is to in a way work backwards, where the appropriate matrix transformations will be defined from world to camera and camera to pixel reference frames. To first understand how the pixels are mapped to a spatial representation in the camera coordinate system, consider the K matrix in equation 20³⁹:

$$K = \begin{bmatrix} f & s & C_x \\ 0 & af & C_y \\ 0 & 0 & 1 \end{bmatrix} \quad (20)$$

Here, f is the camera focal length in pixel coordinates, a is the image aspect ratio, s is a skew term between sensor and optical axes, and C_x and C_y represent the optical center of the image, which is the pixel coordinate of the center of the image and thus half of the total pixel length in the vertical and horizontal direction. Since this matrix represents a transformation from camera to pixel coordinates, the next step is to determine an appropriate transformation matrix from world coordinates to camera coordinates. This is done through a simple Euclidean transformation utilizing a translation from the world origin (the ground station) to the camera's world coordinates, along with a rotation to align the world NED axes to the camera's XYZ axes. The geometry of the camera and imaging plane can be seen in figure 124³⁸, where \mathbf{x} represents the target pixels and \mathbf{X} represents the target in spatial coordinates:

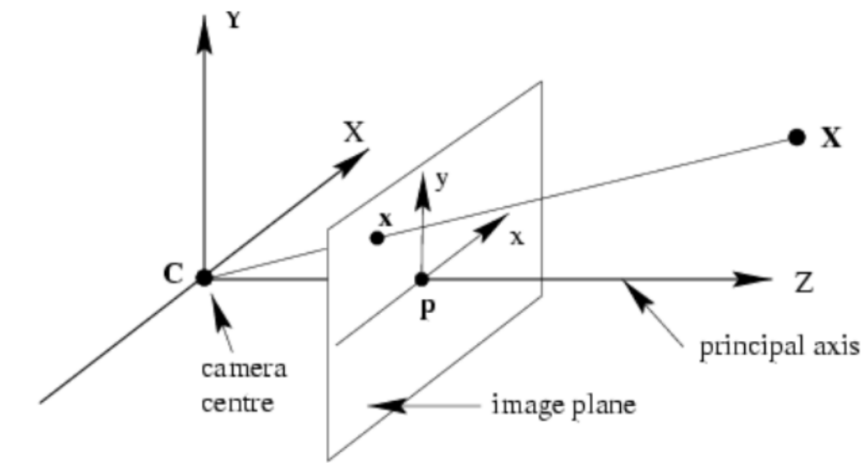


Figure 124. Imaging Plane and Camera Coordinate System

The Euclidean transformation is represented in equations 21 and 22, where R is the rotation matrix represented as the product of a roll (ϕ), pitch (θ), yaw (ψ) Euler angle sequence:

$$E = [R|t] \quad (21)$$

$$R = R_1(\phi)R_2(\theta)R_3(\psi) \quad (22)$$

Finally, the camera matrix and Euclidean transformation matrix can be multiplied to produce the full projection matrix from world coordinates to pixel coordinates. This transformation cannot be directly applied to solve the inverse problem, however, since an extra piece of information is required to transform from pixel to spatial coordinates. By utilizing homogeneous coordinates, an extra dimension is added to the problem, which is where the previously mentioned range in the camera Z coordinate is utilized. Equations 23 through 26 define the full transformation equation using homogeneous coordinates:

$$\tilde{P}\tilde{p}_w = x_s \quad (23)$$

$$\tilde{p}_w = \begin{bmatrix} N(north) \\ E(east) \\ D(down) \\ 1 \end{bmatrix} \quad (24)$$

$$x_s = \begin{bmatrix} u \\ v \\ 1 \\ 1/z \end{bmatrix} \quad (25)$$

$$\tilde{P} = \begin{bmatrix} \mathbf{K} & 0 \\ \mathbf{0} & 1 \end{bmatrix} \begin{bmatrix} \mathbf{R} & \mathbf{t} \\ \mathbf{0}^T & 1 \end{bmatrix} \quad (26)$$

N,E,D are the world coordinates to solve for; u,v are the target pixel coordinates; and z is the spatial distance from the target to the image plane along the Z camera axis. The governing transformation equation can be simply inverted to solve for the world coordinates:

$$\tilde{p}_w = \tilde{P}^{-1}x_s \quad (27)$$

The z range will be equal to the camera altitude when the vehicle isn't banked or pitched, however this value will be explicitly unknown if there is any bank or pitch experienced by the camera. By using the altitude data, however, equation 27 can be solved iteratively with estimated range values until the "Down" component of the world coordinate vector is equal to zero. This software assumes a flat surface, so the Down component of the target will be equal to that of the ground station, which is set to be the local world origin. The range value that produces this solution will then be considered correct, and the North and East components are taken from the vector to geolocate the object in the local world space.

Once the North and East coordinates of the target have been found, the software will then begin to calculate the geodetic coordinates of the target. This is done using the GPS coordinates of the ground station and the vehicle, and the local coordinates of the identified target. MATLAB contains a built-in function to convert from NED to geodetic, using a wgs84 ellipsoid to represent the shape and size of the Earth and an origin with coordinates equal to those of the ground station. Once this conversion is done, the latitude, longitude, and elevation along with the total distance of the target and a general direction relative to the ground station are output to the user, corresponding to the regions of interest that were highlighted in the detection phase. This then concludes the aerospace team's mission with ground software when all regions of interest are geolocated.

To verify that the geolocation software can meet DR 4.2 and locate images within 150 ft of their true location, the maximum uncertainty associated with attitude data corresponding to each image was analyzed. This was done by setting the true location to be within the frame of the image but in the corner of the image that is in the direction of the bank and pitch. This location was then recorded to be truth when zero roll, pitch, and yaw were assumed. From

there, the roll, pitch, and yaw angles were individually increased, and based on the same target pixel within the image, the distance between the truth data at zero roll, pitch, and yaw and the new location with assumed nonzero roll, pitch, and yaw was recorded. The purpose of this was to see how changes in attitude angle affect the ground location of the target, and if a reasonable uncertainty in attitude angles will still allow targets to be located within 150 ft of their true location. Figure 125 provides a plot of this geolocation error as a function of different attitude angle uncertainties, using the same nominal imaging altitude and EE payload specifications.

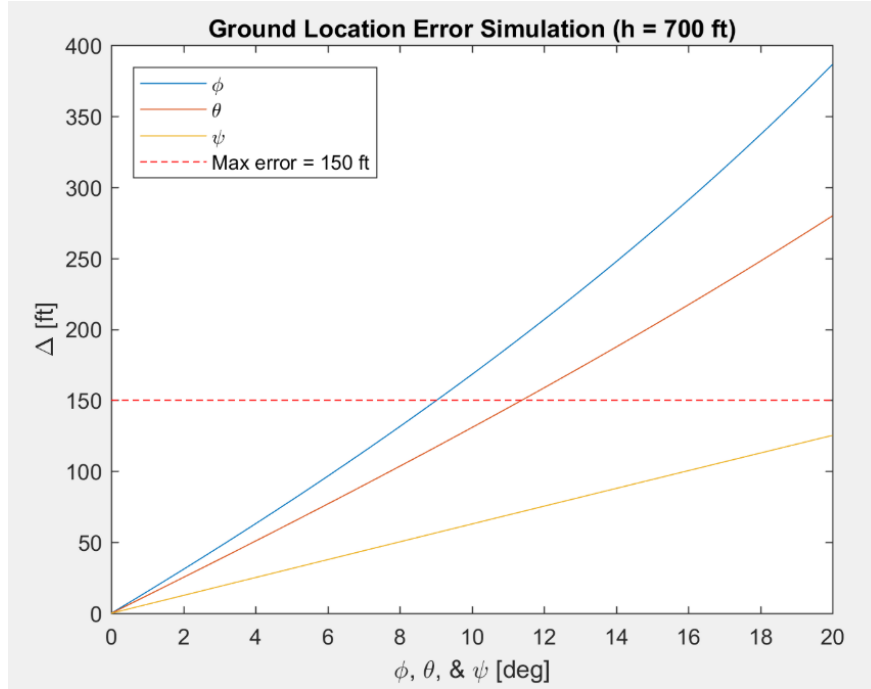


Figure 125. Plot of Geolocation Errors with Uncertainties in Attitude Angles

From this plot, the maximum attitude uncertainties associated with 150 ft of geolocation error are within 8 to 10 degrees in bank and pitch, and much more in yaw. These values are significantly higher than the estimated uncertainty in attitude angles coming from the vehicle to the ground station, so DR 4.2 will be able to be met.

To validate the software, a preliminary test was run using a quadcopter drone and mock target in North Boulder Park. This exact testing procedure will be described in the upcoming verification and validation section, however the results from the test and subsequent output are crucial to the design of the geolocation software. For one of the tests, the drone was taken to 350 ft altitude, and the target was placed on the edge of the FOV of the image. The testers then recorded the true GPS location of the target, and received as part of a telemetry data package the GPS coordinates of the drone. In the full systems test, this vehicle GPS data will be sent to the ground station in real time, however in this preliminary test the data was recorded and then manually input into the software. Along with the GPS data, the yaw angle of the drone was recorded, and the roll and pitch angles were assumed to be zero. The pixel coordinates of the center of the target in the image were then manually input into the software to emulate the output from the ROI determination, and the GPS location of the simulated ground station was input into the software. With the camera specs from the drone known and input into the software, all necessary information is known to be able to begin target geolocation. Figure 126 displays the output of the geolocation software, with the ground station, target estimate, target truth, and vehicle indicated:

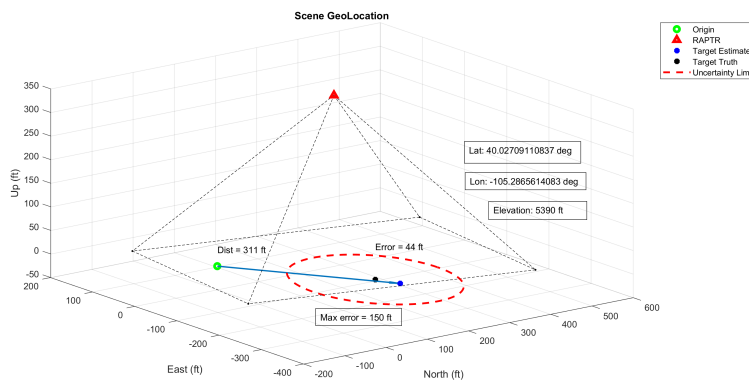


Figure 126. Target Estimate and Target Truth During Drone Test

Since the target estimate of 44 ft fell well within the maximum error bounds of 150 ft, this preliminary test validates the software's capability to accurately geolocate targets. The error in this case was primarily due to uncertain camera specs, uncertain attitude angles, and errors in GPS data. Since most of the developing with the geolocation software is complete, next semester will consist mostly of verification and validation using different target locations within the image, different camera pointing angles, and higher altitudes.

6. Verification and Validation

Author: Greg Clements

6.1. Test Schedule

RAPTR Test Schedule				
Test Name	Date	Brief Description	Location	Requirements
Test Imaging (Software)	11/19/18 04/12/19	Capture images of target with drone for software development/testing	CU South Campus	FR 4
Structural	12/09/19, 01/18/19	Stress test motor mount and wings using weights to verify structural integrity	Senior Projects Room	DR 1.4, 1.4.1, 1.4.2, 1.4.3
Thermal	02/09/19	Static fire of motor positioned near glider fuselage to verify effectiveness of heat shield	Aerospace Welding Shop	DR 5.2.2.1
Controls	04/19/19, 04/26/19	Improve tuning parameters of PixHawk flight controller and verify controllability of vehicle	CUSB, Boulder Model Airport	DR 1.1, 1.1.1, 1.1.4, 6.3
Full Vehicle	04/27/19	Launch vehicle with a weight simulating the payload to verify trajectory/flight path	North/Atlas Site	FR 1, 2, 6
Full Systems	05/05/19	Full systems launch with payload to validate project success	North/Atlas Site	FR 1, 2, 3, 4, 5, 6

Table 89. Test Plan/Schedule

6.2. Test Imaging (Software)

6.2.1. Test Plan

6.2.1.1 Introduction

The purpose of this test is to validate **FR4**; The system shall identify and geo-locate targets present in the captured images. This test will also serve to verify **DR4.1**, **DR4.2**, and **DR4.2.3**. To test the software being developed to achieve this requirement, test images will be captured with a drone at Boulder North Park. The location of the drone during each image capture will be recorded and used as input to the software. The goal of the software being tested is to detect, mark, and provide GPS coordinates of the specified target. A two dimensional target will be constructed out of cardboard and a large, brightly colored, "X" will be taped onto the cardboard. The drone will be flown to 350ft and capture images of the field below containing the target.

6.2.1.2 Test Materials

- DGI Phantom 3 Standard (Drone)
- DGI flight controller
- Mobile device with DGI flight controller application
- 3.8'x3.8' piece of cardboard
- Brightly colored duct tape

6.2.1.3 Features to be Verified/Validated

The primary feature being tested is target detection. In addition, the geolocation feature of the software will be tested. If the specified target is not in the inputted image, the software must provide a negative result. If the target is captured, the software must mark the target in the image and provide GPS coordinates of the target to within 150 ft. This will require that the software can georeference all pixels of the image to the drone's coordinates at the time the picture was captured.

6.2.1.4 Features not to be Verified/Validated

Features of this software that will be included in the final product not being validated in this test include target classification. The final product will be capable of classifying the target between a pre-loaded set of possibilities. This is a feature that is being developed by an electrical engineering sub-team, and will be tested separately by them.

6.2.1.5 Approach

Before testing can begin, a target will be constructed out of a 3.8' x 3.8' piece of cardboard. This target has been scaled down to account for the fact that the drone will be capturing images at only 350ft high instead of 600ft. This corresponds to a factor of 0.583. The resulting area that the scaled down target must cover in order to contain the same number of pixels is therefore $0.583 * 25\text{ ft}^2 = 14.583\text{ ft}^2$ or a 3.8' x 3.8' target. The target will be marked with a large "X" using brightly colored duct tape. Additionally, the battery and controller for the drone will be fully charged. Proper notification will be given to Boulder Municipal Airport, as this is required by law. Finally, the micro SD card of the drone's camera will be cleared to ensure enough storage room for testing images.

To begin testing, the target will be placed in the middle of the field at Boulder North Park in a clearing free of overhead obstructions. The GPS coordinates of this location will be measured and recorded using a phone. The drone will be powered on and commanded via the DGI application to fly 350ft overhead of the target. Images of the target will be captured and saved onto the camera's micro SD card. The drone will then be flown downrange until the target is located at the edge of the camera's FOV. An image will be captured with the camera pointing straight down. Finally, the drone will be flown even further downrange and an image will be captured that does not include the target. For each image that is captured, the GPS coordinates of the drone during imaging will be recorded using the DGI application. Once all images are successfully captured, the drone will be safely landed using the "Return to Home" function of the flight controller.

6.2.1.6 Success/Fail Criteria

The captured images will be considered successful if the target is in clear sight and in focus. If any obstructions are present or the images are not clear (i.e blurry or out of focus) the pictures are a failure and must be re-taken. Additionally, each image must be accompanied by corresponding GPS coordinates of the drone for them to be successful.

For the software to be successful, it must provide a positive result for images which contain the target and a negative for images which do not contain the target. Additionally, for images containing the target, it must accurately mark the target on the image and provide GPS coordinates of the target. These coordinates will be cross-referenced to truth data taken by a cellphone at the actual location of the target. The error between the software's predicted location must be within 150ft of the target's actual location to be successful.

6.2.2 Preliminary Test Results

6.3 Structural Test

6.3.1 Motor Mount Testing

6.3.1.1 Test Overview

The purpose of this test is to verify **DR1.4.1**; The motor mount shall withstand the force generated by the motor at maximum thrust. The motor mount will be 3D printed using PLA plastic and adhered to the balsa fuselage of the vehicle using "Loctite" epoxy. The rocket engine being used will produce a max thrust of around 94.5 N. To verify that the motor mount can withstand this force, a 5 gallon bucket will be hung from the motor mount and increments of water will be added to the bucket until the bond or the mount itself fails. 5 gallons of water weighs roughly 41.7 lb, or 18.9 kg. This translates to a force of roughly 185.22 N, nearly double the maximum thrust generated by the motor.

6.3.1.2 Test Logistics

The test will take place on **12/09/18** in the afternoon. Nick Carvo and Greg Clements will be the members of RAPTR conducting the test. It will take place outside of the Aerospace Senior Projects room. All materials will be purchased at McGuckin Hardware located at 2525 Arapahoe Ave Unit D1 in Boulder, CO. No special access to any other facilities or equipment will be needed for this test.

6.3.1.3 Materials

Item	Quantity	Purchase Required	Cost Estimate
Epoxy	1.69 Oz.	No	\$0
Motor Mount	1	Yes	\$3
Mock Balsa Fuselage	1	Yes	\$7
Clamp	2	No	\$0
5 Gallon Bucket	1	Yes	\$3.99
Water	5 Gal.	No	\$0
2L Measuring Container	1	No	\$0
Stool	1	No	\$0
Sandpaper	1	No	\$0

6.3.1.4 Procedure

1. Clean the adhering surfaces of the balsa wood mock fuselage and motor mount using sandpaper
2. Properly adhere motor mount to the balsa wood mock fuselage using the epoxy
3. Securely clamp balsa wood mock fuselage to one side of the stool so that the motor mount is hanging over the edge of the stool
4. Place a counterweight on the opposite side of the stool.
5. Verify the mock fuselage and motor mount are securely clamped to the stool by pushing and pulling the structure
6. Measure the angle of the fuselage/mount using a level and confirm it is zero.
7. Weigh the mass of the empty 5 gallon bucket and record
8. Hang the 5 gallon bucket from the motor mount at approximately the same location that the motor will be mounted to it
9. Fill the 5 gallon bucket with 2 liters of water
10. Record total volume of water added
11. Repeat steps 7-8 until the bond between mock fuselage and mount fails, the mount itself fails, or the bucket is completely filled.
12. Record the final weight

6.3.1.5 Error/Uncertainty

There are two main sources of error in this test. First, the mount is assumed to be perfectly level with the ground so that all of the weight from the bucket is acting straight down. The level used to verify this was accurate to within ± 1 deg. If the mount was angled at one degree, the total force acting on the mount with a full bucket would then be $\cos(1)*185.22N = 185.19N$. This is only a difference of 0.03N and will not impact the testing significantly. There will also be measurement error in measuring the amount of water being added each increment. The container being used to measure the water is accurate to within $\pm 0.2L$. If this measuring container is used to fill the entire five gallon bucket, or 18.9L, then the actual force being applied to the mount could actually be as low as 182.63N. This is about a 2.59N difference from the expected force. Even with these uncertainties, the test will be capable of verifying that the mount can withstand the maximum force generated by the motor.

6.3.1.6 Success Criteria

DR 1.4 will be validated if the mount and fuselage show no structural damage or failure after the 5 gallon bucket has been filled with water. This amount of water simulates a 185.22 N force acting upon the structure, which is equal to nearly twice the maximum thrust produced by the rocket motor. This is meant to simulate the worst case scenario, where the entire vehicle is held stationary as the engine burns.

6.3.1.7 Results

The mount was able to sustain the force of the weight of the bucket completely filled with water. This was measured to be $16L \pm 0.2$, or $35.2\text{lb} \pm 0.44$. An additional weight was added to the bucket and the mount still did not fail. The bucket of water after this weight was added and removed was weighed along with the weight itself. The bucket and water were measured to be $34\text{lb} \pm 1$ and the weight 37.05 ± 0.01 . The total force acting on the mount was therefore $71.05\text{lbf} \pm 1.01$, or $316.05\text{N} \pm 4.49$. This is just over three times the maximum thrust that the motor will produce.



Figure 127. Test Set-up



Figure 128. Close-up of motor mount

6.3.2. Wing Bending Test

6.3.2.1 Test Overview

The purpose of this test is to verify **1.4.3**; The wings shall withstand the aerodynamic loading experienced during maximum speed. The wings are constructed of laser cut balsa and ply wrapped in MonoKote skin. Due to the composite nature of this construction, it is inherently difficult to accurately model the structural strength. Therefore, it

is necessary to test the structure in order to determine the maximum loading that it can experience before failure. To simulate the elliptical lift distribution acting along the beam, a whiffle-tree will be utilized to apply force at 8 discrete points along the wing. The wing will be constructed without a polyhedral so that it is straight and level for testing. The location where these forces are applied will be computed to closely resemble the lift distribution of the wing. The fuselage/wing structure will be mounted to the edge of a lab cart using clamps so that the wing is cantilever. The whiffle-tree will be hung along the wing similar to Fig. 129 below. Weights will be incrementally added to the bucket hanging at the bottom of the whiffle-tree until the wing fails in either shear or bending. The weight of all structures and the bucket will then be weighed and recorded.

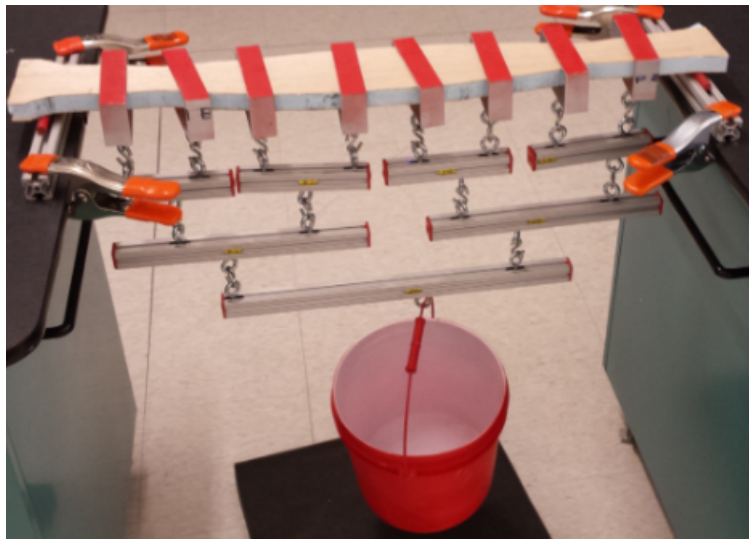


Figure 129. General Whiffle-tree Setup

6.3.2.2 Design of Whiffle Tree Layout.

The lift distribution along the glider wing is assumed to be elliptical and can be modeled using the equation;

$$F(x) = \frac{1}{L} \sqrt{L^2 - x^2} \quad (28)$$

Where L is the length of the wing and x is the location along the span of the wing. This distribution was multiplied by $\frac{1}{L}$ to normalize the lift from 0 - 1. Only the shape of the distribution is what will be of interest throughout this analysis. The goal of the whiffle-tree loading is to as closely match this distribution as possible. The aluminum bars being used to construct the whiffle tree are listed below along with their respective length.

Length	Quantity
6"	4
12"	2
18"	1

The 6" bars will be hung directly from the wing so that 8 discrete forces will act along the wingspan. Locations of the 6" bars were selected to minimize the error between the whiffle-tree loading and actual aerodynamic loading. Fig. 130 shows the comparison of the two distributions.

Because the whiffle tree is a statically determinate structure, equations can be derived to determine how the total force of the bucket is distributed through the whiffle tree structure. For a static structure:

$$\Sigma F_y = 0 \quad (29)$$

$$\Sigma M_z = 0 \quad (30)$$

The free body diagram (Fig. 131) of a bar in the whiffle-tree structure can be used in addition to these equations to compute how the force is distributed. These equations of motion can be used to solve for $\frac{B}{A}$ and F_0

$$F_0 = F_1 + F_2 \quad (31)$$

$$\frac{B}{A} = \frac{F_1 - F_2}{F_0} \quad (32)$$

Starting from the loads at the eight discrete points shown in Fig. 130, the forces and relative locations of the other bars can be computed all the way down the whiffle-tree. Because the lengths of the bars are known, the values of $\frac{B}{A}$ can be used to calculate how far along the length of each bar to place the supports. These locations are tabulated in Tab. 90 and used to plot the set up of the whiffle tree shown in Fig. 132.

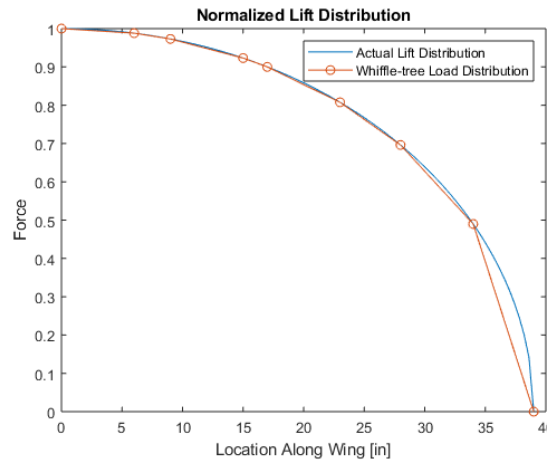


Figure 130. Load Distribution Comparison

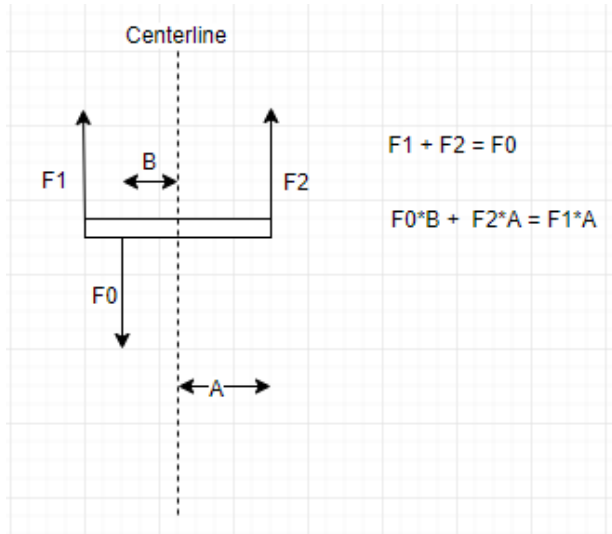


Figure 131. Whiffle-tree FBD

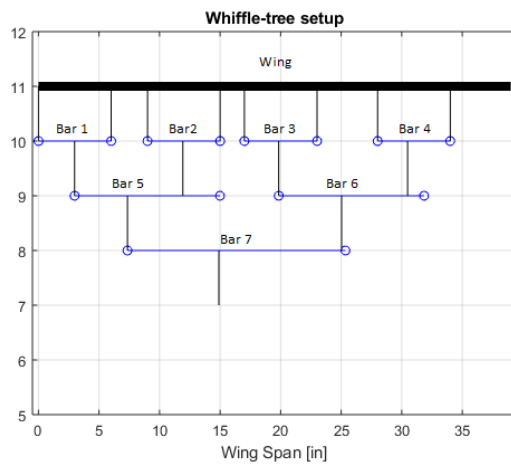


Figure 132. Actual Whiffle-tree Setup

Bar Number	Support Location Along Bar
Bar 1	2.98"
Bar 2	2.92"
Bar 3	2.84"
Bar 4	2.48"
Bar 5	4.36"
Bar 6	5.19"
Bar 7	7.55"

Table 90. Location of eye bolts for each bar

6.3.2.3 Test Logistics

The test will take place inside of the ITLL laboratory. The wing will be mounted to an empty lab cart found within the ITLL. All materials needed for testing other than the wing will be provided by the Aerospace department. Approval to use this equipment has been granted by Bobby Hodgkinson. This includes all necessary clamps, bars, supports, loops, and weights. The test will take place during the week of 12/16/18.

6.3.2.4 Materials

Item	Qty
Wing/Fuselage	1
Lab Cart	1
Foam Pad	1
Aluminum Support	2
Clamps	4
Aluminum Loops	8
6" Aluminum Bar	4
12" Aluminum Bar	2
18" Aluminum Bar	1
Bucket	1
Various Weights	1
Calipers	1

6.3.2.5 Procedure

1. Locate an empty test cart in the ITLL and gather the whiffle tree testing kit
2. Securely clamp the fuselage to the edge of the lab cart using the clamps so that the root of the wing is flush with the edge of the cart and is level with the ground
3. Slide the eye bolts to the correct location of each bar according to Tab. 90 using the calipers and tighten the bolts in place.
4. Measure and mark the eight locations along the wing where the aluminum loops will be placed
5. Slide each aluminum loop around the wing to the previously marked locations
6. Hang the three tiered whiffle tree from the aluminum loops on the wing
7. Hang the bucket from the bottom bar and position the foam pad underneath the bucket
8. Add the weights one by one starting with the heaviest and moving down until the wing fails
9. Place all pieces of the assembly in to the bucket and weigh
10. Record the total weight and the mode in which the wing failed

6.4. Thermal Test

6.4.1. Test Overview

The purpose of this test is to verify **DR 5.2.2.1.** This requires that the thermal tape applied to the fuselage is effectively shielded from the exhaust plume of the rocket engine. The vehicle must not sustain any damage to its MonoKote skin or balsa structures while the engine is burning. Any damage would lead to a critical failure of the entire mission making it crucial that the thermal shielding is verified before flight testing begins. During the first seconds of launch, the vehicle will still be moving relatively slow and there will be minimal airflow acting on the motor and fuselage. It will be at this time that the rocket exhaust is most likely to damage the vehicle. To verify that the selected thermal tape is effective in mitigating this risk, a static launch of the motor will be conducted. The fuselage with thermal tape applied to its belly will be positioned near the motor as it would be in the final assembly. Temperature measurements of the exhaust plume and outside surfaces of the fuselage will be measured using an IR camera. A thermocouple will be attached to the inside of the fuselage to measure the interior temperatures of the vehicle.

Due to the inherent danger in firing a rocket motor, RAPTR personnel conducting this test will follow a strict safety procedure and be familiar with all corresponding accident prevention protocols. Because Aerospace Department equipment and funds will be used for the testing, approval will first need to be given by both Matt Rhode and Bobby Hodgkinson.

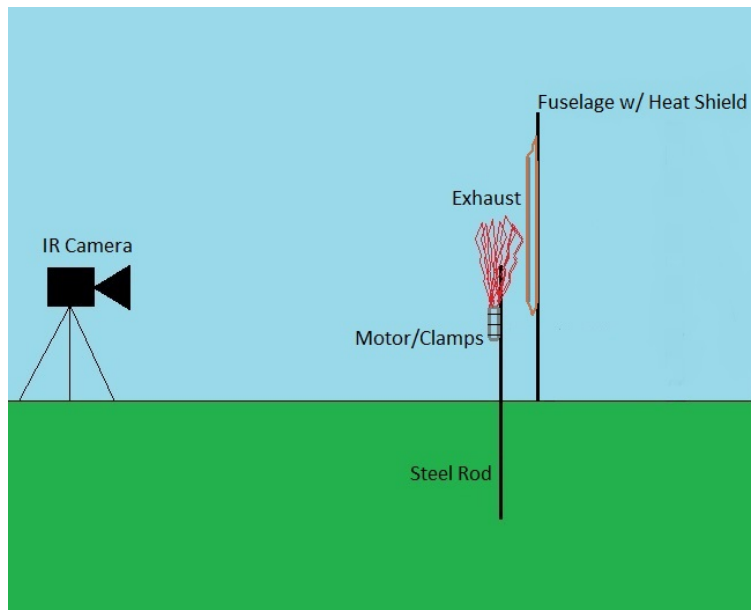


Figure 133. Basic test setup

6.4.2. Test Logistics

6.4.2.1 Testing Site

The test is aimed to take place during the week of **01/13/19** on East Campus. This location has been selected due to the fact that the rocketry club, COBRA, has previously performed static launches at this site. A map of this location is shown in Fig. 135. A 200 feet exclusion zone radius will be enforced for any persons not involved with testing or behind cover. The entrance to the parking lot will be blocked with caution tape and no firings will occur if cars are on the nearby road. The lot will be vacated and all debris within 30 feet of the test stand will be removed before firing.



Figure 134. Location of testing site

6.4.2.2 Local Emergency Services

Service	Contact Info	Response Time
Boulder Community Health	(303) 415-7000	10-20 min
Boulder Fire Station 3	(303) 441-3350	8-12 min

6.4.2.3 Personnel Breakdown

Name	Title	Role
Greg Clements	Safety Officer and Lead Test Engineer	Ensure all safety procedures are followed and all instrumentation is properly installed
Anna Tiberi	Spotter and Test Engineer	Ensure all personnel and bystanders are either behind cover or outside the exclusion zone and assist in test set-up/procedure
Matt Rhode	Facilities Manager	School representative and testing consultant

6.4.3 Materials

6.4.3.1 Materials List

Category	Item	Qty.
Safety Equipment	Safety Glasses	1 for each person
	Fire Extinguisher	1
	Earplugs	1 pair for each person
Motor	Motor Casing	2
	Propellant Grains	6
	Nozzle	2
	Igniter	6
	Launch Controller	1
Test Setup	C Alkline Battery	8
	Steel Rod	2
	Hose Clamp	6
Measurement Devices	Fuselage w/ heat shield	2
	Infrared Camera	1
	Calipers	1
	Tripod	1
Tools	Temperature Sensor Board	1
	Hammer/Mallet	1
	Phillips Head Screwdriver	1

6.4.3.2 Safety Hazards

Hazard	Mitigation
Chemical energy stored in propellant grains	Grains will be stored and carried in antistatic bags to prevent premature ignition. Ignition leads will be shorted until launch countdown. Any personnel handling propellant grains will be electrically grounded.
Heat from motor firing	A hold time of four minutes will be implemented during which no personnel may approach the launch stand. Materials will be handled only after they are cool to the touch
Toxic exhaust fumes	No personnel shall approach the launch stand until four minutes after the completion of the firing when all fumes have dispersed.
Fire	All flammable materials will be removed from the testing zone. A fire extinguisher will be kept on hand to extinguish small, persisting fires after firing

6.4.4. Go/No-Go Criteria

Before the motor firing is initiated, the following criteria must be checked and satisfied;

- Motor securely clamped to test stand (Pre-retreat check, two person verification)
- Temperature sensor package functioning nominally (Pre-retreat check)
- Cameras Recording (Pre-retreat check, two person verification)
- All personnel located behind cover with safety glasses and earplugs
- Exclusion zone is vacated and no cars are driving by on the nearby road

6.4.5. Procedure

6.4.5.1 Pre-Firing Procedure

1. Ensure camera power and storage is sufficient before going to test site
2. Once arriving to the site, unload all necessary materials and gain pad clearance from facility manager
3. Hammer steel rods two feet into the ground leaving 1.8" of space between them
4. Securely clamp the motor casing to the bottom of the steel rod using 3 hose clamps
5. Install temperature sensor package on the inside of the fuselage
6. Clamp the fuselage with thermal tape on to the other steel rod so that the belly covered in thermal tape is facing the motor and the front end of the fuselage is flush with the front end of the motor
7. Position the thermal and video camera 20 feet away from the motor test stand
8. Verify no reflective material is prohibiting the functionality of the thermal camera
9. Power on temperature sensor package and begin recording with cameras
10. Ensure the exclusion zone is clear of people and debris
11. Announce hot pad
12. Remove 1 propellant grain from its antistatic bag at a time and install into the motor casing, ensuring that they are correctly oriented, until all three grains have been added
13. Screw the nozzle onto the end of the motor casing
14. Ensure the safety key of the launch controller is removed
15. Carefully install the igniter into the motor
16. All personnel retreat to safe firing location
17. Verify go/no-go criteria are satisfied
18. Attach igniter leads to the controller leads
19. Install firing key into the launch controller
20. Verify continuity of the ignition system and announce
21. Initiate launch countdown and fire

6.4.5.2 Post-Firing procedure

1. If any small fires persist after firing, one member may approach the test stand after 20s to extinguish with the fire extinguisher
2. If any larger fires persist and begin spreading, contact fire department immediately and do not attempt to fight the fire
3. Otherwise all personnel must wait at least four minutes before entering the exclusion zone
4. Verify that all combustion has completed
5. Stop cameras
6. verify that all equipment including the motor casing, steel rods, and fuselage have adequately cooled down before attempting to handle. Assume all materials are very hot and use extreme caution
7. Remove fuselage from rod and power off the temperature sensor
8. Assess any damage that was sustained by the fuselage and record
9. Remove motor casing from the rod
10. Leave the pad area and ensure all materials have been vacated from the area
11. Ensure all materials in the materials list are accounted for before leaving the site
12. Confirm with facility manager that all requirements have been met

6.4.6 Success Criteria

For the test to be considered successful, the thermal shielding applied to the fuselage must completely have protected the fuselage from any damage. If the fuselage shows damage anywhere throughout the body such as melting or deformation, an alternate thermal shield must be re-tested using the same procedure. Additionally, the thermal camera must capture useful video of the motor burn. It is important to know how hot the plume is and how it interacts with the fuselage. This will be important if different thermal shielding must be selected. The temperature sensor inside of the fuselage must also capture accurate data. This will be important for verifying that the electronics inside will be kept at their respective operating ranges during full systems tests.

6.5 Wind Tunnel Testing

6.5.1 Test Overview

The purpose of this test is to verify **DR1.2**, **DR1.2.1**, and **DR1.2.2**. These requirements relate to the fact the vehicle must have a glide slope of less than 5.7 deg in order to image the entire 2000 ft corridor. In order for this to be met, the vehicle must have a lift to drag ratio of at least 10. CFD analysis has been completed on the vehicle after the motor has detached and showed that the lift to drag ratio is indeed greater than 10. To verify this, a scale model of the glider will be 3D printed and tested in the Aerospace Department's wind tunnel located in the ITLL. It will be mounted to a sting balance which measures the axial and normal forces acting on the scale model which will be used to compute the lift and drag forces. The angle of attack will be varied from -10 to 10 deg in one deg increments.

6.5.2 Test Logistics

This test is aimed to take place during the week of **01/27/19**. It will require special access granted to the wind tunnel by Bobby Hodgkinson. The scale model of the vehicle will be printed using the 3D printers available at the ITLL. It is critical that the wind tunnel is operated safely to avoid causing any damage. This means two people will verify a number of things before powering on the wind tunnel;

- The model is securely mounted to the sting balance
- There are no loose materials located inside of the test section
- Both clamps used to seal the test section are securely locked shut

After these things are verified by two people, the wind tunnel can be slowly brought up to speed. Measurements will be taken at an airspeed of 50 m/s to match the flight conditions of the actual mission.

6.5.3. Materials

- Scale Model Vehicle
- ITLL Wind Tunnel
 - Sting Balance
 - Airspeed Sensor

6.5.4. Procedure

1. Open the test section door and mount the scale model to the sting balance
2. Verify all three criteria listed in test logistics are met
3. Run Labview on a laptop and verify all sensors are operating nominally
4. Rotate the balance so that the model is at -10 deg angle of attack using the measurement displayed on Labview
5. Slowly increase the airspeed to 50 m/s
6. After the measurements becomes stable for a few seconds, save the last 100 points to a file using Labview
7. Repeat taking measurements and saving the data for angles of attack up to 10 deg in one deg increments
8. Verify that the data file contains 2000 lines of measurements
9. Slowly bring the airspeed back down to 0 m/s
10. Close Labview and retrieve all materials from the test section of the wind tunnel

6.5.5. Success Criteria

The measurements of the wind tunnel testing will be post processed in MATLAB to convert the axial and normal forces to drag and lift forces at each angle of attack using the following equations;

$$L = N\cos(\alpha) - A\sin(\alpha) \quad (33)$$

$$D = A\cos(\alpha) + N\sin(\alpha) \quad (34)$$

Where α is the angle of attack, N is the normal force, and A is the axial force. The lift and drag at each angle of attack will then be plotted alongside of the predictions made using CFD. The lift to drag ratio will also be plotted for each angle of attack. If the maximum lift to drag ratio is greater than 10, **DR1.2** has been successfully verified. If it is not, and there is considerable deviations from the wind tunnel results and the CFD analysis, the test has failed. One key error that may cause this to happen is the accuracy of the scaled model. It will be very important to print this model so that it as closely matches the model used for CFD analysis. This means a high quality 3D printer must be used. Additionally it may require that the fuselage and wings are printed separately and fitted together afterwards.

6.6. Communications Integration Test

6.6.1. Test Overview

The purpose of this test is to verify **DR 3.1.1**, **DR 3.2**, and **DR 3.3**. **DR 3.1.1** relates to the fact that the vehicle will include three separate radio transmitters; One will be used for transmitting image data, one will be used to transmit vehicle telemetry data from the PixHawk, and one will be used to manually control the vehicle. The radio controller and payload transmitters will both be operating over the 2.4 GHz frequency. It is therefore critical that these transmitters are operating on appropriate channels as to avoid interference between one another. **DR 3.2** states that all communications must have a range of at least 4000ft, which is the maximum distance the vehicle will be from the ground station over the course of its mission. Finally, **DR 3.3** requires that the vehicle is radio transparent. These requirements all serve to ensure that image and telemetry data is able to be transmitted from the vehicle to the ground station over the entire mission profile. To verify these requirements are met, the communications system will be integrated with the vehicle and data will be sent to a ground station 4000ft away. The integrated system will

include all components of the final system including the PixHawk, imaging payload, and antenna. It must be capable of transmitting all sets of data through the vehicle over a 4000ft distance without interference. The quality of the data received by the ground station will be analyzed to determine whether these three design requirements are verified.

6.6.2. Test Logistics

This test is aimed to take place during the week of **02/03/19**. It will be completed at CU South Boulder Campus located right off of Highway 36. Permission from CU Flight Director Dan Hesselius will be granted prior to testing. This is to ensure the communication system does not interfere with others attempting to fly in that area. A image of the test site is shown below in Fig. 135.

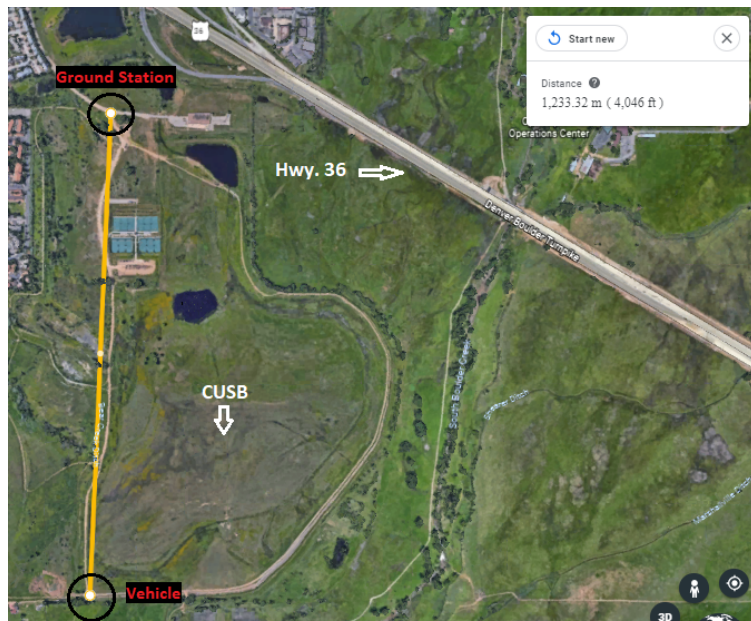


Figure 135. Test Site

6.6.3. Materials

- Fully Built AndREaS Glider
 - PixHawk Flight Controller
 - Imaging Payload
 - Imaging Antenna
 - Batteries
- RC controller
- Ground Station Laptop
- Ground Station Receiver

6.6.4. Procedure

1. Assemble the electronics inside of the vehicle fuselage
2. Drive to "Ground Station" location of CUSB
3. Measure location with GPS using a cellphone and record
4. Power on the vehicle's PixHawk and payload
5. Initiate data transmission and verify it is being received by the ground station

6. One member take the vehicle and drive down the road to "Vehicle" location on map
7. Measure location with GPS using a cellphone and record
8. Continue transmitting data at this location for up to two minutes
9. Members at the "Ground Station" location input commands to the vehicle using RC controller
10. Rendezvous at the "Ground Station" location
11. Power off vehicle electronics and stop transmitting data
12. Review quality of transmitted data throughout testing

6.6.5. Success Criteria

The data being transmitted must be received by the ground station just as it would during full systems testing. The location of the ground station and vehicle measured during testing must be at least 4000ft apart. If any interference between the payload and PixHawk occurs, the payload software will either provide an error message or produce noticeably corrupt images. Additionally, the PixHawk will report connection errors. If interference does occur, different channels will have to be selected for the communication systems and the test must be repeated. If the data stops transmitting before the vehicle is taken to 4000ft away, different hardware may have to be selected to increase the system's range. Finally, if the systems are unable to transmit data through the vehicle itself, different materials for the vehicle may have to be considered. If none of these things occur during testing, then the communications system has been successfully verified.

6.7. Controls Testing/Tuning

6.7.1. Test Overview

The purpose of this test is to verify **DR 1.1**, **DR 1.1.1**, **DR 1.1.4**, and **FR 6**. These requirements relate to the fact that the vehicle must be controlled throughout its flight. While the motor is burning, it must be controlled manually to stabilize the pitch. After the motor is done burning, the vehicle must correct its flight path and be capable of navigating along a specified set of GPS waypoints. Finally, the vehicle must also be capable of performing a controlled landing. To verify these requirements are satisfied, a fully built vehicle will be flown without the rocket engine. The tuning parameters used by the PixHawk flight controller to control the vehicle will be improved using the "AUTOTUNE" function of ArduPilot. After it has been verified that the vehicle is adequately tuned, the vehicle will be flown to verify that is able to perform a turn radius of 350 ft and perform a controlled landing.

6.7.2. Test Logistics

This test is aimed to take place during the week of **02/10/19**. It will take place on the south face of NCAR shown in Fig. 136. This is a popular slope soaring location for hobby RC pilots due to its accessibility and steepness. The test will need to be performed on a day with strong enough winds coming from the south to provide enough lift to the vehicle. If the method of slope soaring the glider deems itself to be too difficult or wind conditions are not ideal, other methods of flying the glider will need to be considered. One of these methods is to use a bungee high start. The AndREaS glider being used is built with a connection on the bottom of the fuselage for this very reason and can be easily used to complete flight tests. Another method that could be considered is using the electric propeller that is optional with this glider kit.

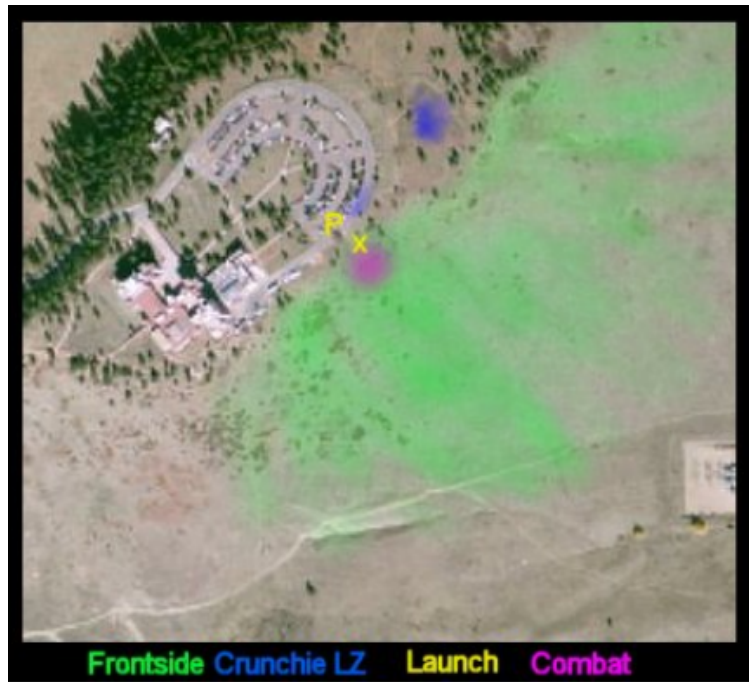


Figure 136. Slope Soaring Location

6.7.3. Materials

- Fully Built Glider
 - PixHawk 4 Flight Controller w/ GPS Module
 - Battery
 - Servos x2
 - FrSky X8R Receiver
 - Airspeed Sensor
 - Telemetry Radio
- FrSky Radio Controller
- Laptop w/ ArduPilot

6.7.4. Procedure

1. Load all equipment into car and drive to the NCAR parking lot
2. Walk to the south face of the slope shown in Fig. 136
3. Power on vehicle electronics
4. Confirm telemetry data is being transmitted and received
5. Confirm wind is blowing up the slope
6. Switch flight mode to "AUTOTUNE"
7. Hand launch vehicle off slope
8. Control vehicle so that it flies in figure eights parallel to the slope, turning into the wind
9. Input maximum yaw and pitch commands in both directions while vehicle is in flight

10. Once the glider loses lift or at least 10 commands for pitch and yaw have been inputted in each direction, land the glider in the landing zone marked in Fig. 136
11. Using the telemetry data gathered in ArduPilot, verify that the demanded vehicle attitude and achieved attitude are equal to each other
12. Repeat flights as necessary to further improve tuning parameters and verify the vehicle can be controlled during flight and landing

6.7.5. Success Criteria

For the test to be a success the vehicle will first need to be properly tuned using the "AUTOTUNE" function. This will be verified by looking at a plot of the demanded attitude and achieved attitude of the vehicle during flight. An example of this plot is shown below in Fig. 137 . Next the vehicle will flown to verify that it is capable of a turn radius of at least 350ft and that it is stable while gliding. This can be verified by looking at the flight path and attitude of the glider in ArduPilot after flight. Finally, the vehicle will be landed to verify that it is capable of a controlled landing. Once all of these requirements are verified, the test can be considered a success.

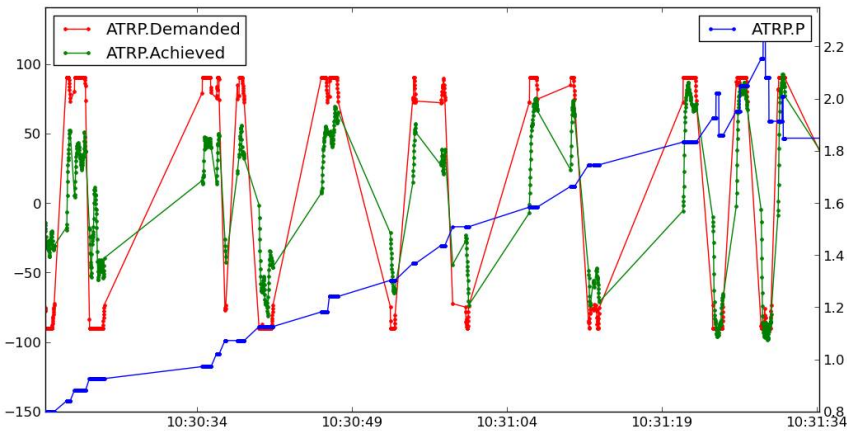


Figure 137. Example tuning plot

6.8. Vehicle Systems Testing

6.8.1. Test Overview

The purpose of this test is to validate **FR 1, 2, and 6**. These requirements relate to the fact the aerial system needs to fly over the region of interest in order to image potential targets. Additionally, the system must be man-portable and comply with all federal and state laws. The test used to validate these functions of the system will be nearly identical to the final full systems tests. For these tests however, the imaging payload will be replaced with a dummy mass. This is because it is important to validate the vehicle design before risking damage to the expensive payload. The otherwise fully-built vehicle will be launched in association with the Northern Colorado Rocketry (NCR) club at their launch site just west of National Pawnee Grassland. After the launch stand is oriented and the vehicle is mounted to it, the rocket will be ignited and the vehicle will be manually controlled during ascent. Once the motor burns out, the pilot will switch the flight mode to autopilot. The mission planner feature of ArduPilot will be used to program the flight controller prior to launch. The waypoints will be specified so that the vehicle navigates 4000ft downrange and then performs a belly landing. The vehicle must fly over the target region (2000 - 4000ft downrange) while at an altitude of 600 - 700ft for **FR 1** to be validated.

Due to the inherent danger of firing a rocket motor, RAPTR personnel conducting this test will follow a strict safety procedure and be familiar with all corresponding accident prevention protocols. Extra caution will be used when handling and installing the propellant grains. Additionally, spotters will be located downrange to maintain a visual line of sight with the vehicle and radio potential abort commands back to the pilot.

6.8.2. Test Logistics

6.8.2.1 Testing Site

There are currently three launch dates that are scheduled by NCR that RAPTR intends to use for vehicle validation testing. These dates are **03/02/19**, **03/09/19**, and **03/30/19**. All of these launches will take place at NCR's Atlas Site shown in Fig. 138. This is located just west of the National Pawnee Grassland in northern Colorado. A 200ft radius safety zone will be enforced as suggested by Tripoli safety codes for "T" class research launches.

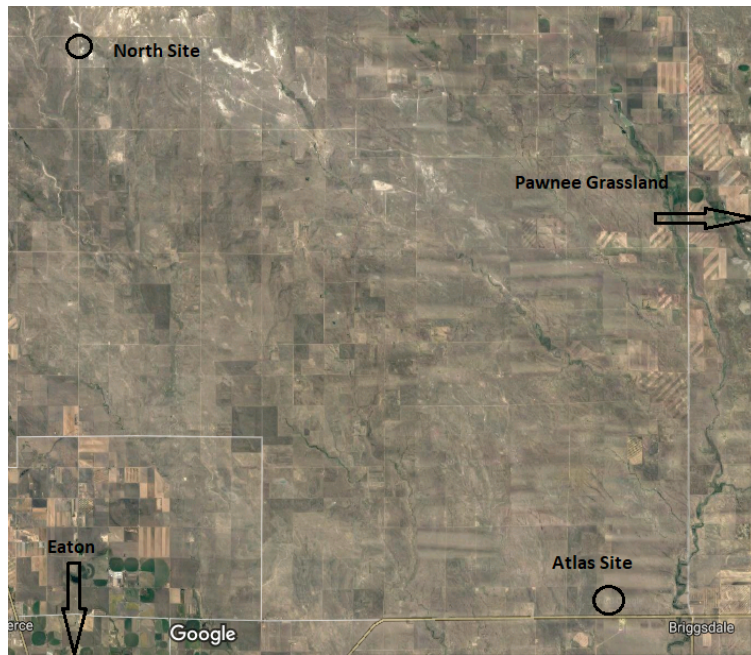


Figure 138. Launch sites

6.8.2.2 Local Emergency Services

Service	Contact Info	Response Time
UCHealth Poudre Valley Hospital	(970) 495-7000	40-60 min
Nunn Volunteer Fire Department	(970) 381-4402	20-30 min

6.8.2.3 Personnel Breakdown

The following table provide a comprehensive breakdown of all RAPTR personnel conducting the test. There will likely be multiple other members of RAPTR available to assist if any of the following people request it. All members present during testing will be made aware of all safety and accident-prevention protocols.

Name	Title	Role
Greg Clements	Safety Officer/Test Engineer	Ensure all safety procedures are followed and coordinate test procedure
Anna Tiberi	Firing Officer	Carry out motor installation and firing
Logan Thomas	Spotter	Ensure safety zone is vacated prior to launch and visual line of sight of vehicle is maintained
Tyler Faye	Electronics Engineer	Assist with electronics installation/verification prior to launch
Zach Donovan	Controls Engineer	Oversee mission planning in ArduPilot software and monitor telemetry data
Dan Hesselius	Pilot	Manually pilot vehicle during ascent and input potential abort commands
Joe Hinton	NCR Point of Contact	Representative of Northern Colorado Rocketry Club

6.8.3. Materials

Below is a list of materials that will be used for each test to be conducted. All electronics will be installed into the vehicle prior to testing. Additionally, the motor mount will be attached and thermal tape will be applied. The battery power of the vehicle battery, radio controller, radios, cameras, and launch controller will all be checked before leaving as well. Enough materials will be brought to each launch day for two launches.

Category	Item	Qty.
Safety Equipment	Safety Glasses	1 per person
	Earplugs	1 pair per person
	Fire Extinguisher	2
Motor	Motor Casing	2
	Propellant Grains	6
	Nozzle	2
Launch Setup	Launch Stand	1
	Igniter	6
	Launch Controller	1
	C Alkline Battery	8
Vehicle	Glider w/ Electronics	1
	Radio Controller	1
	Dummy Payload Mass	1
	Motor Mount	1
Tools/Other	Laptop	1
	Video Camera	2
	Hammer/Mallet	1
	Tongs	2
	Tripod	2
	Radio	4

6.8.3.1 Safety Hazards

Hazard	Mitigation
Chemical energy stored in propellant grains	Grains will be stored and carried in anti-static bags to prevent premature ignition. Ignition leads will be shorted until launch countdown. Any personnel handling propellant grains will be electrically grounded.
Heat from motor firing	A hold time of four minutes will be implemented during which no personnel may approach the launch stand. Materials will be handled only after they are cool to the touch with tongs
Toxic exhaust fumes	No personnel shall approach the launch stand until four minutes after the completion of the firing when all fumes have dispersed.
Fire	All flammable materials will be removed from the testing zone. A fire extinguisher will be kept on hand to extinguish small, persisting fires after firing

6.8.4. Go/No-Go Criteria

Before the motor firing is initiated, the following criteria must be checked and satisfied;

- Vehicle is properly mounted to launch stand (Pre-retreat check)
- Motor grains are properly oriented and installed into motor casing (Pre-retreat check, two person verification)
- All vehicle electronics functioning nominally (Pre-retreat check)
- Cameras Recording (Pre-retreat check, two person verification)
- Mission planner is functioning nominally, telemetry data is being received
- All personnel located outside of safety zone with safety glasses and earplugs
- Spotter is safely located downrange

6.8.5. Procedure

The following test procedure will be used for all vehicle systems tests that are performed. If any failures initially occur that do not destroy the vehicle, the pre-firing procedure will be repeated with the extra propellant grains included in the materials list.

6.8.5.1 Pre-Firing Procedure

1. Ensure all battery power and camera storage is sufficient before going to test site
2. Once arriving to the site, unload all necessary materials and gain pad clearance from facility manager
3. Stake launch stand into the ground and orient rails to directly vertical position
4. Mount vehicle to launch stand
5. Position the video cameras 20 feet away from the launch stand
6. Power on and calibrate vehicle electronics
7. Begin recording with cameras
8. Verify all electronics are functioning nominally including radio controller
9. All personnel vacate safety zone except test engineer and firing officer
10. Announce hot pad
11. Remove 1 propellant grain from its anti-static bag at a time and install into the motor casing, ensuring that they are correctly oriented, until all three grains have been added

12. Screw the nozzle onto the end of the motor casing
13. Ensure the safety key of the launch controller is removed and ignition leads are detached from controller leads
14. Carefully install the igniter into the motor
15. All personnel retreat to safe firing location
16. Spotter assume safe location down range
17. Verify go/no-go criteria are satisfied
18. Attach igniter leads to the controller leads
19. Firing Officer install firing key into the launch controller
20. Verify continuity of the ignition system and announce
21. Initiate launch countdown and fire

6.8.5.2 Flight procedure

1. Pilot control vehicle to maintain a zero angle of attack during ascent
2. Once motor burns out, pitch vehicle and initiate autopilot mode
3. Spotter maintain visual line of site as it glides downrange, alerting pilot if abort is needed
4. Spotter announce when the vehicle lands

6.8.5.3 Post Flight Procedure

1. If any small fires persist after firing, one member may approach the fire after 20s to extinguish with the fire extinguisher
2. If any larger fires persist and begin spreading, contact fire department immediately and do not attempt to extinguish the fire
3. Otherwise all personnel must wait at least four minutes before approaching the launch stand
4. Verify that all combustion has completed
5. Stop cameras
6. Verify that all equipment including the motor casing, launch stand, and vehicle have adequately cooled down before attempting to handle. Assume all materials are very hot and use extreme caution
7. Spotter will retrieve vehicle
8. Assess any damage that was sustained by the vehicle and record
9. Disassemble launch stand
10. Leave the pad area and ensure all materials have been vacated from the area
11. Review flight telemetry data of the vehicle
12. Ensure all materials in the materials list are accounted for before leaving the site
13. Confirm with facility manager that all requirements have been met

6.8.6. Success Criteria

Testing will need to be repeated until the following criteria are met:

- Rocket motor successfully ignited
- Motor mount remained attached to the vehicle and vehicle was successfully propelled off of launch stand
- Cameras captured launch of the vehicle
- Pilot successfully controlled the vehicle during ascent maintaining zero angle of attack
- Motor detached from vehicle after burning and parachute successfully deployed
- Vehicle transmitted all telemetry data back down to ground station throughout entire flight
- Vehicle sustained no structural failure during flight
- Vehicle glided 4000ft downrange while maintaining an altitude of 600 - 700ft
- Vehicle performed a controlled belly landing

6.9. Full Systems Testing

6.9.1. Test Overview

The purpose of this test is to validate all functional requirements of project RAPTR. This test will be nearly identical to the vehicle systems test. For these tests however, the imaging payload will be integrated with the vehicle. The fully integrated vehicle will be launched in association with the Northern Colorado Rocketry (NCR) club at their launch sites just west of National Pawnee Grassland. After the launch stand is oriented and the vehicle is mounted to it, the rocket will be ignited and the vehicle will be manually controlled during ascent. Once the motor burns out, the pilot will switch the flight mode to autopilot. The mission planner feature of ArduPilot will be used to program the flight controller prior to launch. The waypoints will be specified so that the vehicle navigates 4000ft downrange and then performs a belly landing. Once the vehicle reaches the target region (2000 - 4000ft downrange) the imaging payload will begin capturing and transmitting images to the ground station. These images will be run through the target detection, geo-location, and classification software on the ground station. The vehicle must sweep the target region at 600 - 700ft altitude, the imaging payload must capture and transmit images of the target region to the ground station, and the software must detect, classify, and locate any targets. This must all be done in less than 3 minutes for the project to be a success.

Due to the inherent danger of firing a rocket motor, all personnel conducting this test will follow a strict safety procedure and be familiar with all corresponding accident prevention protocols. Extra caution will be used when handling and installing the propellant grains. Additionally, spotters will be located downrange to maintain a visual line of sight with the vehicle and radio potential abort commands back to the pilot.

6.9.2. Test Logistics

6.9.2.1 Testing Site

There are currently three launch dates that are scheduled by NCR that RAPTR intends to use for full systems validation testing. These dates are **04/06/19, 04/13/19, and 05/03/19**. Each of these dates is on a Friday and could potentially be shifted to another day of that weekend if weather is non-ideal. All of these launches will take place at NCR's North Site shown in Fig. 138. This is located just west of the National Pawnee Grassland in northern Colorado. A 200ft radius safety zone will be enforced as suggested by Tripoli safety codes for "I" class research launches.

6.9.2.2 Local Emergency Services

Service	Contact Info	Response Time
UCHealth Poudre Valley Hospital	(970) 495-7000	40-60 min
Nunn Volunteer Fire Department	(970) 381-4402	20-30 min

6.9.2.3 Personnel Breakdown

The following table provide a comprehensive breakdown of all RAPTR personnel conducting the test. There will likely be multiple other members of RAPTR available to assist if any of the following people request it. All members present during testing will be made aware of all safety and accident-prevention protocols.

Name	Title	Role
Greg Clements	Safety Officer/Test Engineer	Ensure all safety procedures are followed and coordinate test procedure
Anna Tiberi	Firing Officer	Carry out motor installation and firing
Logan Thomas	Spotter	Ensure safety zone is vacated prior to launch and visual line of sight of vehicle is maintained
Tyler Faye	Electronics Engineer	Assist with electronics installation/verification prior to launch
Zach Donovan	Controls Engineer	Oversee mission planning in ArduPilot software and monitor telemetry data
James Wells	Imaging Payload Lead	Ensure proper installation of payload and monitor payload data
Jeremy Lane	Software Lead	Setup and monitor ground station
Dan Hesselius	Pilot	Manually pilot vehicle during ascent and input potential abort commands
Joe Hinton	NCR Point of Contact	Representative of Northern Colorado Rocketry Club

6.9.3 Materials

Below is a list of materials that will be used for each test to be conducted. All electronics will be installed into the vehicle prior to testing. Additionally, the motor mount will be attached and thermal tape will be applied. The battery power of all vehicle batteries, radio controller, radios, cameras, and launch controller will all be checked before leaving as well. Enough materials will be brought to each launch day for two launches.

Category	Item	Qty.
Safety Equipment	Safety Glasses	1 per person
	Earplugs	1 pair per person
	Fire Extinguisher	2
Motor	Motor Casing	2
	Propellant Grains	6
	Nozzle	2
Launch Setup	Launch Stand	1
	Igniter	6
	Launch Controller	1
	C Alkline Battery	8
Vehicle	Glider w/ Electronics	1
	Radio Controller	1
	Dummy Payload Mass	1
	Motor Mount	1
	Payload	1
Tools/Other	Laptop	1
	Ground Station Receiver	1
	Video Camera	2
	Hammer/Mallet	1
	Tongs	2
	Tripod	2
	Radio	4
	5' x 5' Marked Target	2

6.9.3.1 Safety Hazards

Hazard	Mitigation
Chemical energy stored in propellant grains	Grains will be stored and carried in anti-static bags to prevent premature ignition. Ignition leads will be shorted until launch countdown. Any personnel handling propellant grains will be electrically grounded.
Heat from motor firing	A hold time of four minutes will be implemented during which no personnel may approach the launch stand. Materials will be handled only after they are cool to the touch with tongs
Toxic exhaust fumes	No personnel shall approach the launch stand until four minutes after the completion of the firing when all fumes have dispersed.
Fire	All flammable materials will be removed from the testing zone. A fire extinguisher will be kept on hand to extinguish small, persisting fires after firing

6.9.4. Go/No-Go Criteria

Before the motor firing is initiated, the following criteria must be checked and satisfied;

- Vehicle is properly mounted to launch stand (Pre-retreat check)
- Motor grains are properly oriented and installed into motor casing (Pre-retreat check, two person verification)
- All vehicle electronics functioning nominally (Pre-retreat check)
- Cameras Recording (Pre-retreat check, two person verification)
- Mission planner is functioning nominally, telemetry data is being received
- All personnel located outside of safety zone with safety glasses and earplugs

- Spotter is safely located downrange

6.9.5. Procedure

The following test procedure will be used for all vehicle systems tests that are performed. If any failures initially occur that do not destroy the vehicle, the pre-firing procedure will be repeated with the extra propellant grains included in the materials list.

6.9.5.1 Pre-Firing Procedure

1. Ensure all battery power and camera storage is sufficient before going to test site
2. Once arriving to the site, unload all necessary materials and gain pad clearance from facility manager
3. Position one target 2500ft downrange and another 3500ft downrange with markings facing up
4. Measure GPS coordinates of each target using cellphone
5. Stake launch stand into the ground and orient rails to directly vertical position
6. Mount vehicle to launch stand
7. Position the video cameras 20 feet away from the launch stand
8. Power on and calibrate vehicle electronics
9. Begin recording with cameras
10. Verify all electronics are functioning nominally including radio controller
11. All personnel vacate safety zone except test engineer and firing officer
12. Announce hot pad
13. Remove 1 propellant grain from its anti-static bag at a time and install into the motor casing, ensuring that they are correctly oriented, until all three grains have been added
14. Screw the nozzle onto the end of the motor casing
15. Ensure the safety key of the launch controller is removed and ignition leads are detached from controller leads
16. Carefully install the igniter into the motor
17. All personnel retreat to safe firing location
18. Spotter assume safe location down range
19. Verify go/no-go criteria are satisfied
20. Attach igniter leads to the controller leads
21. Firing Officer install firing key into the launch controller
22. Verify continuity of the ignition system and announce
23. Initiate launch countdown and fire

6.9.5.2 Flight procedure

1. Pilot control vehicle to maintain a zero angle of attack during ascent
2. Once motor burns out, pitch vehicle and initiate autopilot mode
3. Spotter maintain visual line of site as it glides downrange, alerting pilot if abort is needed
4. Spotter announce when the vehicle lands

6.9.5.3 Post Flight Procedure

1. If any small fires persist after firing, one member may approach the fire after 20s to extinguish with the fire extinguisher
2. If any larger fires persist and begin spreading, contact fire department immediately and do not attempt to extinguish the fire
3. Otherwise all personnel must wait at least four minutes before approaching the launch stand
4. Verify that all combustion has completed
5. Stop cameras
6. Verify that all equipment including the motor casing, launch stand, and vehicle have adequately cooled down before attempting to handle. Assume all materials are very hot and use extreme caution
7. Spotter will retrieve vehicle
8. Assess any damage that was sustained by the vehicle and record
9. Disassemble launch stand
10. Leave the pad area and ensure all materials have been vacated from the area
11. Review flight telemetry data of the vehicle
12. Review image data and software output
13. Ensure all materials in the materials list are accounted for before leaving the site
14. Confirm with facility manager that all requirements have been met

6.9.6 Success Criteria

Testing will need to be repeated until the following criteria are met;

- Rocket motor successfully ignited
- Motor mount remained attached to the vehicle and vehicle was successfully propelled off of launch stand
- Cameras captured launch of the vehicle
- Pilot successfully controlled the vehicle during ascent maintaining zero angle of attack
- Motor detached from vehicle after burning and parachute successfully deployed
- Vehicle transmitted all telemetry data back down to ground station throughout entire flight
- Vehicle sustained no structural failure during flight
- Vehicle glided 4000ft downrange while maintaining an altitude of 600 - 700ft
- Payload captured images of target region and were transmitted and received by the ground station
- Software successfully detected targets within each image
- Software successfully located targets to within 150ft
- Software correctly classified target type
- Successfully detected targets were located and classified within 3 minutes from the time of launch
- Vehicle performed a controlled belly landing

7. Risk Assessment and Mitigation

Author: Logan Thompson

The RAPTR project involved several important risks, which are assembled into a matrix shown in Fig. 139. The largest risks stem from the temperatures generated by the vehicle's rocket motor, the controllability of the vehicle, particularly on ascent, and the interfaces between the electrical and aerospace project teams. The development of the design and the integration into a testable model carries technical challenges, such as the thermal effects of the rocket. Logistically, each risk represents some measure of time necessary to address the technical integration or safety concerns. However, safety is not a prominent risk that is being tracked, and financial risks are minimal as the project is currently far below budget with plenty of margin to correct for any major risk impacts.

The first of the risks is the uneven rocket engine moments. This risk stems from concerns on an earlier design that flowed down from FR 1 and stated that a cluster of rocket motors would generate a differential moment on burnout that would destabilize the rocket in flight. However, the motor cluster idea was shelved, and so this is a low impact risk for safety, finance, logistics, and technical concerns.

The second risk is the integrity of the wing on launch. This again stems from FR 1, as a wing failure would bar the vehicle from being able to fly over the imaging corridor. This presents significant logistical impacts on the project, as well as moderate financial ones to reproduce another vehicle and/or fix the wings.

The third risk is the ascent pitch control authority. Once more, this risk stems from FR 1. Without being able to control the ascent and reach the proper altitude, the vehicle will be unable to successfully traverse the imaging corridor. This presents large technical challenges, particularly with the consolidation of manual control, as well as financial and logistical impacts if the vehicle cannot properly ascend.

The fourth risk is the autopilot adaptation. Relating to FR 1, the autopilot program Ardupilot has to be manipulated to work with the project's unconventional mission profile, as it is mainly used for electric propeller-powered drones and other such unmanned aircraft. Failure of the Ardupilot software represents major and serious risk to the project's logistics and technical aspects. Large delay will stem from a failed autopilot, as the vehicle will likely get nowhere near the desired imaging corridor, and several testing dates will have to be delayed to address the risk.

The fifth risk is the NAR Certification for Launching and permission from the FAA to launch and test. This risk stems from FR 6, and will violate the customer given condition if not met. This represents major logistical problems, as lack of permission to test will push all testing dates by necessity.

The sixth risk is interference between the communications systems of the electrical and aerospace teams. This risk was identified when considering FR 1, FR 2, and FR 4. If the two systems interfere with each other, image data, telemetry data, and commands cannot be properly sent and received, and the mission will fail. This represents huge financial, and logistical impacts. However, the technical aspect is not large, as the two communications systems can simply use different channels on the same frequency.

The seventh risk is the payload weight; this risk stems from FR 1, since a too heavy payload will cause the vehicle to be unstable or otherwise fail in its mission to deliver the payload to and image the imaging corridor. Such a failure represents financial, logistical, and technical concerns in order to accommodate the electrical team's heavy payload or coordinate to scale down the payload's mass.

The eighth risk is the payload volume, stemming from FR 1, in the same vein as the seventh risk. A too large payload cannot be accommodated within the vehicle, and will thus present technical and logistical challenges.

The ninth risk is the physical integration of the aerospace team's vehicle and the electrical team's payload. This risk flows from FR 3, as no images can be transmitted if there are no images to transmit because the payload is incorrectly mounted. While this risk gives no serious implications to the aerospace team, it has technical and logistical implications for the electrical team.

The tenth risk is the thermal effects from the rocket motor mounted on the vehicle. Once again, this stems from FR 1. If the vehicle is too hot to work properly, then the corridor will not be properly reached. This represents major technical, logistical, and safety concerns, and is thus targeted for mitigation.

The eleventh risk is the data transmission rate, stemming from FR 3 and FR 5. Images cannot be properly transmitted in the appropriate time frame if the data is not able to transmit quickly enough. The vehicle is also only airborne for a certain amount of time, limiting ensured transmission time. The risk threatens large technical and logistical impacts.

The twelfth risk stems from FR 4 and involves the synchronization of data from the aerospace and electrical teams. Images from the electrical team must be matched with time-stamped data from the aerospace team in order to match the right locations and images together. Logistical and technical impacts flow from this risk.

The thirteenth risk is the image processing time, stemming from FR 5. In order to make the window, the images must be able to be processed quickly. Such a risk carries logistical and technical challenges, and encroaches on an essential customer requirement.

Credible mitigations intended to reduce the projects two highest risks are displayed in Fig. 140, along with the associated movements of risks caused by those mitigation strategies. A failure due to both risks will almost assuredly mean a mission failure. Successful implementation of this risk mitigations will go a long way to ensuring project success and mission success, as the two risks in question are the highest probable points of failure during the project's mission.

Risk Matrix

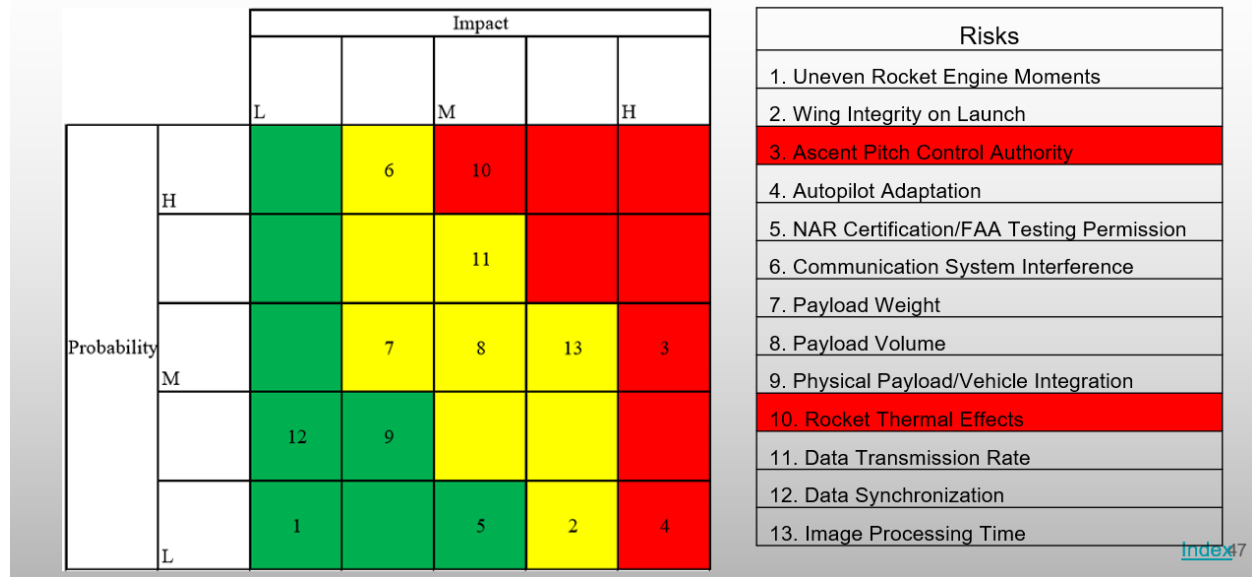


Figure 139. Normal Risk Matrix

Risk Mitigation

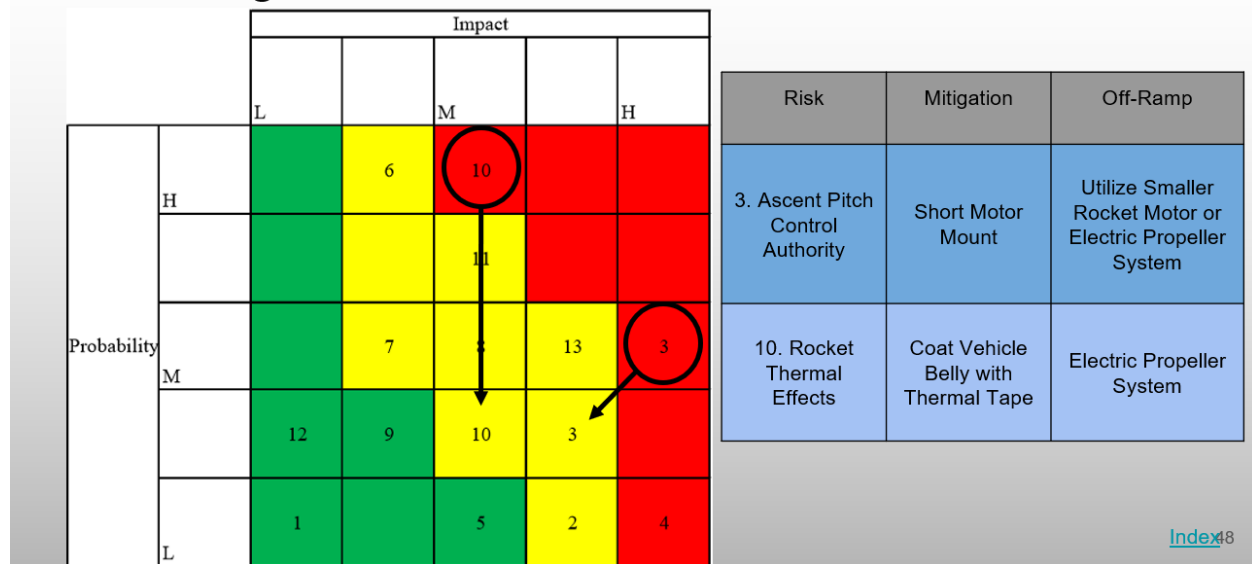


Figure 140. Mitigated Risk Matrix

8. Project Planning

Author: Aubrey McKelvy, Logan Thompson, and Everett Hale

8.1. Work Breakdown Structure

The work breakdown for the RAPTR project may be viewed in Fig. 141. Each sub-team's major milestones for the duration of the project are displayed, with those already completed in green and those that will be completed throughout the remainder of the project in red. Although comparatively small on the chart, the Integration and Test component of each sub-team will take the longest amount of time, since this will likely be a month long endeavour.

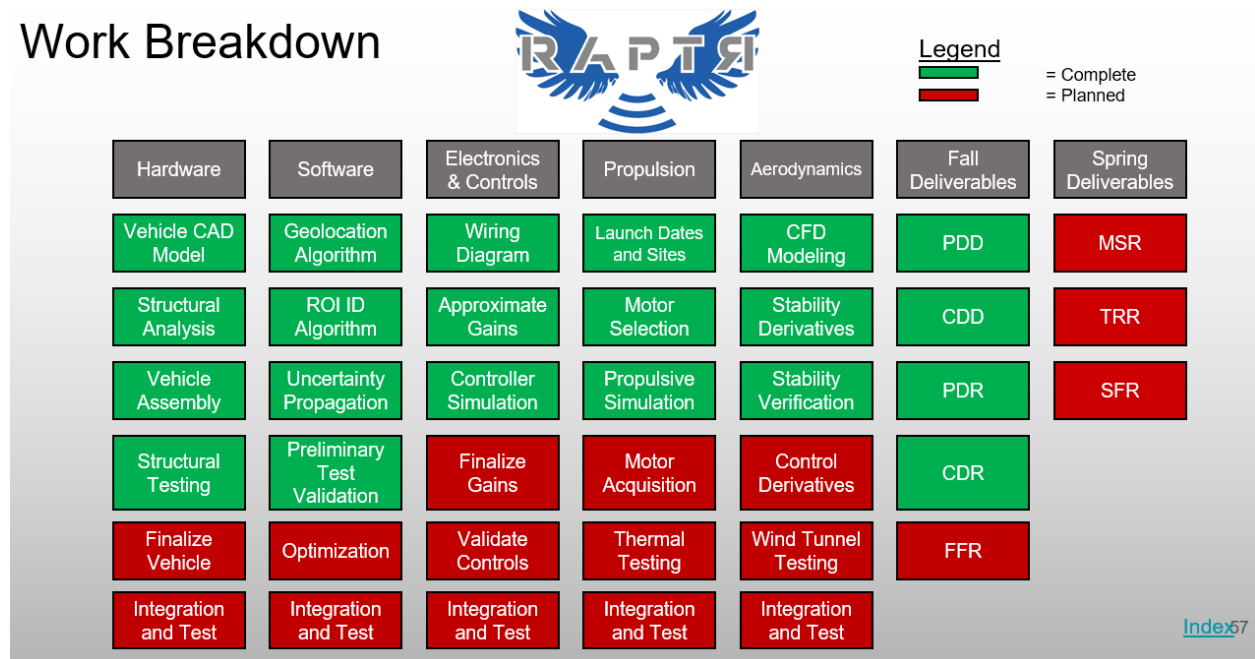
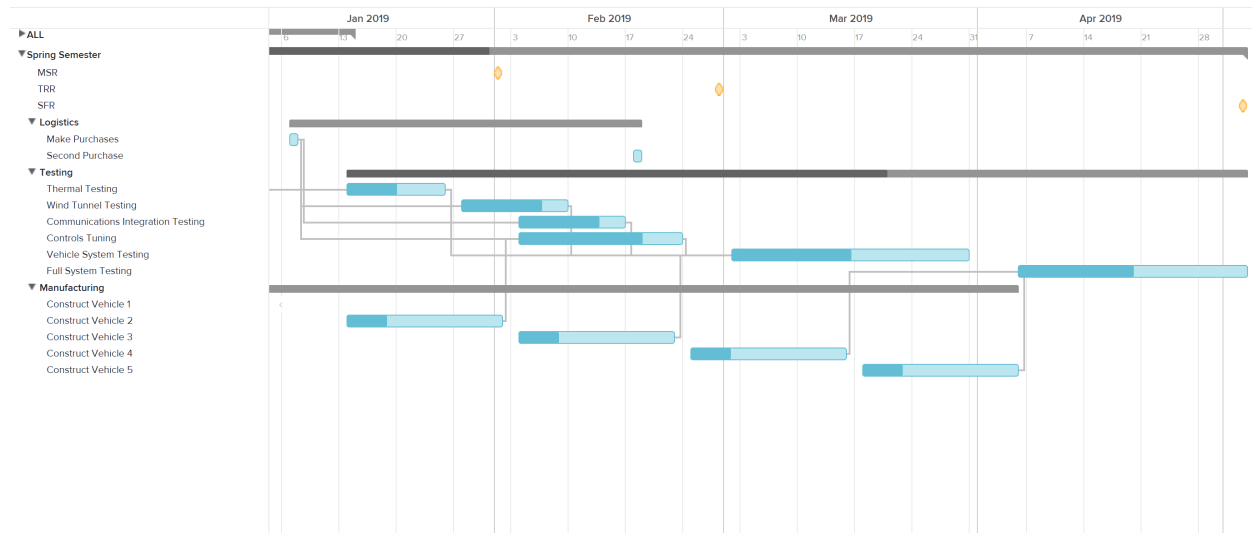


Figure 141. Work Breakdown

8.2. Work Plan

The schedule for the items listed in the work breakdown is visualized with a Gannt chart shown in figure 142. The left side of the figure lists the items and is organized into four sections. The first is Spring presentations or milestones, the second is purchasing logistics, the third is testing, and the last is manufacturing. The shapes to the right of each of these items indicate the task and its duration. The shading indicates the margin.

**Figure 142. RAPTR Spring Gantt Chart**

The three Spring milestones are the Manufacturing Status Review, the Test Readiness Review, and the Spring Final Review. These will be the administrative items driving the progress of the project.

The purchasing logistics section includes two dates for purchasing. The reason for this is to prevent a bulk order of unneeded components or faulty components. The first purchase will supply the testing and manufacturing up to about halfway through the semester. At this point, the project will have matured significantly and a more educated decision for purchasing can be made.

In the testing section, all the tests on the test plan are laid out. They are ordered such that the smaller sub-system tests are conducted first and the larger vehicle test and final full systems test are conducted last. The sub-system tests include a static motor fire for the thermal test, a wind-tunnel test of a scale model, a communications integration test, and a controls tuning un-powered test flight. The vehicle testing will finalize the vehicle's construction and functionality prior to the integration with the EE payload. The full systems testing will be to verify the vehicle and payload functionality and will require a test flight similar to the scenario detailed in the CONOPS.

The final section shows the schedule for manufacturing the vehicles. There will be four vehicles manufactured throughout the semester. One vehicle is being manufactured in pieces in addition to this but will be used entirely for destructive testing. The reason for manufacturing four vehicles is that the testing is likely to damage any vehicle that is flown and this will allow for multiple tests even if they destroy the vehicles. The budget was also more than sufficient to support these purchases.

The critical path starts with the first round of purchasing and leads into the thermal testing. The margin on the thermal testing is 100% to allow for delays in test approval or the need for repeat testing. Next is the communications testing, the margin for this testing is 30% to allow for testing issues, but there are no big potential stoppers that could delay it further, so the margin is fairly low. Then the first vehicle manufacture which has a margin of 300 % to allow room for any snags. The margin is so large because it is hard to quantify how long the construction will take as it depends on experience and there is plenty of room for snags. The next item is the pixhawk tuning, which has a slightly larger margin than the communications because this test depends on the completion of the first vehicle. After these, the next critical item is the vehicle testing which is scheduled to begin in early march. The margins for this test are 100% in-case there is a delay with the sub-system test. The final critical item is the full systems test which also has a 100% margin for the same reason as the vehicle test.

8.3. Cost Plan

A high level breakdown of the cost plan for the project can be seen below in Figure 143. The following sections have tabulated versions of a more detailed cost breakdown for each individual subteam with required expenses. A spreadsheet fully detailing the budget can be found in Appendix 10.1.

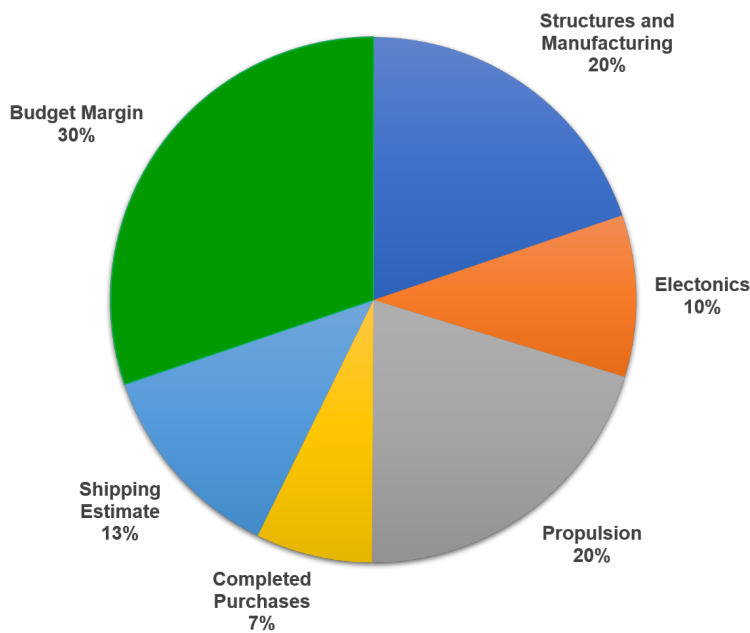


Figure 143. Pie Chart Visualizing the Project Budget

8.3.1. Electronics Subteam Cost Breakdown

Table 91. Detailed Cost Breakdown for the Electronics Subteam

Item	Quantity	Cost per Unit
Pixhawk 4 and GPS Module	1	\$211.00
Digital Airspeed Sensor	1	\$64.59
FrSky X8R Receiver	1	\$34.99
HKPilot Telemetry Radio Set	1	\$45.00
Telemetry Cable	1	\$19.99
Futaba Servo	2	\$40.99
Turnigy Graphene Panther 950 mAh Battery	1	\$12.24
Voltage Regulator	6	\$0.54
Diode	6	\$1.57
PCB (cost per 10 units)	1	\$15.00
Total:		\$497.45

8.3.2. Propulsion Subteam Cost Breakdown

Table 92. Detailed Cost Breakdown for the Propulsion Subteam

Item	Quantity	Cost per Unit
Nose Cone	3	\$24.94
Parachute	3	\$7.49
I-55 Engine	10	\$40.00
HAZMAT Shipping	1	\$50.00
38mm Cesaroni 3 Grain Casing	3	\$39.75
2240 PS-II Launch Controller	1	\$39.99
Total:		\$706.53

8.3.3. Structures and Manufacturing Subteam Cost Breakdown

Table 93. Detailed Cost Breakdown for the Manufacturing and Structures Subteam

Item	Quantity	Estimated Tax per Unit (VAT)	Cost per Unit
Hyperflight Andreas	4	\$27.55	\$137.73
Oracover Oralight	12	\$3.90	\$19.48
Carbon Rod	4	\$1.10	\$5.48
Low-Profile Sleeve Bearing Carriage	1	\$0.00	\$6.26
27mm Guide Rail for Bearing Carriage	1	\$0.00	\$15.00
Total:			\$1026.04

8.3.4. Already Completed Purchases

As of FFR, there have been 3 separate purchases made for this project for the purpose of preliminary testing. The first purchase made occurred on November 14 and was the largest purchase so far. This purchase consisted mainly of parts and materials needed to manufacture a single glider model for preliminary structural testing. The second purchase was made on November 29 and consisted of more materials that were necessary for manufacturing the glider model. The third purchase was a small purchase made to acquire materials to test the structural integrity of the engine mount. The total cost of these purchases came out to \$358.99 and spreadsheets detailing these purchases can be found in Appendix 10.1.1.

9. Individual Report Contributions

9.1. Austin Abraham

- Assisted with "Vehicle Trade Study" section of FFR
- Wrote "Analytic Wing Bending Model" section of FFR
- Assisted with writing "Modifying Fuselage for Flight Hardware" section of FFR
- Developed Matlab model for wing bending analysis
- Designed Separating Engine Mount Mechanism
- Created Solidworks model for engine mount initial design
- Started building first glider for testing/manufacturing purposes
- Made plan for modifying the glider and adding payload
- Assisted with derived requirement development
- Assisted with developing structural test plans
- Researched materials for structural and thermal failure mitigation

9.2. Nick Carvo

- Assisted with "Vehicle Trade Study" section of FFR
- Wrote "Detachable Engine Mechanism Design"
- Wrote "Engine Mount Structural Analysis"
- Assisted with writing "Modifying Fuselage for Flight Hardware"
- Wrote "Vehicle and Payload Integration"
- Created the SolidWorks model of the RAPTR Vehicle
- Provided SolidWorks renderings and drawings for the document
- Provided Ansys structural analysis and corresponding images
- Started construction on first glider for testing purposes
- Assisted with the design of the motor mount system

9.3. Greg Clements

- Section 3 - Performed and wrote trade study for landing methods
- Section 4 - Changed/Added requirements and filled out the V&V for each requirement
- Section 5 - MATLAB and FAA Compliance subsections of propulsion design. Contributed to thermal effects subsection
- Section 6 - All
- Assisted with overall propulsion system design
- Completed test imaging for software and motor mount stress testing
- Researched all relevant regulations and safety codes for high-powered rockets and unmanned aerial systems
- Contacted necessary parties for testing approval

9.4. Zach Donovan

- Section 3 (Concept Design) - Wrote sensor suite design trade study
- Section 5 (Detail Design) - Aided in electrical component selection, performed analysis of servos in Matlab, and experimental tested the Pixhawk
- Section 5 (Detail Design) - Performed/wrote about of ArduPlane code, controls architecture, PID gain approximation
- Wrote all PID code
- Developed control CONOPs and flowchart
- FFR proofreading and formatting

9.5. Tyler Faye

- Created and updated circuit and wiring diagrams throughout design process
- Created comprehensive solution with a backup to eliminate the potential for radio interference
- Created complete power budget including idle, operating, and max current draw conditions
- Modified relevant derived requirements to more accurately reflect project necessities
- Wrote section 6.4.1 of the FFR, detailing the vehicle electronics
- Wrote section 6.4.2 of the FFR, detailing vehicle transmission and reception
- Assisted other sections of the FFR with feedback as it relates to the vehicle electronics

9.6. Thad Gleason

- Performed CFD analysis on the Solidworks model
- Calculated stability derivatives using the data from the CFD results
- Performed further stability analysis using USAF Digital Datcom
- Calculated glide slope angle using the lift and drag results from the CFD analysis
- Various sections in the FFR pertaining to aerodynamics including the design and test sections

9.7. Everett Hale

- Performed trade study on autopilot platform for conceptual design.
- Assisted with development of software test plan.
- Assisted in the writing of the software section of detailed design.
- Created the bill of materials found in the appendix
- wrote the cost plan section of project planning.

9.8. Jeremy Lane

- Wrote trade study on imaging sensors
- Defined levels of success for software capability
- Assisted in developing all requirements detailing software performance
- Developed software CONOPs and flowchart
- Wrote majority of software detailed design
- Wrote all code for target detection
- Wrote all code for target geolocation
- Perform preliminary software test with Greg and validated software with results

9.9. AJ McKelvy

- Wrote project purpose section
- Uploaded and Updated CDD content for conceptual design section
- Uploaded objectives table from PDD and spoke to it in Objectives section
- Uploaded current requirement breakdown into requirements section.
- Wrote Gantt chart section
- performed performance analysis and spoke to performance plots
- Wrote the baseline design portion of conceptual design section

9.10. Logan Thompson

- Created updated CONOPs and FBD Diagrams and revised/wrote descriptions of each in FFR Section 2
- Revised and updated requirements to more accurately fit current mission profile and be more verifiable
- Created and tracked risk matrices along with their mitigation strategies and their descriptions for FFR Section 9
- Created work breakdown diagram and its description
- Performed trade study on payload mounting method and the analysis of the results

9.11. Anna Tiberi

- Section 3 - Performed and wrote trade study for deployment methods.
- Section 4 - Reviewed requirements and changed/edited where necessary.
- Section 5 - Propulsion Subsection: Wrote and modeled all of this subsection (excluding the MATLAB model overview)
- Propulsive system design: Engine choice and modeling, parachute calculations, modeling of the full system and 3D CAD model for both software.
- Remained in contact with the president of the Northern Colorado Rocketry Club (Joe Hinton) and spoke with him many times about the feasibility of the design.
- Thermal characteristics and numerous attempts to model the thermal effects and plume characteristics.
- Assisted in static firing test idea.

References

- [1] ArduPilot Dev. ArduPlane (2016), <http://ardupilot.org/plane/>
- [2] Hippert, Roy. AndREAS - F3-RES. HyperFlight, www.hyperflight.co.uk/products.asp?code=ANDREASname=andreas-f3-res
- [3] Horrizon Hobby. UMX Radian BNF with AS3X (2018), <https://www.horizonhobby.com/umx-trade%3B-radian-reg%3B-bnf-with-as3x%C2%AE-technology-eflu2980>
- [4] Coker, J. (n.d.). Cesaroni I55. Retrieved from <http://www.thrustcurve.org/motorsearch.jsp?id=1045>
- [5] Components, I. A. (n.d.). Cesaroni - P38-3G Mellow (I55). Retrieved from https://www.apogeerockets.com/Rocket_Motors/Cesaroni_Propellant_Kits/38mm_Motors/3-Grain_Motors/Cesaroni_P38-3G_Mellow_I55
- [6] RAPTR Team, Project Definition Document, September 2018
- [7] RAPTR Team, Preliminary Design Review, October 2018.
- [8] RAPTR Team, Conceptual Design Document, October 2018.
- [9] RAPTR Team, Critical Design Review, December 2018.
- [10] Fossey, Paul L. RockSim Program Guide. *Apogee Rockets*. Retrieved from <https://www.apogeerockets.com/downloads/PDFs/Rocksim.pdf>
- [11] Mechanical Properties of Continuous Fibers. Mechanical Properties of Continuous Fibers, Markforged, 2016.
- [12] Niskanen, Sampo. OpenRocket Technical Documentation. 2013-05-10. *Source Forge*. Retrieved from <http://openrocket.sourceforge.net/techdoc.pdf>
- [13] Kamthai, Suthaphat, and Rathanawan Magaraphan. Thermal and Mechanical Properties of Polylactic Acid (PLA) and Bagasse Carboxymethyl Cellulose (CMC_B) Composite by Adding Isosorbide Desters. Thermal and Mechanical Properties of Polylactic Acid (PLA) and Bagasse Carboxymethyl Cellulose (CMC_B) Composite by Adding Isosorbide Desters.
- [14] Ultimaker. Technical Data Sheet ABS. Farnell.com, 28 Feb. 2017, www.farnell.com/datasheets/2310520.pdf
- [15] Parametric Elliptical Nose Cone. Retrieved from <https://www.thingiverse.com/thing:507830>.
- [16] Parachute Descent Calculations. Retrieved from <http://www.rocketmime.com/rockets/descent.html>.
- [17] Wasp III Factsheet. Retrieved from <https://archive.is/20120723101353/http://www.af.mil/information/factsheets/factsheet.asp?id=10469>.
- [18] RQ-20 Puma data sheet. Retrieved from http://www.avinc.com/downloads/PumaAE_0910.pdf.
- [19] 1010 Conformal Rail Guide 38mmC. Retrieved from <https://www.rocketryforum.com/media/1010-conformal-rail-guide-38mmc.346666/>.
- [20] Folding Model Rocket Launch Pads & Accessories: FLP-48 Model - Our Largest Folding Launch Pad. Retrieved from http://knight-mfg.com/folding_launch_pads.
- [21] LAUNCH RAIL (STANDARD 1010). *Apogee Rockets*. Retrieved from https://www.apogeerockets.com/Launch_Accessories/Launch_Pads/Launch_Rail_Standard.
- [22] Hobby King. Turnigy Graphene Panther 950mAh 2S 75C Battery Pack, <https://cdn-global-hk.hobbyking.com/media/catalog/product/cache/1/image/660x415/17f82f742ffe127f42dca9de82fb58b1/1/9/191845.jpg>
- [23] ArduPilot. Common Power Module, http://ardupilot.org/copter/_images/3DR-current-sensor-top.jpg
- [24] DIY Drones. Pixhawk (and APM) Power Consumption, <https://diydrones.com/profiles/blogs/pixhawk-and-apm-power-consumption>

- [25] Dronecode. PX4 User Guide, https://docs.px4.io/en/flight_controller/pixhawk4.html
- [26] Get FPV. Holybro Micro M8N GPS Module, <https://www.getfpv.com/holybro-micro-m8n-gps-module.html>
- [27] jDrones. Digital airspeed sensor, http://store.jdrones.com/digital_airspeed_sensor_p/senair02kit.htm
- [28] Amazon. YKS 3DR Radio Telemetry Kit 915Mhz Module Open Source for APM 2.6 2.8 Pixhawk RC Quadcopter, <https://www.amazon.com/YKS-Telemetry-915Mhz-Pixhawk-Quadcopter/dp/B0196LF6PW>
- [29] FrSky. X8R, <https://www.frsky-rc.com/product/x8r/>
- [30] ServoDatabase. Futaba S3152 - Servo Digital Standard Hi-Torque, <https://servodatabase.com/servo/futaba/s3152>
- [31] Meyers, J. M. ME 239: Rocket Propulsion Over- and Under-expanded Nozzles and Nozzle Configurations. *University of Vermont, Mechanical Engineering*. Retrieved from <http://www.cems.uvm.edu/~jmmeayers/ME239/Slides/04%20-%20Over%20and%20Under%20Expansions%20and%20Nozzle%20Configurations%20v1.pdf>.
- [32] Jarvinen, P. O., Hill, J. A., Draper, J. S., & Good, R. E. (1966, June). High Altitude Rocket Plumes. Retrieved from <https://apps.dtic.mil/dtic/tr/fulltext/u2/807649.pdf>.
- [33] Lunar Lander Plume Impingement. *Department of Aerospace Engineering and Engineering Mechanics at the University of Texas, Austin*. Retrieved from <http://cfpl.ae.utexas.edu/lunar-lander-plume-impingement>.
- [34] Aerospace Specification Metals Inc. *Aluminum 6061-T6*, Retrieved: 15th December 2018, Retrieved from: <http://asm.matweb.com/search/SpecificMaterial.asp?bassnum=ma6061t6>
- [35] Engineers Edge, LLC. *AISI Carbon Steel Mechanical Characteristics*, Retrieved: 15th December 2018, Retrieved from: <https://www.engineersedge.com/materials/carbon-steel-properties.htm>
- [36] Rock West Composites, Inc. *ROD - PULTRUDED UNIDIRECTIONAL - 0.236 X 78 INCH*, West Jordan, UT 84088, Retrieved: 15th December 2018, Retrieved from: <https://www.rockwestcomposites.com/rods-shapes/round-pultruded-solid-rod/carbon-round-pultruded-solid-rod/r-rnd-236>
- [37] Schachter, Bruce J. Automatic Target Recognition. Second Edition. Retrieved on 15 September 2018. Retrieved from: [https://app.knovel.com/web/view/khtml/show.v/rnid:kPAtRE0005/cid:kt011ER1X2/viewerType:khtml//root_slug:2-target-detection-strategies/url_slug:target-detection-strategies?b-toc-cid:kPAtRE0005&b-toc-root-slug=&b-toc-url-slug:target-detection-strategies&b-toc-title=Automatic%20Target%20Recognition%20\(2nd%20Edition\)&page=18&view=collapsed&zoom=1](https://app.knovel.com/web/view/khtml/show.v/rnid:kPAtRE0005/cid:kt011ER1X2/viewerType:khtml//root_slug:2-target-detection-strategies/url_slug:target-detection-strategies?b-toc-cid:kPAtRE0005&b-toc-root-slug=&b-toc-url-slug:target-detection-strategies&b-toc-title=Automatic%20Target%20Recognition%20(2nd%20Edition)&page=18&view=collapsed&zoom=1)
- [38] Szeliski, Richard. Computer Vision: Algorithms and Applications. Retrieved on 25 October 2018. Retrieved from: http://szeliski.org/Book/drafts/SzeliskiBook_20100903_draft.pdf
- [39] Collins, Robert. CSE 486, Penn State. Lecture 12: Camera Projection. <http://www.cse.psu.edu/~rtc12/CSE486/lecture12.pdf>

10. Appendix

10.1. Project Budget

Part Name	Relevant Subcat	Part Number (if applicable)	Weight [g]	Weight [lb]	Cost (USD)	Quantity	Tax per Unit (USD)	Source	Total Cost (USD)
Pixhawk 4 and GPS Module	Electronics	20064	37.8	0.0833	\$211.00	1	0.00	https://shop.holybro.com/pixt	\$211.00
Digital Airspeed Sensor	Electronics	SENAIR02KIT	12	0.0265	\$64.59	1	0.00	http://store.jdrones.com/digit	\$64.59
FrSky X8R Receiver	Electronics	236000056-0	16.8	0.0370	\$34.99	1	0.00	https://www.amazon.com/FrS	\$34.99
HKPilot Transceiver Telemetry Radio Set V2 (915Mhz)	Electronics	N/A	20	0.0441	\$45.00	1	0.00	https://www.amazon.com/YK	\$45.00
Telemetry Cable	Electronics	N/A	2.5	0.0063	\$19.99	1	0.00	https://www.amazon.com/YK	\$19.99
Servo - Futaba S3152	Electronics	S3152	41	0.0904	\$40.99	2	0.00	https://www.amazon.com/Fut	\$81.98
Turnigy Graphene Panther 950mAh Battery	Electronics	9067000367-0	50	0.1102	\$12.24	1	0.00	https://hobbyking.com/en_us	\$12.24
Voltage Regulator	Electronics	NCP1117ST50T3G	3	0.0066	\$0.54	6	0.00	https://www.digikey.com/proc	\$3.24
Diode	Electronics	DMV1500MFD	2.4	0.0053	\$1.57	6	0.00	https://www.digikey.com/proc	\$9.42
Printed Circuit Board (per 10)	Electronics	N/A	20	0.0441	\$15.00	1	0.00	https://ilcpcb.com/	\$15.00
							Electronics Total:		\$497.45
38MM FIBERGLASS OGIVE 4:1 NOSE CONE	Propulsion	20265	71.4	0.1574	\$24.94	3	0.00	https://www.apogeerockets.c	\$74.82
Parachute: 12" Plastic Chute	Propulsion	29121	2	0.0044	\$7.49	3	0.00	https://www.apogeerockets.c	\$22.47
Engine (I-55)	Propulsion	CTI I55-9A	437	0.9634	\$40.00	10	0.00	http://www.moto-joe.com/ind	\$400.00
HAZMAT Shipping	Propulsion	N/A			\$50.00	1	0.00		\$50.00
38mm Cesaroni 3 grain casing	Propulsion	CTI P38-3G	121.9	0.2687	\$39.75	3	0.00	http://www.moto-joe.com/ind	\$119.25
2240 PS-II Launch Controller	Propulsion	2240	N/A	N/A	\$39.99	1	0.00	https://www.estesrockets.com	\$39.99
Launch Stand - FLP-48	Propulsion	FLP-48	N/A	N/A	\$229.99	1	0.00	http://knight-mfg.com/folding_	\$229.99
Launch Rail - AI-1010	Propulsion	7697	N/A	N/A	\$81.45	1	0.00	https://www.apogeerockets.c	\$81.45
							Propulsion Total:		\$1,017.97
Hyperflight Andreas	Structures	N/A	518	1.1419	\$137.73	4	27.55	https://www.hyperflight.co.uk	\$661.10
Oracover Oralight	Structures	N/A	N/A	N/A	\$19.48	12	3.90	https://www.hyperflight.co.uk	\$280.51
Carbon Rod	Structures	N/A	21	0.0462	\$5.48	4	1.10	https://www.hyperflight.co.uk	\$26.30
Low-Profile Sleeve Bearing Carriage	Structures	6723K11	8.8	0.0194	\$6.26	1	0.00	https://www.mcmaster.com/6	\$6.26
27 mm Wide Guide Rail for Low-Profile Sleeve Bearing Carr	Structures	6723K2	13.6	0.0300	\$15.00	1	0.00	https://www.mcmaster.com/6	\$15.00
							Structures Total:		\$989.18
							Total Without Shipping:		\$2,504.60
							Shipping Estimates (~25%)		\$626.15
							Previous Purchases:		\$314.05
									\$8.08
									\$36.86
							True Total:		\$3,489.74
							Total Budget Remaining:		\$1,555.20

10.1.1. Completed Purchases

Source	Date Purchased	URL	Items Purchased	Cost	Purchase Subtotal	Shipping + Tax	Total Cost	Total Spent on Purchase	Budget Left		
Hyperflight	11/14/2018	https://www.hyper	AndREas-F3-RES	142.37	167.56	57.21	224.77	314.05	4685.95		
			https://www.hyper ORALIGHT-T-BLUE	19.71							
			https://www.hyper CARBON-ROD-5MM	5.48							
Amazon	11/14/2018	https://www.amazon	TruMed 1001 Disposable Scalpels	10.95	10.95	0	10.95				
Top Flite	11/14/2018	http://www.monok	Top Flite Sealing Iron	29.99	61.97	16.36	78.33				
			http://www.monok Top Flite Monokote Hot Sock Iron Cover	3.99							
			http://www.monok Top Flite Trim Seal Tool	27.99							

Source	Date Purchased	Items Purchased	Quantity	Part Number	Cost per Unit	Cost	Total Cost	Budget Left
McGuckin Hardware	11/29/2018	T pins 35 count	1	M3140775	\$3.41	\$3.41	\$36.86	\$4,649.09
		Quick Set Apoxy	1	12286	\$3.59	\$3.59		
		CA glue	1	M9401520	\$7.19	\$7.19		
		CA glue accelerator	1	M9401550	\$14.39	\$14.39		
		100 grit sandpaper	3	10690	\$0.89	\$2.67		
		220 grit sandpaper	3	11388	\$0.44	\$1.32		
		400 grit sandpaper	3	11398	\$1.43	\$4.29		

Source	Date Purchased	Items Purchased	Quantity	Part Number	Cost per Unit	Tax	Cost	Total Cost	Budget Left
McGuckin Hardw	12/1/2018	McGuckin 5GI Bucket	1	124152	\$3.59	\$0.00	\$3.59	\$8.08	\$4,641.01
		Balsa 1.5x2x1in	1	M6525740	\$4.49	\$0.00	\$4.49		